STACKING OF IGBT DEVICES FOR FAST HIGH-VOLTAGE HIGH-CURRENT APPLICATIONS

Thesis presented for the degree of
Doctor of Philosophy in Electrical Engineering
of the University of Strathclyde

Zarir Ghasemi, BSc (honours), MSc (honours)
2007

Department of Electronic and Electrical Engineering
University of Strathclyde
Glasgow, UK

DECLEARATION OF AUTHOR'S RIGHTS

ABSTRACT

The development of solid-state switches for pulsed power applications has been of considerable interest since high-power semiconductor devices became available. However, the use of solid-state devices in the pulsed power environment has usually been restricted by device limitations in either their voltage/current ratings or their switching speed. The stacking of fast medium-voltage devices, such as IGBTs, to improve the voltage rating, makes solid-state switches a potential substitute for conventional switches such as hard glass tubes, thyratrons and spark gaps. Previous studies into stacking IGBTs have been concerned with specific devices, designed or modified particularly for a specific application. The present study is concerned with stacking fast and commercially available IGBTs and their application to the generation of pulsed electric field and the switching of a high intensity Xenon flashlamp. The aim of the first section of the present study was to investigate different solid-state switching devices with a stacking capability and this led to the choice of the Insulated Gate Bipolar Transistor (IGBT). It was found that the collector-emitter voltage decreases in two stages in most of the available IGBTs. Experiments and simulation showed that a reason for this behaviour could be fast variations in device parasitic parameters particularly gate-collector capacitance. Choosing the proper IGBT, as well as dealing with problems such as unbalanced voltage and current sharing, are important aspects of stacking and these were reported in this study. Dynamic and steady state voltage imbalances caused by gate driver delay was controlled using an array of synchronised pulses, isolated with magnetic and optical coupling. The design procedure for pulse transformers, optical modules, the drive circuits required to minimise possible jitter and time delays, and over-voltage protection of IGBT modules are also important aspects of stacking, and were reported in this study.

The second purpose of this study was to investigate the switching performance of both magnetically coupled and optically coupled stacks, in pulse power applications such as Pulse Electric Field (PEF) inactivation of microorganisms and UV light inactivation of food-related pathogenic bacteria. The stack, consisting of 50 1.2 kV IGBTs with the voltage and current capabilities of 10 kV, 400 A, was incorporated

into a coaxial cable Blumlein type pulse generator and its performance was successfully tested with both magnetic and optical coupling.

As a second application of the switch, a fully integrated solid-state Marx generator was designed and assembled to drive a UV flashlamp for the purpose of microbiological inactivation. The generator has an output voltage rating of 3 kV and a peak current rating of 2 kA, although the modular approach taken allows for a number of voltage and current ratings to be achieved. The performance of the switch was successfully tested over a period of more than 10^6 pulses when it was applied to pulse a xenon flashlamp.

Chapter 1
INTRODUCTION

Many established and emerging technologies use devices and systems that require high peak powers at high voltages. These cover a wide range of applications and include high power microwave sources [1,2], ion beam generation and acceleration [3], lightning simulation [3,4], nuclear weapons simulation [5], high power ultrasound sources for rock fracturing [6,7], electronic pasteurisation and sterilisation of foodstuffs [8-10], and environmental applications such as the treatment of hazardous water or waste and flue gases [11]. Pulsed power systems provide the ability to store large amounts of electrical energy over a relatively long period of time (typically millisecond to seconds), followed by release of this energy in a very rapid time scale (usually less than a few microseconds) to allow high peak powers of up to hundreds of MW to be produced.

Switching devices are essential components in pulsed power systems and the levels of the voltage and the other key parameters of the output pulses depend directly on the characteristics of the switches. Advances in the field of pulsed power technology in relation to pulse-forming networks and compression techniques involve increased energy storage, increased power density, and larger voltage handling. However, the overall performance of pulsed power systems with high pulse repetition rate is limited by the speed and reliability of the switching devices.

The advent of high-power semiconductor devices has led to the development of solid-state switches for pulsed power applications. However, the use of solid-state devices in the pulsed power environment has been somewhat restricted by limitations in voltage/current rating and switching speed. For the past two decades, a large number of researchers have attempted to use semiconductor switches in pulsed power systems as a substitute for conventional switches such as hard glass tubes, thyratrons, and spark gap switches [12,13]. The results of these studies reveal that the advantages of solid-state switching devices for pulsed power applications over conventional switches are: *longer lifetime, no degradation, high repetition frequency, no warm-up time, zero maintenance, consistent characteristics, no in-life adjustment of the ancillary circuits*

and *higher efficiency* [12-16]. This has led to the gradual replacement of conventional switches such as the thyratron by solid-state switching devices such as the MOSFET [14].

Most of the previous work on stacking solid-state switching devices has focused on specific devices, which have been designed or modified particularly for a specific pulsed power application [17-19]. This, in addition to the high cost of these devices, has limited their applications. The present investigation is concerned with stacking fast solid-state switching devices, designed for fast power applications, and their application to the generation of pulsed electric field and the switching of a high intensity xenon flashlamp.

The first part of this study was to investigate different solid-state switching devices with a stacking capability for use in fast pulse power applications. Various potentially suitable semiconductor devices were examined and compared in terms of their availability, switching characteristics and stacking capability. This study led to the choice of the Insulated Gate Bipolar Transistor (IGBT), and, in order to fully understand IGBT operation, a study of IGBT characteristics was undertaken, and suitable models for analysis are discussed and reviewed. A comprehensive review of the various methods for operating IGBT devices in series and parallel is presented and a suitable method for fast pulse power application then selected. Equal voltage and current sharing, and simultaneous turn on of all devices are some of the difficulties encountered with series and parallel-connected semiconductors. In order to control the dynamic and steady state voltage imbalances caused by gate driver delay, an array of synchronised pulses, isolated from each other, is required, and this was provided using magnetic and optical coupling. The design procedures for the pulse transformers, optical emitter/receiver modules and the drive circuits required to minimise possible jitter and time delays are important aspects of stacking, and are reported in this study. The success of the overall design was confirmed by simulation and experiment. Over-voltage protection of the stack was achieved by limiting the supply voltage to no more than 80% of the IGBT rated value, and auxiliary protection was provided by connecting fast voltage suppressor devices such as *Transil, Transient Voltage Suppressor, Tranzorb and Voltage Dependent Resistor* across the IGBT modules.

The second objective of this study was to investigate the switching performance of both magnetically coupled and optically coupled stacks, in pulse power applications such as Pulse Electric Field (PEF) inactivation of microorganisms and UV light inactivation of food-related pathogenic bacteria. The semiconductor switch, consisting of IGBT devices, was incorporated into a coaxial cable Blumlein type pulse generator in order to investigate the effect of pulsed electric fields on the inactivation of a microbial population suspended in liquids in static and flow systems. One of the important and complicated components of the PEF processing system is the treatment chamber. Several designs of static and flow chamber were investigated, and a coaxial geometry test cell was selected. The coaxial test cell was optimised in terms of the electric field distribution across the gap and its performance was confirmed by simulation and experiment. The PEF experiments were carried out for *E.coli* and *Bacillus cereus* with different numbers of pulses. As a second application of the semiconductor switch, a fully integrated solid-state Marx generator was designed and assembled to drive a UV flash lamp for the purpose of microbiological inactivation. The reduction in microbial viability is discussed for the inactivation of food-related pathogenic bacteria such as *E.coli* and *Salmonella*.

Chapter 2 provides a review of pulsed power techniques and devices suitable for switching, with an emphasis on semiconductor devices. The choice of the Insulated Gate Bipolar transistor (IGBT) for fast pulse power applications is validated. In Chapter 3, the switching characteristics of the IGBT are discussed and a comprehensive review is provided of the various techniques for operating IGBT devices in series and parallel. Experimental arrangements for the tests carried out on different IGBTs are described in Chapter 4. The switching speed of the different IGBT devices is evaluated by experiment and computer simulation. The stacking procedure for 600 V and 1.2 kV IGBTs, together with the operating performance of the stacked IGBTs are also discussed in Chapter 4. Chapter 5 covers the approach and procedure for stacking 1.2 kV IGBTs using optical coupling. A prototype optical system is introduced and the stack performance in terms of switching speed is discussed and compared with that of the stack assembled using magnetic coupling. In Chapter 6, the operational performance of the optically coupled IGBT stack in an application involving the use of high-intensity pulsed electric fields (PEF) is discussed. In Chapter 7, another approach to cell inactivation is described using UV radiation again using an

optically coupled stack of IGBTs. The design and performance of a fully integrated solid-state Marx generator that drives a UV flashlamp is described in this chapter.

Chapter 2

REVIEW OF HIGH VOLTAGE SWITCHING DEVICES

2.1 Pulsed power techniques

The primary aim of a pulsed power system is to produce high output powers from low input power sources. This is achieved through the use of pulse compression, where the energy is supplied to a storage device over a long time period and is released from the energy storage device in very short time. A typical pulsed power system is assembled from four basic elements. These are a primary power source, an intermediate energy store, a pulse forming network (PFN) and at least one high-power switch. A generalised diagram for a pulsed power system with examples of the system components is shown in Figure 2.1. Initially, the PFN element is charged through a capacitive or inductive energy store by the primary power source. The PFN element may be a coaxial cable, a stripline or a water-filled[1] line and is usually the section of the circuit that determines the main pulse characteristics. A suitable resistance or inductance controls the flow of energy to the PFN. The PFN is charged to the same voltage level as the primary power supply in the case of resistive charging, and to a maximum of twice the primary power supply in the case of resonant charging.

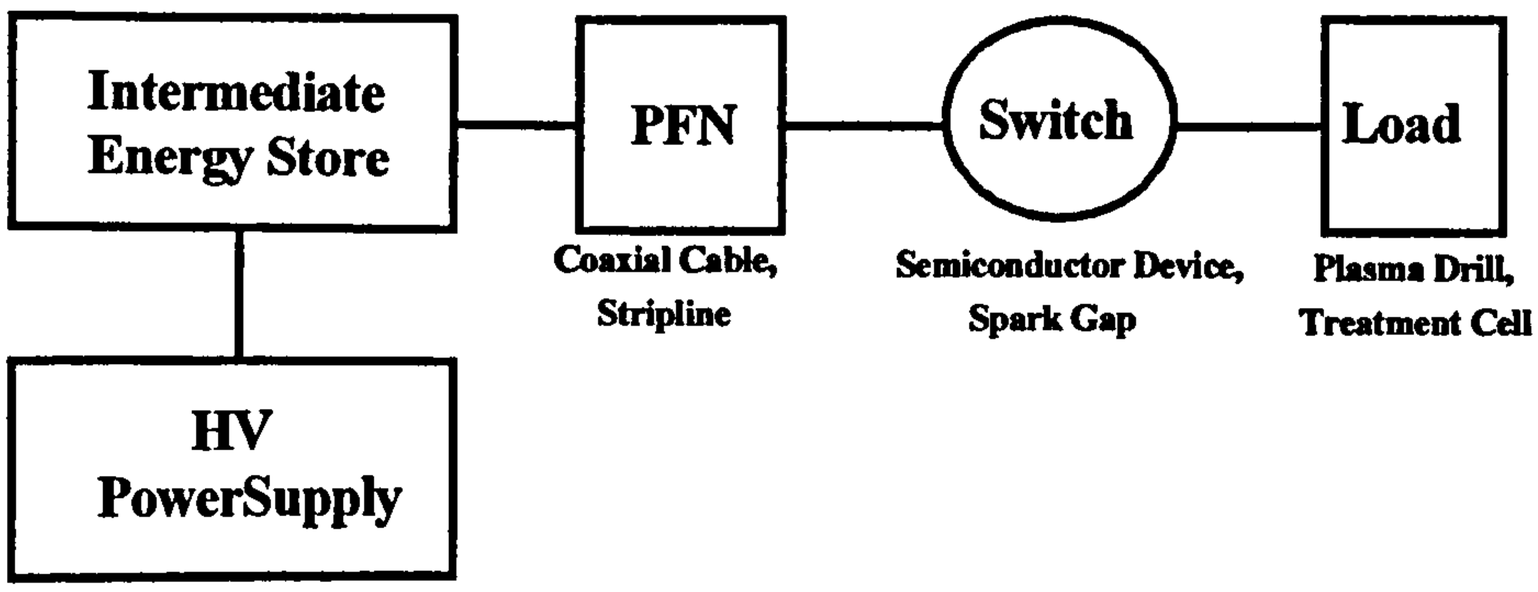

Figure 2.1 Pulsed power system with examples of system components.

[1] Water-filled line would need to be pulsed charged due to ionic conduction losses.

The PFN delivers its stored energy to the load through a high voltage switch in times of between ns and μs and allows very high peak powers to be generated. The speed of the switch is one of the factors that determine the pulse generator performance and it is critical that the switch can safely handle the charge transfer, whilst exhibiting fast closure time and high dI/dt. Typically, the switching device can take the form of either a closing switch or an opening switch. Closing switches are used to produce high power pulses with capacitive storage circuits. In these circuits, upon closure of the switch, energy is transferred from the capacitor to the load. Opening switches are used where energy is stored in the form of an electromagnetic field around an inductor. Upon opening the switch, the current flowing through the inductor is interrupted and the energy stored in the electromagnetic field is transferred to the load. Given the inherent difficulty in developing opening switches capable of transferring high peak powers, more extensive use is made of closing switches.

In pulsed power applications, the switch is an essential component and the levels of the voltage and other key parameters of the output pulses depend directly on the characteristics of the switch [15]. The characteristics of an ideal switch suitable for fast-pulsed power applications include efficient voltage and current handling capability, high dI/dt (up to 10^{15} A s^{-1}), and fast closure time in the range of nanoseconds. It is difficult however to obtain all of these characteristics with one device and this places limitations on voltage, energy per pulse or pulse repetition rate and thereby on the overall system performance. The following section (2.2) details the basic design and operation of the most commonly used closing switches. These are the self-closing spark gap, the triggered spark gap, the thyratron, and the ignitron [for pulsed power applications]. In 2.3, some semiconductor switches used for pulsed power applications are introduced and their switching characteristics discussed.

2.2 Closing switches

2.2.1 Self-closing spark gap

One of the simplest forms of closing switch is a self-closing or overvoltaged spark gap. Basically, a spark gap consists of two uniform field, or quasi-uniform field electrodes, separated by an insulating gas or gas mixture. As the breakdown voltage in a uniform DC field is a function of pressure and distance as governed by Paschen's law [20], for ideal gases, the breakdown voltage can be adjusted simply by adjusting the gap spacing, the gas pressure or the gas type. Self-closing spark gaps are typically used for circuit or component protection, where, upon application of a high voltage pulse above the determined safe level, the pulse is diverted to ground through the discharged gap [21].

2.2.2 Triggered spark gap

For spark gaps, the switching discharge is initiated by overvolting the gap. However, in order to achieve a low jitter and higher degree of synchronisation, a trigger method is usually employed. This offers faster conduction and pulse risetimes than those available from a conventional spark gap switch, and allows control of the spark gap in terms of pulse initiation and repetition rate. The trigger method can be mechanical, electrical or optical. The trigatron, field-distortion (FD) gap and rotary spark gap are examples of triggered closing switches [21,22].

A trigatron is constructed from a pair of parallel high voltage electrodes, with a third trigger electrode situated in, but insulated from, the earth electrode. The switch operates by being set to a voltage level, which is just beneath the self-breakdown voltage for the switch. A fast trigger pulse applied to the trigger electrode forms a small plasma channel between the trigger electrode and the main earthed electrode. The resultant ionisation of gas atoms and molecules and emission of UV photons in the region near the plasma channel results in rapid photoionisation and electron avalanches in the region between the main electrodes. This allows plasma formation and breakdown to occur in the main gap, thus closing the switch [21-24].

A field-distortion (FD) switch is also a three-electrode spark gap, but in this case, the third electrode is a knife-edge ring electrode situated between the two main electrodes. Application of the trigger pulse to the trigger electrode distorts the field within the switch. This distortion causes breakdown between the main electrode and the trigger electrode, which overvolts the remaining half of the switch. This results in a second discharge initiation, which has the effect of closing the switch.

A rotary spark gap switch is an example of a mechanically triggered spark gap switch. The basic principle involves altering the spark gap path length through the inclusion of a metal conductor (usually brass or stainless steel) in the spark gap. To trigger the switch, a rotating electrode is moved towards a pair of fixed circuit electrodes, initiating breakdown of the gap. A rotary spark gap exhibits some degree of timing jitter between pulses as a result of mechanical variations in the path of the moving trigger electrode.

2.2.3 Thyratron

The thyratron is a low-pressure switch that was originally developed in the 1940s for repetitive radar applications. It has found use in a number of applications such as in gas lasers and microwave sources, where a high repetitive capability is required [25,26]. The rapid rate of voltage recovery (typically of the order of a few tens of μs) makes the thyratron very suitable for applications with high pulse repetition rate (~ a few kHz). However, the thyratron has limited voltage (a few tens of kV) and current (a few kA) handling capabilities and is not as robust as the spark gap. The voltage and current ratings of thyratron switches can be improved by using series and parallel combinations of thyratrons [27].

2.2.4 Ignitron

The ignitron, like the thyratron, is a low pressure device. It is suitable for relatively low voltage (tens of kV) and high current (hundreds of kA) applications such as the discharge of large capacitor banks and crowbar circuits, high power lasers, arc welders and electromagnetic railguns. The ignitron is constructed of an anode, a mercury-pool cathode and an ignitor or starting electrode immersed in the mercury pool. All electrodes are housed in a stainless steel vessel, which is evacuated. The

ignitron requires a voltage pulse of a few kV for triggering. The ignitron has a very slow recovery after closure and this makes it suitable for single-shot or low repetition rates only [21,28,29]

2.3 Semiconductor switches

Semiconductor switches offer a number of advantages over conventional switching technology, such as longer lifetime, zero maintenance and consistent characteristics. A variety of power semiconductor devices is used in power electronics switching applications, and these can be divided into the following three groups [18]:

1. Unipolar devices, where charge conduction is due mainly to flow of one type of carrier, usually electrons. These include Schottky diodes, Junction-Field-Effect-Transistors (JFET), Metal-Semiconductor Field-Effect Transistors (MESFET), Metal–Oxide-Semiconductor Field-Effect Transistors (MOSFET), and Static-Induction-Thyristors (SIT).
2. Bipolar devices, where drift-diffusion processes of both electrons and holes contribute to current flow. These include power Bipolar-Junction-Transistors (BJT), Insulated-Gate-Bipolar-Transistors (IGBT), Gate-Turn-Off Thyristors (GTO), MOS-Controlled Thyristors (MCT), Reverse-Conducting-Thyristors (RCT), and MOS-Assisted-Gate-Triggered-Thyristors (MAGT).
3. Bulk avalanche devices that often require optical triggering. These devices have high dark resistivity (> 10^4-10^8 Ωcm^2) and large anode-to-cathode separation, and this allows them to be implemented in very high power (~ 1 MW) switching systems.

Because of the absence of minority-carrier stored charge, the switching speed of unipolar devices is fast and in most cases, the gate-drive power requirements are low and simple. Compared to unipolar devices, bipolar devices exhibit lower conduction

losses and lower switching speeds. Bulk avalanche devices are commonly constructed from III-V compound semiconductors, especially Gallium Arsenide (GaAs), to improve switching speed and achieve high values of blocking voltage [18]. In the following section, some of the semiconductor switches, which have been used in pulsed power applications, are introduced, and their switching characteristics discussed.

2.3.1 Thyristor

The thyristor, or silicon-controlled rectifier (SCR), was the first solid-state power electronic switch. It has a four-layer n-p-n-p junction structure as shown in Figure 2.2. It differs from the transistor in that it is a latching device, which is turned on by a gate pulse and remains conducting until the current falls to zero. The peak gate current is the only parameter that affects the pulsed anode current dI/dt capability of the thyristor, and to achieve a short turn-on time, a large trigger current pulse must be used [15].

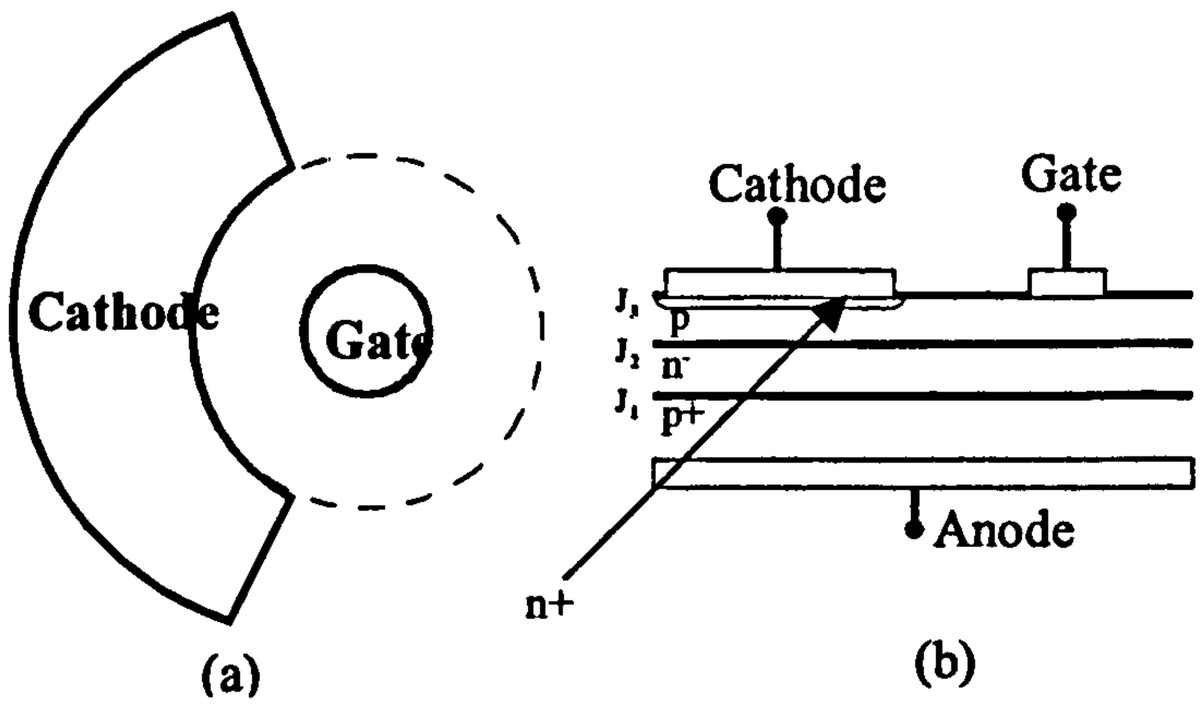

Figure 2.2 Diagram of a thyristor, (a) top view, (b) side view.

When a conventional thyristor turns on, the conducting area is localised around the gate lead and then spreads relatively slowly over the whole silicon chip. The turn-on time of the whole chip is therefore relatively long, resulting in a limit on the dI/dt rating of the thyristor [30]. This is the main reason that the use of the thyristor for

fast-pulsed power applications has been limited [15]. Where a thyristor with a high dI/dt is required, special manufacturing techniques must be used [31]. The most direct approach is to use an iterdigitated gate structure (Interdigitating means modifying the gate-cathode geometry such that there are many small cathode and gate regions intermixed), such that several areas around the chip periphery are triggered simultaneously. In this case, a much larger gate current is required since the gates are, in effect, connected in parallel. The forward blocking capability of a thyristor is normally less than the reverse blocking capability. However, the forward blocking capability can be improved by short-circuiting the p-base region to the n^+ layer as shown in Figure 2.3. This structure is referred to as the *cathode-shorted structure*. Thyristors with a cathode-shorted structure have a much better switching performance than thyristors with an interdigitated gate structure [32].

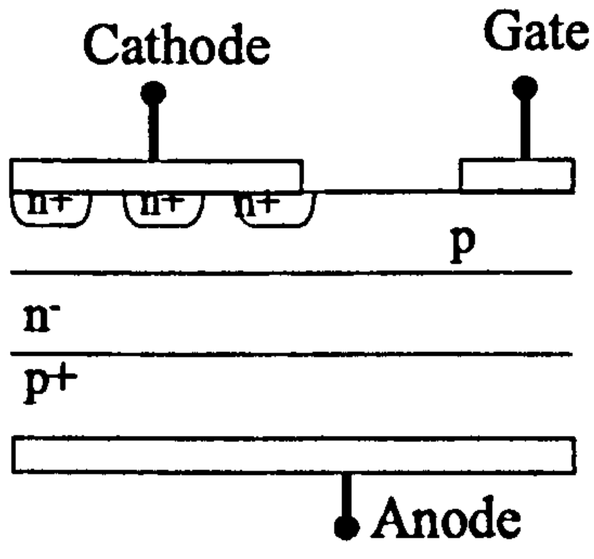

Figure 2.3 Cathode-shorted thyristor.

Thyristors have the potential to replace gas switches over the pulse parameter ranges 1-10 kV, 1-100 kA, 1-10 kA/μs [15,33].

2.3.2 Gate-Turn-Off Thyristor (GTO)

The gate turn-off thyristor (GTO) is similar in construction to a thyristor but with four layers rather than three. It is turned on by current flowing into the gate terminal, as for a conventional thyristor, but it can be turned off by taking current out of the gate, that is, with a negative gate current. There are two different structures of GTO; *symmetrical* and *anode-shorted* [13]. Figure 2.4 shows the structure of a GTO that is anode-shorted. This structure is used to decrease the turn-off time of the device. As a result, however, the reverse blocking voltage capability is reduced to 20-30 V. A GTO thyristor with an anode-shorted structure (called a Reverse Conducting

Thyristor, RCT) is specially suited for pulse applications, because the asymmetric design allows an optimum combination of low power losses, high blocking voltage and pulse repetition frequencies in excess of 20 kHz [34].

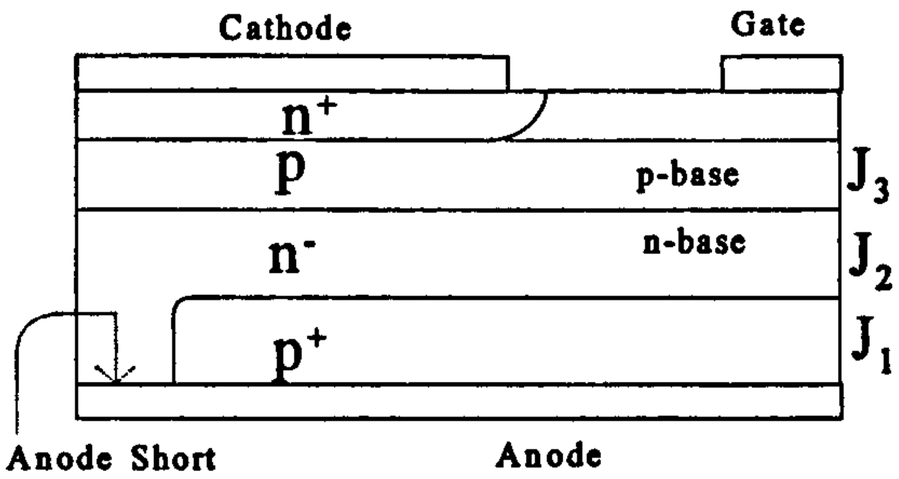

Figure 2.4 Anode-shorted GTO.

A GTO thyristor with a symmetrical structure has a reverse blocking voltage up to 80% of the forward voltage, and this makes it suitable for pulse applications [13]. Compared to a standard thyristor, a GTO has a similar high forward blocking voltage rating, a higher voltage drop and a higher latching current. The gate drive needs to be maintained for a longer period during turn-on to ensure that the higher latching current is reached. [31]. It is not possible to construct a GTO with an internal amplification thyristor as in a conventional thyristor, and so to achieve a high dI/dt during turn-on and turn-off, high gate currents (typically 30% of the anode current) are required. The maximum rate of rise of current during turn-on for GTO is 600A/μs. However, it has been shown that it is possible to improve the dI/dt capability of a GTO by using a ring gate-cathode structure and high interdigitation. These devices (called Fast-High-Current-Thyristors, FHCT), have very short cathode-gate distances and extremely long gate-cathode periphery. This leads to dynamic plasma spread at turn-on so that the device conducts extremely rapidly [17]. GTO thyristors can offer an alternative to conventional valve technology in pulse applications.

2.3.3 Metal–Oxide-Semiconductor-Field-Effect-Transistor (MOSFET)

The Metal-Oxide-Semiconductor-Field-Effect-Transistor (MOSFET) is a voltage-controlled device, which uses the continuous application of a gate-source voltage in order to remain in the on state after turn-on. The gate current is only applied during

transitions from the on to off state or vice versa in order to charge or discharge the gate capacitance. The voltage drop across the MOSFET during conduction is 1 V to 10 V, which is greater than for other devices. The inherent pulse capability of the MOSFET, typically peak currents of 4 times the continuous rating, allows it to handle large current surges (a few 100 A) and makes it attractive for pulsed power applications [12,16]. The MOSFET is a majority-carrier device and in contrast to the Bipolar Junction Transistor (BJT), has no stored charge that must be removed during conduction [31]. As a result, MOSFET switches turn on and off very rapidly. In addition, the positive temperature coefficient of MOSFET switches makes it easy to use them in parallel [35]. As shown in Figure 2.5, a MOSFET contains an integral diode from the p-base region to the drain terminal, which is called the body diode. The body diode allows reverse current to flow when the MOSFET is in the off state. An external diode is normally shunted with a MOSFET to allow the reverse current to flow through the external diode rather than through the inherent reverse diode of the device. As a result, a MOSFET usually has no reverse blocking voltage capability [16].

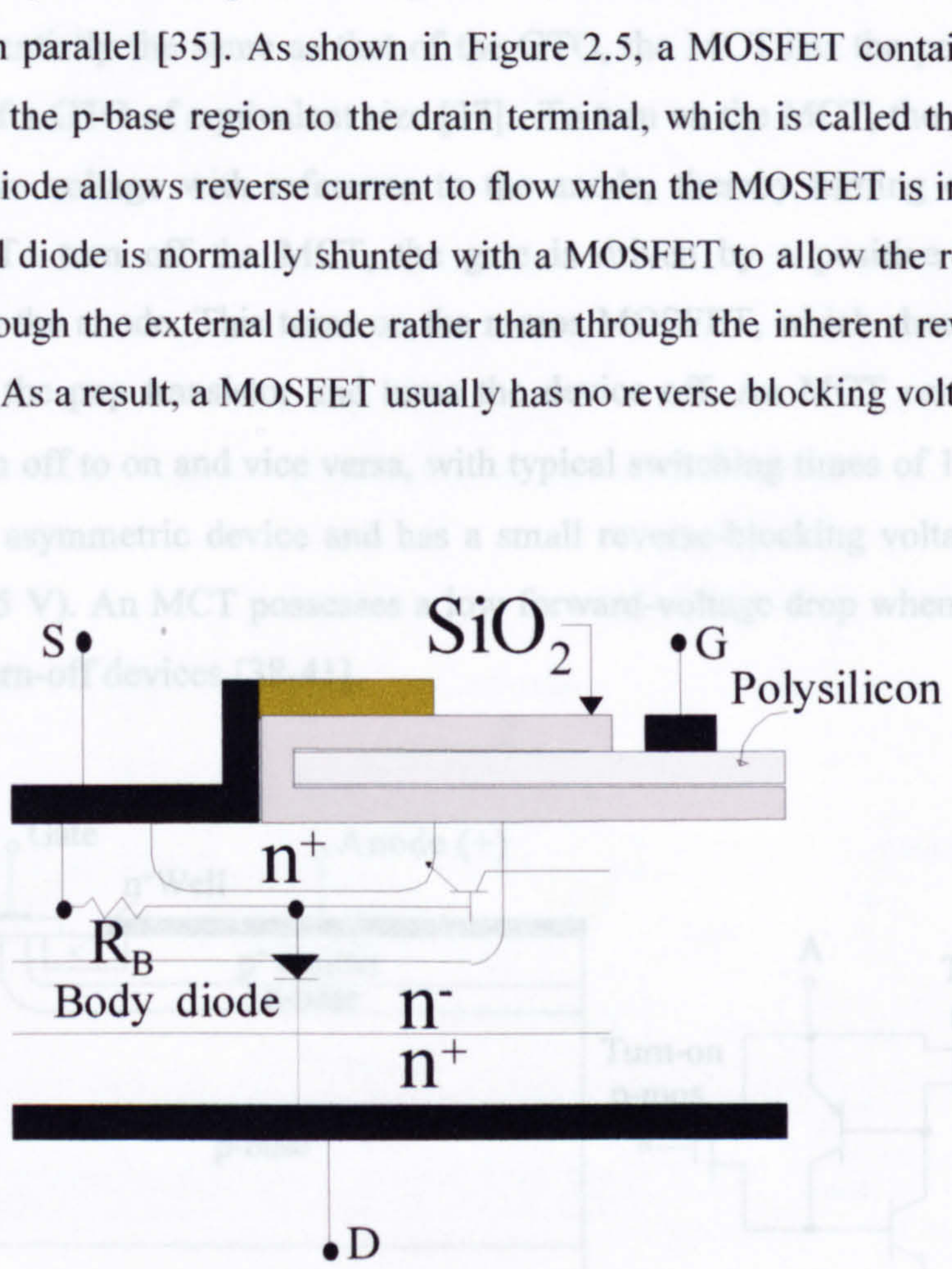

Figure 2.5 Power MOSFET and body diode.

Single MOSFET devices with voltage and current ratings of a few hundreds of volts and a few tens of amperes are available.

2.3.4 MOS-Controlled-Thyristor (MCT)

The need to maintain a low on-state voltage, while reducing gate drive requirements, has led to the development of a new type of device known as the MOS-Controlled-Thyristor (MCT). The MCT is basically a GTO thyristor with two MOSFETs built into the gate structure. One of the MOSFETs is responsible for turning the device on and the other is responsible for turning it off [31-36]. The structure and equivalent transistor of an MCT is shown in Figure 2.6. Because the I-V characteristic of the MCT is essentially the same as that of the GTO, the MCT has the power handling capability of a GTO of equivalent size [37]. To turn on the MCT, the gate is driven to a negative voltage with reference to the anode, thereby turning on the p-mos MOSFET. To turn off the MCT, the gate is driven by a positive voltage with reference to the anode. This turns on the n-mos MOSFET, which shorts the emitter junction of the pnp transistor and turns the device off. An MCT can be switched rapidly from off to on and vice versa, with typical switching times of 1 μs [38]. The MCT is an asymmetric device and has a small reverse-blocking voltage capability (typically 25 V). An MCT possesses a low forward-voltage drop when compared to other fast turn-off devices [38-41].

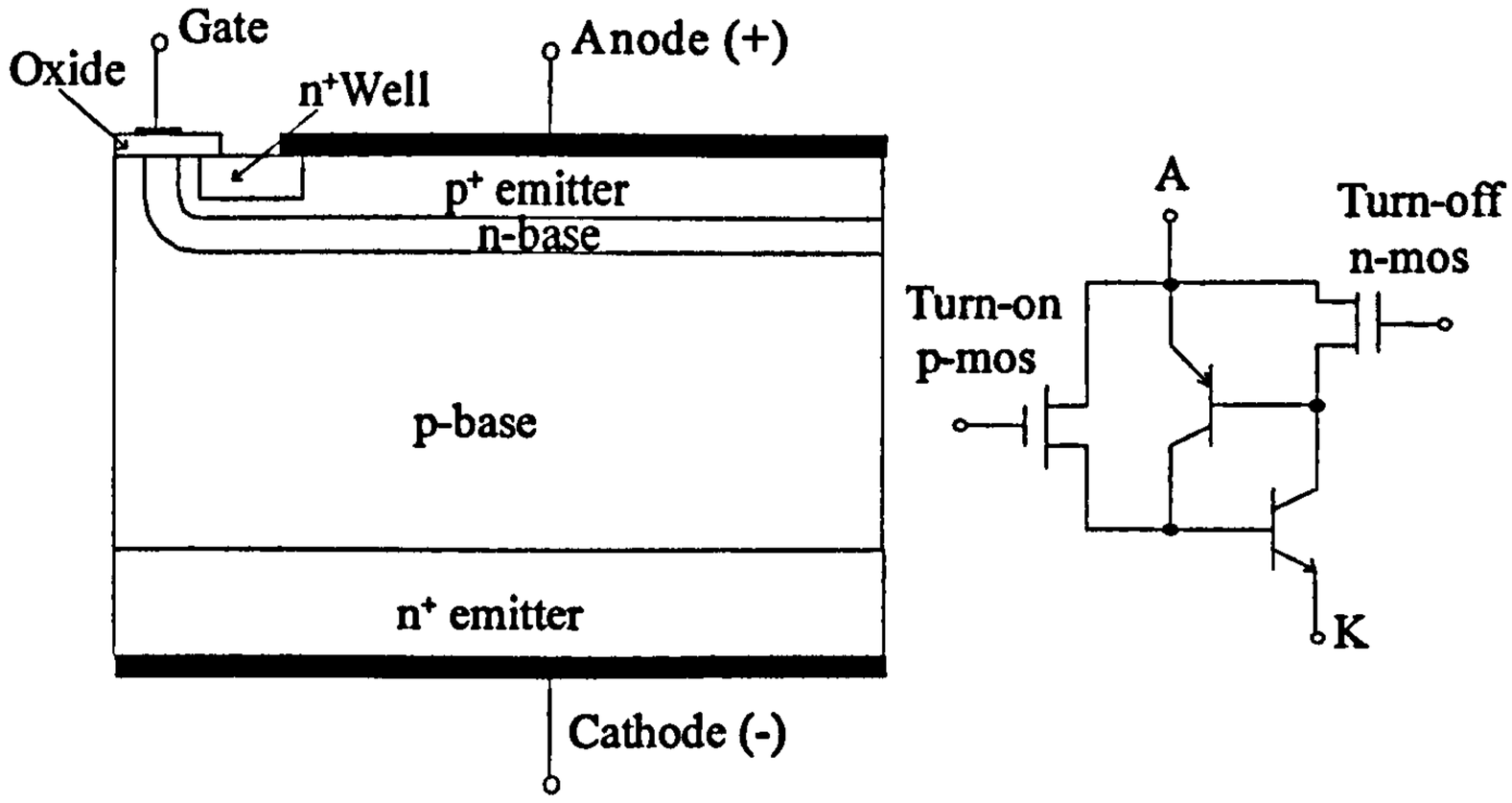

Figure 2.6 Structure and equivalent transistor of an MCT.

The dV/dt limitation of an MCT is the same as for a GTO, (typically 500-1000 V/μs) and this can be increased by minimising the resistance of the gate-drive circuitry [42].

2.3.5 MOS-Assisted-Gate-Triggered -Thyristor (MAGT)

The MOS-Assisted-Gate-Triggered-Thyristor (MAGT) is specially designed for high-repetition-rate pulsed power operation [43]. The MAGT has both the high-power handling capability of a thyristor and the fast turn-on capability of a MOSFET. The maximum current and dI/dt rate for an MAGT have been measured to be 8.5 times and 5.3 times respectively the values obtained for conventional thyristors. A maximum current of 8 kA, a blocking voltage of 2.5 kV and a dI/dt of 21 kA μs^{-1} at a pulse duration of 0.1 μs have been obtained from a single MAGT device [44]. The basic structure and equivalent circuit of the MAGT is shown in Figure 2.7. The MOS gate electrode is placed on the edge of the p-base layer in order to turn on the thyristor with a high dI/dt ratio. The base electrode is placed on the p-base layer to ensure high dV/dt immunity at high repetition rate.

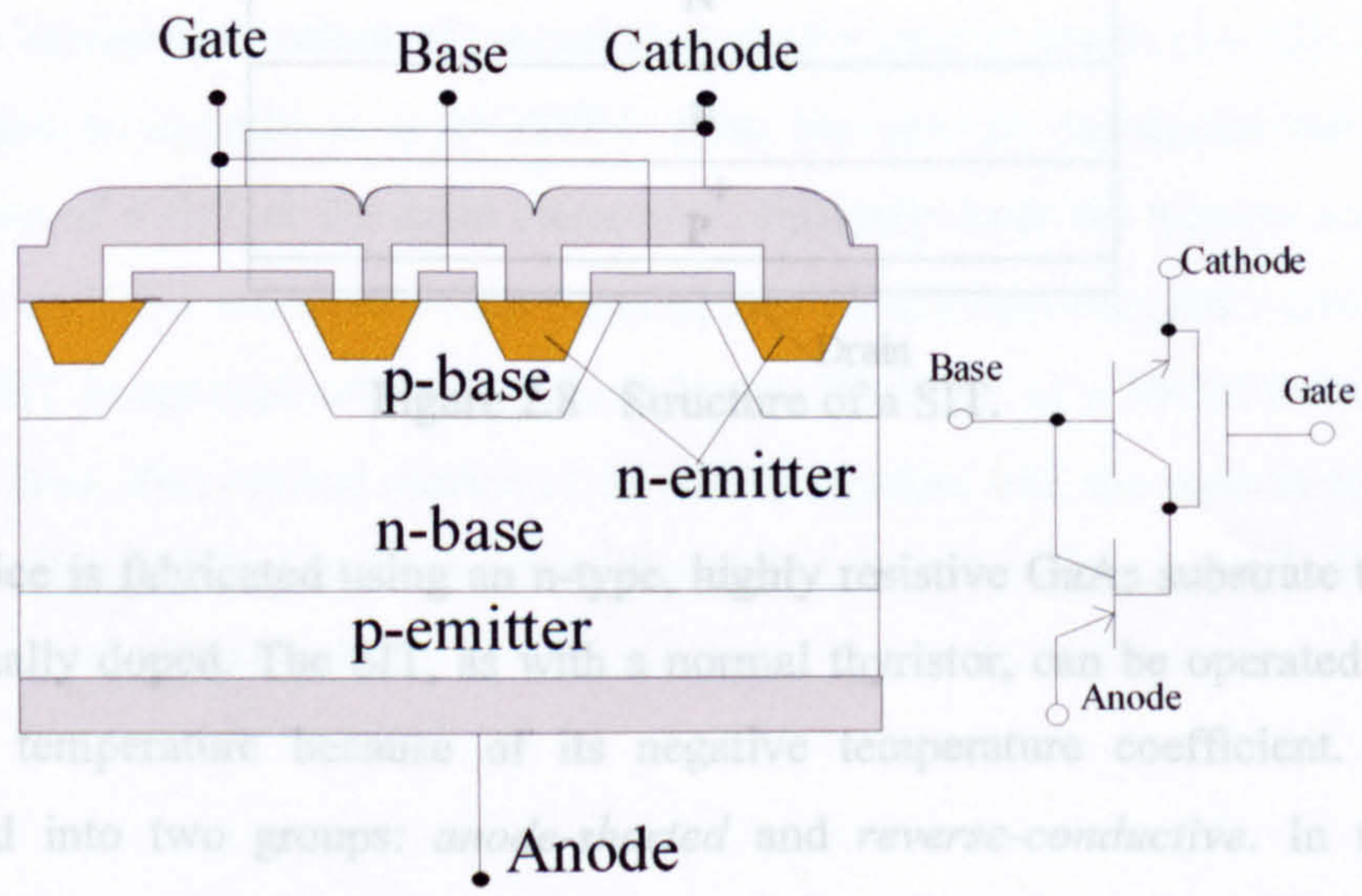

Figure 2.7 Structure and equivalent transistor for an MAGT.

In the MAGT, a high-speed turn-on occurs because electrons are injected from the cathode into the n-base layer through the MOSFET. Furthermore, the p-base width is

optimised to produce high emitter injection efficiency so that the device turns on quickly. In MAGT device, only one MOSFET is present and is responsible for turn-on. Hence MAGTs have fast turn-on times, as for MCTs, but their turn-off times are similar to those of conventional thyristors.

2.3.6 Static-Induction-Thryistor (SIT)

The Static-Induction-Thyristor (SIT) is a vertical channel field-effect device, which exhibits fast switching speeds (<20 ns), high dI/dt (1 kA μs^{-1}) and dV/dt (1 kV μs^{-1}) capability and low forward-voltage drop. The vertical channel geometry allows for fabrication of interdigitated structures, which leads to higher current ratings [45,46] The SIT structure is shown in Figure 2.8.

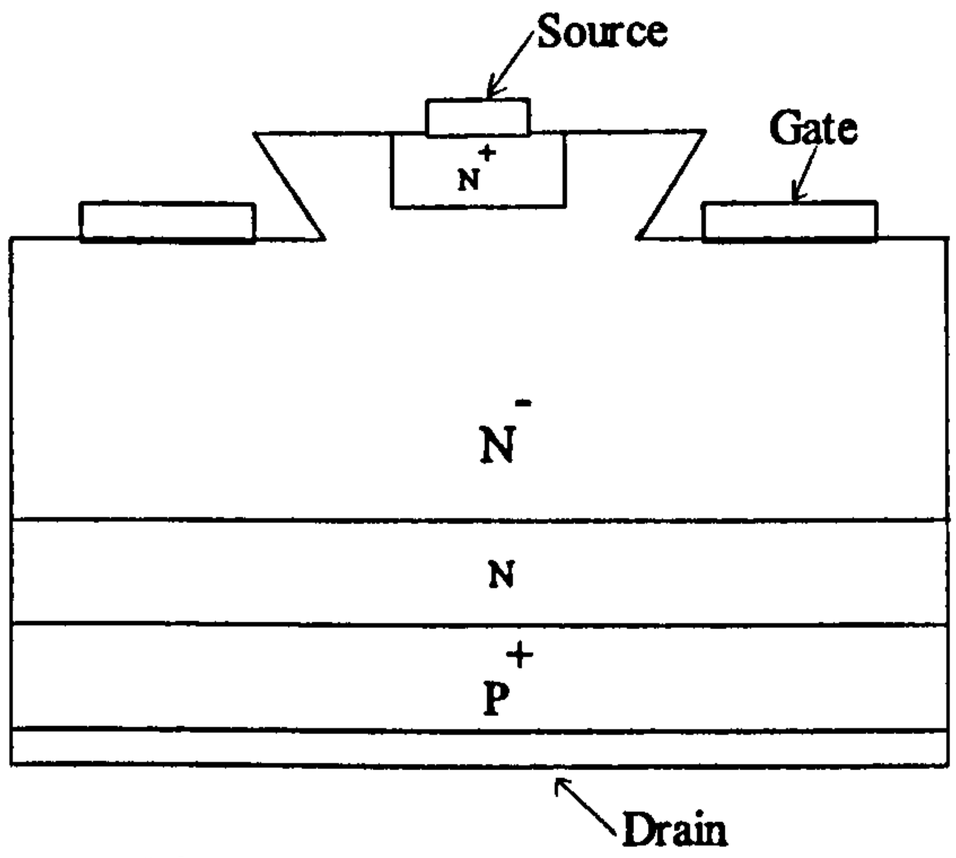

Figure 2.8 Structure of a SIT.

The device is fabricated using an n-type, highly resistive GaAs substrate that is not intentionally doped. The SIT, as with a normal thyristor, can be operated at a high ambient temperature because of its negative temperature coefficient. SITs are classified into two groups: *anode-shorted* and *reverse-conductive*. In the latter, reverse polarity diodes are connected in parallel to allow reverse current flow. Each group is divided further into two types depending on the differences in the structure of the n-region between anode and cathode. These are termed *nonpunch-through* (NPT) and *punch-through* (PT). The n-buffer layer between the p^+ drain contact and

the n^- drift layer is not essential for the operation of the SIT and some SITs are in fact made without it and termed *nonpunch-through*. Compared to the NPT-type, the PT-type SIT has a shorter current rise time, a larger voltage drop and a shorter turn-on time. This makes the PT-type more suitable for pulsed power application in the medium power region [47-50].

2.3.7 Insulated-Gate- Bipolar-Transistor (IGBT)

In the low and medium power range, Bipolar Junction Transistors (BJTs) have been the most commonly used power semiconductors, despite some limitations due in part to the current drive (which can be uneconomic in terms of the number of components and the dimensions of the resulting circuits), and also the fact that minority carrier conduction places a limit on the maximum frequency of use. The introduction of power MOSFET devices now allows much simpler voltage drives to be used, and has made operation at much higher frequencies possible, as conduction occurs with majority carriers. The use of this device has grown rapidly in low voltage applications, but the dissipation characteristics in conduction have limited its use at high voltages. Insulated-Gate-Bipolar–Transistors (IGBT)[2] are a newer class of high voltage device which combine the simplicity of drive of the MOS structure with the ability to handle high values of current typical of a bipolar device [51-53]. The IGBT is intended to operate as a MOSFET from the control standpoint but with the advantages of a BJT at the main electrodes. Typically both the turn-on and turn-off times for an IGBT are slower than those of a MOSFET, but the peak current density in an IGBT is approximately five times higher than that of a MOSFET having the same die area. The vertical section of the IGBT together with the equivalent circuit is shown in Figure 2.9. Conductivity in the collector-drift region is controlled by the injection of minority carriers.

---

[2] The IGBT terminals are labelled collector, gate and emitter. This terminology retains compatibility with the BJT, which the IGBT has replaced in many applications.

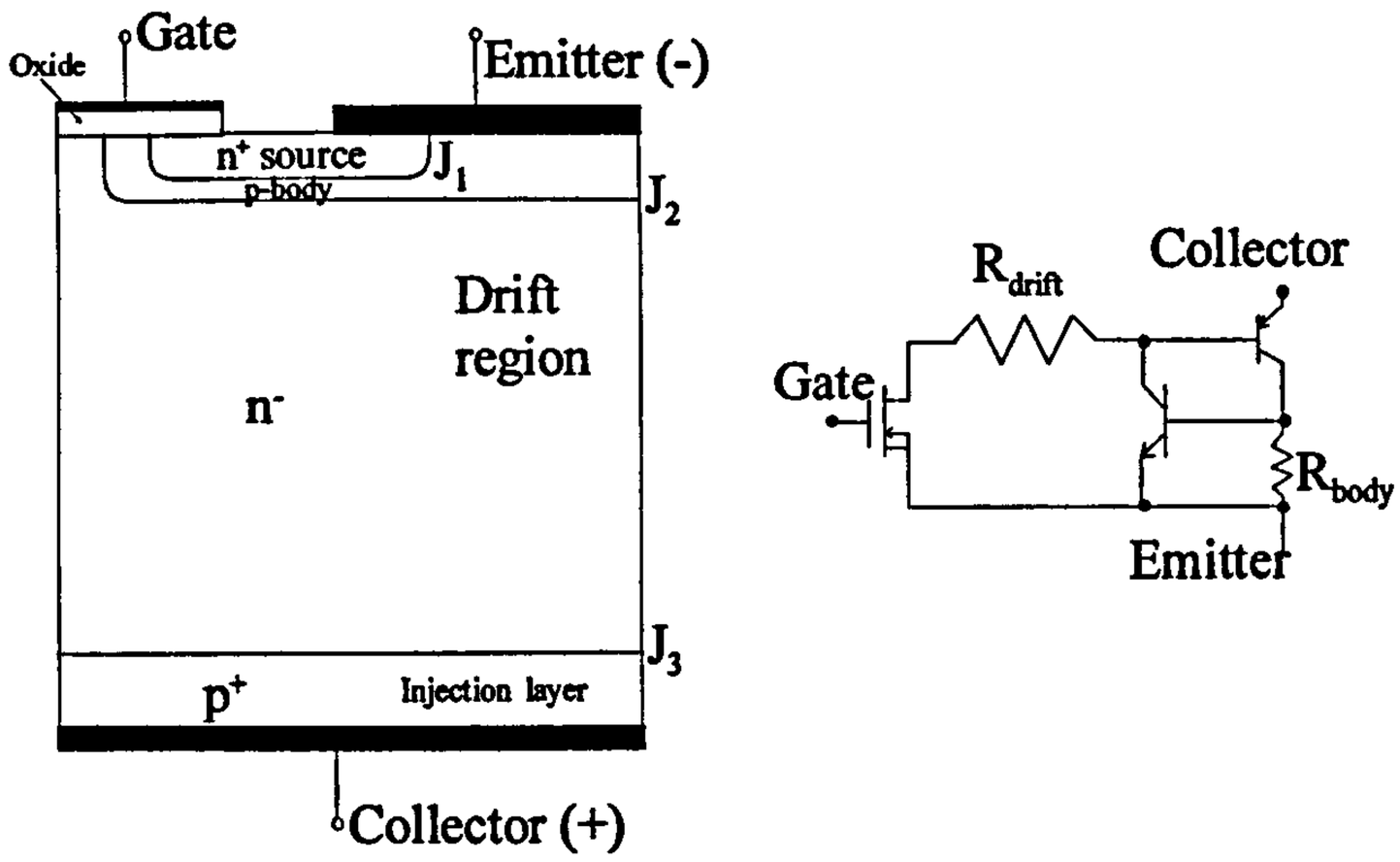

Figure 2.9 Structure and equivalent transistor of an IGBT.

Although the IGBT is structurally a 4-layer device like the thyristor, its operation is fundamentally different, as it is designed to prevent thyristor action with a metal short between the n^+ source region and the p-body. The resulting structure is essentially equivalent to that of a vertical n-channel MOSFET, except it has a p^+ injection layer instead of n^+. In this way a junction is created with the n^- area of the collector; such a junction injects holes into the n^- area during conduction, modulating the resistance and significantly reducing the $V_{CE(sat)}$ of the device. In the forward conducting state, when a positive voltage is applied to the gate conductor with respect to the emitter conductor, the p^- n^- junction (J_2) is reverse biased. The depletion layer extends into the n^- drift region and provides the forward blocking-voltage capability. The forward and reverse blocking voltage capabilities of the IGBT are approximately equal because of the involvement of the common n^- drift region [pe-agrawal]. If the positive voltage at the gate is greater than the threshold voltage V_T, an n-channel is formed in the p-region just beneath the gate terminal, in a manner similar to that in the MOSFET. Electrons flow from the n^+ emitter to the n^- drift region through the n-channel. These electrons constitute the base current of the pn^-p^+ transistor. The emitter of this transistor (p^+ region) injects holes into the base (n^- region). Thus there is double injection into the n^- region. The density of the injected carriers increases with the increase in the positive bias on the collector of the IGBT. As a consequence, the conductivity of the n^- drift region increases very significantly and the IGBT is in

the on-state. To turn the IGBT off, the channel is cut off by setting the gate voltage to below the threshold voltage. The channel current is a significant proportion of the total IGBT current, and therefore, under a constant collector-emitter voltage, the change in gate voltage results in an immediate reduction of the total current depending on the circuit conditions. The remaining current corresponds to the removal of injected holes and electrons from the n^- drift region. This is usually a slow removal, so that the IGBT exhibits a tail current. The removal of stored charge can be greatly enhanced with the addition of an n^+ buffer layer, which acts as a sink for the excess holes and significantly shortens the turn-off time. This device structure is referred to as Punch-Through (PT) IGBT while the structure without the n^+ buffer region is referred to as a Non-Punch-Through (NPT) IGBT. NPT-IGBTs have positive temperature coefficient regarding the forward voltage drop V_{Cesat} over the whole current range, a great advantage for paralleling modules. The tail-current in NPT-IGBTs is low, so that their turn-off losses are lower than those in PT-IGBTs. When a negative voltage is applied to the collector of an IGBT with respect to its emitter, the p^+n^- junction (J_3) is reverse biased. The depletion layer extends into the n^- drift region and provides the reverse blocking-voltage capability. The combination of two transistors in the structure of the IGBT constitutes a parasitic thyristor. This is undesirable but unavoidable. In first-generation devices this parasitic element caused latch-up conditions so that the gate of the MOSFET could lose extinction control. The introduction of further p^+ diffusion in the base body region is one of the methods used to cancel the effects of the parasitic thyristor. Other methods of fabrication to avoid latch-up in IGBTs are also available [36,54,55].

2.4 Choice of IGBT

Solid-state switches have the potential to replace conventional switches for both sub-microseconds pulsed switching at high frequencies (several kHz) and 50-1000 μs pulsed switching at low frequencies (0.01 – 50 Hz) [54-58]. Following this review of the parameters of solid-state switches, their general properties are compared in table

2.1, the IGBT was determined to be the preferred device for stacking in HV switching applications.

Table 2.1 Comparison of solid-state switching devices.

	Voltage Rating	Current Rating	Speed	Availability	Cost
Thyristor	High (1-10 kV)	High (1-100 kA)	Low (μs)	Readily available	Low
GTO	High	High	Low	Medium	Medium
MOSFET	Low (Under 1kV)	Low (Under 100 A)	High (Under 100ns)	Readily available	Low
MCT	High	Medium (Under 1kA)	Medium (Under 1μs)	Special order only	High
MAGT	Medium (1-3 kV)	High	High	Special order only	High
SIT	Medium	Medium	High	Special order only	High
IGBT	Medium	Medium	High	Readily available	Low

Chapter 3

SWITCHING CHARACTERISTICS AND OPERATION OF THE IGBT

3.1 General

An IGBT is a device for which the control characteristics are similar to that of a power MOSFET, and the output characteristics (V versus I) are similar to those of a bipolar junction transistor. The controlling parameter is an input voltage, normally, the gate-emitter voltage, rather than an input current. Figure 3.1 shows the complete I-V characteristics of an IGBT.

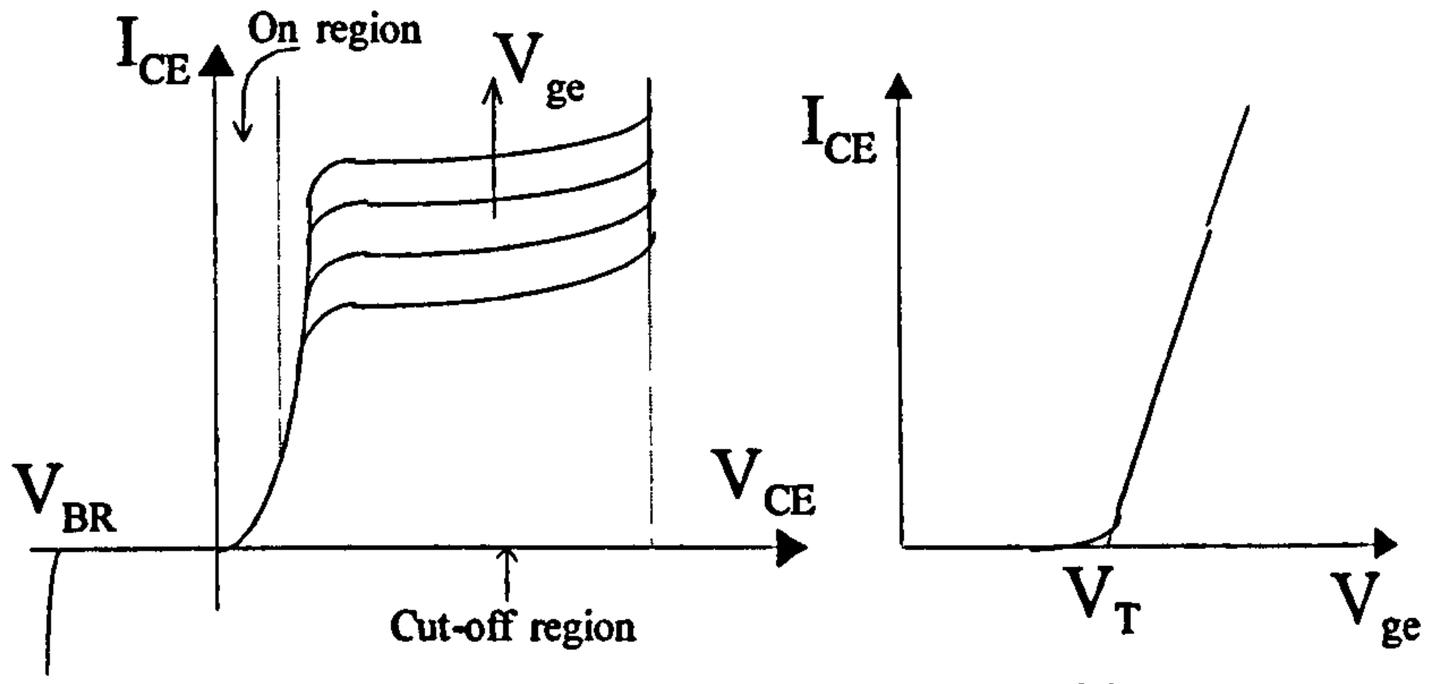

(a) (b)

Figure 3.1 The I-V characteristics of an IGBT cell.

As can be seen in Figure 3.1, the IGBT has three regions of operation.

1. A cut-off region, where $V_{GE} \leq V_T$.
2. A pinch-off, saturation or active region, where $V_{CE} \geq V_{GE}-V_T$ and $V_{GE} > V_T$.

   In this region, the collector current is given approximately by [59]

$$i_C = \frac{1}{2} g_m (v_{GE} - V_T)^2 \tag{3.1}$$

   The transconductance g_m depends on the device geometry and is defined as

$$g_m = \frac{\Delta I_C}{\Delta v_{GE}} \tag{3.2}$$

   The transfer characteristic of the IGBT is almost linear over a wide range of output current, becoming non-linear only at low collector currents where the

gate-emitter voltage approaches the threshold value. The transconductance of an IGBT is significantly larger than (typically 2 times) the g_m of a MOSFET.

3. A linear or ohmic region, where $V_{CE} \leq V_{GE}-V_T$ and $V_{GE} > V_T$.

   The output resistance, $r_o = R_{CE}$, defined as $R_{CE} = \frac{\Delta v_{CE}}{\Delta i_C}$, is normally very high in the pinch-off region, typically of the order of MΩ, and is very small in the linear region, typically of the order of mΩ [59].

For switching actions, IGBTs must be operated in the linear region with a low collector voltage. A gate-to-emitter voltage of about 15 V has to be established to turn on the IGBT and maintain its operation in the ohmic region of operation.

3.2 IGBT gate drive consideration

For gate-insulated devices such as MOSFETs and IGBTs, it is the charge on the input capacitance that creates the n-channel for conduction. To speed up the switching of these devices, the input capacitor must be charged quickly. This means that the gate-circuit current controls the speed of the switching action. Therefore, for fast switching, current pulses are preferred to voltage pulses. For insulated-gate devices, switching efficiency depends strongly on stray capacitance and depletion-layer capacitance [60-63]. The switching behaviour of an IGBT, on the other hand, depends on gate-emitter capacitance C_{ge} and gate-collector capacitance C_{gc}, while the collector-emitter capacitance plays no role. A simple approach to the analysis of switching transients in an IGBT may be taken by considering only C_{ge} and C_{gc}, for both cases of driving the gate by current and voltage pulses, and this is done here for both (i) a current pulse driving the gate, and (ii) a voltage pulse driving the gate.

3.2.1 Driving the IGBT gate by current

Although IGBT and MOSFET devices are supposed to be driven by voltage pulses, in practice, their switching speed and power dissipation are practically optimised by controlling the gate current during switching [64-69]. Figure 3.2 shows typical gate-

charge curve and static characteristics of insulated-gate devices during a turn-on transient, while a constant current is injected into the gate.

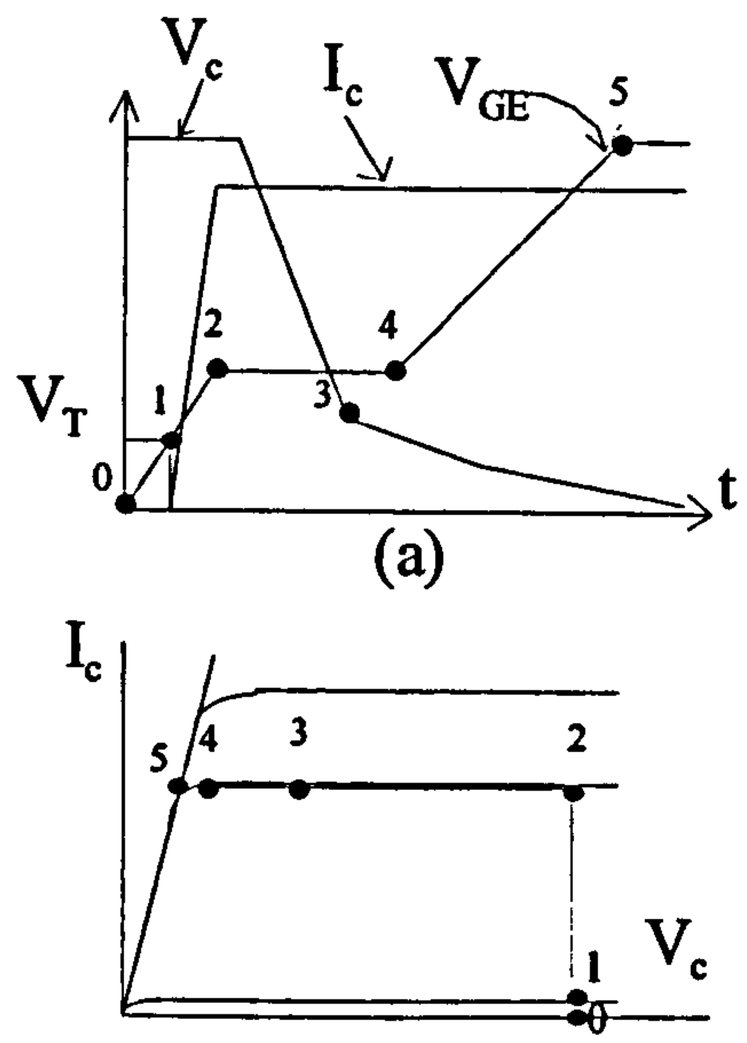

Figure 3.2 Gate charge of insulated gate devices during a turn-on transient. (a) switching transient traces and (b) static characteristics with the corner points reported in (a).

With reference to Figure 3.2, at the beginning, the collector current (I_c) is very small until V_{GE} reaches a threshold voltage (V_T) at point 1. As long as the voltage V_{GE} remains below V_T, no drain current will flow. The time taken for the gate voltage to reach the threshold voltage represents a turn-on delay period, namely t_d. During the t_d interval, the input capacitance is (C_{ge}+C_{gc}) and the gate voltage, V_{GE} rises linearly and is obtained from the following equation:

$$t_d = \frac{Q}{I_g} = \frac{V_T(C_{ge} + C_{gc})}{I_g} \tag{3.3}$$

The collector current begins to flow after the gate voltage reaches the threshold voltage. By considering the case of an IGBT with linear characteristics, the collector current will increase in proportion to the gate voltage. Since the device is now in its active region, the collector current flows and reaches its maximum value I_c at point 2.

Between points 2 and 4, the Miller effect[1] occurs and the input capacitance appears to be infinite since the gate voltage remains constant even though the gate circuit is supplying current to the gate. This constant voltage is known as the Miller voltage, and is around 4 to 6 V, depending on the level of current being switched. Using linearized transfer curve, the collector-current slope in the pinch-off region can be calculated as follows:

$$i_C \approx g_m v_{GE} \tag{3.4}$$

$$di_C/dt \approx g_m \cdot dv_{GE}/dt \tag{3.5}$$

$$di_C/dt \approx g_m \cdot I_g/C_{ge} \tag{3.6}$$

Equation (3.6) shows that the collector-current slope is determined by the rate of supply of charge to the gate during the first slope of the gate voltage. While the Miller effect takes place, the collector-emitter voltage is related to the rate of supply of charge to the gate and the equation for its slope is given by

$$\frac{dv_{CE}}{dt} = \frac{dv_{CG}}{dt} + \frac{dv_{GE}}{dt} \tag{3.7}$$

Since the gate voltage is constant, all the input current flows into the C_{gc} and consequently;

$$\frac{dv_{CE}}{dt} = \frac{I_g}{C_{gc}} \tag{3.8}$$

From equation (3.8), the collector-voltage slope is related to the rate of supply of charge to the gate in the Miller effect zone. Because the collector voltage exhibits two different slopes during this phase, two different capacitances $C_{gc(1)}$ and $C_{gc(2)}$ are defined and consequently;

$$\frac{dv_{CE}}{dt} = \frac{I_g}{C_{gc(1)}} \quad \text{(first slope)} \tag{3.9}$$

$$\frac{dv_{CE}}{dt} = \frac{I_g}{C_{gc(2)}} \quad \text{(second slope)} \tag{3.10}$$

---

[1] The Miller effect is a way of dealing with a situation where the voltages at both ends of a capacitor change at the same time, either independently or dependently. In certain circuits, instead of taking into account what actually happens with the voltage, we can say that this is equivalent to having a larger capacitor. The Miller effect states that the simultaneous switching of both terminals of a capacitor will modify the effective capacitance between the terminals.

As soon as the Miller effect ends, the gate voltage can begin to increase again, reaching its final value at point 5.

3.2.2 Driving the IGBT gate by voltage

In this case, a step voltage V_d drives the gate-insulated device. The turn-on waveform for this case can be divided into three phases over the times t_1, t_2 and t_3 shown in Figure 3.3.

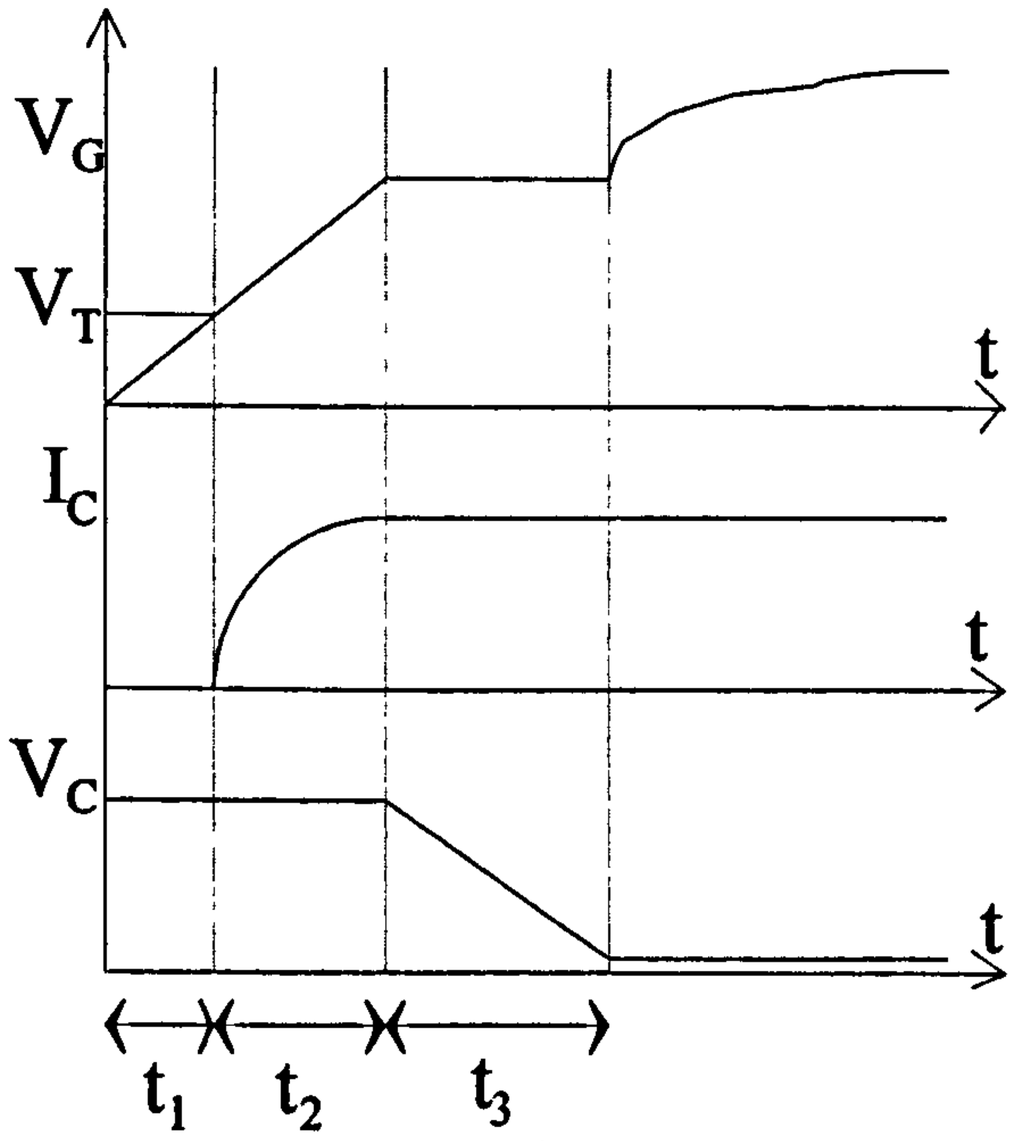

Figure 3.3 Turn-on transient of a gate-insulated device for the case of a step voltage applied at the gate terminals.

As long as the gate voltage V_{GE} remains below the threshold voltage V_T, no collector current will flow. The time t_1 taken for the gate voltage to reach V_T that is, the turn-on delay is obtained from equation (3.11) where R_G is the total resistance in the gate-emitter circuit.

$$t_1 = R_G(C_{ge} + C_{gc}) \ln\left[\frac{1}{1-\left(V_T/V_d\right)}\right] \tag{3.11}$$

Collector current begins to flow after t_1 and the gate-emitter voltage rises exponentially and can be expressed by equation (3.12).

$$v_{GE} = V_d\left\{1 - e^{-\left[\frac{t}{R_G(C_{ge}+C_{gc})}\right]}\right\} \tag{3.12}$$

The equations for collector current and its slope are

$$i_c = g_m(V_d - V_d e^{-\left[\frac{t}{R_G(C_{ge}+C_{gc})}\right]} - V_T)^2 \tag{3.13}$$

and

$$\frac{di_c}{dt} = \frac{2g_m}{R_G(C_{ge}+C_{gc})}V_d^2 . e^{\frac{t}{R_G(C_{ge}+C_{gc})}} . (1 - \frac{V_T}{V_d} - e^{\frac{t}{R_G(C_{ge}+C_{gc})}}) \tag{3.14}$$

If a linear transfer characteristic as described by equation (3.4) is used, the slope of the collector current is obtained from

$$\frac{di_c}{dt} \approx \frac{g_m}{R_G(C_{ge}+C_{gc})} . (V_d - V_T - \frac{i_c}{g_m}) \tag{3.15}$$

If the stray inductance L_{ge} in the gate-emitter path is considered, equation (3.15) must be rearranged as follows

$$\frac{di_c}{dt} \approx \frac{g_m}{\left[R_G(C_{ge}+C_{gc}) + L_{ge}.g_m\right]} . (V_d - V_T - \frac{i_c}{g_m}) \tag{3.16}$$

At the end of phase t_2, the collector current reaches its maximum value. If the stray inductance L_s in the collector-emitter path is small, then the Miller effect is negligible and the gate voltage will continue to rise. In Figure 3.3, transient characteristics have been shown for the case where L_s is very small and because of this, there is no Miller-effect zone in the gate voltage during phase t_2. Beyond phase t_2, the drain voltage begins to fall to the on-state voltage of the device. Because the drain current is now constant, according to equation (3.4), the gate voltage is also constant and all the input current flows into the capacitance C_{gc} during this period. In addition, the slope of the collector voltage can be expressed as follows;

$$\frac{dv_{CE}}{dt} = \frac{I_g}{C_{gc(1)}} \approx \frac{V_d - V_T - \frac{i_c}{g_m}}{C_{gc(1)}} \qquad \text{(first slope)} \tag{3.17}$$

$$\frac{dv_{CE}}{dt} = \frac{I_g}{C_{gc(2)}} \approx \frac{V_d - V_T - \frac{i_c}{g_m}}{C_{gc(2)}} \qquad \text{(second slope)} \tag{3.18}$$

The gate voltage may continue to rise beyond time t_3, but this will not influence the collector current or voltage because both have reached their steady-state levels.

The dynamic behaviour of IGBTs is affected by unavoidable parasitic capacitance in the form of the structure, often referred to as C_{ge}, C_{gc} and C_{ce}. Equation (3.14) shows that the rate of rise of collector-current during turning on can be controlled by R_G. A high dI/dt that leads to fast switching requires a very small R_G. Moreover, in the selection of the value of R_G for power application, two other factors must be considered; to minimise power consumption, R_G must be low, while to minimise electromagnetic interface (EMI) generation, a high value of R_G is needed. Therefore, a compromised value for R_G must be chosen in order to achieve relatively low-power losses, together with acceptable rates of rise of collector-current and EMI level. High-power dissipation occurs during the intervals t_2 and t_3 (Figure 3.3) and after point 1 in Figure 3.2, where the device sustains both high current and high voltage simultaneously. It would be possible to accelerate the collector-emitter voltage, and thus the switching speed, by shaping the gate current, without increasing the collector-current slopes and EMI levels. This could be achieved by charging the input capacitance quickly, which would not change the slope of the collector current and would consequently increase the rate of rise of the collector voltage [70]. It has been shown that if the gate voltage applied to the device is decreased, the ability of the IGBT to withstand short circuits during fault will be improved. When a short circuit occurs in a circuit that includes an IGBT, the current rises rapidly, pulling the IGBT out of its full conduction state. V_{CE} is increased and causes a current to flow through the Miller capacitance. Due to the presence of a high R_G, the gate-emitter voltage increases to a higher peak value and the fault current rises again, potentially damaging the device. Lowering the value of R_G during turn-off improves clamping of the gate-emitter voltage, thus reducing the fault current magnitude significantly [71]. Therefore, a trade off has to be made by the designer based on the other considerations, and the drive circuit can be configured to allow the use of two different values of gate resistance, one for turn-on $R_{G(on)}$, and the other for turn-off $R_{G(off)}$.

A corresponding analysis can be performed for device turn-off [60]. The above observations remain valid for power MOSFETs during turn-off but not for IGBT devices. At turn-off, IGBTs show a tail during the fall of the collector voltage due to the time required for the excess carriers in the epitaxial collector region to recombine. This tail is responsible for large losses and its effect cannot be reduced by means of the driving circuit [64].

3.2.3 Off-state negative gate voltage requirements

Negative gate bias is not necessary to turn off or hold off an IGBT. But certain dynamic conditions, such as fast $\frac{dv}{dt}$, may turn on the device. This false turn-on is dependent on voltage across the IGBT, voltage rise time, gate bias voltage, gate impedance, and temperature. Spurious triggering can be avoided totally, by using negative gate bias voltage (a reverse bias of less than –5 v) and a low gate impedance ($\leq 20\ \Omega$) [72-74].

3.3 Series operation of IGBTs

In order to increase the voltage rating of IGBT devices, a wide drift region must be used and this increases the on-state resistance of the device. Although it is possible to decrease the on-state resistance by injecting a high level of charge into the collector, this slows down the IGBT speed and consequently increases the switching losses. The series connection of medium-voltage (< 1.5 kV) devices is more practical for high-speed switching [75]. There exists an optimum number of series IGBTs that give the best on-state voltage for given voltage and current ratings. The complexity of the overall switch, the acceptable losses per IGBT, and the overall cost affect the optimum number of devices used in a switch [76]. In designing a high-speed switch made up of IGBTs in series, the problems of isolation and voltage sharing have to be addressed. Switching pulses have to be

level shifted across a high-voltage barrier with minimum stray capacitance-to-earth. Voltage sharing has to be ensured both during switching and in the steady state. In the steady state, parallel resistors are commonly used. The resistor value need only be an order of magnitude lower than the IGBT off-state resistance, which is very high (> 10 MΩ). The losses in the resistors are therefore quite negligible. Timing errors in switching pulses, non-identical gate circuit components, and stray capacitances to ground are the reasons that make non-equal voltage sharing across the devices connected in series. Different delays during the turn-on transient can produce spike voltages across the slowest device, and during the turn-off transient the leading switching pulse produces an over-voltage across the fastest device. In power applications, if delays are limited to less than 0.3 μs, they do not create significant over-voltages, switching times being in the scale of μs. However, in pulsed power applications with pulse lengths of a few hundred nanoseconds, the delay between switching pulses must be limited to a few nanoseconds. Stray capacitances to ground can result in unequal voltage sharing, with the device farthest from ground carrying the highest voltage. During fast rising voltages across a stack of devices, these stray capacitances draw significant amounts of current and therefore cause unequal voltage distribution across the elements in the stack [77]. This is an issue for IGBT modules because they are normally connected to a copper base plate via an insulating ceramic substrate, and this results in a high collector to ground capacitance. Although device selection can be adopted to minimise the extra cost involved in the sharing circuits, it is unpopular because it is impractical if more than a few devices are used. Small differences are to be expected between IGBT parameters such as threshold voltage, transconductance, and gate-emitter capacitance. The techniques available to ensure that the voltage is shared equally across the devices in the transient and steady states may be classified, as shown in Figure 3.4. The techniques used to design the sharing circuits can be divided into load-side (passive snubber), and gate-side (active snubber).

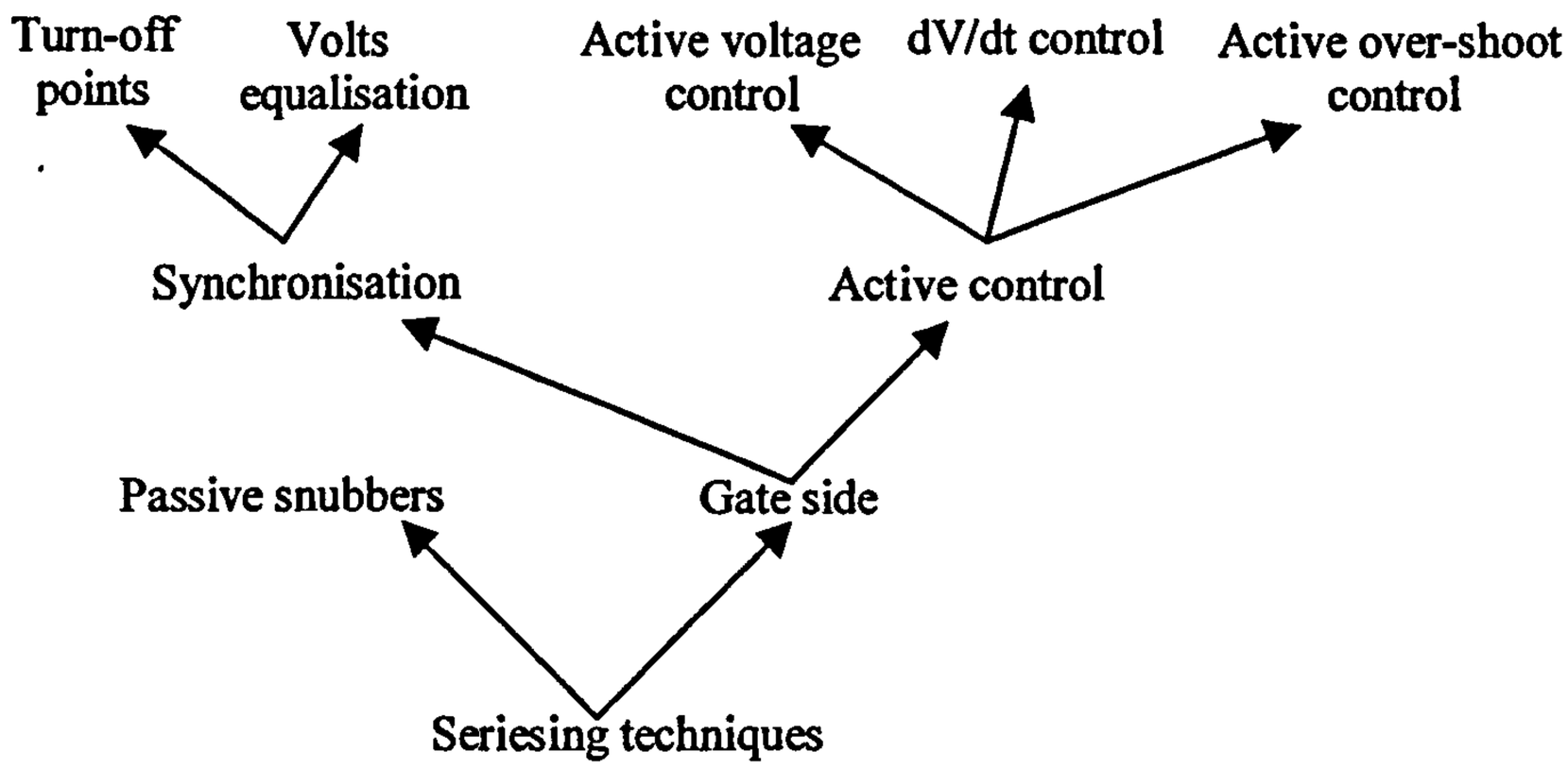

Figure 3.4 The techniques available to ensure equal voltage sharing

3.3.1 Load-side techniques (passive snubber)

A load-side technique is designed to slow down the $\frac{dv}{dt}$ of all the devices to the speed of the lowest device, using extra components such as snubbers on the load side. As shown in Figure 3.5, this technique typically employs equalising networks of resistors and capacitors to eliminate any differences in IGBT switching speed and to ensure that the voltage is shared nearly equally during a turn-off transient.

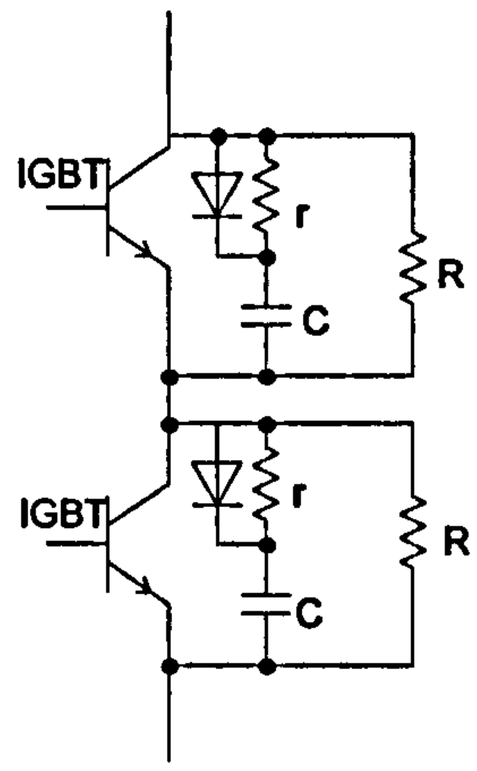

Figure 3.5 Equalising network of resistors and capacitors.

3.3.1.1 Equalising network of resistors

Assuming that the range of maximum leakage current for devices is from $I_{b(max)}$ to $I_{b(min)}$, the maximum voltage imbalance occurs when the first device in the string has a leakage current of $I_{b(min)}$ while all the remainder have $I_{b(max)}$. By assuming $I_{b(min)} = 0$, V_D as the maximum blocking voltage for each device, V_S as the maximum blocking voltage of the string, and n as the number of devices which are placed in series, the value of the maximum allowable resistance is obtained from [78]:

$$R \leq \frac{nV_D - V_S}{(n-1)I_{b(\max)}} \tag{3.19}$$

If resistors with tolerance of a are used, the worst case occurs when the first device has a parallel resistance at the upper tolerance while all the others have parallel resistance at the lower limit. Therefore, the appropriate maximum resistance is given by [78];

$$R \leq \frac{V_D(n-1)(1-a) - (V_S - V_D)(1+a)}{(n-1)(1-a^2)I_{b(\max)}}, \quad \text{n} \geq 2 \tag{3.20}$$

3.3.1.2 Equalising network of capacitors

During the steady state, resistors alone are sufficient to ensure equal voltage sharing in the string, but as mentioned earlier, during turn-off, different delays on switching pulses time can cause a transient unequal voltage distribution across the devices in the string. This problem can be solved by the use of equalising networks of capacitors. The capacitor action is to provide a transient current path by bypassing a recovered device to allow slower devices to recover. In a method similar to that for calculating the sharing resistors, the values of capacitors are given by;

$$C \geq \frac{(n-1)Q_{\max}}{(nV_D - V_S)(1-a)} \tag{3.21}$$

When Q_{max} is the maximum stored charge and a is the capacitor tolerance [78].

3.3.2 Gate-side techniques (active snubber)

In gate-side techniques, attention is focussed on the control side to ensure voltage sharing. This approach may be further split into methods that control the point of turn-off to achieve voltage sharing, and those that employ the gate-controlled active

regime of operation. As the turn-off time of an IGBT may be temperature dependent, the synchronisation approach is not very attractive for use with IGBTs. The gate-controlled active regime of operation offers superior voltage-sharing performance at the cost of increased switching loss. Some examples of gate-side technique are active over-shoot control, active voltage control, and $\frac{dv}{dt}$ control. The active over-shoot-control method is an adaption of that used with series connection of conventional thyristors. In this method, an active overvoltage-control circuit, effectively clamping the peak voltage attained by each device, replaces the over-voltage crowbar circuit. In this method, for optimum performance, the IGBTs should be matched, as uneven switching times increase the switching loss in the fastest device. In the active-voltage-control method the collector voltage is controlled directly within a feedback loop, and each IGBT voltage follows a given reference-input voltage using a closed-loop control. In the $\frac{dv}{dt}$-control technique, the rate of voltage rise is limited using large gate resistors (Z_g) during turn-off. An external collector-to-gate feedback capacitor is inserted, so that the collector-voltage rate-of-rise is controlled independently of turn-off delay. In this method, since the voltage is not directly controlled, voltage sharing is not guaranteed. In addition, any stray inductance included in the IGBT collector connections will cause unstable oscillations. This tends to degrade the closed-loop performance.

3.3.3 Choice of snubber for fast switching

In power applications with switching times in the scale of μs, active snubbers can ensure equal voltage sharing during transient and steady state, particularly in the turn-off transient. But because active-gate-control methods rely on sampling the voltage or voltage rise across the IGBTs, there is an inherent delay between the times at which each of the devices reacts. This makes active-gate-control methods slow and unsuitable for fast pulsed power applications where pulse lengths are a few hundred nanoseconds. Therefore, in the present study, attention is focused on the passive snubbers.

3.4 Parallel operation of IGBTs

In order to increase the current rating of the switch, several devices have to be connected in parallel. Current sharing, balance of losses, balance of temperature and thermal stability are the main issues in the parallel operation of IGBTs. An attractive feature of the IGBT is that, at approximately the rated current (and lower for the NPT-IGBT), it has MOSFET-like behaviour where the on-state voltage increases with current, making parallel operation less demanding. Since temperature directly affects the reliability of an IGBT, close thermal coupling to reduce temperature differences between parallel devices is essential [79]. In order to successfully parallel IGBTs, attention is required in the following design aspects;

The circuit layout must be symmetrical, both for the gate-drive circuit and the main power circuit. Failure to ensure this may cause imbalances during switching, with possible device over-heating. Such dynamic imbalances are especially important in high-current, fast-switching circuits. Stray inductances should be minimised as they can produce parasitic oscillations ranging between 1 and 300 MHz, which may cause gate rupture by overheating the gate and increasing switching losses and increasing electromagnetic interference (EMI), High thermal stability is obtained by mounting the parallel devices on the same heat sink. For optimum switching performance of parallel IGBTs, it is necessary to drive the IGBT gates with only one gate resistance [78,80]. In contrast to BJTs, connecting external resistors in series with the emitters of the IGBTs cannot improve the current balance during the turn on state. This is because the gate voltage rarely influences the value of $V_{CE(Sat)}$, [80].

Chapter 4
PRACTICAL SYSTEMS

In previous chapters, the IGBT was introduced as the suitable candidate for stacking and switching in fast pulsed power applications. This chapter describes tests carried out on different IGBTs: these are investigated in terms of their voltage, current rating and speed. The experimental arrangements for the tests are described. For fast 600 V IGBT devices, it was observed that they can handle a peak current of five times their nominal current rating during short-pulse conducting, if they are driven by fast gate pulses. For 1.2 kV devices, however, problems have been encountered when rapid switching is employed (<100 ns). The slope of the collector-emitter voltage collapse may be distorted when a 1.2 kV device is stressed to facilitate rapid turn-on. This undesirable switching behaviour and its possible reasons are investigated using both computer simulation and experiment.

General issues associated with the stacking of 600 V and 1200 V IGBTs including gate-drive circuits for series IGBTs, signal isolation, and stack over-voltage protection are discussed. The chapter concludes with a description of the switching performance of a 10 kV, 400 A stack consisting of 50 IGBTs.

4.1 Experimental systems

4.1.1 High-voltage, low-power DC supplies

The high-voltage DC supplies used in this study were a Brandenburg, model 475R capable of supplying 2 kV and 3 mA, a Glassman model PS/WR100R2.5-22, capable of supplying 20 kV and 30 mA (600 W), and an A.L.E Systems Power Supply model 202A-40 kV-pos-pfc, capable of supplying 40 kV and peak charging rate of 2200 J/s. The power supplies were connected to the experimental system through decoupling resistor chains. These resistor chains served to isolate the power supply from the rest of the circuit in the event of a fault, and to limit the maximum current that could be drawn from the supply while the switch was closed.

4.1.2 Blumlein cable generators

The most basic type of cable pulse generator consists of a single length of coaxial cable connected to a load through a switch. The cable is charged through a charging resistor or inductor and then the energy stored in the cable is released to the load upon closure of the switch. The output voltage of this type of generator is restricted to the charging voltage level for an open-circuit load and to half the charging voltage level for a matched load. Blumlein cable generators offer a method of producing higher voltage levels by charging a number of lengths of coaxial cable in parallel, and then discharging them in series. The schematic diagram of an X2, non-inverting Blumlein cable generator that was constructed to provide a unit voltage gain into a matched load is shown in Figure 4.1. The generator is one length of coaxial cable generator, with the outer braid removed between points b and c. A total of four X2 Blumlein generators were used throughout this study. Different lengths of coaxial cable were used in the construction of each generator, and this provided four different output pulse durations. The four generators were:

Blumlein generator 1: switched input impedance 10 Ω, output pulse duration 200 ns
Blumlein generator 2: switched input impedance 25 Ω, output pulse duration 250 ns
Blumlein generator 3: switched input impedance 50 Ω, output pulse duration 250 ns
Blumlein generator 4: switched input impedance 25 Ω, output pulse duration 1 μs

The four generators were used to investigate the performance of IGBT devices and modules for different operating parameters, such as pulse duration and current. The Blumlein generators were constructed using URM 43 coaxial cable, rated at 40 kV DC.

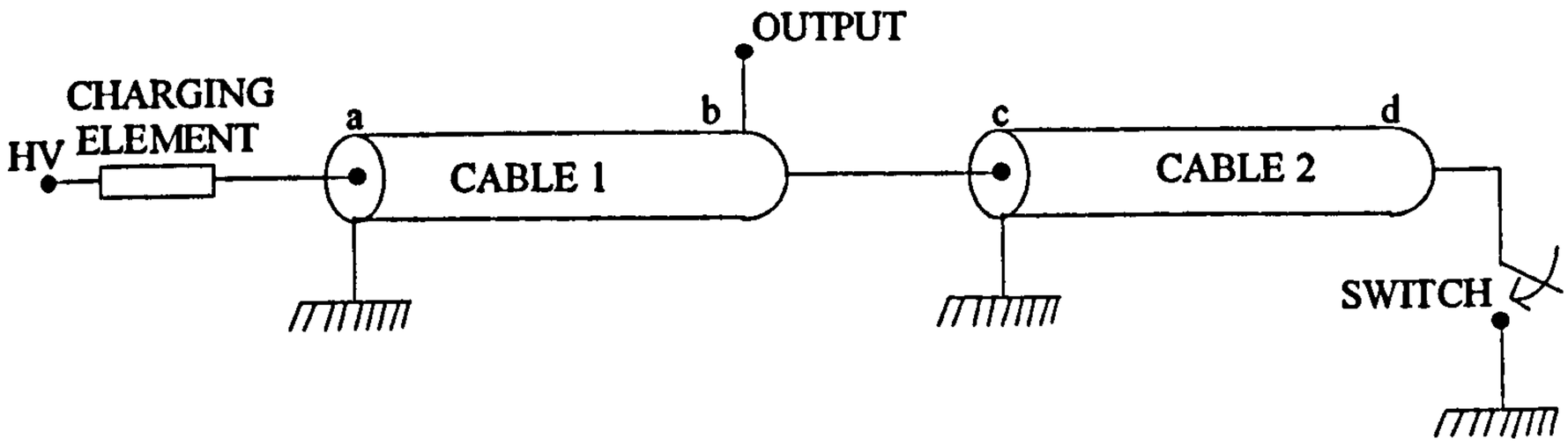

Figure 4.1 Diagram of an X2 non-inverting Blumlein cable generator.

Initially, the transmission lines are charged to a DC voltage, E. Upon closure of the switch, a negative pulse of magnitude E is created along the cable 1. Once this negative pulse reaches point b, a voltage of $2E$ is produced between b and c for an open circuit load. The duration of the output pulse is twice the transient time of cable 1 or cable 2.

4.2 Evaluation of IGBT switching speed

4.2.1 Experiment

Initial experiments carried out on single 600 V IGBTs, which are commercially available, showed that most of them have the capability of stacking and can be used in fast pulse power applications, if proper drive circuits are used. For 1.2 kV devices, it was observed that when rapid switching is employed (<100ns), the slope of the collector-emitter voltage collapse may be distorted. These variations in the collector-emitter voltage collapse during fast turn on (switching) are referred to as *dual degradation*. The effect on circuit performance caused by dual-degradation behaviour can be reduced by using a saturable inductance or a magnetic assist (MA) in series with the switch to create a delay between the voltage fall and the current rise [77,81]. However, applying this remedial method to most types of high-speed pulse generator, such as the Blumlein cable generator, causes perturbations and deviations in the shape of the output pulse. In order to explore the dual-degradation phenomenon in several 1.2 kV IGBT devices, samples from different manufacturers were characterised. The components of interest were single chip plastic encapsulated IGBTs, in packages such as TO-247 and TO-220. A comparison of the published parameters for each sample device examined is given in Table 4.1. These include the input capacitance C_{iss}, the reverse transfer capacitance C_{rss}, the output capacitance C_{oss}, the peak pulsed collector current I_{peak}, the rise time t_r, and the fall time t_f.

Table 4.1 Comparison of published parameters for different types of 1.2 kV IGBT

Device	Manu.	C_{iss} (pF)	C_{rss} (pF)	C_{oss} (pF)	I_{peak} (A)	t_r (ns)	t_f (ns)
IRG4PH40U	Inter. Rec.	1800	18	120	120	18	130
IRG4PH50KD	Inter. Rec.	2800	53	140	90	100	200
MGW12N120D	Motorola	1003	106	126	~80	87	575
BUP313D	Siemens	1000	70	150	64	45	70
GT15Q301	Toshiba	~900	~160	~250	30	50	160

Two pulse generators, with switched input impedances of 10 Ω and 50 Ω, and pulse durations of 200 nsec and 250 nsec, respectively, were used for this evaluation of IGBT performance under different input impedance conditions. Initially, the two transmission lines that comprise the input stage of the generator were charged to a DC voltage, and the generator fired by closure of the IGBT. A drive circuit, with a peak current of a few tens of amperes, was used to charge the IGBT input capacitance in less than 100 ns in order to speed up the switching time of the IGBT. The device IRG4PH40U was tested with the 10 Ω input impedance pulse generator at 1.2 kV and its collector-emitter voltage was monitored and recorded as shown in Figure 4.2.

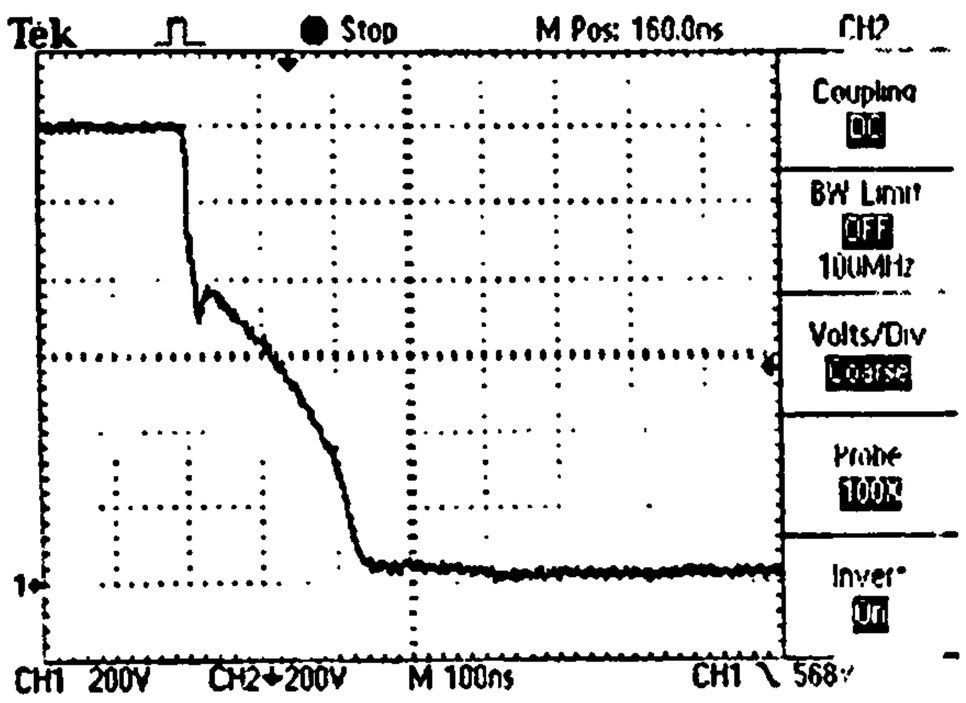

Figure 4.2 Voltage waveform across IRG4PH40U for a 10 Ω input impedance pulse generator (voltage amplitude 200 V/div and time base 100 ns/div).

As can be seen, the rate of voltage fall across the IGBT occurs in two distinct stages. The voltage collapses quickly during the first stage and thereafter a slower rate is observed during the second stage termed *dual degradation*. As would be expected, this switching behaviour significantly affects the shape of the output pulse of the generator. This effect can be seen in Figures 4.3 - 4.6, which display similar voltage collapse profiles for the different devices tested, along with the corresponding output pulse from the Blumlein generator. In all cases, the temporal nature of the voltage switching is reflected in the output pulse from the generator. The 100 ns time delay between voltage waveforms is due to the wave propagation along the cable 2 in figure 4.1.

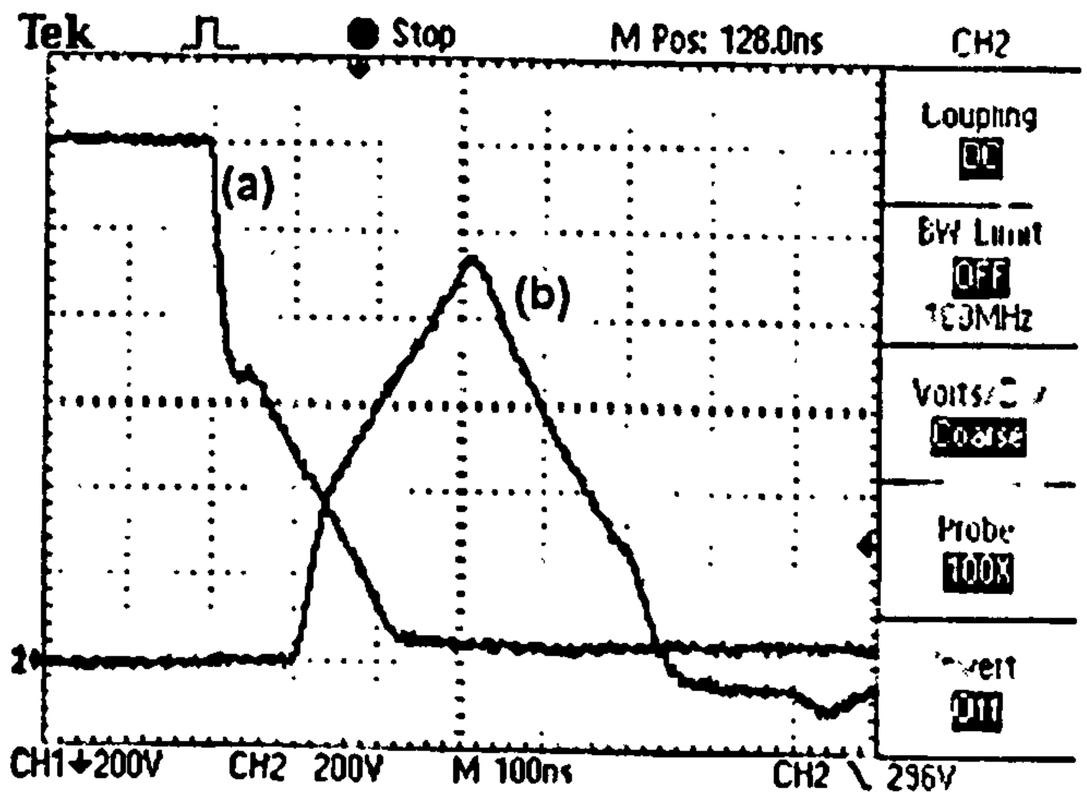

Figure 4.3 Voltage waveform across IRG4PH50KD (a) and output voltage pulse (b) for a 10 Ω input impedance pulse generator (both traces amplitude 200 V/div and time base 100 ns/div).

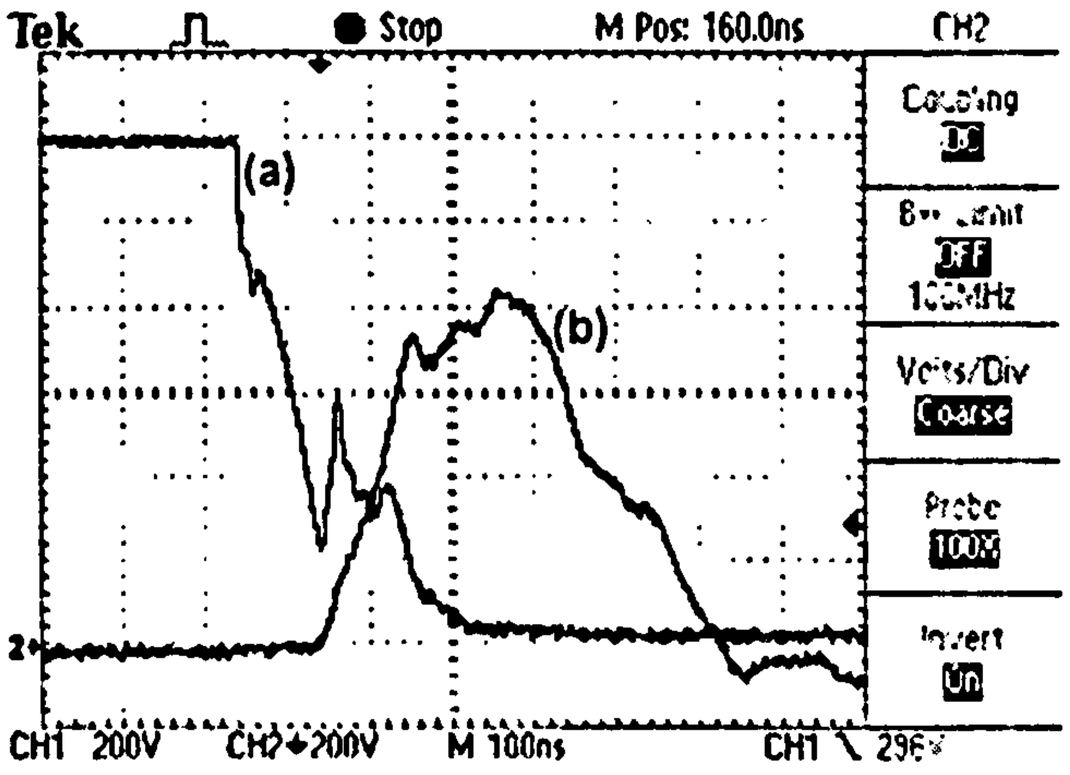

Figure 4.4 Voltage waveform across MGW12N120D (a) and output voltage pulse (b) for a 10 Ω input impedance pulse generator (both traces amplitude 200 V/div and time base 100 ns/div).

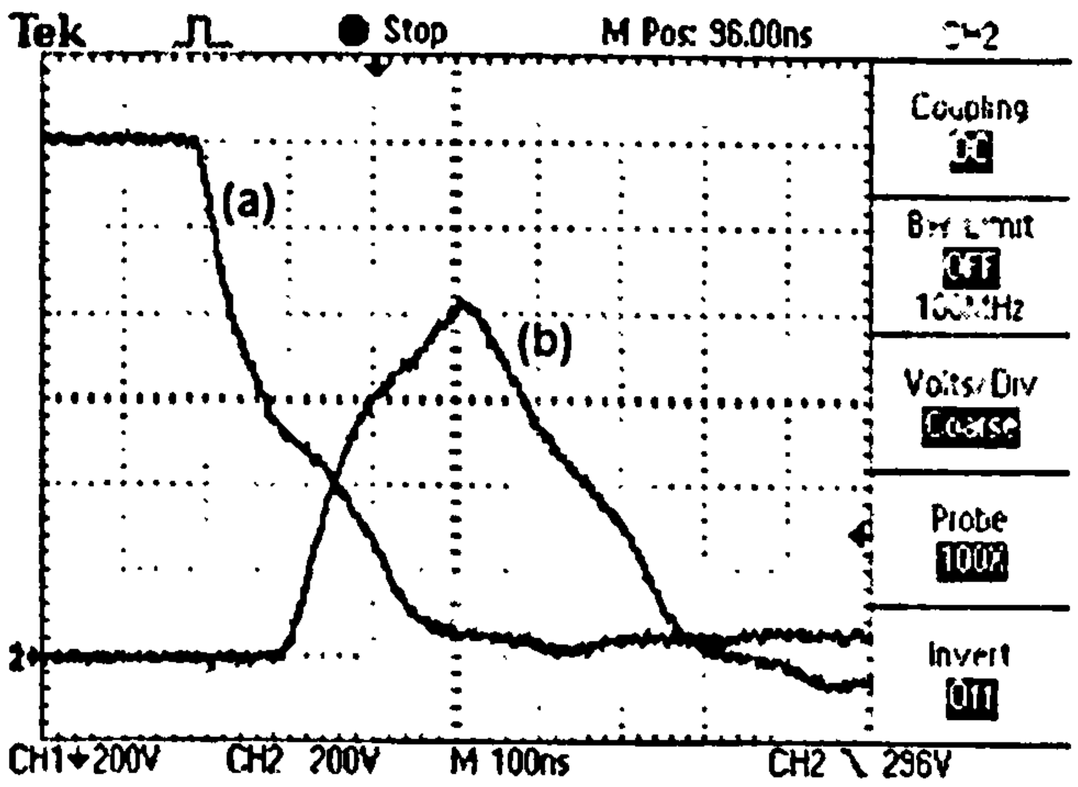

Figure 4.5 Voltage waveform across BUP313D (a) and output voltage pulse (b) for a 10 Ω input impedance pulse generator (both traces amplitude 200 V/div and time base 100 ns/div).

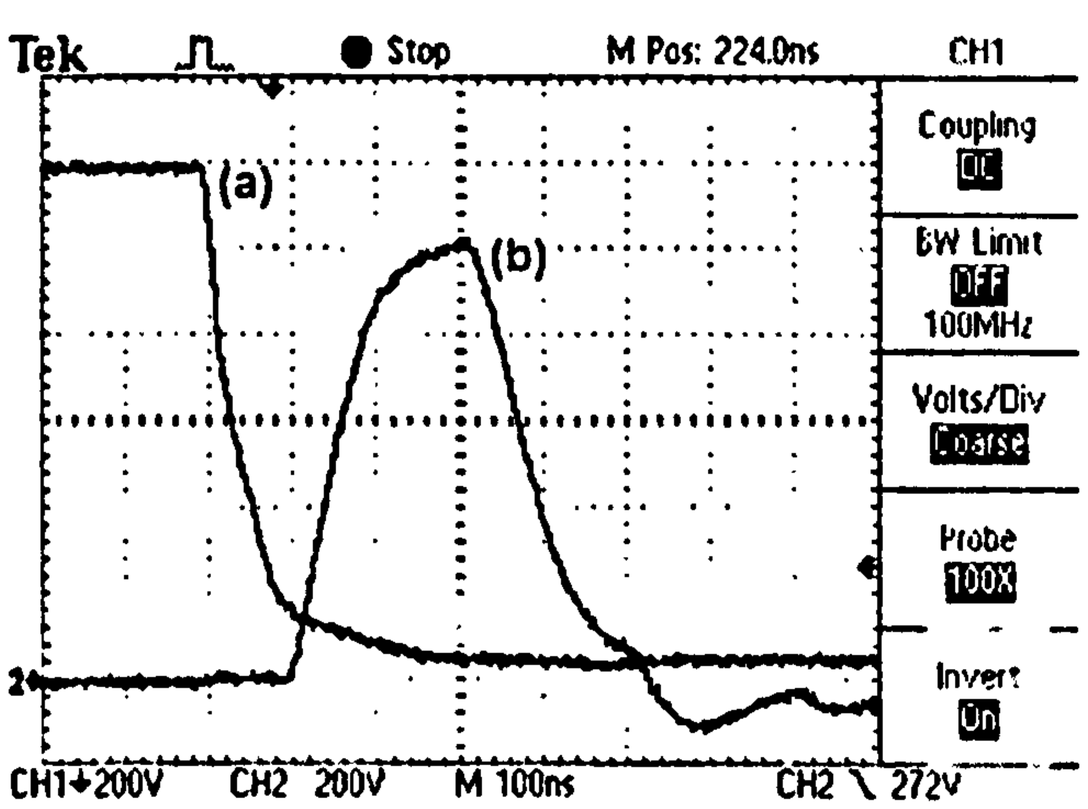

Figure 4.6 Voltage waveform across GT15Q301 (a) and output voltage pulse (b) for a 10 Ω input impedance pulse generator (amplitude 200 V/div and time base 100 ns/div).

It is apparent from the results that the dual-degradation effect does not exist for the GT15Q301 device (Figure 4.6) but is present in the other four devices, being most significant for the IRG4PH40U device. The IRG4PH40U device was further tested with the 10 Ω pulse generator and the voltage across the switch was varied from zero

to the rated switching voltage. This experiment was also carried out for two parallel IRG4PH40Us, and it was observed that dual degradation existed even at very low operating voltages. The voltage collapse across the switch and the generator output pulse are shown in Figure 4.7, for an applied voltage of 1.2 kV.

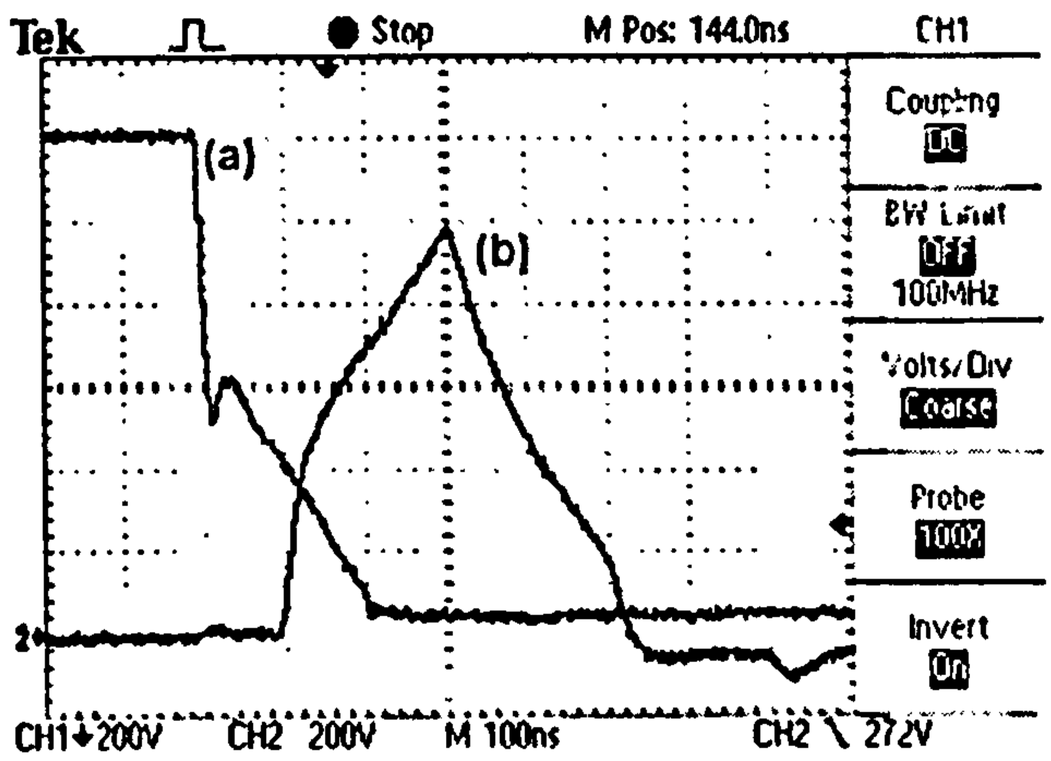

Figure 4.7 Voltage waveform across two parallel IRG4PH40Us (a) and output voltage pulse (b) for a 10 Ω input impedance pulse generator (amplitude 200 V/div and time base 100 ns/div).

These results indicate that the dual-degradation effect is not simply related to the magnitude of the current passing through the device. For example, the IRG4PH40U was tested in a 50 Ω input-impedance pulse-generator circuit and, as shown in Figure 4.8, the dual-degradation effect is still apparent.

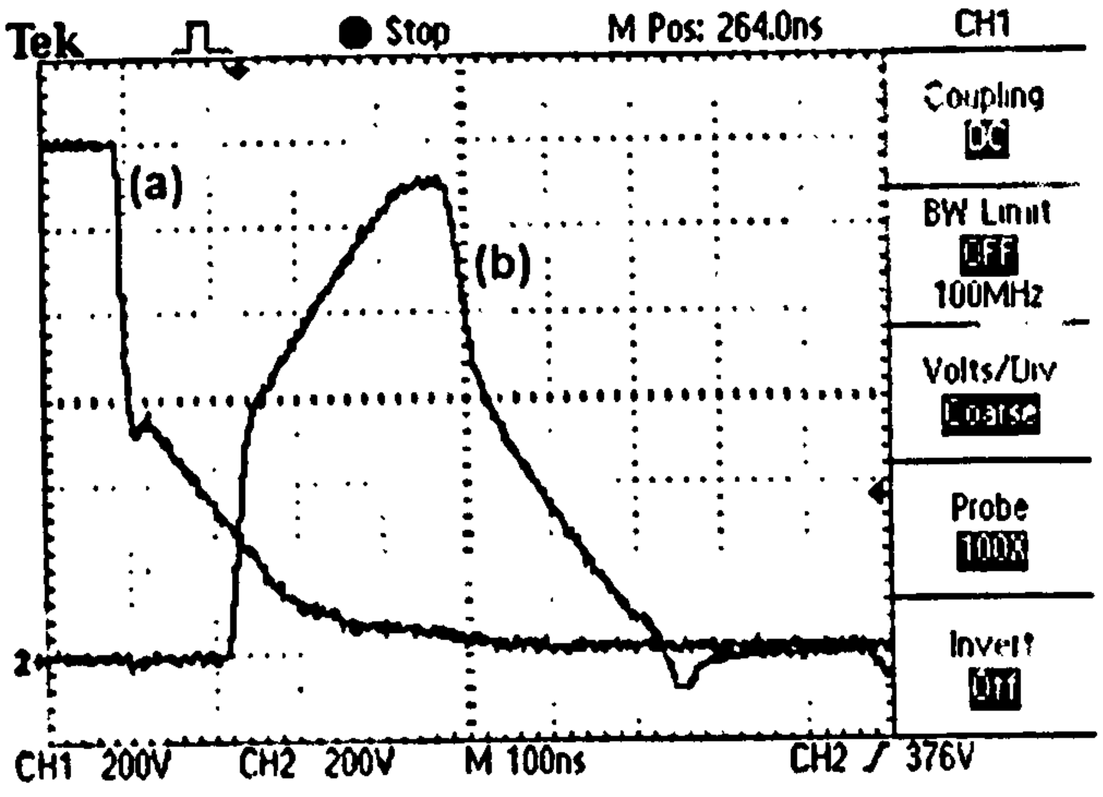

Figure 4.8 Voltage waveform across IRG4PH40U (a) and output voltage pulse (b) for a 50 Ω input impedance pulse generator (amplitude 200 V/div and time base 100 ns/div).

The voltage across the switch, and the values of the collector-emitter voltage where the transition occurs between the fast and slow rates of fall are referred to as V_0 and V_B respectively. The ratio of V_B to V_0 can therefore be described as a loss factor η, which reflects the switching characteristic of the device. The way in which η changes as a function of V_0 for the IRG4PH40U is shown in Figure 4.9. It can be seen that at low operating voltages, the deviation accounts for ~40% of the switching waveform whereas at higher voltages, this increases to 65%.

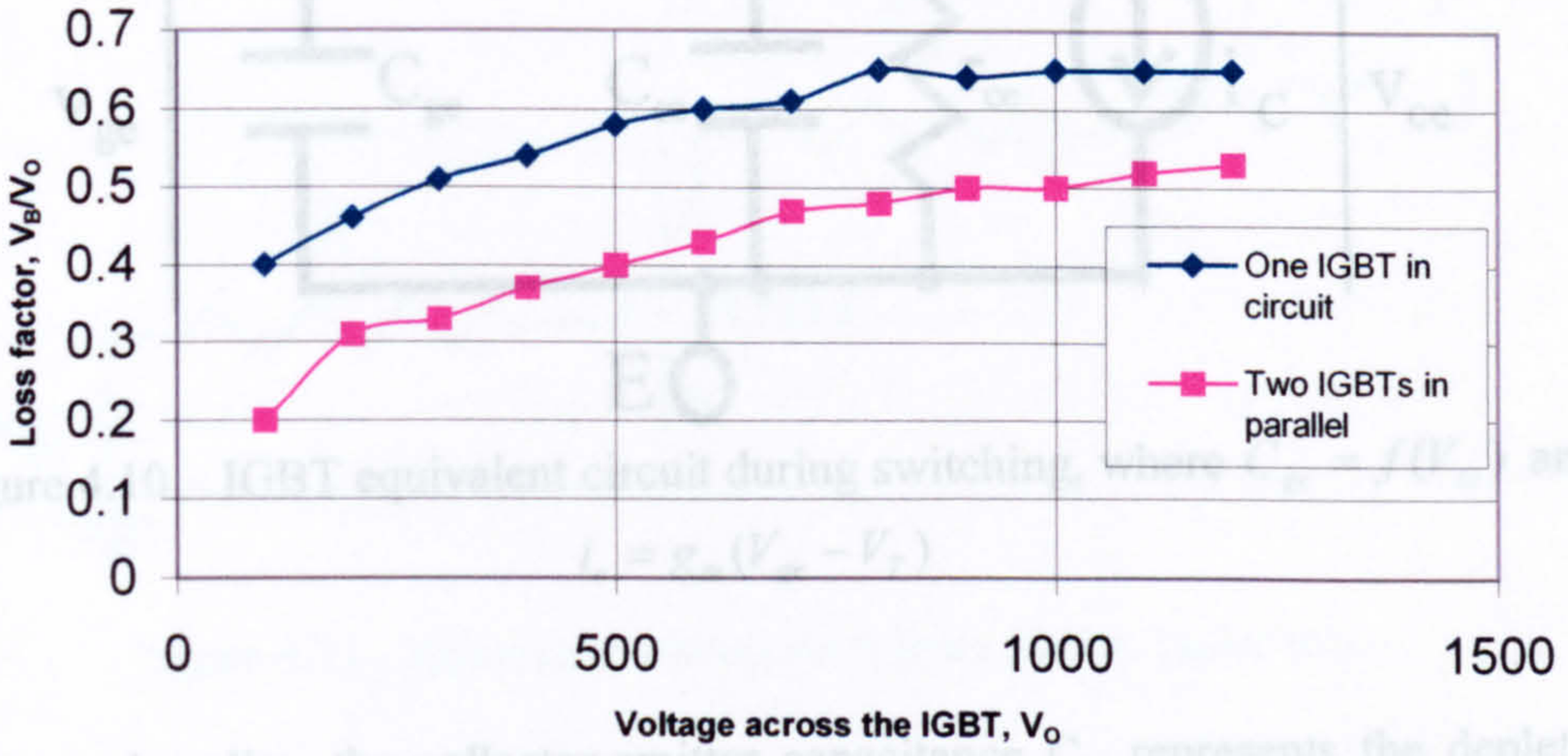

Figure 4.9 η - V_0 characteristic for IRG4PH40U in a 10 Ω input impedance pulse generator.

By connecting two devices in parallel, and consequently passing less current through each device, some reduction in the loss factor is achieved.

4.2.2 Discussion

Assuming that the voltage and current are linear functions with respect to time during switching, maximum instantaneous power in the switch occurs at 50% of the voltage collapse. If dual degradation is due to over-rating of the peak instantaneous power, it would be expected to occur prior to 50% of the voltage collapse and the corresponding loss factor in this case would be greater than 0.5. However, according to the experimental data obtained for η using 10 Ω, 25 Ω and 50 Ω pulse generators, dual degradation occurs with loss factors of less than 0.5. Therefore, these results suggest that dual degradation is not simply due to over-rating of the peak instantaneous power of the IGBTs.

The role of parasitic capacitance in dual degradation was then examined. Figure 4.10 represents the equivalent circuit of an IGBT during switching. V_T represents the gate threshold voltage, g_m is the transconductance gain and r_{ce} is the collector-emitter resistance.

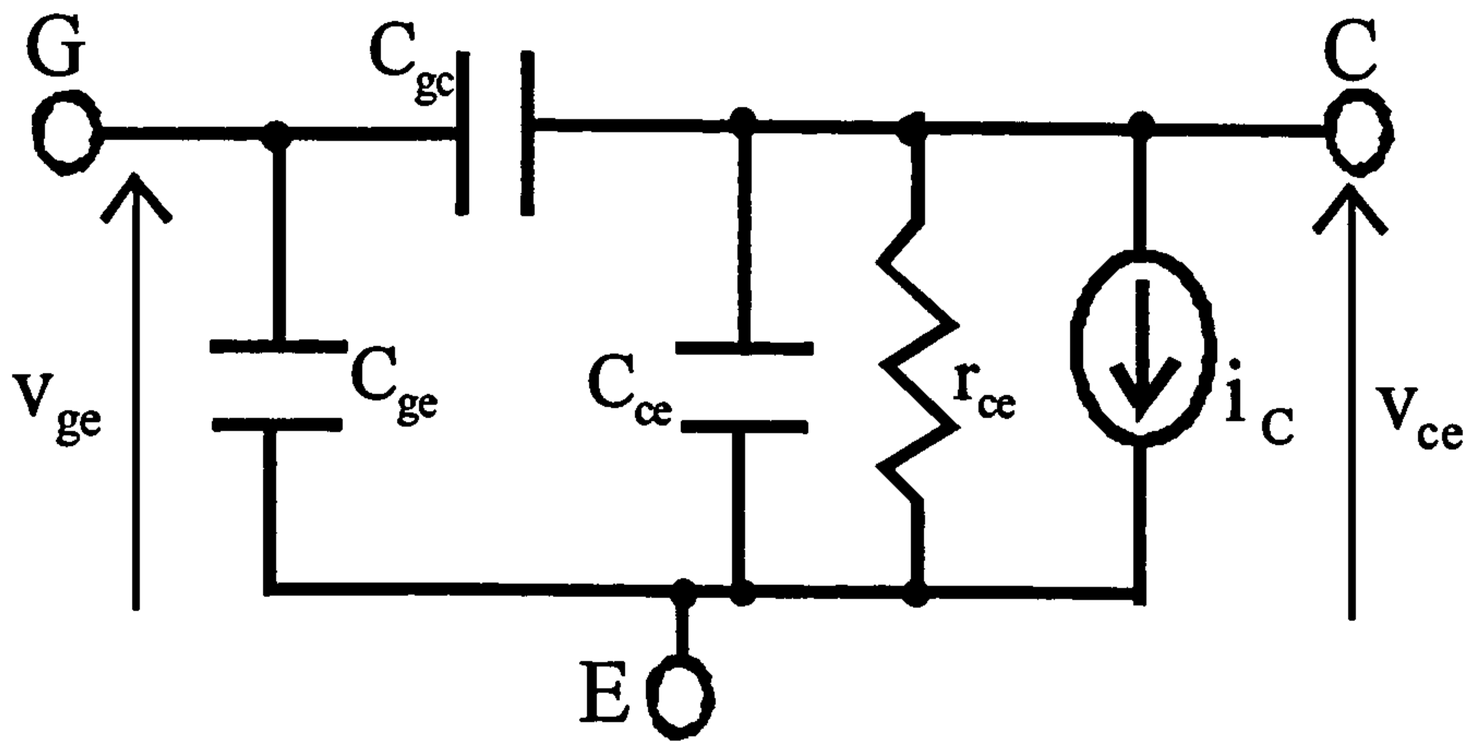

Figure 4.10 IGBT equivalent circuit during switching, where $C_{gc} = f(V_{ce})$ and $i_c = g_m(V_{ge} - V_T)$

As discussed earlier, the collector-emitter capacitance C_{ce} represents the depletion layer capacitance in the drift region and it has no significant effect on the switching characteristics of the IGBT. The gate-emitter capacitance C_{ge} is a combination of the electrostatic capacitance of the oxide layer in series with the capacitance of the depletion layer and this has only a limited effect on the switching characteristics. The most significant capacitance affecting the switching performance is the gate-collector capacitance C_{gc}, representing the extended drift-region depletion-layer capacitance. The magnitudes of the parasitic capacitances depend upon the geometry and topology in the IGBT structure, with higher current devices having larger capacitances [81]. The values of these capacitors are also a function of the operating voltage, and because the voltage across C_{ce} is much larger than that across C_{ge}, the gate-emitter capacitance does not vary significantly and is usually assumed to be constant during switching [82-84]. To investigate further the influence of the gate-collector capacitance on the switching behaviour, a computer simulation of the equivalent circuit was carried out.

4.2.3 Computer simulation

In order to simplify the simulation while focusing on the influence of the gate-collector capacitance, the simplified circuit of the Blumlein pulse generator has been used. The equivalent circuit seen from the switch (IGBT), has been drawn as shown in Figure 4.11. The parameters V_0, L_c, Z_0, R_g and V_{ge} are the maximum charging voltage, circuit stray inductance, switch input impedance, IGBT gate drive circuit resistance and triggering pulse voltage, respectively.

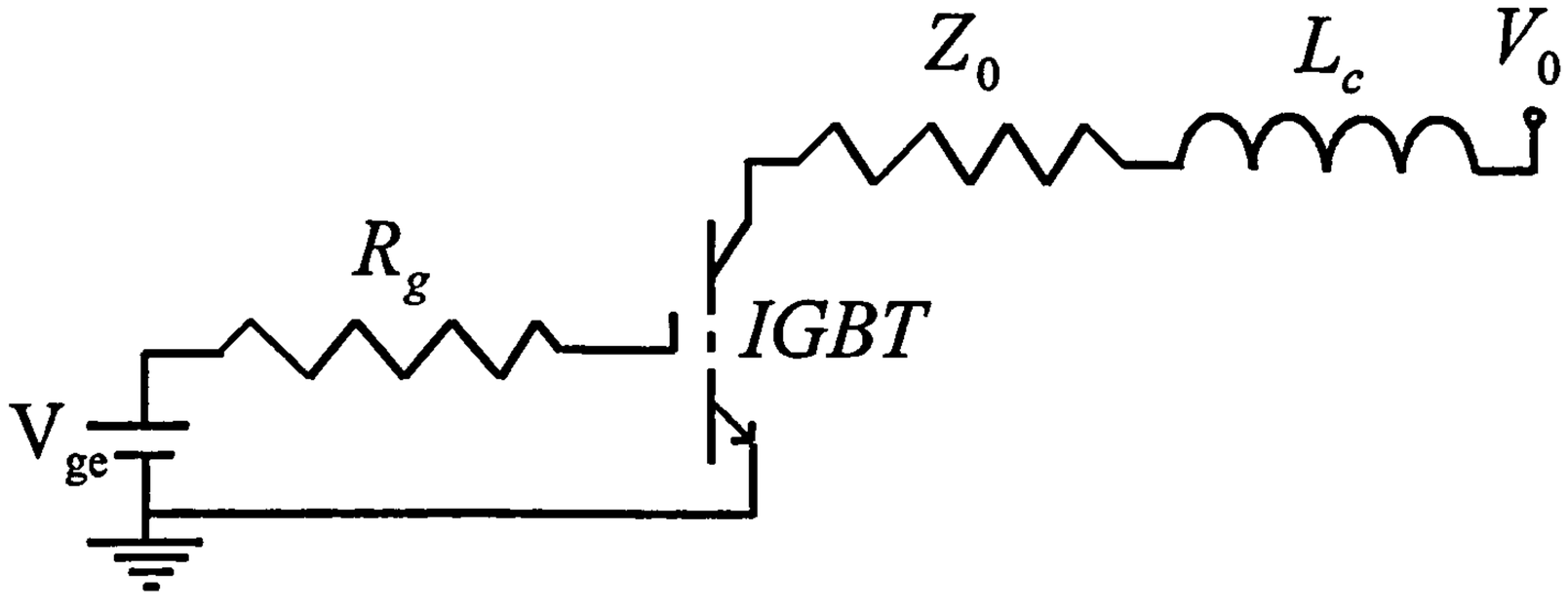

Figure 4.11 Equivalent circuit seen from device under test.

According to the circuit shown in Figure 4.11, the output-circuit equation can be written as:

$$V_0 = L_c \cdot \frac{di_c(t)}{dt} + Z_0 i_c(t) + v_{ce}(t) \tag{4.1}$$

Where $i_c(t)$ is the instant collector current, and $v_{ce}(t)$ is the collector-emitter voltage drop.

In addition,

$$\frac{dv_{ge}(t)}{dt} = \frac{i_g(t)}{C_{iss}} = \frac{V_{ge} - v_{ge}(t)}{R_g C_{iss}} \tag{4.2}$$

where $C_{iss} \cong C_{ge} + C_{gc}$, $v_{ge}(t)$ is the instant gate-emitter voltage, and $i_g(t)$ is the instant gate current.

The reduction in the collector-emitter voltage during switching causes the voltage across C_{gc} to decay, resulting in an additional current i_{Gm} flowing in the gate circuit. This increases the voltage drop V_m across the gate resistor and slows the rate of rise of the gate-emitter voltage through negative feedback (Miller effect). Therefore, equation (4.2) has to be modified to:

$$\frac{dv_{ge}}{dt} = \frac{V_{ge} - V_m - v_{ge}(t)}{R_g C_{iss}} = \frac{V_{ge} - R_g i_{Gm} - v_{ge}(t)}{R_g C_{iss}}$$

$$\frac{dv_{ge}}{dt} = \frac{V_{ge} - C_{gc} R_g \frac{dv_{ce}}{dt} - v_{ge}(t)}{R_g C_{iss}} \tag{4.3}$$

As the value of parasitic capacitance specified in most data sheets is for a static collector-emitter voltage of 25 V, to obtain realistic results from a computer simulation, C_{gc} in the above equations has to be considered as a function of the collector-emitter voltage. Considering equations (4.1-4.3) and other equations of the IGBT characteristics presented in Chapter 3, the block diagram shown in Figure 4.12 is taken to summarise the previous analysis. As shown in this block diagram, the variation of gate-emitter capacitor appears as a negative feedback on the device switching performance. This slows the rate of rise of gate-emitter voltage and consequently changes the turn-on speed and switching characteristics of the IGBT.

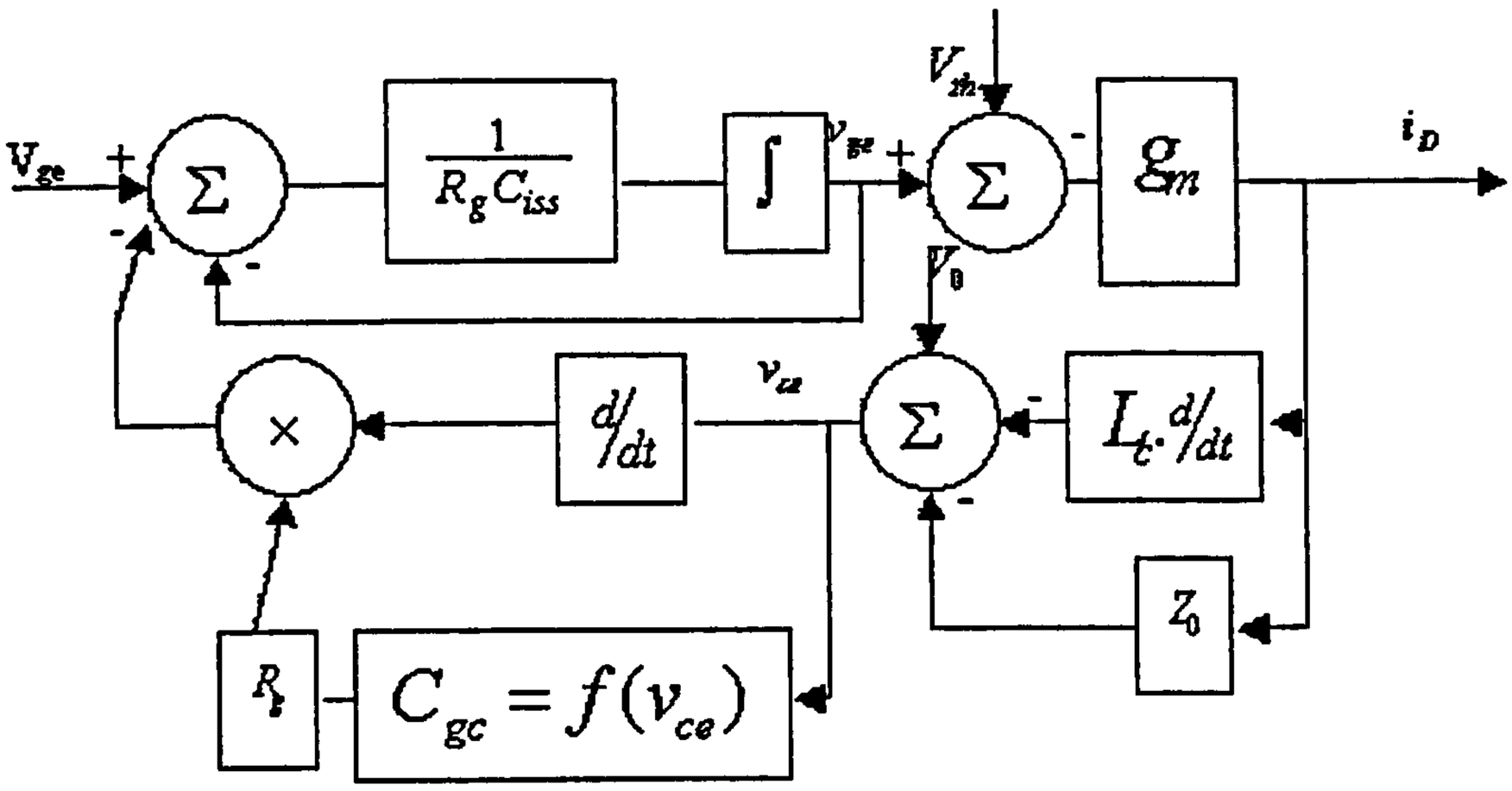

Figure 4.12 Block diagram showing IGBT and circuit parameters affecting the turning-on behaviour.

Computer simulation was carried out for two types of IGBT; the IRG4PH40U and the GT15Q301. Published information for the value of C_{gc} and other parameters were taken from IGBT data sheets. Attention was paid to the effect of C_{gc} on the shape of the voltage collapse across the device, as C_{gc} varied as a function of the collector-emitter voltage. The simulation was carried out using *MATLAB SIMULINK* and according to the block diagram shown in Figure 4.13. A small inductance (~0.1 mH)

was included to represent the overall inductance of the circuit and switch. An input pulse signal with a rise time of 100 ns was selected as triggering pulse and the program was run for different values of $C_{gc} = f(v_{ce}(t))$, given in Table 4.2, to represent two different IGBT devices (IRG4PH40U and GT15Q301). Collector-emitter and gate-emitter voltage waveforms were recorded for both IGBTs, as shown in Figure 4.14.

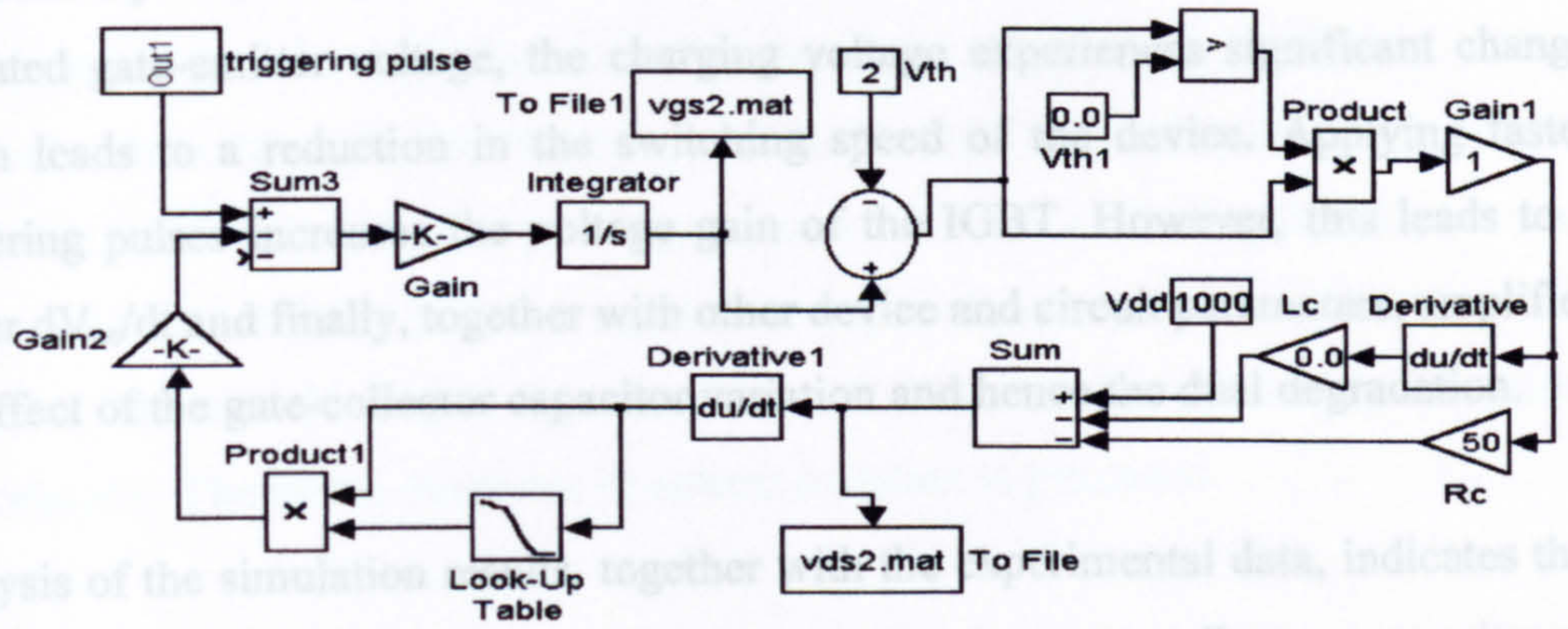

Figure 4.13 Simulated block diagram.

Table 4.2 Gate-Collector capacitance for two different IGBT devices

Voltage V_{CE} (V)		900	800	700	600	500	400	300	200	100
Capacitance C_{GC}(pF)	GT15Q301	20	30	40	45	50	65	75	80	85
	IRG4PH40U	5	8	10	15	15	20	25	30	50

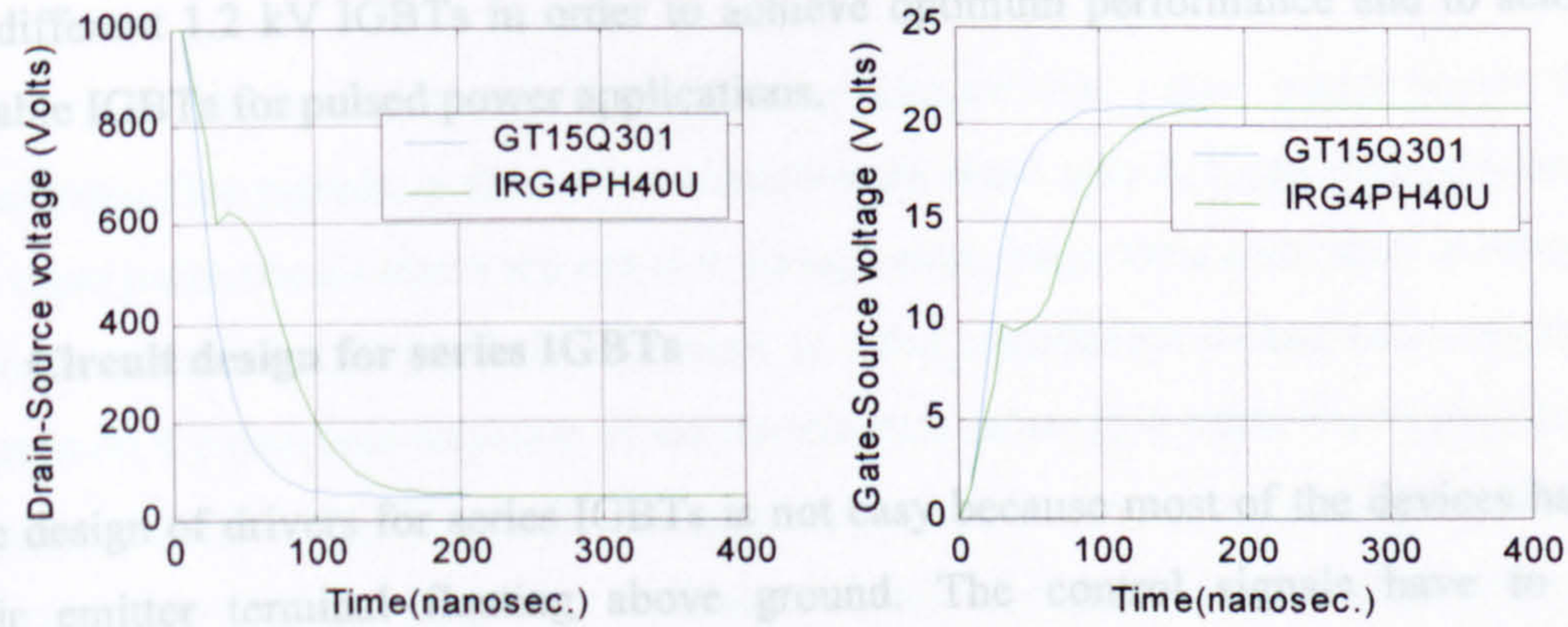

(a) Collector-emitter voltage (b) Gate-emitter voltage

Figure 4.14 Switching characteristic waveforms for IRG4PH40U and GT15Q30.

The simulated collector-emitter curves of Figure 4.14a appear similar to those obtained experimentally and shown in Figures 4.2, 4.6 and 4.8. The difference in behaviour of the two IGBTs examined here also shows up in the gate-emitter voltage, as seen in Figure 4.14b. According to this Figure, by applying the triggering pulse across the gate-emitter of the GT15Q301, the gate-emitter capacitor starts charging exponentially with a consistent time constant. For the IRG4PH40U, at around 40% of the rated gate-emitter voltage, the charging voltage experiences significant change which leads to a reduction in the switching speed of the device. Applying faster triggering pulses increases the voltage gain of the IGBT. However, this leads to a higher dV_{ce}/dt and finally, together with other device and circuit parameters, amplifies the effect of the gate-collector capacitor variation and hence the dual degradation.

Analysis of the simulation results, together with the experimental data, indicates that the circuit and device parameters, particularly the gate-collector capacitance, determine the IGBT switching performance under fast pulse conditions. A reason for the dual degradation observed for the collector-emitter voltage could be the rapid variations in device parasitic parameters such as gate-collector capacitance. From the results obtained for the loss factor for pulse generators with different input impedances, the dual-degradation phenomenon cannot be due to over-rating the peak instantaneous power, nor is it associated with exceeding the current capability of the device. The simulation developed can be used to predict the switching performance for different 1.2 kV IGBTs in order to achieve optimum performance and to select suitable IGBTs for pulsed power applications.

4.3 Circuit design for series IGBTs

The design of drivers for series IGBTs is not easy because most of the devices have their emitter terminal floating above ground. The control signals have to be synchronised and transported across a large voltage barrier, in this case up to over 10 kV. For pulsed power applications where the goal is to turn the device on very quickly, a fast, large gate current (tens of amperes) is required during turn-on but little power is needed thereafter. Likewise, during turn-off, a large current must be drawn

from the gate-emitter capacitance. Therefore, the gate drive circuit must be capable of sourcing and sinking these currents at the required repetition rate. The power required in drive circuits has to be provided across the high voltage barrier. Paralleling IGBT devices also necessitates increasing the output power of the gate driver. This leads to using a current amplifier as the last stage of the gate drivers.

The level shifting of switching pulses to the high voltage side can be achieved by various methods. Although the use of commercial IGBT driver modules (silicon devices) such as *TC-4426*, *HCPL-3120*, and *HCPL-2300* seems attractive, they cannot be used in applications requiring voltages above 1 kV and cascading IGBTs, because of the variation of delay between input and output signals (a delay of ~100 ns was measured between the output signals of two HCPL-3120 devices during the initial experiments). Therefore, magnetic or optical isolation is preferred.

A common approach to transmission of switching signals across a high voltage barrier, in order to trigger multiple devices in series, is to use pulse transformers. This method offers impedance matching, DC isolation and a desirable synchronisation between switching pulses. However the duty cycle of the pulse to be transmitted is limited and the parasitic elements of each winding and its associated element must be well matched and minimised in order to avoid increasing the switching time. The problem of limited pulse duration is not so important in applications with pulse durations of a few microseconds.

In order to check the possibility of using commercial pulse transformers for transferring fast signals, a few pulse transformers were tested. Experiments proved that these pulse transformers are not fast enough even when their secondary windings are open circuited. This has led to a review of pulse transformer design with attention focused on the rise-time response of the transformer rather than other parameters such as pulse duration. Pulse transformer response near the front edge of the pulse is determined by the high-frequency equivalent circuit of Figure 4.15, which is obtained from the transformer equivalent circuit by neglecting the effect of magnetising inductance [85].

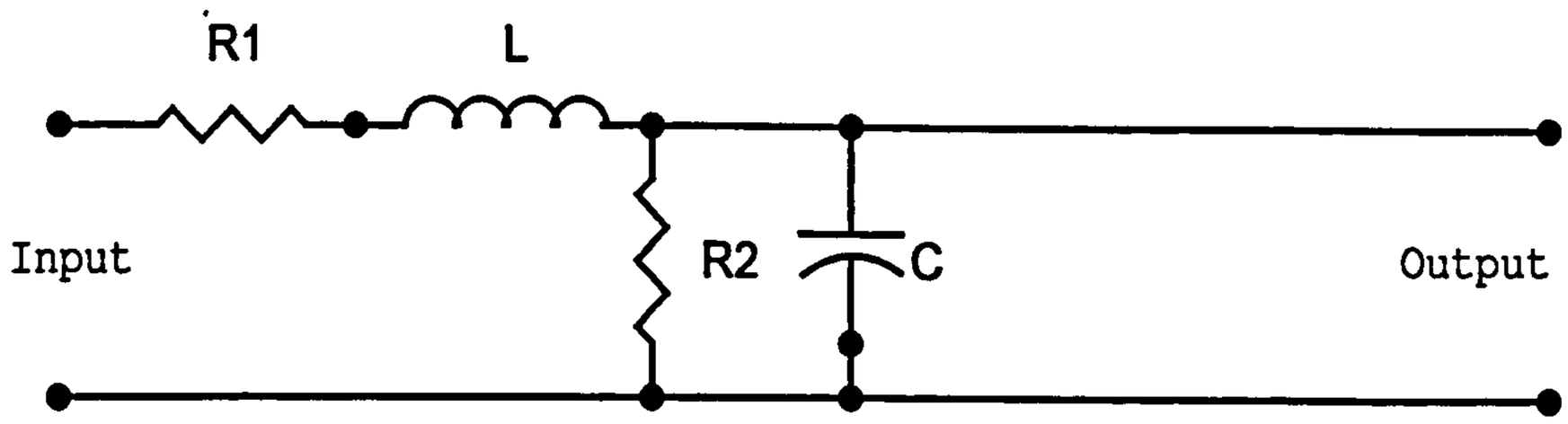

Figure 4.15 High frequency equivalent circuit of a pulse transformer, where R1 represents the primary winding resistance, R2 the combination of the load resistance and the secondary winding resistance, L the leakage inductance, and C shunt capacitor [85].

By assuming the rise-time t_r to be the time interval required for the output voltage to rise from 0.1 to 0.9 of its final value, t_r is expressed as [85]:

$$t_r = 1.06\pi\sqrt{LC\lambda} \qquad 4.4$$

where λ is the amplification factor defined as $\lambda = \frac{R2}{R1+R2}$

According to equation 4.4, in order for the output pulse to rise rapidly, the leakage inductance and the shunt capacitance must be kept small. The rise-time may also be decreased by reducing λ, although a small value of λ will result in a highly attenuated output voltage. Large step-up ratios are rarely used in pulse transformers, because the gain n can be obtained only at the price of increasing the rise-time by the factor n [85].

Several pulse transformers including air-core and ferrite-core transformers were built and tested. For air-core transformers, the output pulses were fast, but their performance was very sensitive to noise, particularly when the trigger circuit was not far from the high voltage source. For ferrite-core transformers, it was observed that for optimum performance, the secondary winding must have a symmetrical position relative to the primary winding; otherwise, a significant time-delay (~ 75 nsec) occurs between their output pulses. Therefore, single turn, ferrite-core pulse transformers with only one secondary winding were chosen.

To generate a fast pulse at the secondary of a pulse transformer, the current level in the primary winding must change rapidly. In low-inductance drive circuits, by using a fast closing switch, the current increases quickly. In inductive drive circuits, opening the circuit quickly is possible by using fast opening switches to rapidly increase the level of current. Here, the first method was applied using the circuit shown in Figure 4.16. Initially capacitor C is charged to 50 V and then it is discharged through the primary winding of the transformer by closure of switch. A 22 V Zener diode is connected at the secondary winding to clamp the amplitude of the output pulse to 22 V and protect the gate of the IGBT against over-voltage.

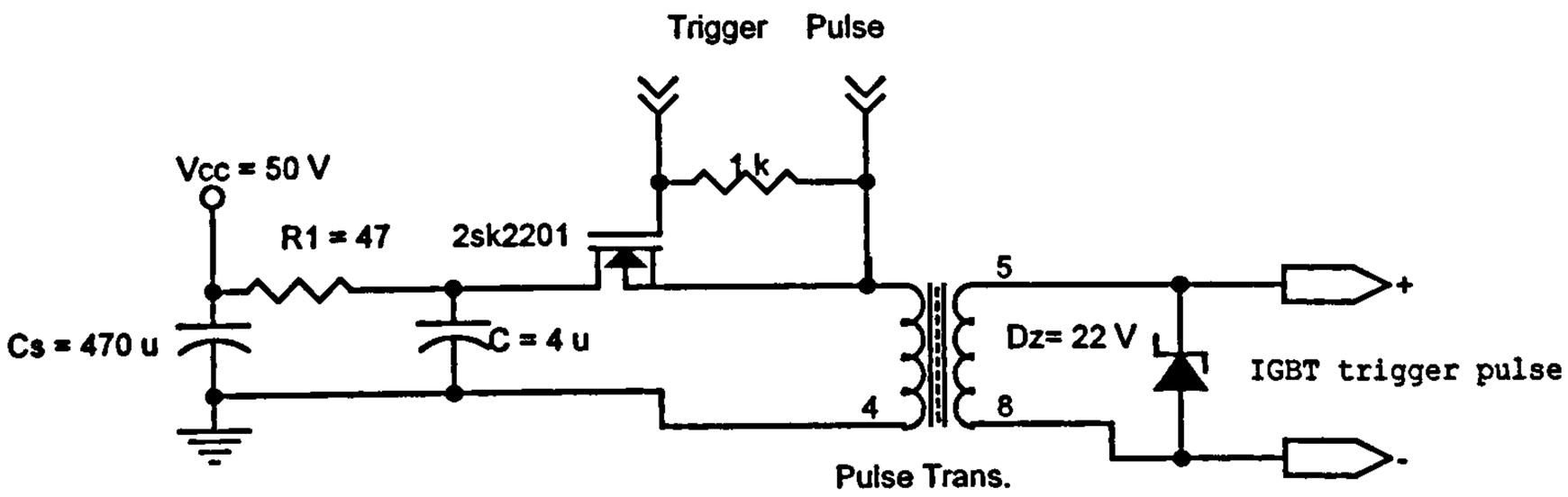

Figure 4.16 Gate-drive circuit for driving a ferrite-core pulse transformer.

For driving more than one pulse transformer, primary windings were connected in series to keep the delay between output pulses to a minimum. However, it was observed that for more than three transformers, the output pulse rise-time increases and therefore, connecting the primary windings in parallel was preferred. In addition, it was observed that for 1.2 kV IGBTs, these transformers cannot provide the required energy to charge the gate-emitter capacitance quickly and some modification to winding turns and drive circuit is necessary. This issue will be discussed later in section 4.5.1, where the stacking of 1.2 kV IGBTs is discussed.

For high voltage applications where an isolation of more than 10 kV is required, pulse transformers with bigger cores are required. This leads to significant changes in the design and necessitates extra circuitry. This isolation problem can be addressed by incorporating opto-coupler devices or optical fibre links. Opto-coupler devices tend to be slow and are available with maximum isolation voltage of a few thousands volts. In addition, device-to-device delay and jitter limit their application in the fast

switching of IGBTs. The use of optical fibre links provides virtually unlimited isolation voltage. Their use requires consideration of methods for keeping device–to-device delay at a low level, and the following chapter deals with optical isolation, including consideration of device-device delay.

4.4 Stacking 600 V IGBTs

The first attempt to stack the IGBT devices was carried out using 600 V IGBTs (HGTP7N60C3 manufactured by Harris semiconductor) with a collector current, continuous and pulsed (pulse width limited by maximum junction temperature) of 14 A and 56 A, respectively. The aim was to make a closing switch with voltage and pulsed current of 2.5 kV and 250 A respectively. Therefore, the value of the static voltage sharing resistance was calculated for a stack of 5×5 IGBTs using the maximum collector-emitter leakage current of the IGBT as published in its data sheet (250 μA) and equation 3.20 from chapter 3. The sharing resistors and IGBTs were mounted vertically around aluminium plates as shown in Figure 4.17. All five IGBT stages were triggered using single pulse transformers with their primary windings connected in parallel and driven using the circuit shown in Figure 4.16.

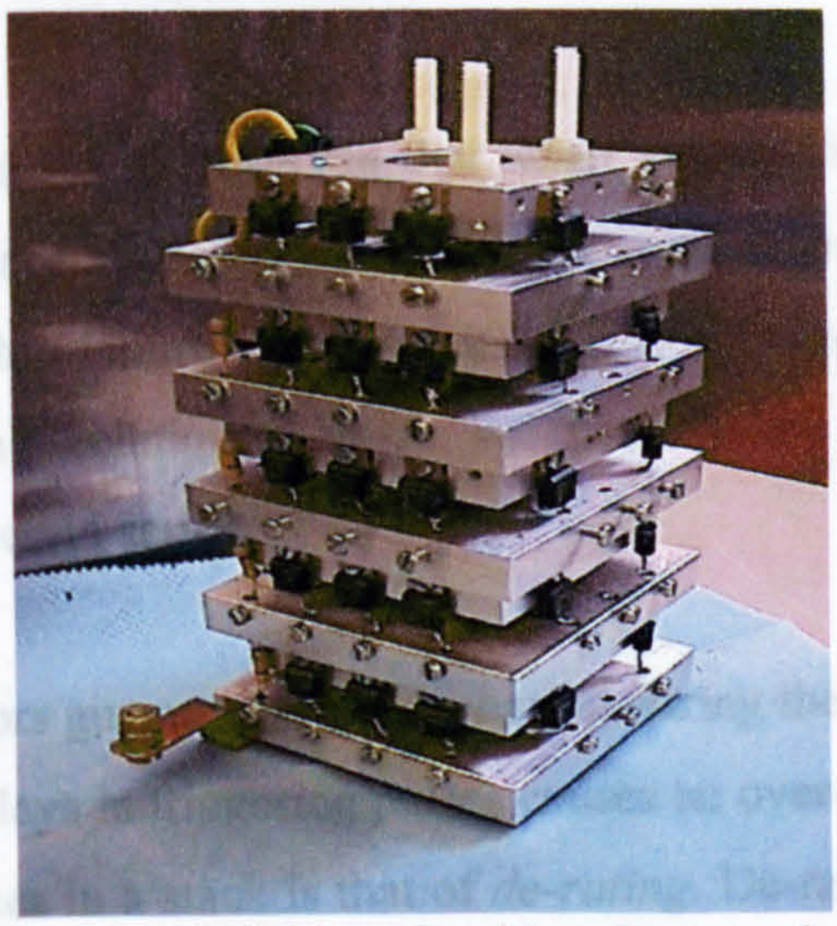

Figure 4.17 Photograph of 5×5 IGBT stack with voltage and current ratings of 2.5 kV and 250 A, respectively.

Voltage sharing between the modules was investigated by monitoring voltage across each of the IGBT modules and the total voltage across the stack. All of the modules were found to turn on simultaneously so that none of the modules experienced over-voltage. No significant difference between the voltage fall-time of a single IGBT and the stack was observed. This stack was used to produce rectangular pulses with rise-time of about 50 ns from a 10 Ω, 200 ns, Blumlein pulse generator. The voltage waveform across the stack and output voltage pulse are shown in Figure 4.18.

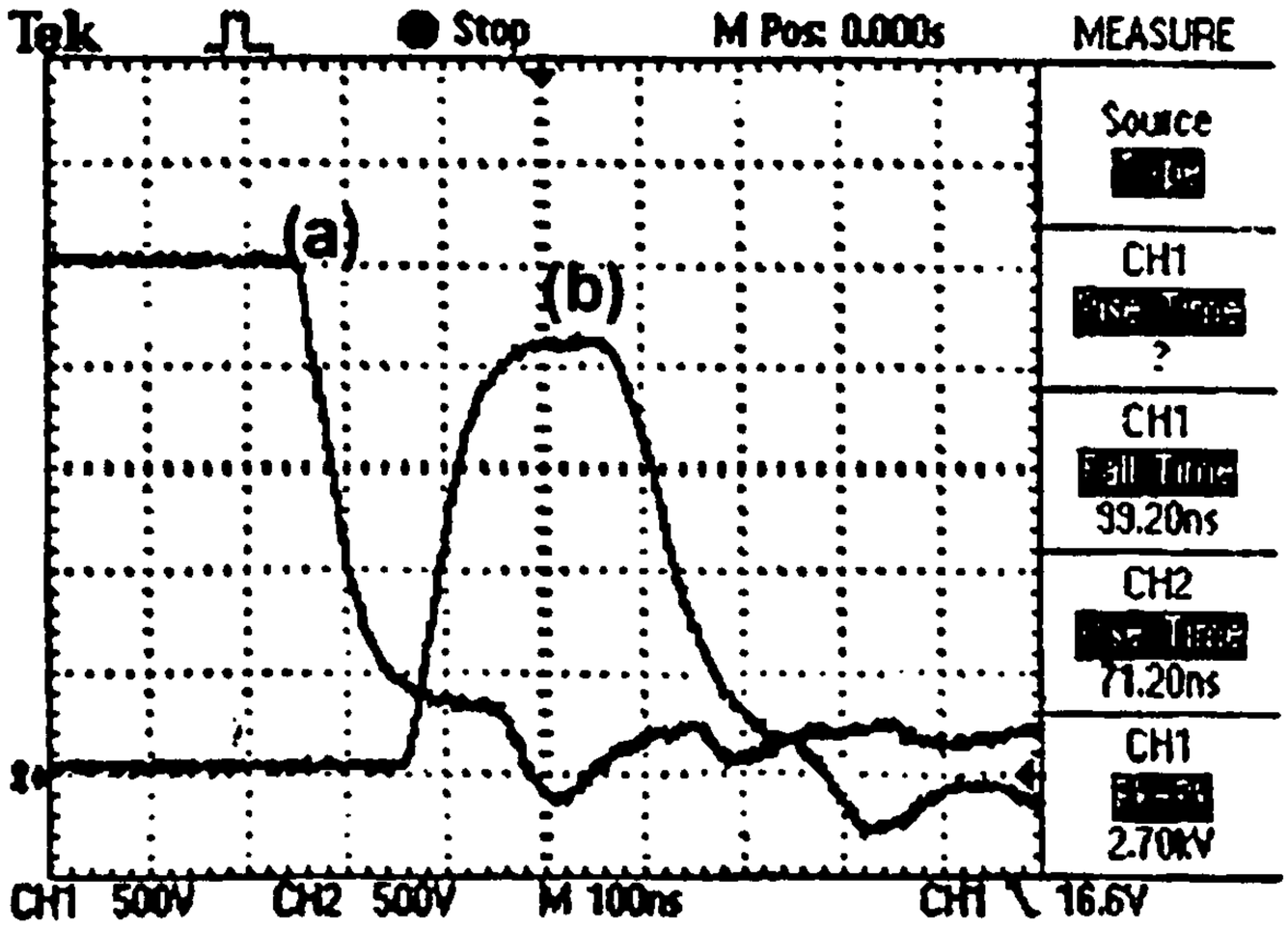

Figure 4.18 (a) Voltage across the stack and (b) the output voltage pulse in a 10 Ω Blumlein pulse generator.

During the experiments, it was observed that when a device/module fails as a short circuit, the applied voltage appears as an increased voltage on the remaining devices. This leads to catastrophic failure of the stack. Therefore, careful design, monitoring and failure-prevention techniques must be used when a large number of devices/modules are used in series.

In a stack, equal resistors guarantee voltage sharing during the off state. However, the probability of small delays in triggering pulses causes an over-voltage. One method to protect all of the devices in a stack is that of *de-rating*. De-rating is accomplished by placing in series more than the minimum number of devices required at a given voltage. This prevents sequential over-voltage of the remaining devices and catastrophic failure of the stack. In practice, primary protection against voltage

breakdown is achieved by limiting the supply voltage to no more that 80% of the IGBT-rated value. Auxiliary protection can be achieved by connecting fast non-linear voltage arresters such as a *Transil, Transient Voltage suppressor, Transorb or Voltage Dependent resistor* across the IGBT modules in a stack.

Initially, in order to investigate the transient behaviour of these devices, fast pulses with amplitudes higher than the DC voltage rating of devices were applied across them. It was observed that the amplitude of the applied pulses is clamped at voltages 60% higher than the DC voltage claimed in the datasheets. For example, when using the *VR500*, which is a transient voltage suppressor with DC voltage clamp of 500 V, the amplitude of the applied pulse is clamped at 800 V. By connecting more devices in parallel, the difference between the practical clamp voltage and the voltage claimed in the device datasheet could be decreased. In order to examine the behaviour of the voltage arresters in real situations, the arrangement shown in Figure 4.19 was used.

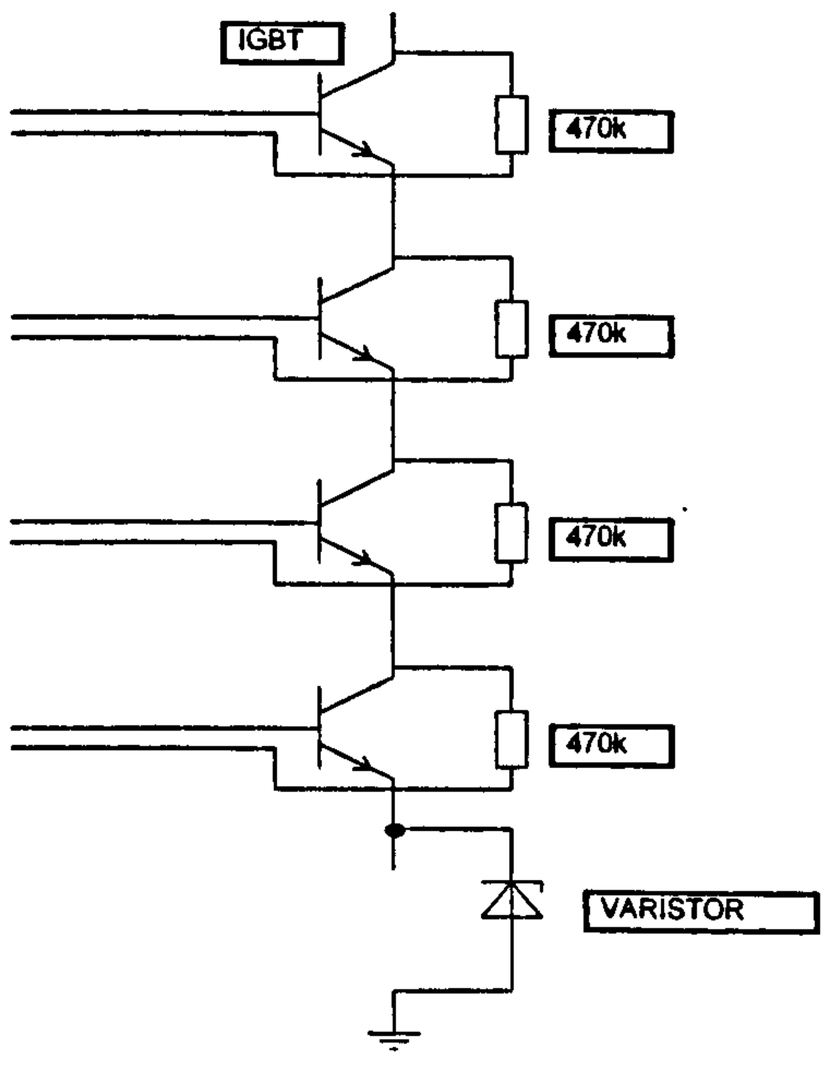

Figure 4.19 Investigating the transient behaviour of a voltage arrester in real situations.

To simulate the real situation of the stack, when one of the stages fails or is fired with a delay, the bottom IGBT of the stack was replaced by a voltage arrester, as shown in Figure 4.19. By applying a voltage of 2 kV across the stack and firing all the IGBT modules, the total voltage of the stack appears across the voltage arrester. The voltage

waveforms across the voltage arrester and across the stack were recorded for different types of voltage arrester. In Figure 4.20, the waveforms are shown for the 1.5KE400A transient voltage suppressor that has a DC voltage clamp of 400 V. Similar waveforms were observed for other voltage arresters.

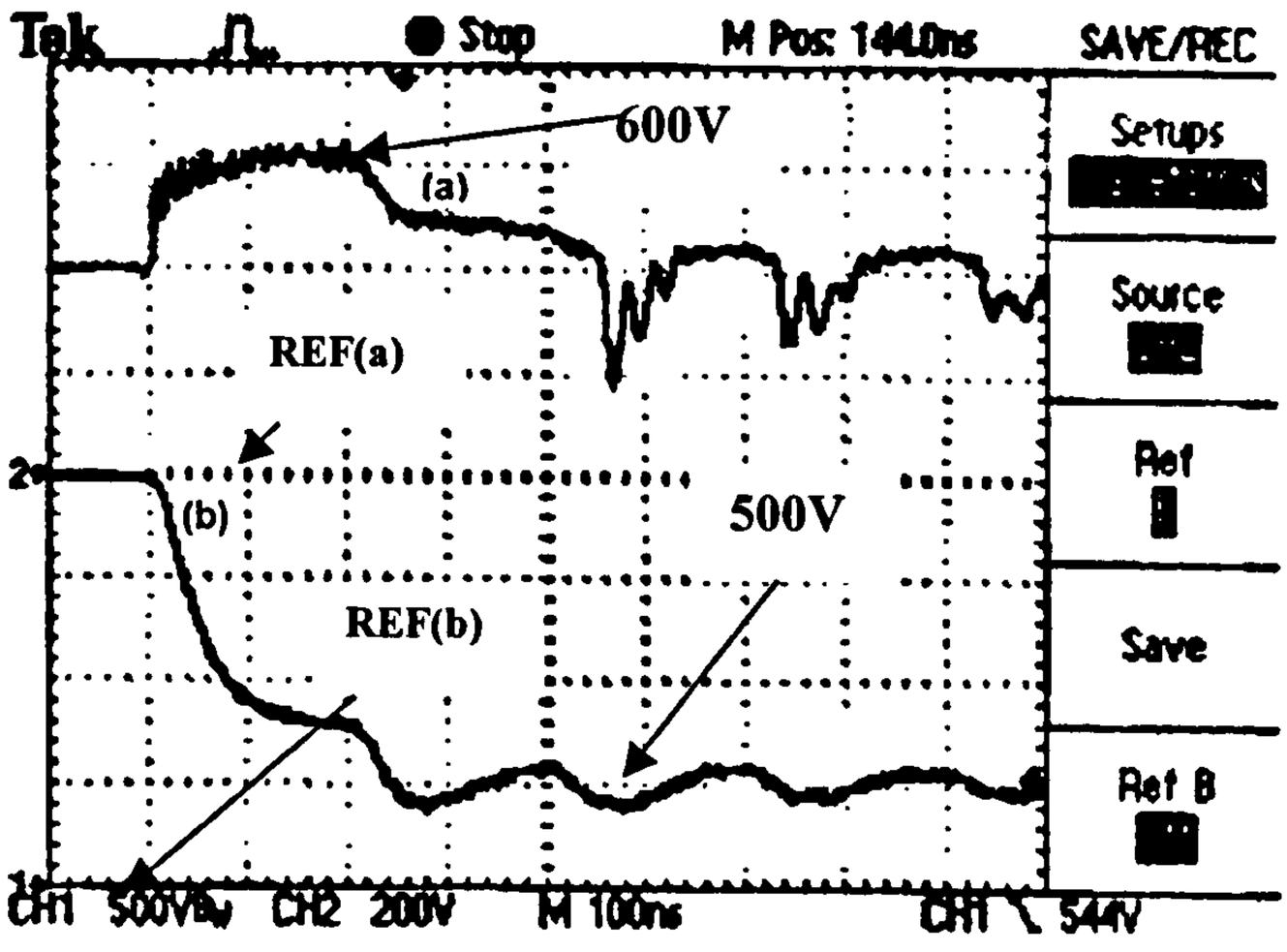

Figure 4.20 (a) Voltage across the transient voltage suppressor, *1.5KE400A,* and (b) voltage across the stack in the circuit of Fig 4.19.

Figure 4.20 shows that the voltage across the 1.5KE400A is clamped to 600 V for the first 200 ns after firing the stack, after which it falls to 500 V. Hence by using 600 V IGBTs, each with a 1.5KE400A device in parallel, and only 400 V applied across it (34% de-rating), the IGBTs can be protected against any over-voltages.

A pulse generator in the form of a 2.5 kV IGBT stack, with a 1.5KE400A device connected across each IGBT stage, was successfully operated with a pulse repetition rate of 1 kHz.

4.5 Stacking 1.2 kV IGBTs

One of the purposes of this research programme is to develop a practical semiconductor switch for a Blumlein pulse generator used in the investigation of the effect of Pulsed Electric Fields (PEF) on the inactivation of microbial populations

suspended in liquids [9]. Typical performance requirements that need to be satisfied by such a switch are listed in Table 4.3. Based on these requirements, a prototype switch using an IGBT stack of 1.2 kV devices was assembled and tested. The comparative study of IGBT devices from several vendors, presented in section 4.2, led to the selection of the GT15Q301 device manufactured by Toshiba. The GT15Q301 has a 1200 V maximum collector-emitter rating, an average current rating of 15 A, and a pulsed current rating of 30 A for a pulse width of 1 ms. Initial evaluation experiments have shown that this device can handle pulsed currents up to 100 A if the pulse width is limited to a few microseconds.

Table 4.3 Performance requirements

Parameter	Requirement
Output Voltage	10 kV into 50 Ω
Voltage Rise/Falltime	≤ 50 ns (10-90%)
Flattop Pulse-width	250 ns, 1 μs

To ensure that the total voltage across the switch is evenly distributed across each stage during steady state operation, a resistive biasing network was used. There is an absence of leakage current information in IGBT data sheets although leakage current is known to be a function of case temperature. A single module consisting of 5 IGBTs in parallel was thermally cycled and its leakage current measured using the experimental set-up shown in Figure 4.21.

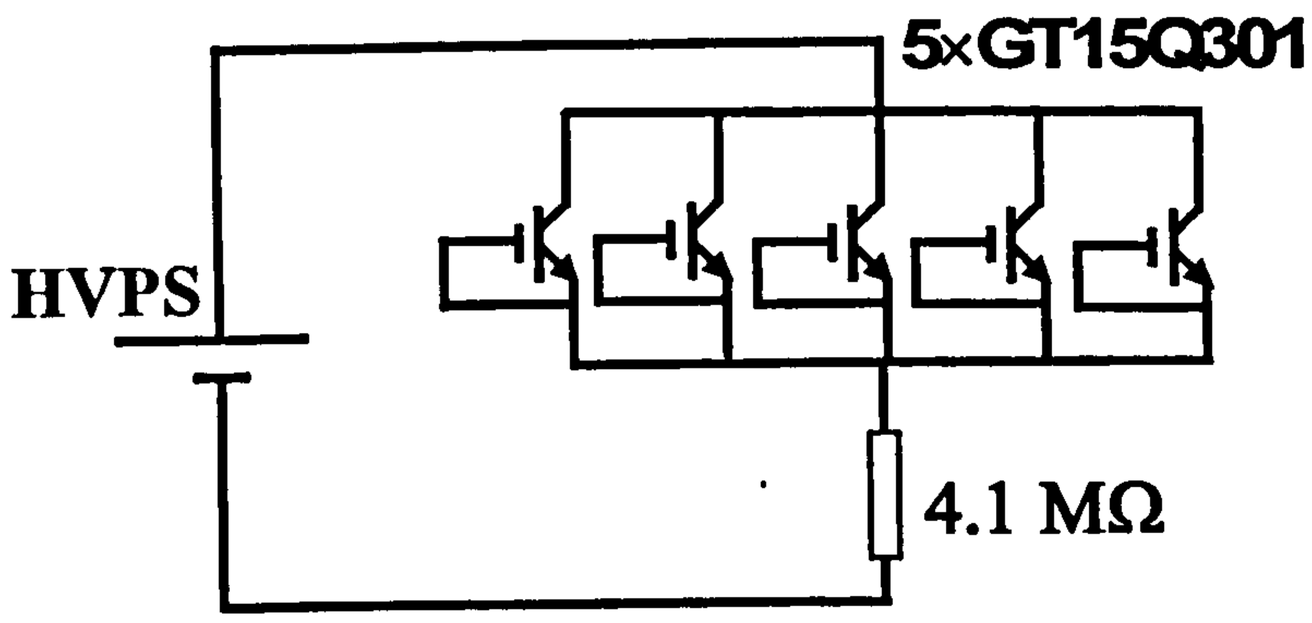

Figure 4.21 Experimental arrangement for measuring leakage current of IGBT modules.

The resultant variation of IGBT leakage current with temperature is shown in Figure 4.22.

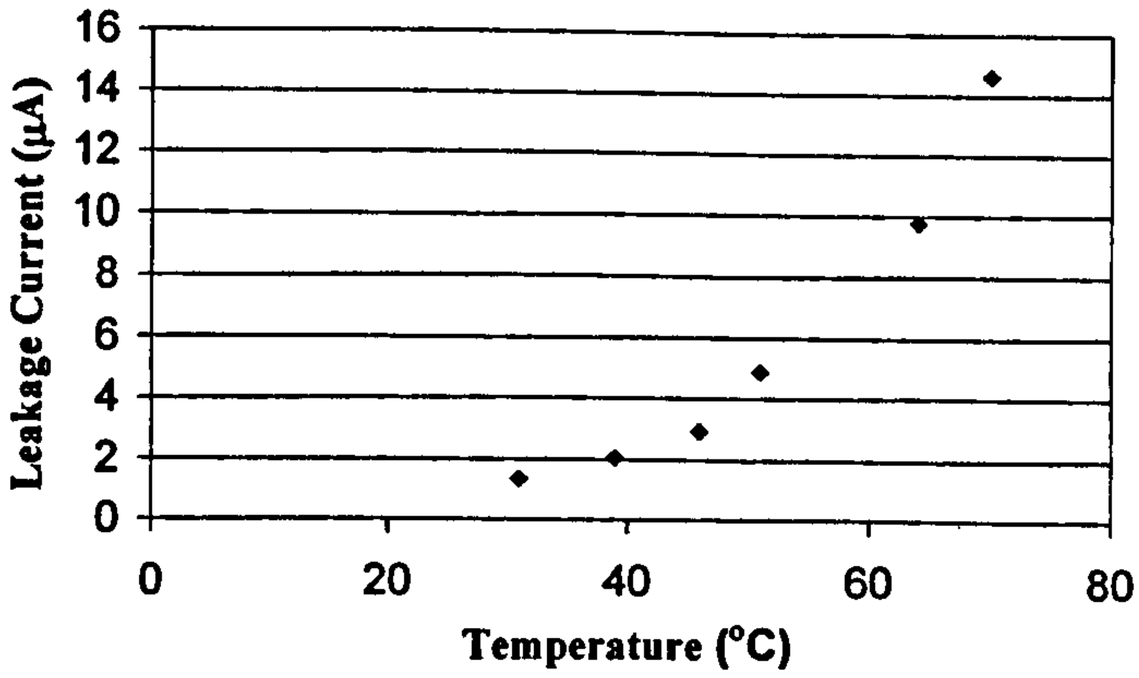

Figure 4.22 Leakage current of a module of 5 1.2 kV IGBTs as a function of temperature.

It can be seen that increasing the case temperature leads to higher leakage current, and this effect must be incorporated into calculations of values of sharing resistors. Therefore, the values of the steady-state voltage-sharing resistors were calculated using the maximum leakage current, assuming that the temperature of the IGBTs is maintained below 70°C. Using equation 3.20 from chapter 3 and by assuming a 5% resistor tolerance, 10 modules of IGBTs in series, and a total blocking voltage of 10 kV for the stack, the maximum value for the resistive network was calculated to be about 8 MΩ.

4.5.1 Stack configuration

From the results obtained on stacking 600 V IGBTs, it was noted that during the stacking of single-chip plastic-encapsulated IGBT devices, in packages such as TO-247:

- The circuit layout for all of the devices in the stack must be identical to prevent any timing error in switching.
- Stray capacitances to ground can result in unequal voltage sharing, and so must be minimised.
- It must be possible to easily remove faulty stages/devices, without dismantling the entire stack.

- Stray inductances cause a delay between voltage and current and this limits the application of the stack in pulsed power applications. Hence wiring between devices and modules must be maintained as short as possible.
- At frequencies in excess of kilohertz, the power dissipated in the stack is significant and suitable heat sinking must be included.

With these conditions in mind, a proper configuration for stacking of IGBTs was designed. Two circular aluminium plates as shown in Figure 4.23 were used for connecting 5 IGBTs in parallel in each stage.

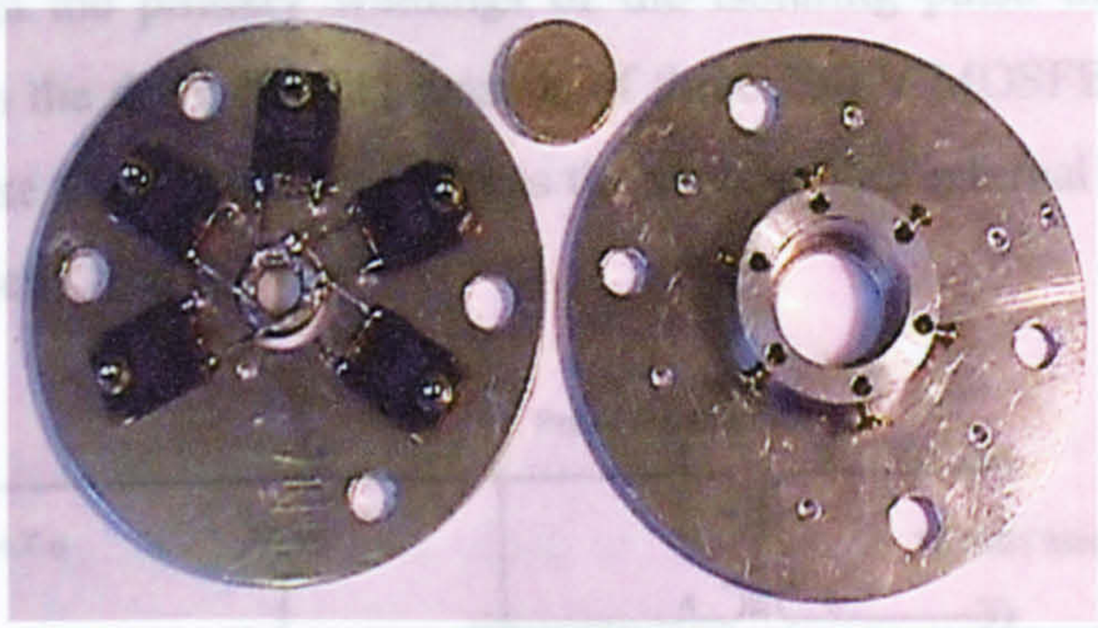

Figure 4.23 Photograph showing the connection of IGBTs in parallel.

The two aluminium plates shown in Figure 4.23 were connected through 14 mm plastic spacers and a voltage-sharing resistor was connected between the two plates using "O" ring brass washers as shown in Figure 4.24.

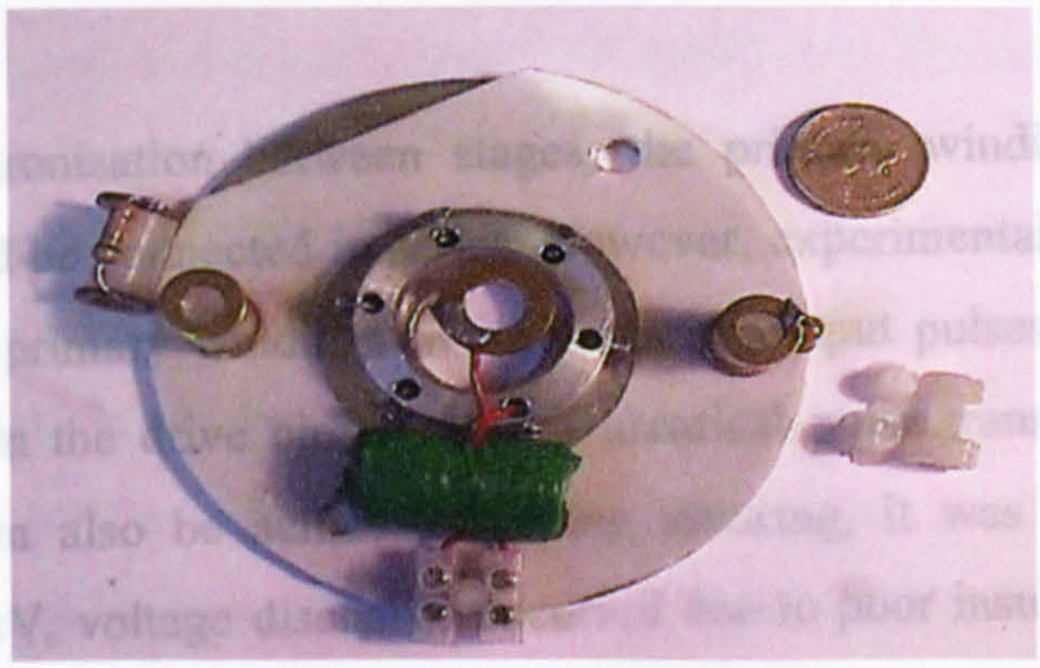

Figure 4.24 Photograph showing how the voltage-sharing resistor is placed in the IGBT module.

Results from stacking 600 V IGBTs have shown that pulse transformers with cylindrical ferrite cores and unit primary and secondary turns have good operating performance in terms of speed and output-pulse magnitude. However, it was observed that when driving five 1.2 kV IGBTs in parallel, pulse transformers with single turn windings cannot deliver the required energy for charging the gate-emitter capacitance. In order to deliver the energy required, their primary and secondary winding turns must be increased to three. A diagram of a suitable drive circuit is shown in Figure 4.25. In this circuit, the drive capacitor is initially charged to 100 V and then discharged through the primary windings of the isolating pulse transformers. The main switch, Q_2 in the drive circuit, consists of three 200 V MOSFETs connected in parallel to minimise the voltage drop across the switch. The external triggering signal is applied via switch Q_1 to Q_2.

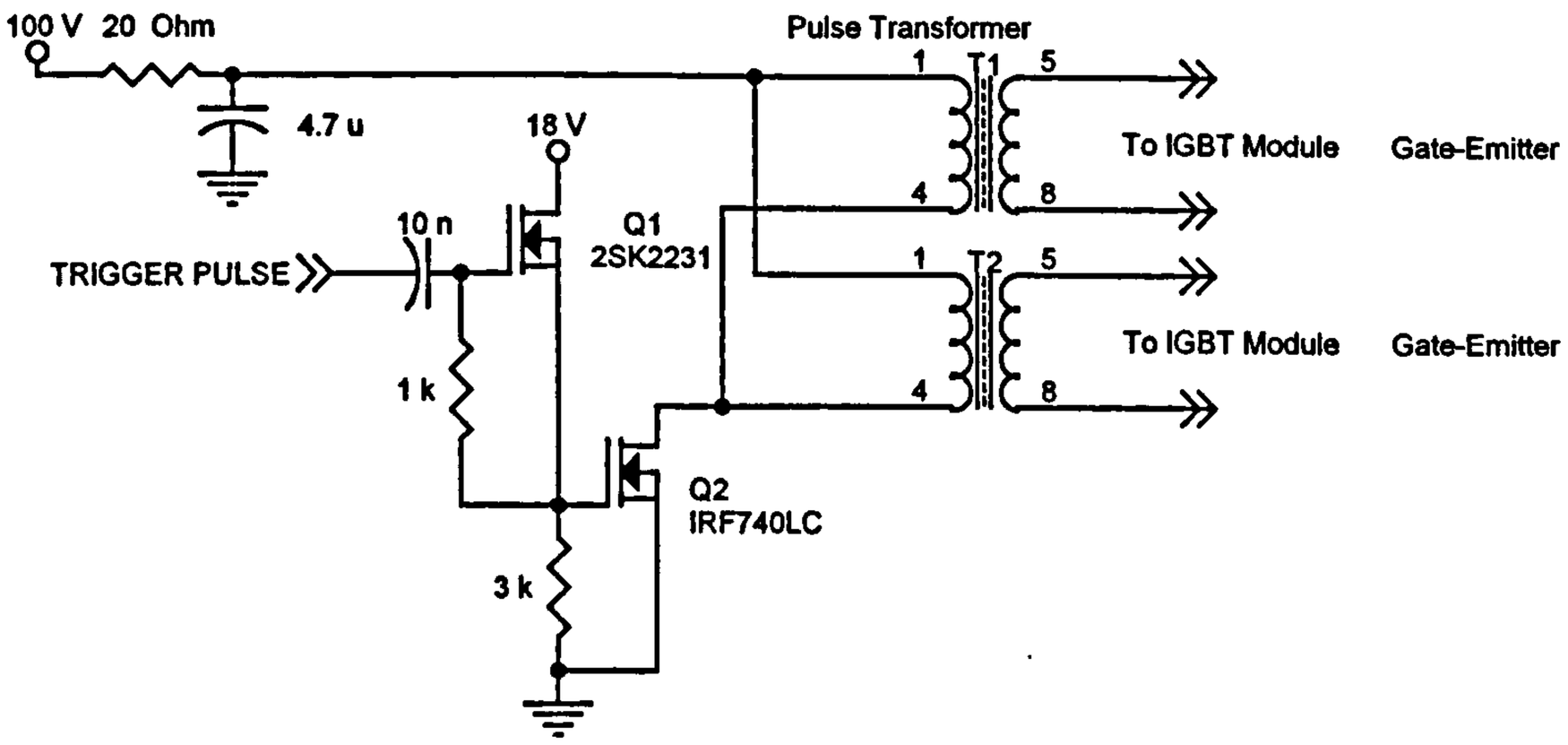

Figure 4.25 Circuit for driving IGBT modules.

For optimal synchronisation between stages, the primary windings of the pulse transformers should be connected in series. However, experimental results show that by connecting the primary windings in parallel, the output pulses are faster due to lower inductance in the drive circuit, and if identical pulse transformers are used, synchronisation can also be achieved. During stacking, it was observed that for voltages above 6 kV, voltage discharge occurred due to poor insulation between the windings of the pulse transformers and the aluminium plates. This problem was overcome by placing an insulating sheet between the pulse transformers and aluminium plates as shown in Figure 4.24.

4.5.2 Stack over-voltage protection

As discussed earlier, over-voltage protection of IGBTs in a stack can be achieved by connecting fast non-linear voltage arresters such as the *Transil* or *Transient Voltage suppressor* across the IGBT modules. Experimental results reveal that these devices can only be used for low voltage IGBTs (< 600 V). By connecting them in series, the difference between their rated voltage and the clamp voltage is increased, and so the voltage rating cannot be improved by placing them in series. This limits their application for stacking 1.2 kV IGBTs.

It is apparent that any undesirable over-voltage across the stack modules appears as an additional voltage across the bottom stage of the stack. Therefore, if the voltage across the bottom stage is monitored and compared with a reference voltage, over-voltages can be detected. This method can be used to improve the immunity of the total stack to short and long-term over-voltages. Using a resistive voltage divider, a fraction of the voltage across the bottom module is sampled and compared with an adjustable reference level. If the voltage across the module exceeds the limit, then a disable signal is sent to the high voltage power supply to stop charging the pulse-forming network (PFN).

The power supplies used in this study were WR series from Glassman High Voltage Inc. providing high voltages to 20 kV. Some of the available terminals on the back of these power supplies are INTERLOCK (pin 3), COMMON (pin 2) and HV ENABLE (pin 11). The COMMON terminal is the instrumentation/measurement return. Normally, COMMON is at ground potential. The INTERLOCK terminal must be connected to COMMON to enable the supply. There is a jumper that connects these two terminals that can be removed and replaced by an external switch/relay. If the external switch is opened, the supply output will drop to zero. When the switch is again closed, the front panel HIGH VOLTAGE ON pushbutton must be depressed to re-enable the supply. The HV ENABLE terminal must be connected to a positive 2.5-15 V source (with respect to COMMON) to enable the supply. A 0-1.5 V signal at this

input will disable the supply. In order to use these facilities on the power supplies for stack over-voltage protection, the circuit shown in Figure 4.26 was designed.

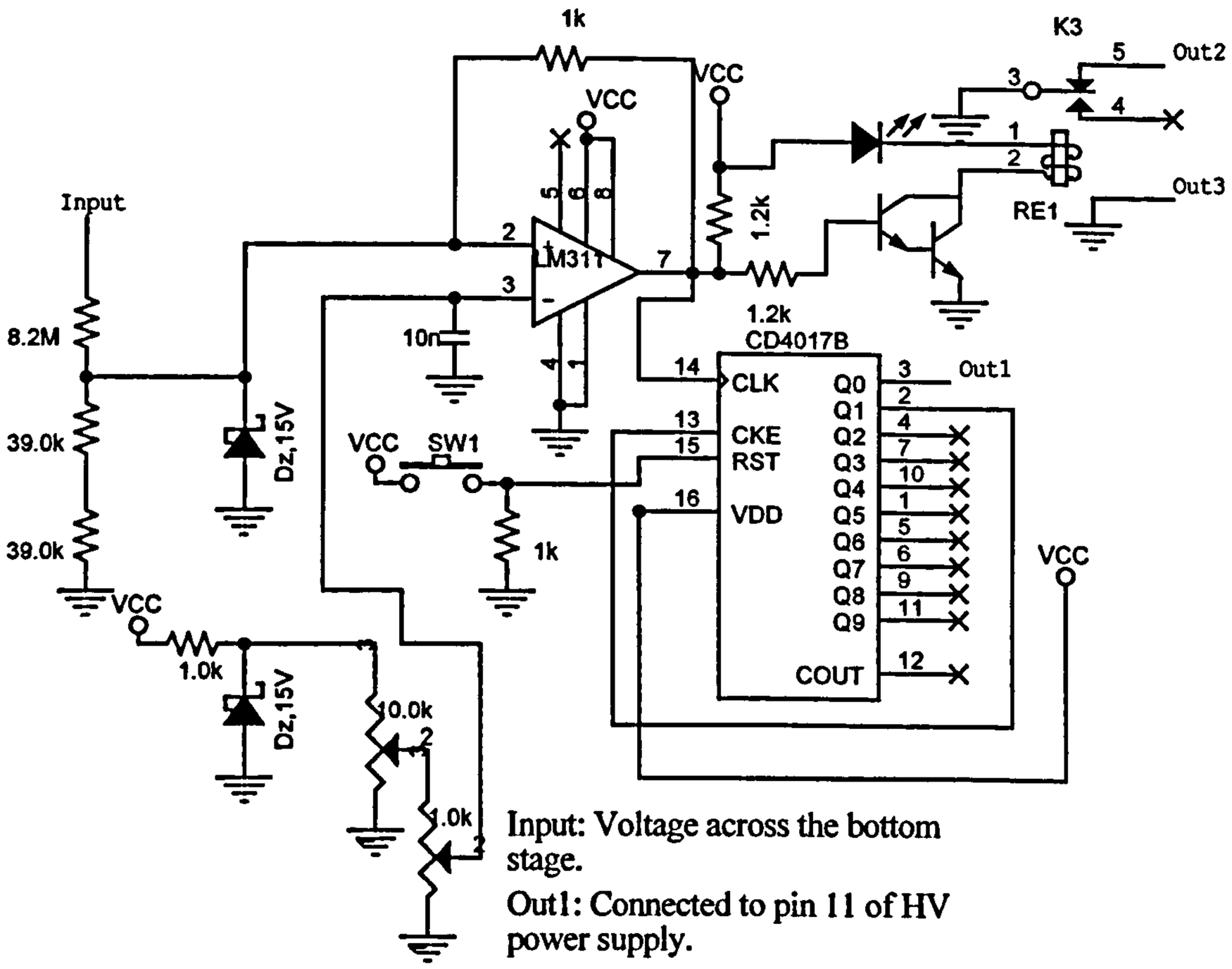

Figure 4.26 Circuit for over-voltage protection of IGBTs in a stack of 10 kV.

Using the voltage divider, 0.94% of the voltage across the bottom module in the stack is sampled and compared with a reference signal that has been set for a maximum voltage of 1 kV across the bottom stage in the stack. If the sampled voltage exceeds the reference voltage, the output of comparator, LM311, jumps from low (~0 V) level to high (~18 V) level. Relay RE1 is activated and pin 3 of the HV power supply is disconnected from ground. This disables the HV power supply. The HV power supply can be restarted by pressing its reset pushbutton. Initial experiments showed that this technique could not be applied for fast and short time over-voltages due to the long reaction time of the relay. Therefore the circuit was modified using a decimal counter

CD4017. In the normal operation of the stack, the Q0 output of the counter which has been connected to pin 11 of the HV power supply, remains at high level and therefore enables the power supply. If the sampled voltage exceeds the reference voltage, a pulse is applied to the CLK of the counter. This changes the Q0 output of the counter (connected to pin 11 of the HV power supply) from high to low and the output Q1 (Pin 3) from low to high level. Then both the HV power supply and the counter are disabled. Pressing the reset pushbutton SW1 restarts the HV power supply. Therefore, for short term over-voltages, the disable signal only inactivates the power supply, and pressing the reset pushbutton on the drive circuit returns the voltage to the switch. For long-period over-voltages, the disable signal switches off the power supply, and to restart the system, the power supply must be reset.

4.5.3 Stack switching performance

A photograph of the completed IGBT stack, consisted of 10×5 1.2 kV IGBTs in a series/parallel configuration is shown in Figure 4.27.

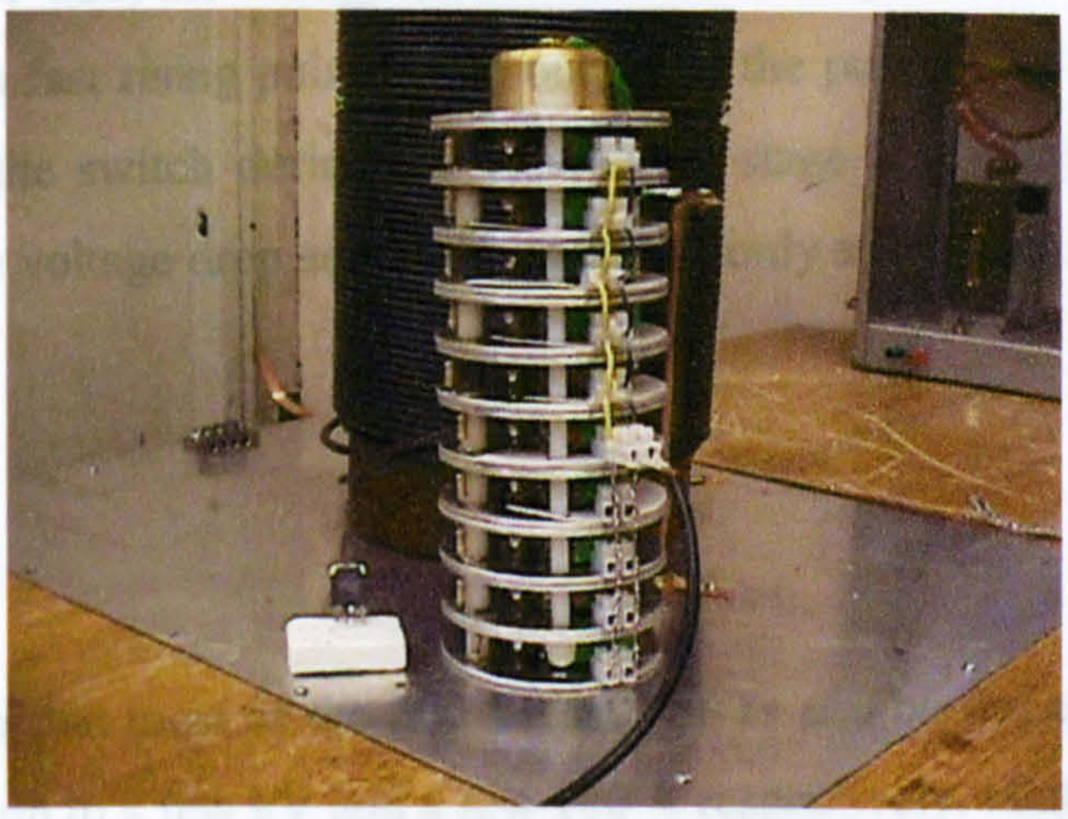

Figure 4.27 Photograph of 10 kV, 400 A stack of IGBT modules consisting of 10×5 1.2 kV IGBTs.

The switching performance of the stack shown in Figure 4.27 was investigated using the 25 Ω input-impedance, 250 ns Blumlein pulse generator. The pulser was terminated in a matched (50Ω) load (Copper sulphur resistance), and switch successfully operated at its voltage and current ratings (400 A and 10 kV). Voltage

waveforms across different stages were monitored simultaneously and no significant over-voltages were observed. Voltage waveforms recorded across the switch and generator output are shown in Figure 4.28.

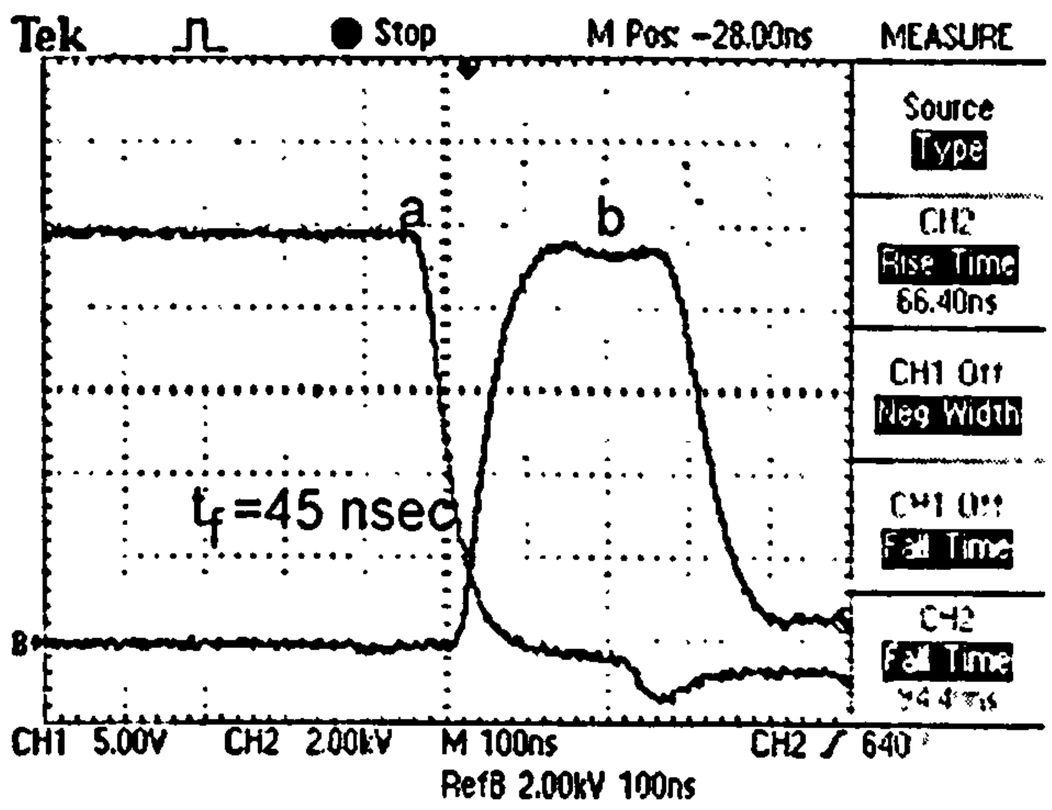

Figure 4.28 Voltage waveform across the switch (a) and output voltage pulse (b) for a 25 Ω input impedance pulse generator (amplitude 2 kV/div and time base 10(ns/div).

As shown in Figure 4.28, the voltage across the stack collapses in less than 50 ns (10-90%), leading to a fast rising pulse at the output of the pulser. The negative voltage appearing across the switch during the conducting stage is a result of a diagnostic instrument and the voltage drop across the switch is only a few tens of volts.

4.6 Summary

It has been shown that most of the 600 V fast IGBTs can be stacked for voltage and current ratings of up to a few kV and a few 100 A respectively. Higher ratings are also possible, but this leads to slower switching speed. A prototype 2.5 kV, 250 A stack consisting of 25 × 600 V IGBTs was constructed and tested with a 10 Ω input impedance, Blumlein pulse generator.

For 1.2 kV IGBTs, dual degradation of the collector-emitter voltage was found to exist in some of them. A reason for this behaviour may be fast variations in device parasitic parameters such as gate-collector capacitance. Operating 1.2 kV IGBTs in fast pulse

circuits leads to a higher voltage gain resulting in an increased Miller effect. This leads to further disruption of the voltage collapse across the IGBTs. Therefore, care must be taken when choosing the 1.2 kV IGBTs for stacking in pulsed applications. Using a computer simulation program, the switching performance of different types of 1.2 kV IGBT devices was investigated and the most suitable devices for stacking were selected. A prototype stack of commercially available 1.2 kV IGBTs was designed and built for use as a closing switch in a 25 Ω input impedance, Blumlein pulse generator using a magnetic isolating technique. The switch was operated at voltage and current ratings of 10 kV and 400 A, respectively, with a voltage fall-time of about 45 ns. The output pulse had a flattop pulse-width of about 200 ns in 250 ns Blumlein pulse generator. These satisfied the performance requirements of Table 4.2.

In chapter 5, the use of optical isolation rather than magnetic isolation will be described. This allows the use of an increased number of devices and hence an increase in voltage rating for the switch. It will also be shown to improve the operating performance of the switch in terms of jitter and switching speed.

Chapter 5

IGBT STACKING USING OPTICAL COUPLING

As discussed in section 4.3, when stacking IGBT devices with isolation of more than 10 kV, pulse transformers with bigger cores must be used and this requires additional circuitry. The isolation problem can however be addressed in a more efficient way through optical coupling. Opto-coupler devices are commercially available with maximum isolation voltages of a few thousands volts, but initial experiments show that they tend to be slow and have significant device-to-device delay. Optical fibre links, on the other hand, provide virtually unlimited voltage isolation, and they can be tailored to keep device-to-device delay at a low level.

This chapter discusses the approach and procedure leading to the system finally adopted for stacking ten 1.2 kV IGBT devices using optical coupling.

5.1 Basic Optical System

A basic optical isolating system consists of a light source (transmitter), a length of optical fibre and a light detector (receiver). The emitter converts the initial electrical signal into an optical signal that then propagates along the fibre; the optical signal is collected by the detector and converted back into an electrical signal, which in an ideal system will be the same as the initial electrical signal. In order to achieve this the three components of the optical isolation system need to be carefully matched. For example, the spectrum of the source should closely match the responsivity of the detector and the fibre should be capable of transmitting the light with minimum loss. Furthermore, the divergence of the source should match the numerical aperture (NA) of the fibre so that there is good light collection and similarly the NA of the fibre should match well with the collection angle of the detector for the same reason.

For the present work, the light source has to be capable of being switched on and off rapidly, that is, it should have a high frequency of modulation. This means that it

needs to be a low electrical power device so that rapid switching is readily achieved. The light sources that satisfy this condition most closely are solid-state devices, namely light-emitting diodes (LEDs) and laser diodes. The main differences between the two are in

(i) their modulation frequency – modulation bandwidths of LEDs are limited to below about 300 MHz, whereas laser diodes can readily be modulated at frequencies up to 1 GHz, and

(ii) their optical power spectrum - a typical LED has a spectral linewidth of between 20 nm and 100 nm, while the typical spectral linewidth of a laser is between 1 nm and 5 nm.

For long-distance, large bandwidth communications, laser diodes are used because of their large bandwidth and narrow linewidth. They are used in conjunction with single-mode optical fibres made from silica. This type of fibre shows little dispersion and attenuation, and maintains the shape of the initial optical pulse during transmission over hundreds of kilometres. In the present work, dispersion and attenuation are not critical since the optical signal is transmitted only over a very short distance (50 cm), and so multimode plastic fibres can be used. This allows fibres with a large NA to be used so that as much of the divergent light of the emitter as possible can be collected and transmitted to the detector.

In this project, ten modules of IGBTs are to be stacked. This requires ten isolated switching pulses. The switching pulses have to be matched, synchronised and the delay between them needs to be not more than a few nanoseconds.

5.2 Prototype optical system

Initial tests were carried out using optical emitters and detectors available in modular form. The results showed however that optical modules could not be used for optical coupling of muti-unit systems because of significant differences between modules in performance characteristics. The alternative was to use optical devices, which are available either in component form, or aligned in SMA/ST style housing offering PCB or bulkhead-mounting option. Modular optical devices aligned in SMA/ST housing are more expensive than the individual components, a significant part of the

manufacturing cost of a module being associated with the optical alignment. To reduce overall costs for the present IGBT-stacking system, individual components were used in conjunction with the alignment unit shown in Figure 5.2. Fibre and emitter or detector were placed in position and aligned for optimum transmission by making small adjustments to fibre, emitter and detector positions.

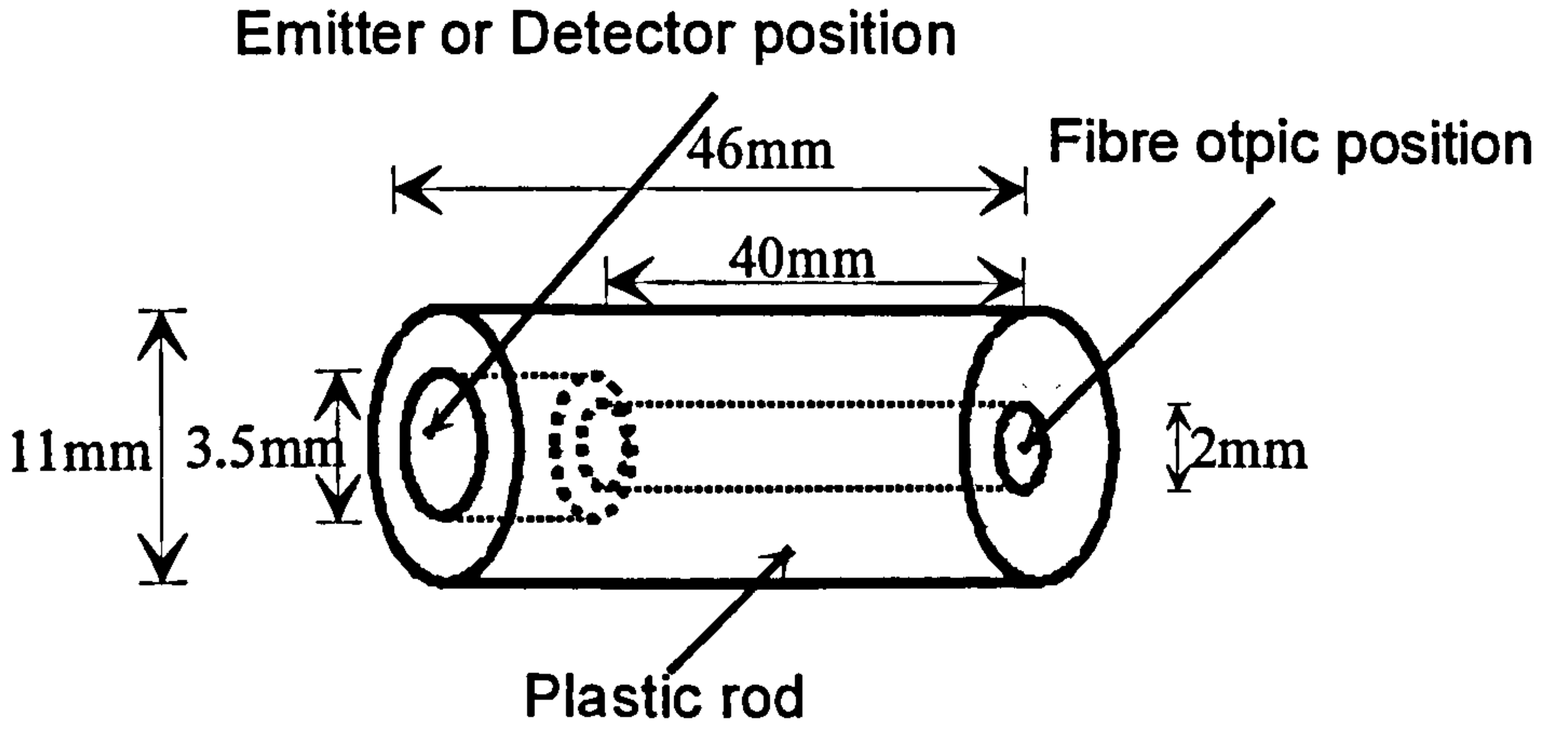

Figure 5.2 Alignment unit for fibre and optical components.

Different types of fast emitter such as the *OD-880L* (opto-diode GaAlAs emitter manufactured by Opto-Diode), the *GL514* (silicon phototransistor manufactured by Sharp), and the *3 mm ultra-bright red LED* (manufactured by Ledtech) were tested using the unit shown in Fig 5.2 according to the circuits recommended by the manufacturers. Initial results showed that to minimise delays between firing signals, the emitters have to be driven by current pulses with a magnitude of a few amperes. As the power dissipation in the device cannot exceed the rating given by the manufacturer, the pulse duration has to be reduced. This required some improvement in the drive circuits recommended for the emitters and detectors. The diagram of the first drive circuit for the optical emitters is shown in Fig 5.3. In this circuit, the duration of the current passing through the emitters is controlled by the voltage pulse applied to the MOSFET switch. Upon firing the MOSFET switch, the power supply voltage appears across resistor R2 and the optical emitters. Resistor R2 has been bypassed by capacitor C2 to increase the initial peak current and to improve the turn-on speed of the emitters.

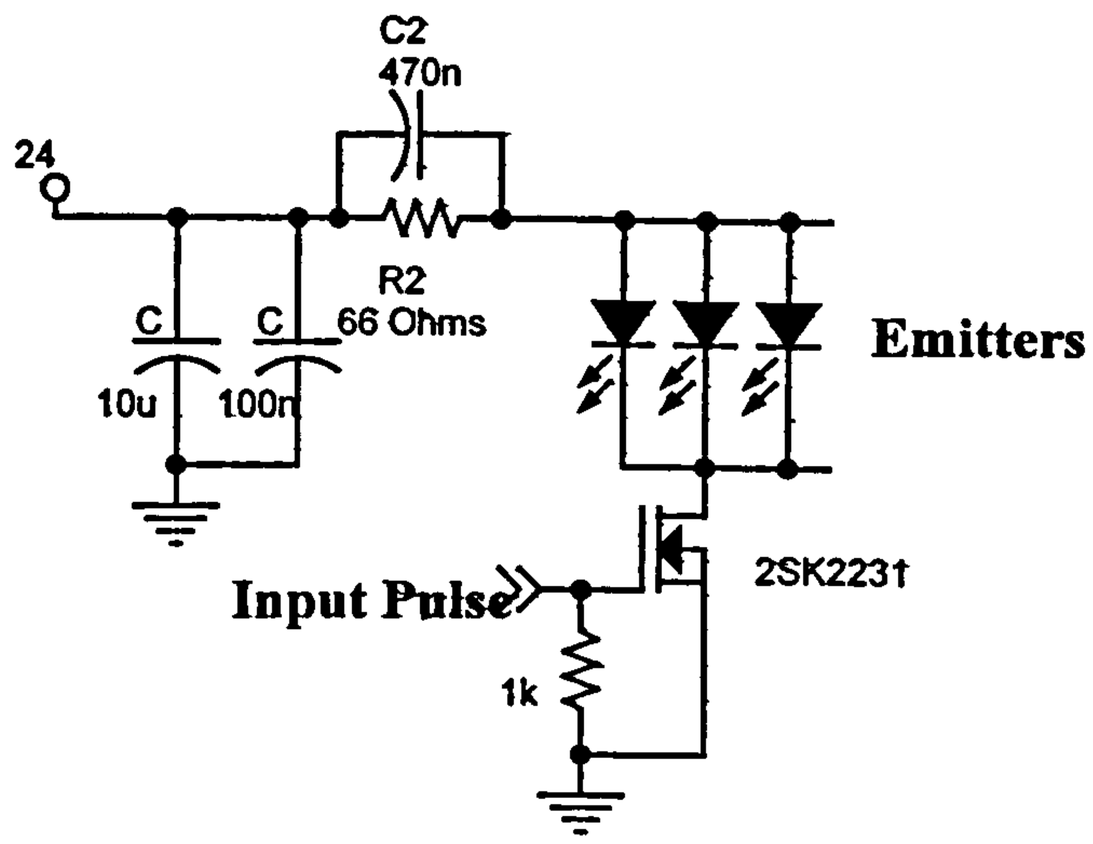

Figure 5.3 Diagram of the drive circuit for optical emitters.

The performance of the drive circuit was satisfactory over a period of time, but the following issues led to a redesign of the circuit:

- Applying a long trigger pulse across the gate-source of MOSFET 2SK2231 could damage all the optical emitters.
- In the case of a spurious switch short circuit, the power supply will be short circuited via the optical emitters and resistor R1. This results in major damage to the emitters and power supply.
- Switching on and off the power supply can create a transient in the circuit, leading to failure of the emitters.

The drive circuit was therefore modified as shown in Figure 5.4.

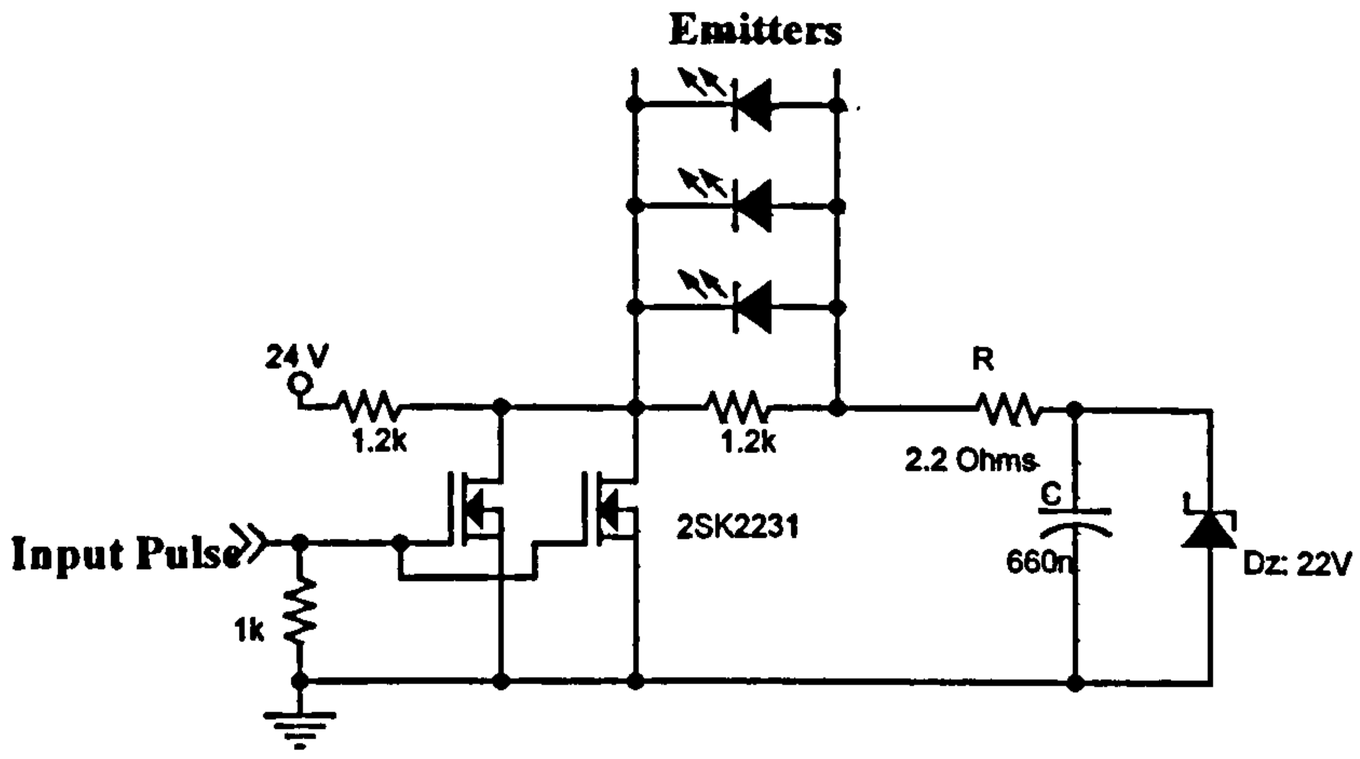

Figure 5.4 Diagram of the improved drive circuit for the optical emitters.

Capacitor C in Figure 5.4 is initially charged through the 1.2 kΩ resistors and resistor R to the voltage of the Zener diode (22 V). Upon firing the MOSFET switches, capacitor C is discharged through resistor R and the optical emitters, which have been connected in parallel. Resistor R and capacitor C, respectively, control the peak discharge current and the maximum energy dissipated in the optical emitters. For the component values in Figure 5.3, a peak current of a few tens of A with a small rise-time (50 ns) passed through each of the emitters. By tailoring the rates of rise of current through the optical emitters and minimising turn-on delays, it was possible to produce homogeneous switching of the assembly.

At the detector, a current proportional to the intensity of the optical radiation is generated. In optical communications, the reverse current of the detector is amplified using a pre-amplifier, and finally using a comparator, the logic voltage is produced. This technique cannot be applied in multi-unit optical-decoupling systems as the comparator causes variable delays between receiver outputs. Therefore a drive circuit based on single solid-state components, as shown in Figure 5.5, was designed and tested. Here the optical pulse at a detector is converted to a voltage pulse using a Darlington transistor. This provides the required gain. In the second stage, the pulse magnitude and rate of rise are increased using a fast PNP transistor and finally, in the final stage, the trigger pulse for charging the gate-emitter of an IGBT module is generated by reducing the output impedance of the circuit using a MOSFET driver. A 33 kΩ resistor connects the base of the Darlington transistor to ground to limit the input impedance of the drive circuit and improve the noise immunity of the circuit.

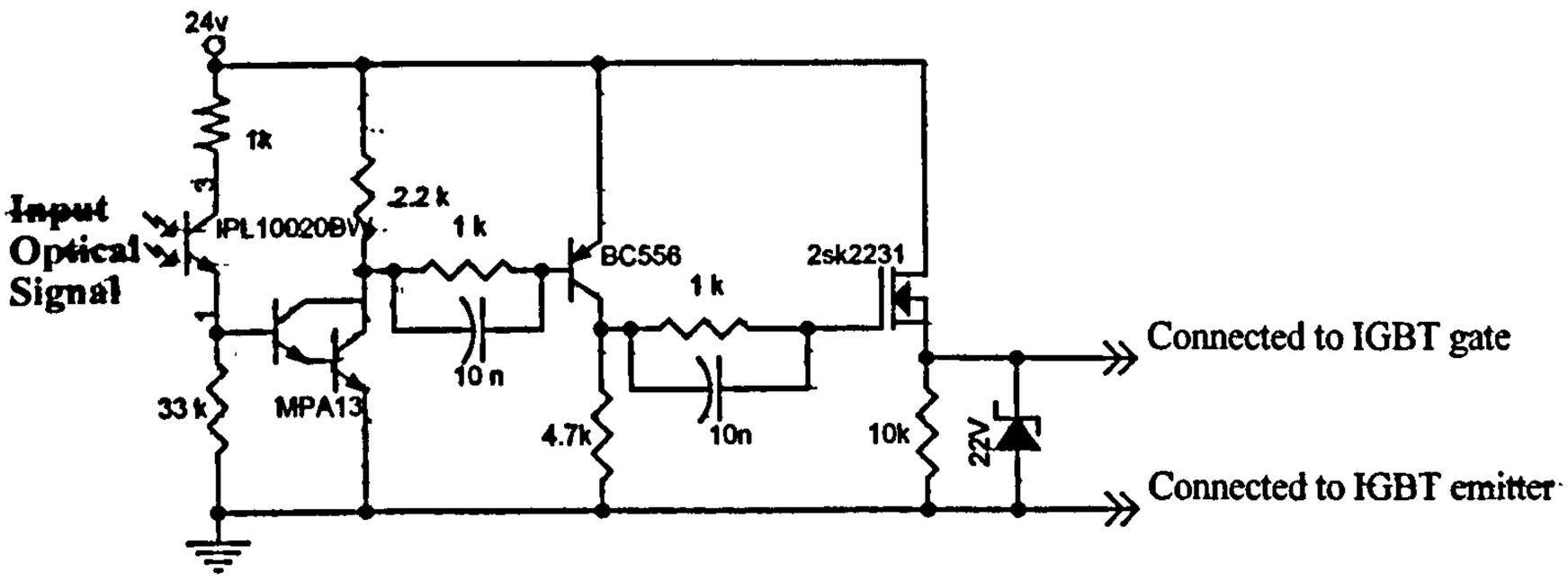

Figure 5.5 Circuit diagram of the driver for the optical detectors.

Different types of detector such as the *BPX65/BPX65RT* (manufactured by Centronic), the *AEPX65* (manufactured by Centronic) and the *IPL10020BW* (manufactured by Texas Instruments) were tested using the drive circuit of Figure 5.5 with the unit shown in Figure 5.2. The emitter and detector tests led the choice of a *3 mm ultra-bright red LED* as source and an *IPL10020BW* as detector. This emitter and detector displayed better performance in terms of the rate of rise of output pulse compare to other tested devices. They have peak spectral responses of 660 nm and 750 nm, respectively. Three identical optical-coupling modules, each consisting of an *IPL10020BW* and a *3 mm ultra-bright LED* were assembled in conjunction with the drive circuits shown in Figure 5.4 and Figure 5.5. The DC power supply for the circuits was provided using three 9 V batteries for each module. Voltage waveforms at different nodes of the drive circuits were observed and compared in terms of speed and delay. For example, the voltage waveforms at the collectors of the Darlington transistors of the three modules are shown in Figure 5.6. There is a time delay of about 50 ns between the voltage waveforms at the collectors of the Darlington transistors. This led to a similar delay between the final triggering pulses.

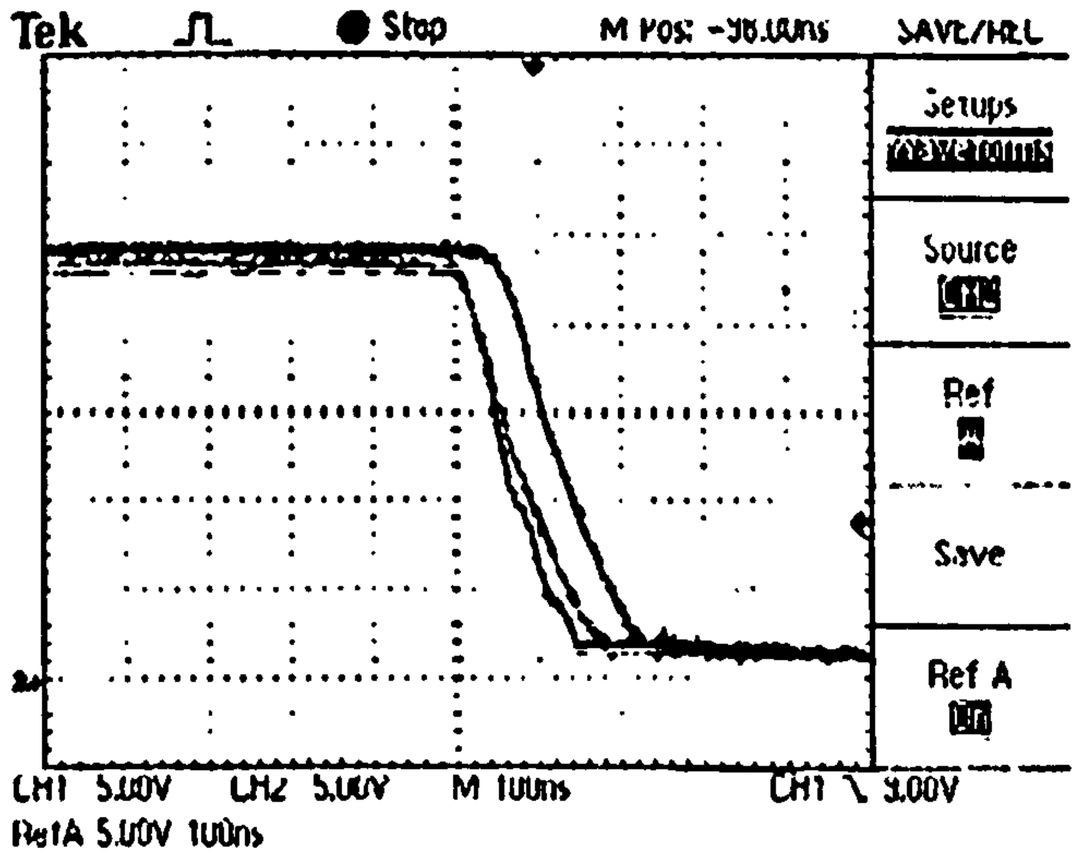

Figure 5.6 Voltage waveforms for three optical coupling modules, as measured at the collector of the Darlington transistor in the drive circuit of each..

This delay between modules is believed to be due to the different switching speeds of the optical detectors. Using a potentiometer to control the bias currents of the Darlington transistors, the voltage pulses can be synchronised. It was found however that any small variations in pulse repetition frequency or duty cycle of the optical pulses required the potentiometer to be readjusted. It was also observed that any

slight movement of a fibre could cause changes in the delay and rate of rise of an output pulse. This problem was solved by polishing the fibre ends and ensuring that the ends were perpendicular to the fibre axes.

Solid-state switching devices have a very low jitter. However, when these devices are stacked and driven through optical coupling systems, the jitter associated with the drive circuit may cause additional jitter in the voltage across each device and stack. In order to obtain a measure of this jitter, two modules, each of five IGBTs in parallel, were used in two 800 V identical charge/discharge systems as shown in Figure 5.7. Both modules were triggered optically via a common pulse.

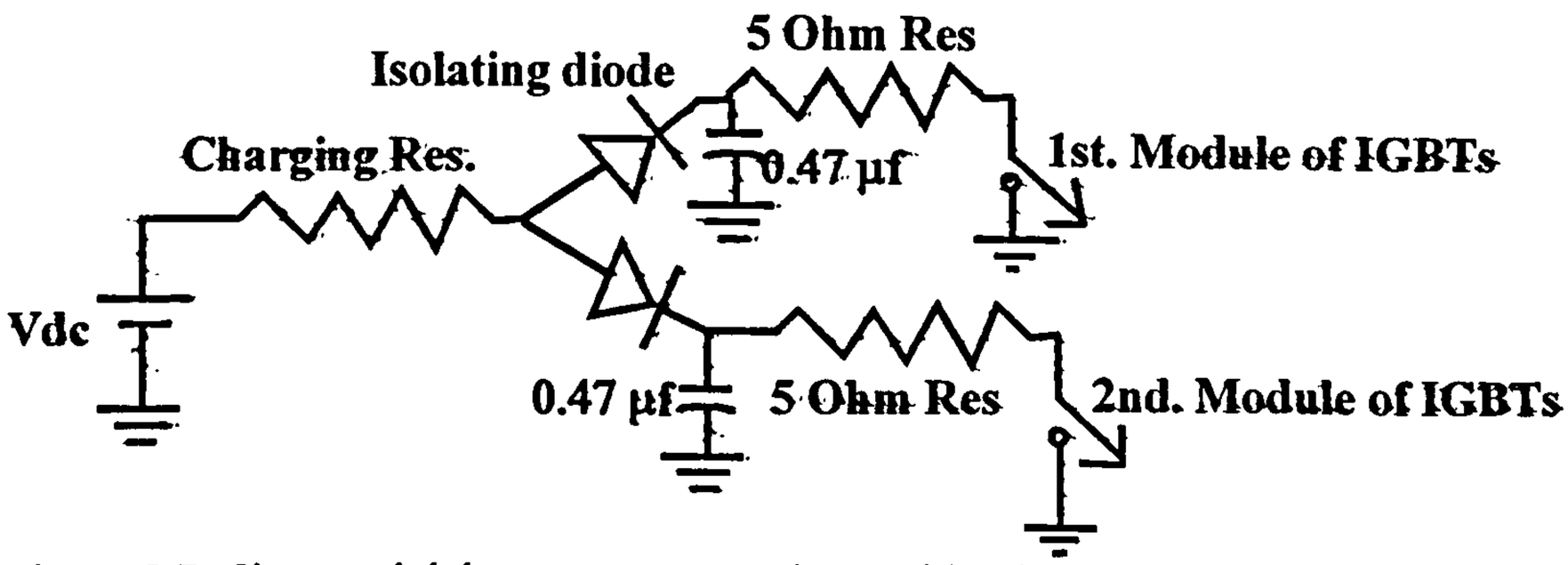

Figure 5.7 Jitter and delay measurement in two identical optically triggered IGBT modules.

Voltage waveforms across both IGBT modules were monitored and the delay between them (the measurements were carried out at a point where the voltage reached half of its maximum value) was measured at four different switching frequencies; 0.1 Hz, 1 Hz, 10 Hz and 20 Hz, for 15 shots in each case. The delay and jitter between the voltage waveforms across the IGBT modules were found to be independent of switching frequency and had maximum values of 6.8 ns and 0.8 ns, respectively. These small values are considered to be acceptable.

5.3 Final optical system

The results of driving IGBT modules using *3 mm ultra-bright LED* and *IPL10020BW* devices were satisfactory and showed the possibility of using the devices in stacking IGBT modules. However, during experiments and stack assembly it was observed that

optimum performance required careful adjustment of fibre and emitter/detector positions within the alignment units of Figure 5.2. Clearly, this is not acceptable if a robust and reliable system is to be produced. It was decided therefore, somewhat reluctantly, that it was necessary to move to higher-cost optical components such as emitters and receivers aligned in SMA/ST style housings. An *FFT2000BHR* (bulkhead emitter with peak wavelength of 660 nm, Honeywell Optoelectronics) and an *FDR850IR* (bulkhead receiver with peak wavelength of 850 nm, Honeywell Optoelectronics) are devices that offer PCB or bulkhead-mounting options and which are suitable for optical coupling of many units.

The DC voltage required by the drive circuit of the *FDR850IR* detectors could be provided from the voltage across the IGBT modules (self-excited drive-circuit) by adding some components to the circuit shown in Figure 5.5. As shown in Figure 5.8, a 220 nF capacitor is charged to 44 V from the voltage across the IGBT module (~ 1.0 kV) through a 680 kΩ charging resistor.

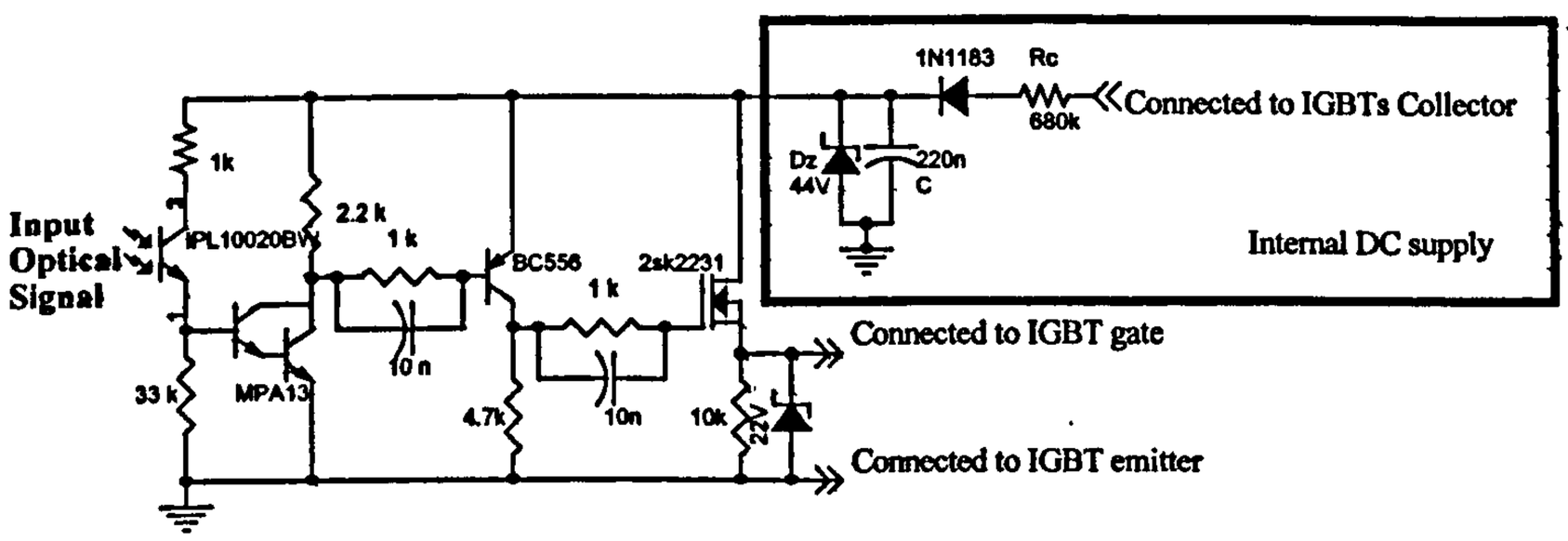

Figure 5.8 Using the voltage across the IGBT modules to drive the optical detectors (self-excited drive-circuit).

Capacitor C and resistor Rc determine the maximum operating frequency of the drive circuit. For long pulse durations, C has to be large enough to maintain the required charge for driving the components of the drive circuit. A large value of C means a small value of R_c, which increases the leakage current of the IGBT stack. Therefore a balance has to be struck in component selection and design according to the stack operating conditions.

The self-excited drive-circuit was tested using the components depicted in Figure 5.8. The delay and jitter existing between two optical coupling units were also measured in a circuit similar to that in Figure 5.7. The delay and jitter were independent of the operation frequency and had maximum values of 2.2 ns and 0.3 ns, respectively. The delay and jitter for the self-excited drive-circuit are lower than those recorded for the drive circuit powered by batteries, and this is likely due to the use of a higher DC voltage (~ 44 V) in the drive circuit, which leads to faster charging of the gate-emitter capacitors of the IGBT devices.

5.4 Stacking IGBT devices using optical coupling

In order to assemble a solid-state pulser using optical coupling for a switching system with the same performance requirements as that presented in Table 4.2, a procedure similar to that used for IGBT stacking with magnetic coupling was used. The same configuration was found to be suitable for mounting the IGBT devices and the only change was the replacement of the pulse transformer in each stage by the circuit shown in Figure 5.8.

The components of the circuit for driving the optical emitters (ten *FFT200BHR* devices in parallel) were transferred from the strip board to a printed circuit board (PCB) and the circuit was housed in an EMI/RFI shielded aluminium alloy diecast box. The circuit was powered by three PP3, 9 Volt batteries in series. Use of shielding and batteries minimised electromagnetic and radio interference. A typical current waveform passing through one of the emitters is shown in Figure 5.9.

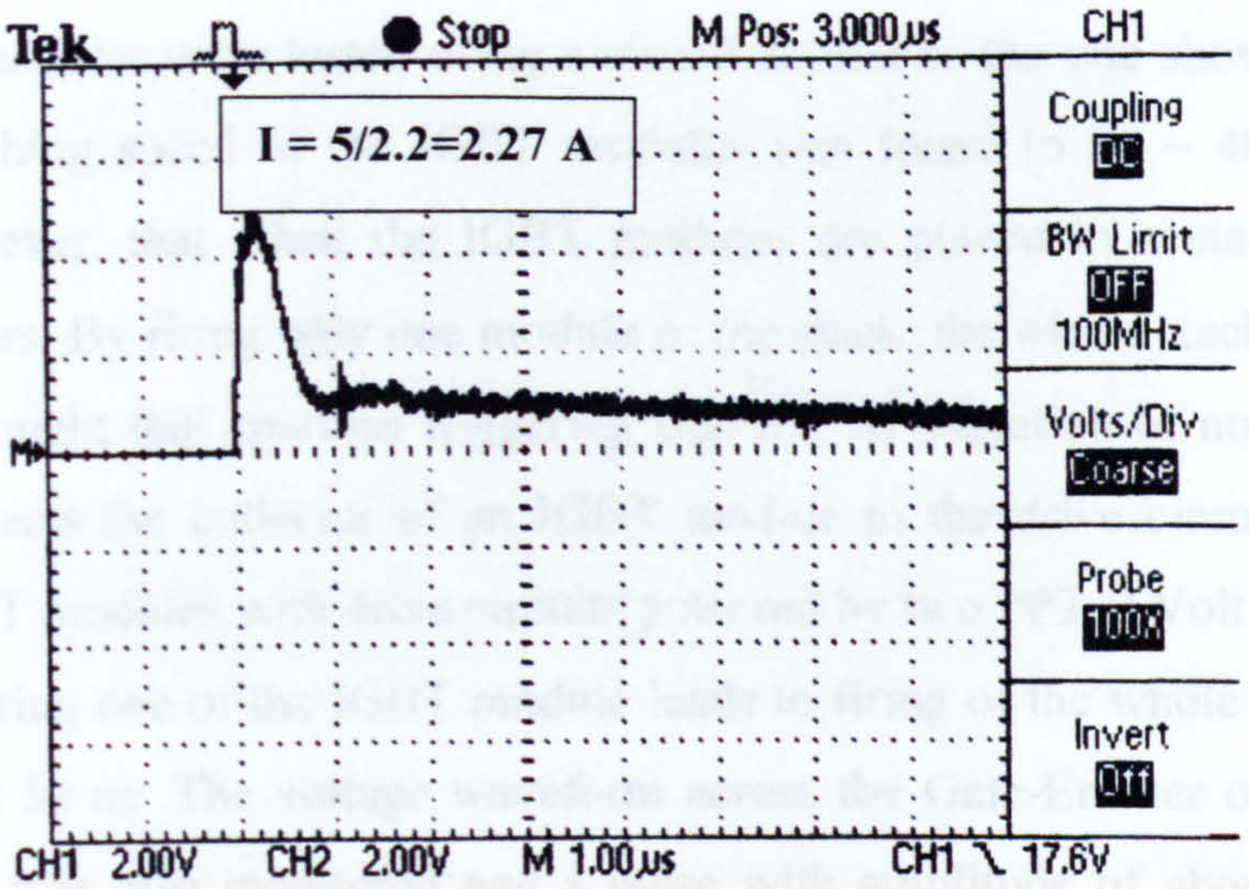

Figure 5.9 Current waveform passing through an emitter measured in drive circuit of Figure 4.4 .

The initial peak current passing through a *FFT200BHR* was about 2.2 A and much higher than the continuous current specified for this device (~ 50 mA). As described earlier, this initial peak current helped to increase the switching speed and hence reduce the delay between the triggering pulses. The drive circuit of the detectors was also transferred to a PCB, as shown in Figure 5.10, and placed beside the IGBTs in the gap provided between the two aluminium plates.

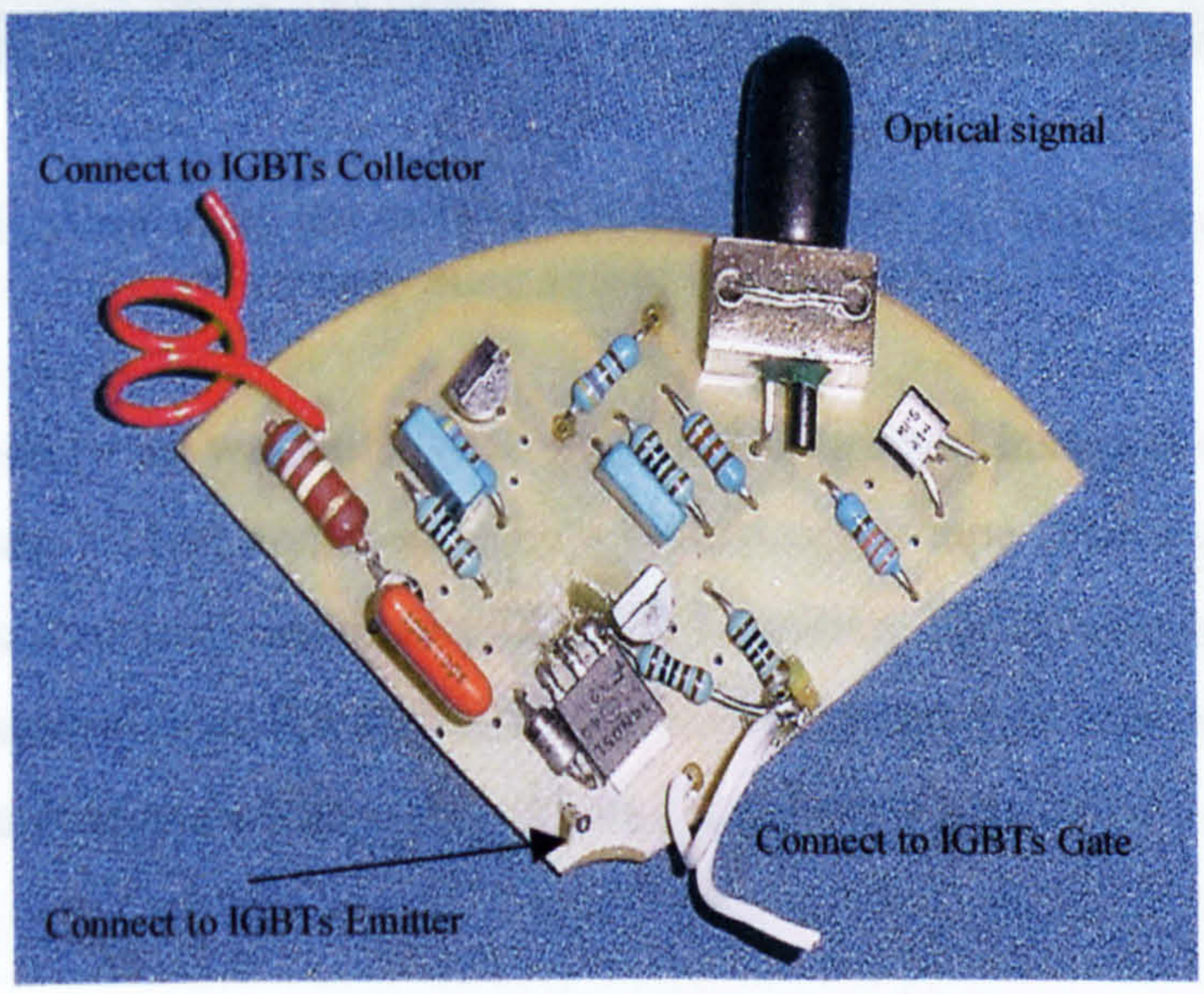

Figure 5.10 Photograph of the final PCB for driving detectors.

Single IGBT modules were tested using a circuit similar to the one shown in Figure 4.1. The switching speed of the IGBT modules was found to be ~ 40 ns. It was observed, however, that when the IGBT modules are placed in a stack, spurious triggering occurs. By firing only one module in the stack, the whole stack is fired. At first, it was thought that spurious triggering was due to induction of noise from the path that connects the collector of an IGBT module to the drive circuit. But even when two IGBT modules with drive circuits powered by two PP3, 9 Volt batteries are stacked, triggering one of the IGBT module leads to firing of the whole stack after a delay of about 50 ns. The voltage waveform across the Gate-Emitter of the second IGBT module was also monitored and a pulse with amplitude of about 40 V was observed. Next, the drive-circuit PCBs were placed far from the high-voltage parts and some improvement was achieved. The spurious triggering was therefore assumed to be due to electromagnetic interference (EMI), and in order to protect the drive circuit from EMI, shielding as shown in Figure 5.11 was used.

(a) (b)

Figure 5.11 Protecting the drive circuit against EMI, (a) Insulating, and (b) Shielding using parcel copper tapes.

The drive-circuit board was initially covered with a layer of insulator (parcel tape) as shown in Figure 5.11(a) and then shielded with copper tape. The copper layer was soldered to the terminal connected to the IGBT emitter. The board was then covered with another layer of insulator and finally placed beside the IGBTs as shown in Figure 5.12. This shielding procedure eliminated any spurious triggering.

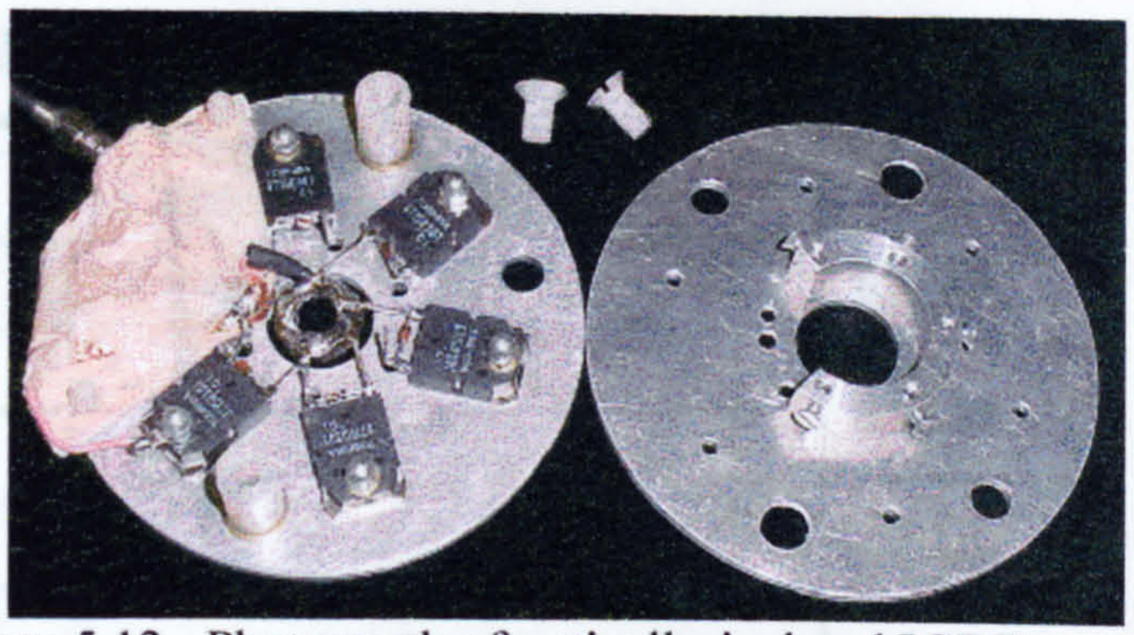

Figure 5.12 Photograph of optically-isolated IGBT module.

A photograph of a completed module of five IGBTs in parallel with optical triggering is shown in Figure 5.13.

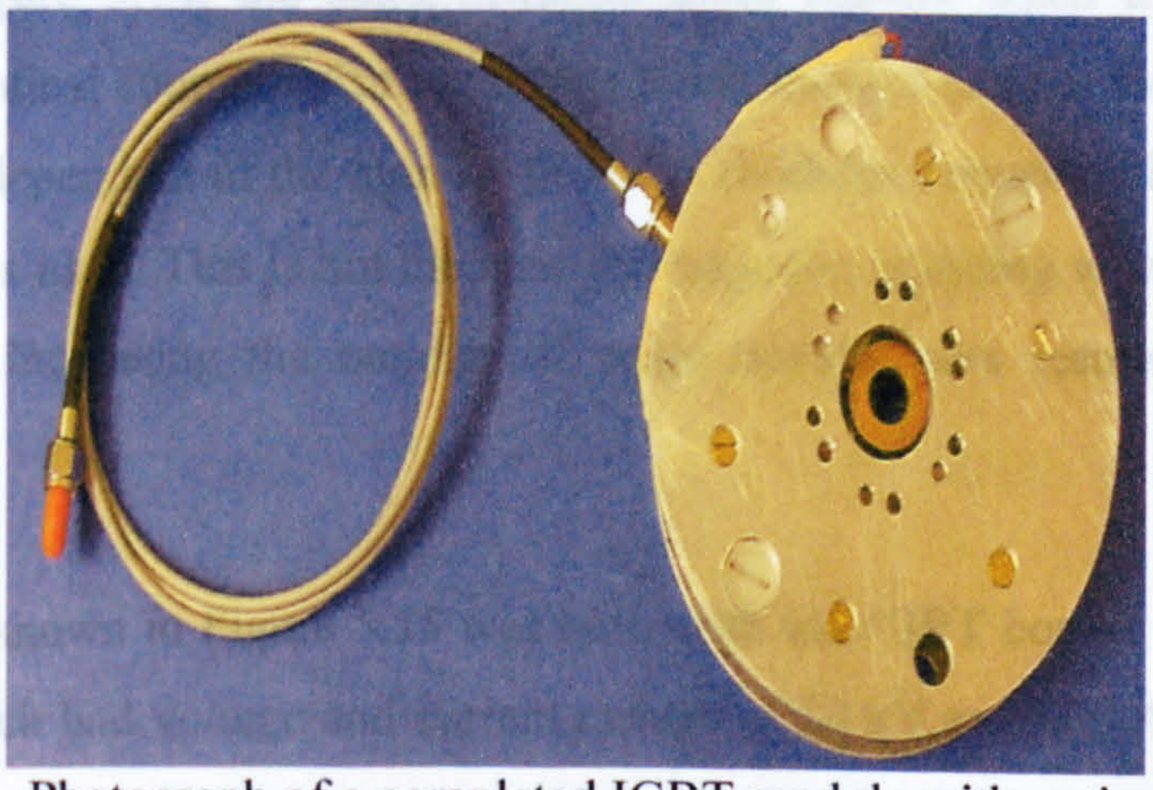

Figure 5.13 Photograph of a completed IGBT module with optical triggering.

The switching performance of this IGBT module was tested in a 1 μs standard Blumlein pulse generator similar to that in Figure 4.1. The voltage waveforms across the switch and the output pulse of the generator were recorded and compared with the results achieved with magnetic coupling. The comparison showed no significant differences between the switching speeds of modules. It was found, however, that by increasing the number of IGBT modules in series, optical coupling provides better performance than magnetic coupling. The voltage waveforms across the stack for both magnetic coupling and optical coupling are shown in Figure 5.14.

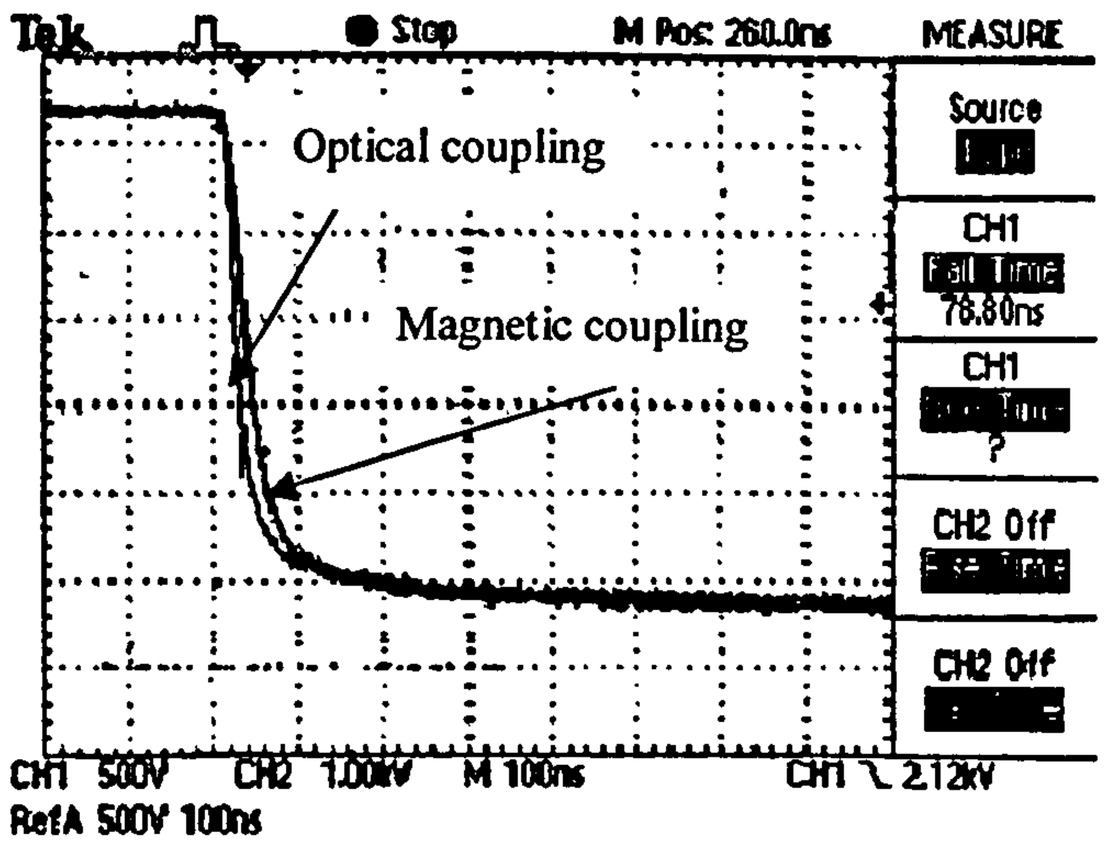

Figure 5.14 Comparison the switching speeds of a stack of three 5 IGBTs in two cases of triggering through isolated transformers and fibre optics.

According to Figure 5.14, the stack switches more rapidly when the IGBTs are triggered using optical coupling. Further experiments showed that the switching speed of the stack is independent of the number of IGBT modules connected in series when optical coupling is used. This is not the case for magnetic coupling where loading the drive circuit by increasing the number of pulse transformers results in a slower switching speed.

The IGBT stack shown in Figure 5.15 was built with ten IGBT boards operating at 1 kV each. The stack had voltage and current ratings of 10 kV and 400 A respectively. The stack switching-performance was investigated using the 25 Ω input impedance, 1 μs Blumlein pulse generator. Over-voltage protection of the IGBT modules was provided by the same protection circuit described in Chapter 4 for an IGBT stack with magnetic coupling.

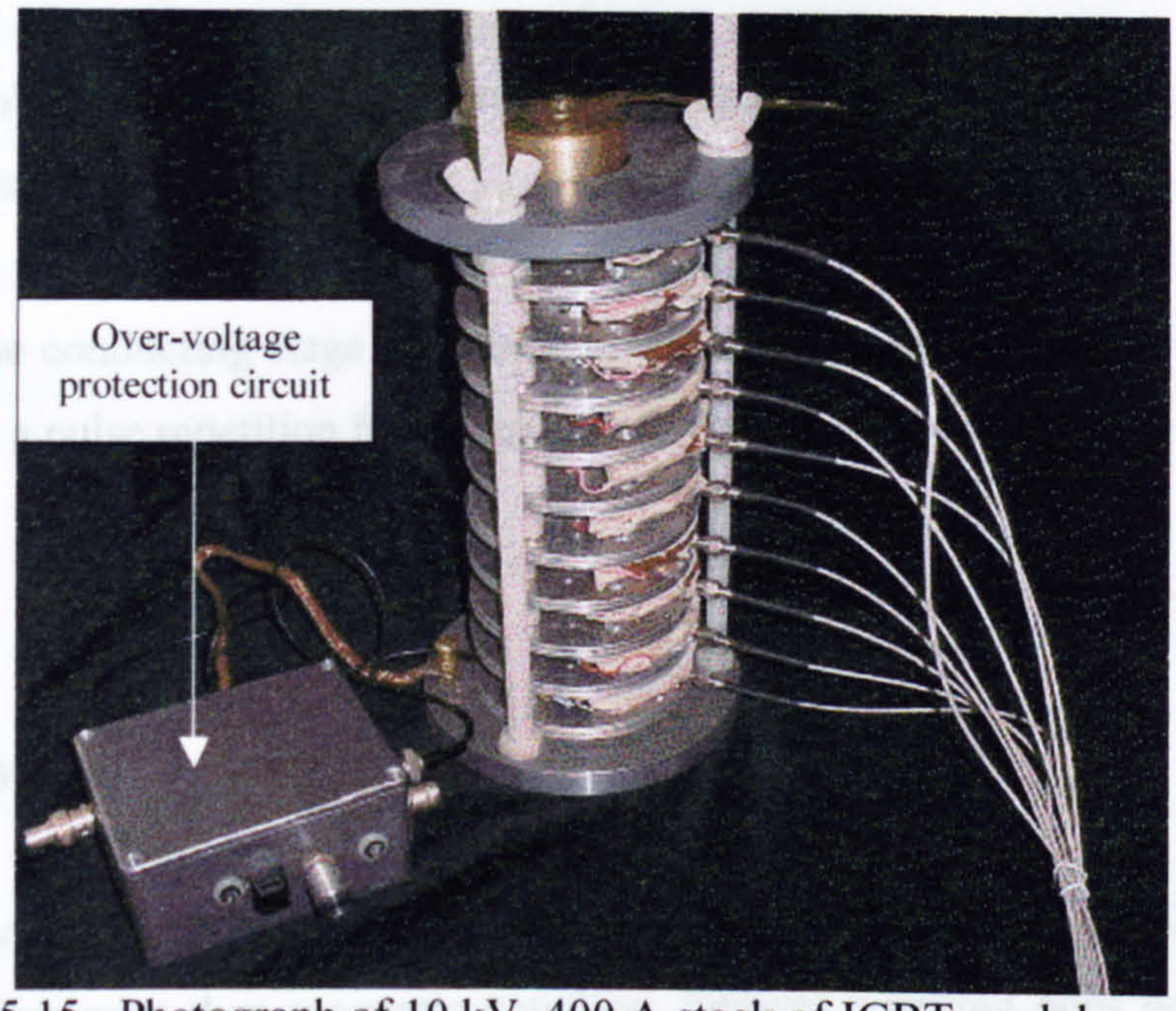

Figure 5.15 Photograph of 10 kV, 400 A stack of IGBT modules, optically triggered.

The pulser successfully operated at a voltage of 10 kV with its output terminated in a matched (50 Ω) load (copper sulphur resistance). The voltage waveform across the switch and the voltage pulse of the generator were monitored and recorded simultaneously as shown in Figure 5.16.

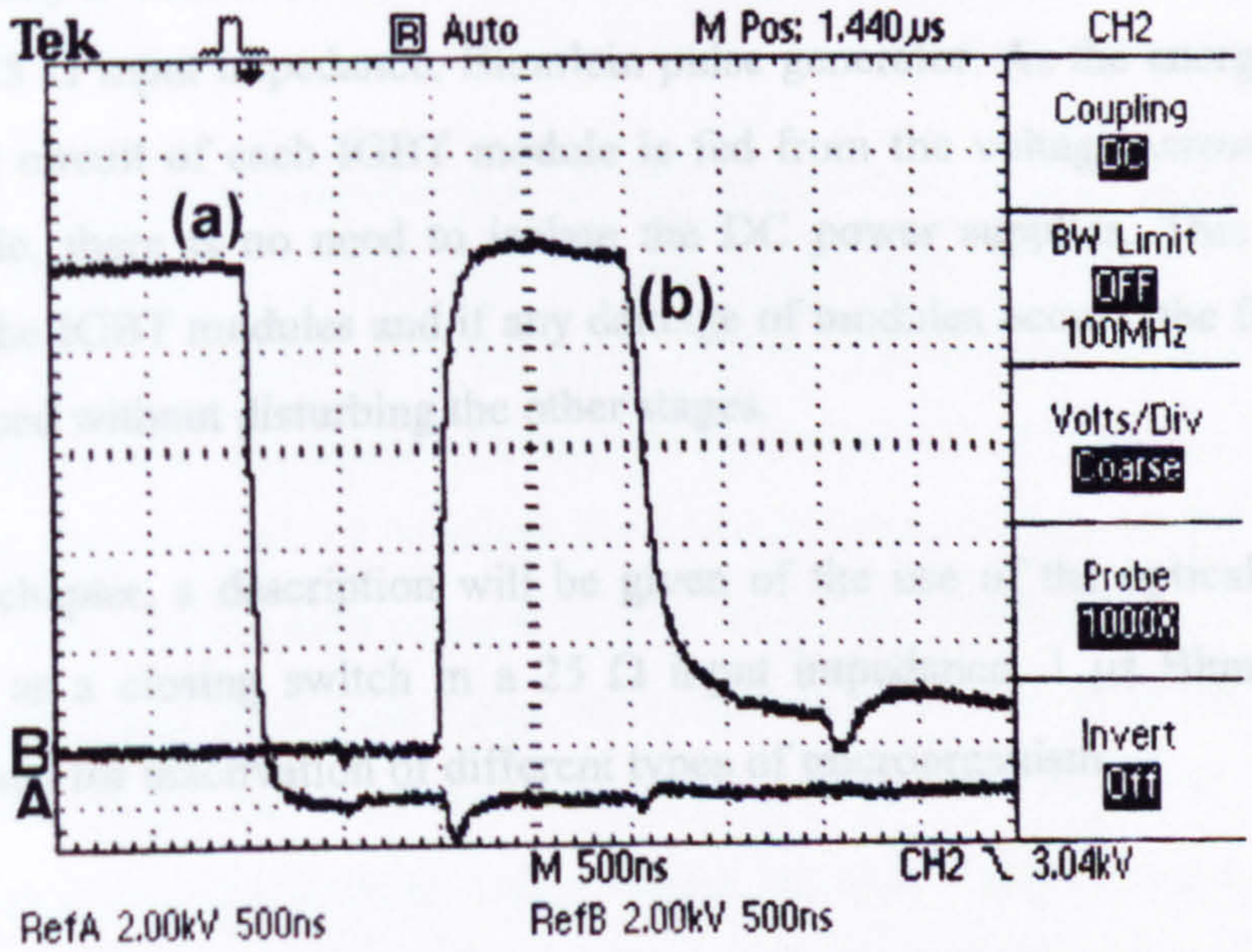

Figure 5.16 Voltage waveform across the switch (a) and output voltage pulse (b) for a 25 Ω input impedance pulse generator (amplitude 2 kV/div and time base 500 ns/div)

The voltage collapse across the stack has a fall-time of less than 40 ns (10-90%), leading to a fast rising pulse at the output of the pulser. The voltage drop across the stack is only a few tens of volts and the small negative voltage appearing across the stack during the conducting stage is caused by a diagnostic instrument. Operation of the pulser with a pulse repetition frequency of a few hundred Hz was also successfully tested.

5.5 Summary

It has been shown that driving IGBT modules with optical coupling provides better switching performance than magnetic coupling. Optical coupling does not produce any limit in the level of the isolating voltage and therefore, on increasing the number of stages in a stack, no extra components need to be added to the drive circuit. The possibility of using single optical devices (without any standard housing) in order to reduce the overall cost of stacking was investigated and the results showed that single optical devices are not suitable for stacking due to alignment errors caused by connection of the ends of optical fibres to optical devices. An optically-coupled stack of commercially available 1.2 kV IGBTs was designed and built for use as a closing switch in a 25 Ω input impedance, Blumlein pulse generator. As the energy required for the drive circuit of each IGBT module is fed from the voltage across the same IGBT module, there is no need to isolate the DC power supplies. This facilitates stacking of the IGBT modules and if any damage of modules occurs, the faulty stage can be replaced without disturbing the other stages.

In the next chapter, a description will be given of the use of the optically-coupled IGBT stack as a closing switch in a 25 Ω input impedance, 1 μs Blumlein pulse generator, used for inactivation of different types of microorganism.

Chapter 6

APPLICATION OF THE SOLID-STATE PULSER TO THE INACTIVATION OF MICROORGANISMS

6.1 Introduction

In this chapter, the operational performance of the optically-coupled IGBT stack is considered in an application involving the use of high-intensity pulsed electric fields (PEF) for non-thermal food processing. Traditionally, pasteurisation or heat processing is used to reduce the level of bacteria, spores, and other agents that cause spoilage of liquid foods or other perishable media. As these methods are energy intensive, and can adversely affect the nutritional qualities and flavour of the preserved food [88], interest has developed in non-thermal sterilization processes. A highly effective non-thermal process is pulsed electric field (PEF) processing. The critical advances in PEF processing were made in the early 1960's, while recent advances in the field of high-voltage pulse-power technology have provided an impetus for further development. In PEF processing, the perishable medium in fluid form is passed through a small treatment chamber, where it is subjected to short pulses (tens of ns to 100 μs) of pulsed electric field, with a magnitude usually greater than 20 kV/cm [89].

Although the fundamental mechanisms of PEF inactivation of microorganisms have still to be elucidated, it is believed that the inactivation is caused by structural disruption of the cell membrane by the accumulation of charge across it as a result of charge migration under the action of the applied electric field [88]. It has been shown that a voltage difference of ~ 1 V across the cell membrane will cause disruption; this corresponds to an electric field strength in the suspending medium in the range of 1 to 25 kV/cm depending on a wide range of conditions. Electric field strength, pulse duration, pulse shape and total treatment time are the four main PEF parameters governing microbial inactivation. Other factors such as medium conductivity, the temperature and pH of the suspending medium, cell age and cell size may also affect the PEF treatment [90].

A PEF processing system consists of a pulser and treatment chamber, together with voltage, current and temperature probes. Up to the present, the primary limitation to commercialisation of PEF processing has been the inability to generate economically high voltage pulses with sufficient peak power. Typical laboratory systems have used vacuum tubes or spark gaps, which are expensive and inefficient. Advances in solid-state switching devices, particularly IGBTs, show promise in providing an economic means of pulsing for food processing by PEF.

6.2 Design and construction of prototype treatment chamber

A PEF processing system is made up of a pulse source and treatment chamber. Several designs of static and continuous treatment chamber have been suggested [91]. The treatment chamber must provide matched impedance with the pulser and a uniform electric field. The distance between the electrodes in a chamber is designed according to the voltage rating of the applied pulses to provide an electric field of more than 25 kV/cm, since this is the field required for irreversible electric breakdown of the cell membrane. It is important to take precautions in the design of a treatment chamber to avoid dielectric breakdown of the medium being processed. Dielectric breakdown occurs when the applied electric field strength exceeds the dielectric strength of the medium. The maximum electric field within the chamber is limited to 30 kV/cm to prevent electrical breakdown of the air above the medium. Electrode surfaces need to be mirror polished and the edges have to be rounded to minimise field-enhancement effects. In this work, a 3 mm gap space between the electrodes was selected to match the 10 kV voltage rating of the pulser. Different types of electrode arrangement such as plate-plate or needle-plate can be selected. A chamber with a plate-plate configuration is easiest to assemble, but the 3 mm gap between the electrodes means that the sample has to be introduced through a small aperture, and this is difficult. As a result, treatment chambers with co-axial configuration were preferred.

The aim of the PEF treatment chamber design was to attain a relatively uniform high-intensity electric field in the treatment region to achieve rapid, uniform microbial inactivation. This is best achieved using a co-axial test chamber. Co-axial chambers

can be readily manufactured and give well-defined electric field distributions. The electric field in a coaxial chamber is not uniform and depends on radial position within the chamber. The field intensity E and resistance R between two electrodes of a co-axial test chamber, as shown in Figure 6.1, can be represented by the following equations [92].

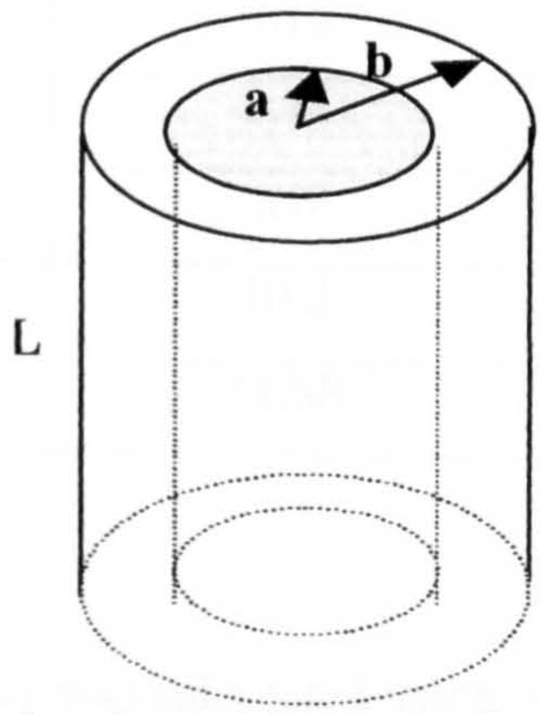

Figure 6.1 Co-axial test chamber with inner and outer conductor radii of a and b and length L.

$$R_{ab} = \frac{\ell n(b/a)}{2\pi\sigma L} = \frac{\ell n(1+\frac{g}{a})}{2\pi\sigma L} \tag{6.1}$$

where $g = b - a$, and

$$E = V_{ab}\frac{1}{r\ell n(b/a)} = V_{ab}\frac{1}{r\ell n(1+g/a)} \tag{6.2}$$

σ is the conductivity of the medium between two conductors, and r is the radial distance from the axis of the central conductor.

The suspension used throughout the PEF experiments was 0.1% bacteriological peptone in distilled water. In order to have a chamber with resistance matched to the output impedance of the pulse generator, the conductivity of the suspension must be known. A 1.9 ml volume parallel-plate test chamber with 10 mm gap was loaded with the suspension of 0.1% peptone in distilled water and connected at the output of a Blumlein pulse generator of output impedance 100 Ω. The open-circuit voltage V_{oc} and the voltage across the chamber V_m were measured and recorded for different values of charging voltage as shown in Table 6.1.

Table 6.1 Data for chamber containing 0.1% peptone in distilled water

V_m(kV)	V_{oc}(kV)	Z_l(Ω)	
0.72	0.88	450	
1.08	1.34	415	
1.80	2.16	500	
2.96	3.84	336	
4.6	5.6	460	
8.24	10.3	400	
9.76	11.80	478	Z_{avg} = 434

The impedance of the chamber was calculated using $Z_l = \frac{V_m}{V_{oc} - V_m} \times Z_0$, where Z_0 = 100 Ω. Using the average impedance calculated for the chamber and by considering the chamber dimensions, a conductivity of σ = 0.0115749 Ω^{-1} m^{-1} was calculated. By substituting g = 3 mm, σ = 0.0115749 Ω^{-1} m^{-1} and R_{ab}= 50 Ω in Equation (6.1), the following relationship between the length and the inner radius of the chamber is obtained:

$$L = 0.275\ell n(1 + \tfrac{3}{a}) \qquad (6.3)$$

By taking into account the availability of brass rods with the maximum diameter size of 50 mm, a = 7.5 mm and L = 92.5 mm were selected. A diagram and a photograph of the prototype co-axial design of a cylindrical treatment chamber are shown in Figure 6.2 and Figure 6.3, respectively. A nylon spacer (seen in the centre of Figure 6.3) separated the two brass electrodes; one rod-shaped (on the right in Figure 6.3) was the inner electrode and it was placed inside the hollowed-out outer electrode (on the left in Figure 6.3). The treatment volume and gap between the electrodes of the chamber were 16 ml and 3 mm, respectively.

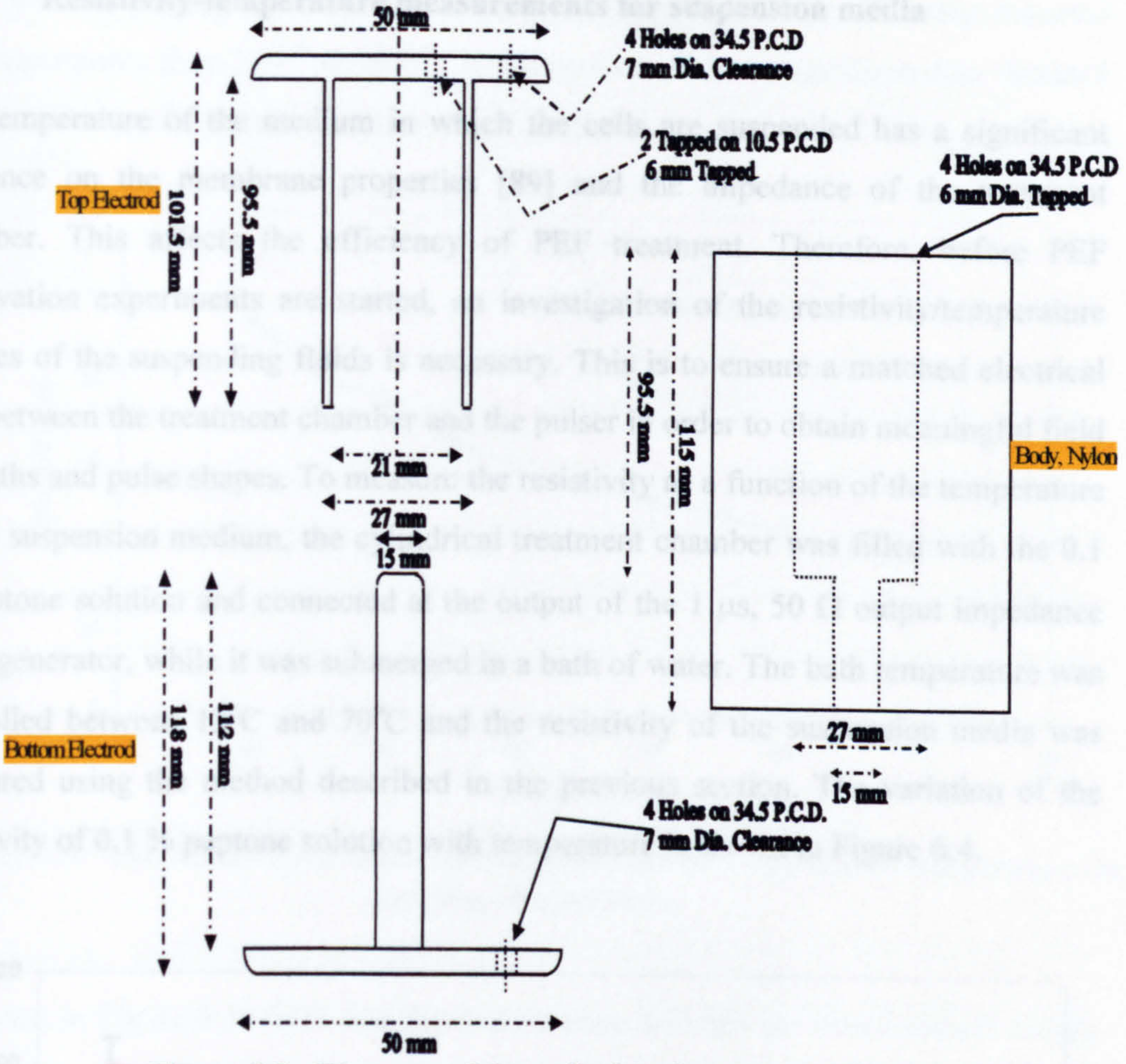

Figure 6.2 Diagram of the cylindrical treatment chamber.

Figure 6.3 Photograph of the cylindrical shaped co-axial treatment chamber.

6.3 Resistivity-temperature measurements for suspension media

The temperature of the medium in which the cells are suspended has a significant influence on the membrane properties [89] and the impedance of the treatment chamber. This affects the efficiency of PEF treatment. Therefore, before PEF inactivation experiments are started, an investigation of the resistivity/temperature profiles of the suspending fluids is necessary. This is to ensure a matched electrical load between the treatment chamber and the pulser in order to obtain meaningful field strengths and pulse shapes. To measure the resistivity as a function of the temperature of the suspension medium, the cylindrical treatment chamber was filled with the 0.1 % peptone solution and connected at the output of the 1 μs, 50 Ω output impedance pulse generator, while it was submerged in a bath of water. The bath temperature was controlled between 15°C and 70°C and the resistivity of the suspension media was measured using the method described in the previous section. The variation of the resistivity of 0.1 % peptone solution with temperature is shown in Figure 6.4.

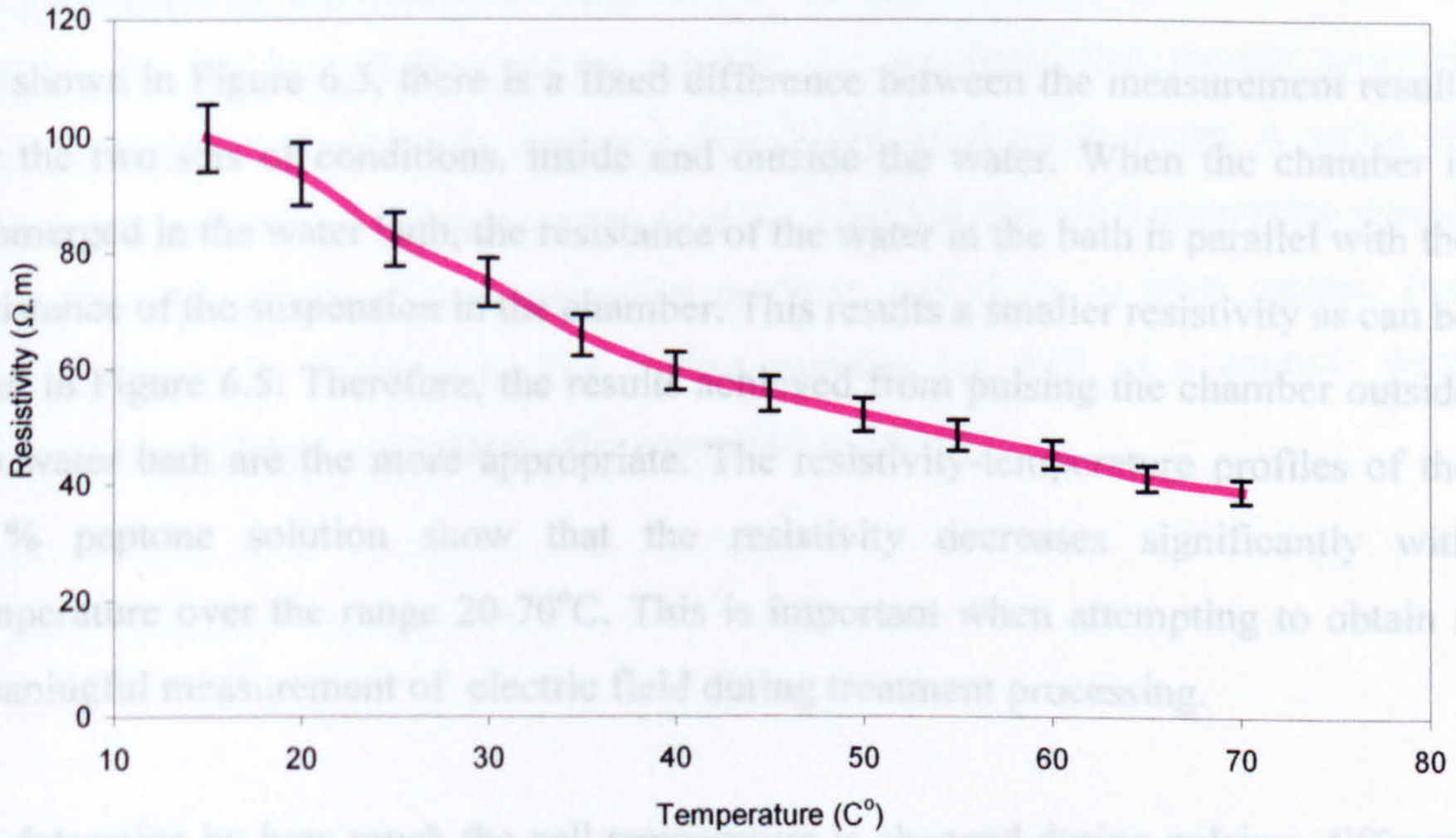

Figure 6.4 Variation of the resistivity of 0.1 % peptone solution with temperature.

The resistivity of the peptone solution was measured again under different conditions. After submerging the treatment chamber in the water bath and allowing it to reach thermal equilibrium with the water in the bath, the test cell was removed from the

water bath for pulsing and hence for measuring the pulse voltage. This was repeated for temperatures from 20 C° to 70 C°. A comparison of the temperature data obtained for the two sets of conditions is shown in Figure 6.5.

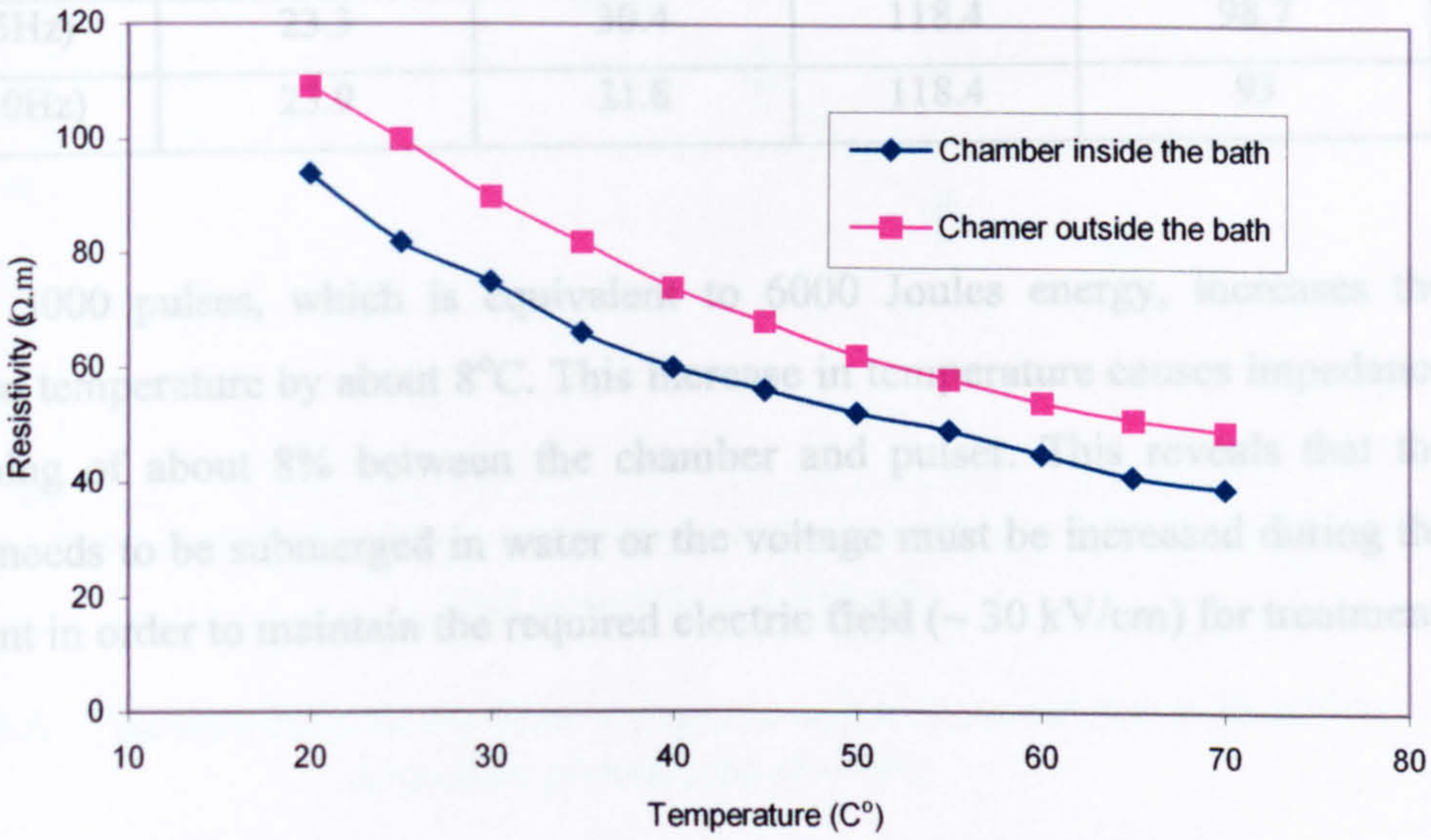

Figure 6.5 The resistivity of the suspension medium as a function of temperature for two sets of conditions.

As shown in Figure 6.5, there is a fixed difference between the measurement results for the two sets of conditions, inside and outside the water. When the chamber is submerged in the water bath, the resistance of the water in the bath is parallel with the resistance of the suspension in the chamber. This results a smaller resistivity as can be seen in Figure 6.5. Therefore, the results achieved from pulsing the chamber outside the water bath are the more appropriate. The resistivity-temperature profiles of the 0.1% peptone solution show that the resistivity decreases significantly with temperature over the range 20-70°C. This is important when attempting to obtain a meaningful measurement of electric field during treatment processing.

To determine by how much the cell temperature is changed during pulsing, different numbers of 10 kV, 1 μs pulses with pulse repetition rates of 5 Hz and 10 Hz were applied to the chamber, while it was filled with a 0.1 % peptone solution. The results are shown in Table 6.2.

Table 6.2 Variation in the solution temperature after different numbers of shots

Number of shots	Init. Temp. (C°)	Fin. Temp. (C°)	Init. ρ(Ω.m)	Fin. ρ(Ω.m)
1500(5Hz)	22	26	118.4	104.8
3000(5Hz)	23.3	30.4	118.4	98.7
3000(10Hz)	23.9	31.8	118.4	93

Applying 3000 pulses, which is equivalent to 6000 Joules energy, increases the suspension temperature by about 8°C. This increase in temperature causes impedance mismatching of about 8% between the chamber and pulser. This reveals that the chamber needs to be submerged in water or the voltage must be increased during the experiment in order to maintain the required electric field (~ 30 kV/cm) for treatment.

6.4 Cell population effect on the resistivity of suspension media

The impedance of the treatment chamber can be adjusted to the desired value by changing the dilution of the peptone solution. It was found that for the co-axial chamber, the best matching is achieved with 0.06% peptone in water. A series of experiments was carried out to examine whether a seeded microbial population would affect the conductivity of the suspending medium, and if so, to what degree. The result is shown in Figure 6.6. The treated samples (as well as a control) were numerated on nutrient agar plates after overnight incubation.

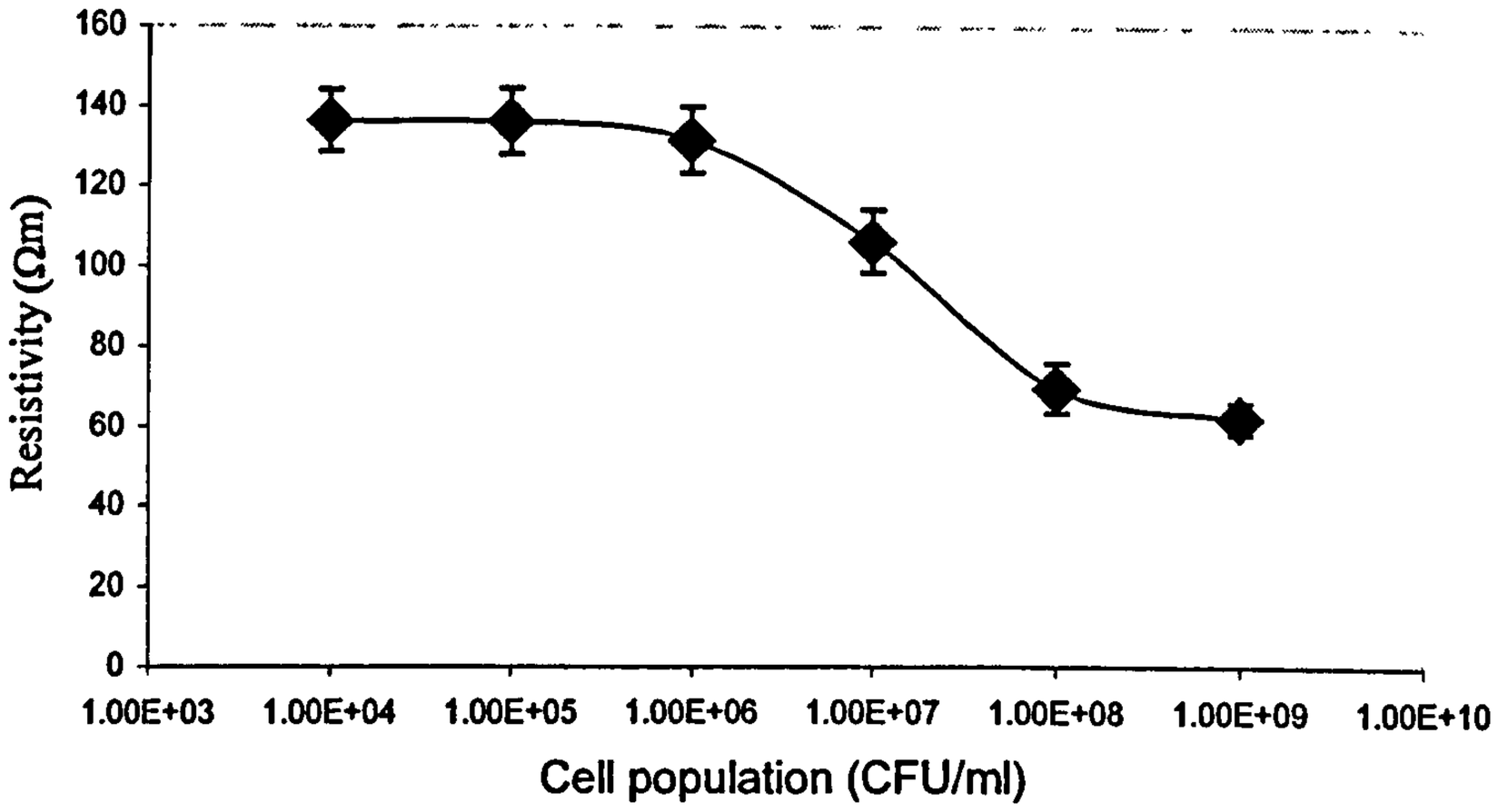

Figure 6.6 The resistivity of the 0.06 % peptone solution inoculated with different microbial populations (*E-coli*).

According to Figure 6.6, the resistivity of the 0.06% peptone solution remains constant for a cell population less than 10^6 CFU*/ml For a cell population greater than 10^6, the resistivity of the peptone solution falls until the cell population reaches a value of around 10^9 CFU/ml where the resistivity of the peptone solution begins to level off at ~ 35 Ωm. The optimal experimental resistivity value for the treatment chamber is 90 Ωm which corresponds to a test-cell impedance of 50 Ω and cell population of ~ 10^7 CFU/ml. Furthermore, if the cell population exceeds a value of ~ 10^7 CFU/ml, the resistivity of the suspension is too low for the generation of an optimal electric field. Therefore, a maximum cell population of 10^7 CFU/ml was used for the experiments carried out using the 0.06% solution.

6.5 PEF treatment of microorganisms using prototype chamber in static mode

A series of experiments was carried out in a static fluid to investigate the performance of the co-axial treatment chamber for microbial inactivation. The 10 kV, 1 μs solid-

* A CFU is a colony-forming unit, which is a bacterial cell that is capable of developing into a colony of bacteria when grown in laboratory conditions.

state pulser described in chapter 5 with the capability of delivering electric pulses of 2 J per pulse, was used. Two bacterial species, *Escherichia coli*, National Collection of Typed Cultures (NCTC) 9001, and *Bacillus cereus*, *NCTC* 11145, were examined. *E.coli* is one of the most characteristic members of the normal intestinal flora of mammals and is responsible for such intestinal flora infections as bacterial dysentery, typhoid fever and bacterial food poisoning. *B.cereus* is a highly motile, flagellate, gram-positive, rod-shaped bacterium commonly found in cereals, herbs and starches that can cause food poisoning characterised by vomiting and diarrhea. The preparation steps, culture and enumeration protocols have been described [94]. The treatment was conducted by exposing suspensions of artificially inoculated *E.coli* to different numbers of pulses, while the pulser was operating with a PRF of 5 Hz. The viability of samples before and after treatment was assayed by counting colony-forming units. The inactivation results for two series of experiments are shown in Figure 6.7.

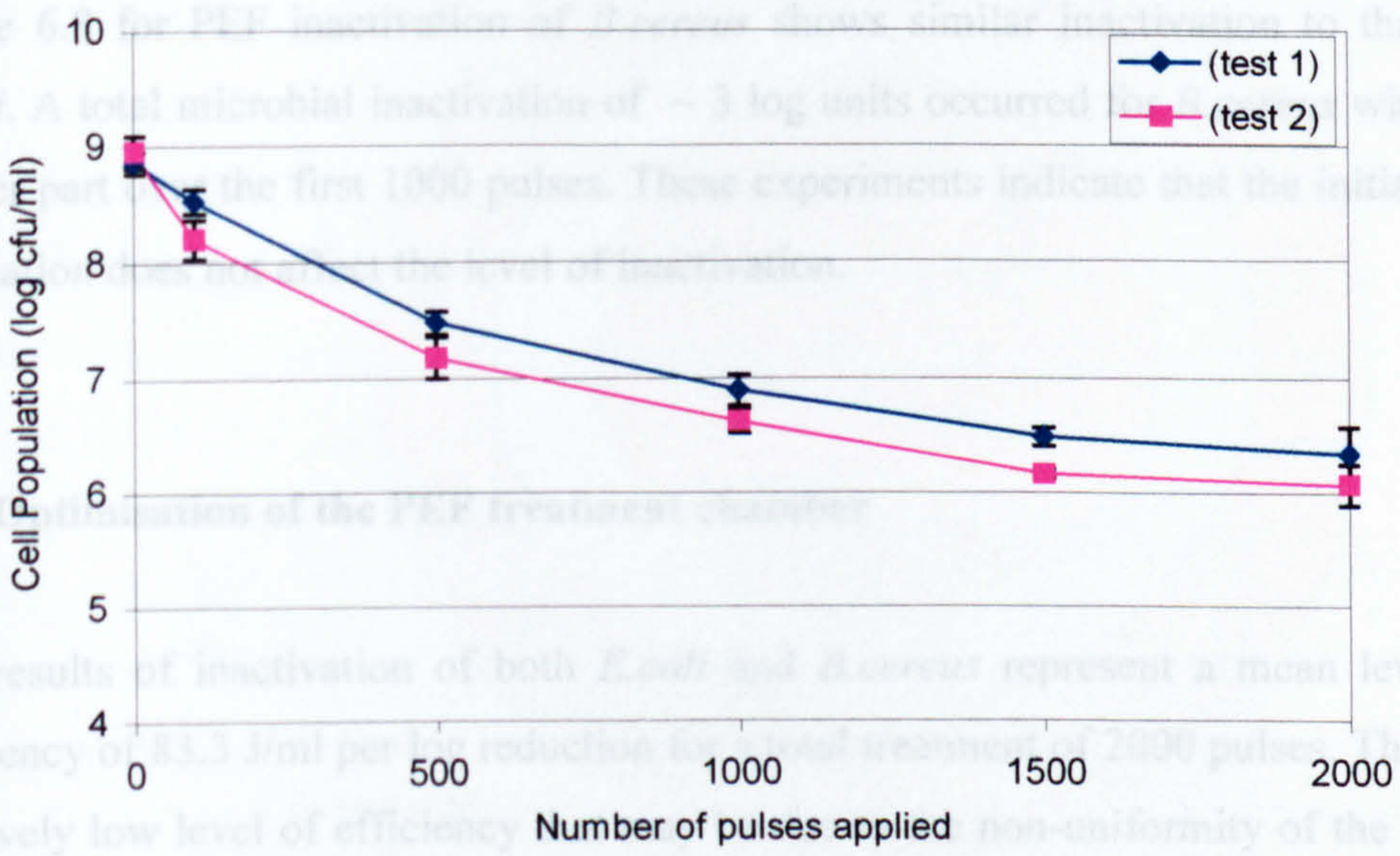

Figure 6.7 PEF treatment of artificially inoculated *E.coli* cell using co-axial chamber and solid-state pulser.

A mean microbial inactivation of ~ 3 cfu log units was accomplished by applying 2000 pulses with an energy of 2 J per pulse. The rate of microbial inactivation was highest (~ 2.2 log reduction) over the first 1000 pulses, with a further 1000 pulses producing a further 0.8 log reduction. The inactivation of *B.cereus* was also examined using the same procedure, but with three different initial cell population levels. The results are shown in Figure 6.8.

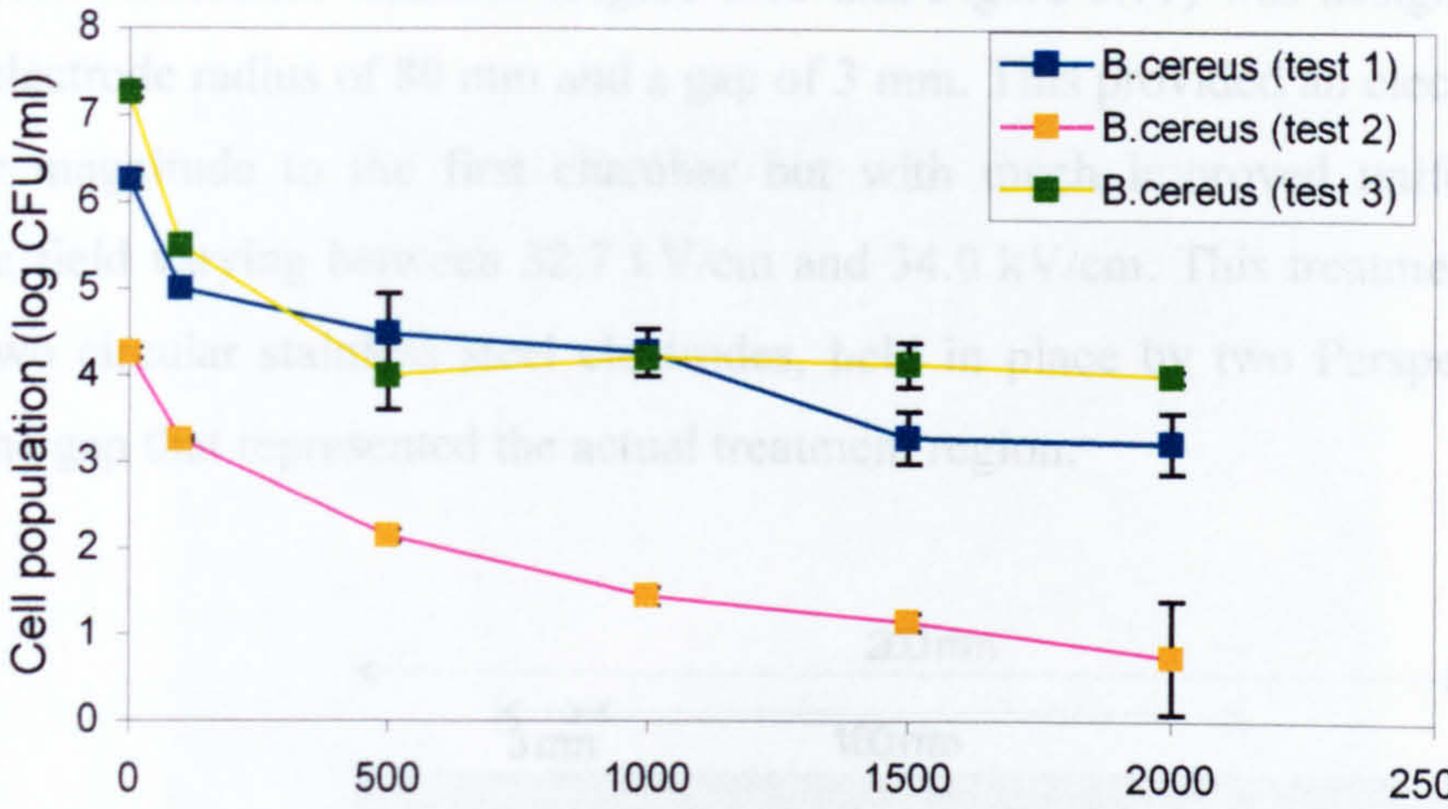

Figure 6.8 PEF treatment of artificially inoculated *B.cereus* cell using co-axial chamber and solid-state pulser.

Figure 6.8 for PEF inactivation of *B.cereus* shows similar inactivation to that for *E.coli*. A total microbial inactivation of ~ 3 log units occurred for *B.cereus* with the greater part over the first 1000 pulses. These experiments indicate that the initial cell population does not affect the level of inactivation.

6.6 Optimisation of the PEF treatment chamber

The results of inactivation of both *E.coli* and *B.cereus* represent a mean level of efficiency of 83.3 J/ml per log reduction for a total treatment of 2000 pulses. This is a relatively low level of efficiency that may be due to the non-uniformity of the radial electric field and existence of dead zones in the treatment area. The electric field distribution across the gap between the electrodes for the 16 ml co-axial treatment chamber was calculated using Equation 6.1, and its magnitude was found to vary from 28.3 kV/cm to 39.6 kV/cm. The uniformity of the electric field in a co-axial treatment chamber improves as the gap between the electrodes is reduced relative to the radius of the outer electrode.

Another treatment chamber was therefore designed to minimise the dead zone and provide a more uniform electric field distribution between the electrodes.

The second treatment chamber (Figure 6.10 and Figure 6.11) was designed with an inner electrode radius of 80 mm and a gap of 3 mm. This provided an electric field of similar magnitude to the first chamber but with much improved uniformity, the electric field varying between 32.7 kV/cm and 34.0 kV/cm. This treatment chamber used two circular stainless steel electrodes, held in place by two Perspex plates to form the gap that represented the actual treatment region.

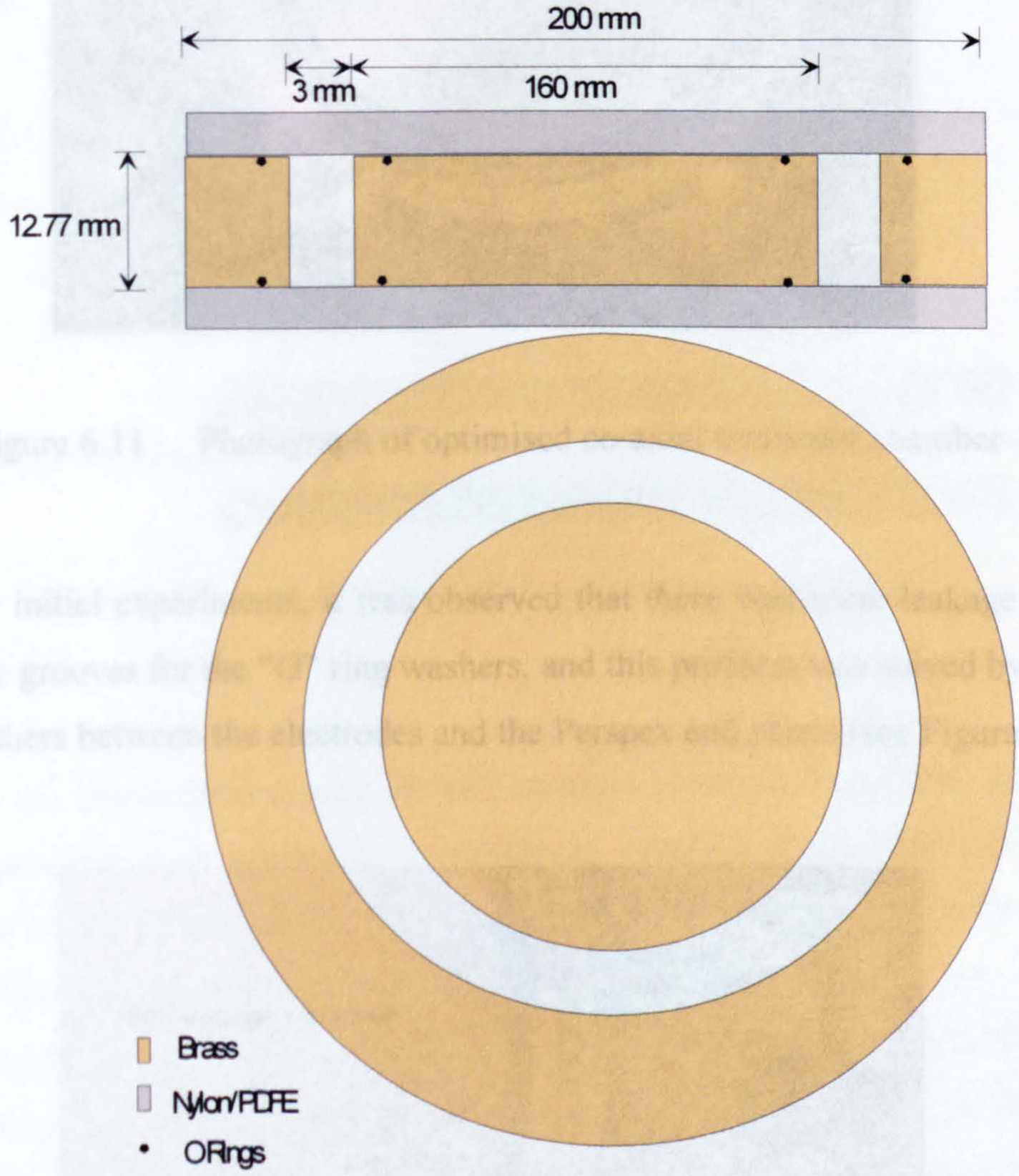

Figure 6.10 Diagram of the optimised co-axial treatment chamber.

Figure 6.11 Photograph of optimised co-axial treatment chamber

During the initial experiments, it was observed that there was some leakage of fluid through the grooves for the "O" ring washers, and this problem was solved by placing plastic washers between the electrodes and the Perspex end plates (see Figure 6.12).

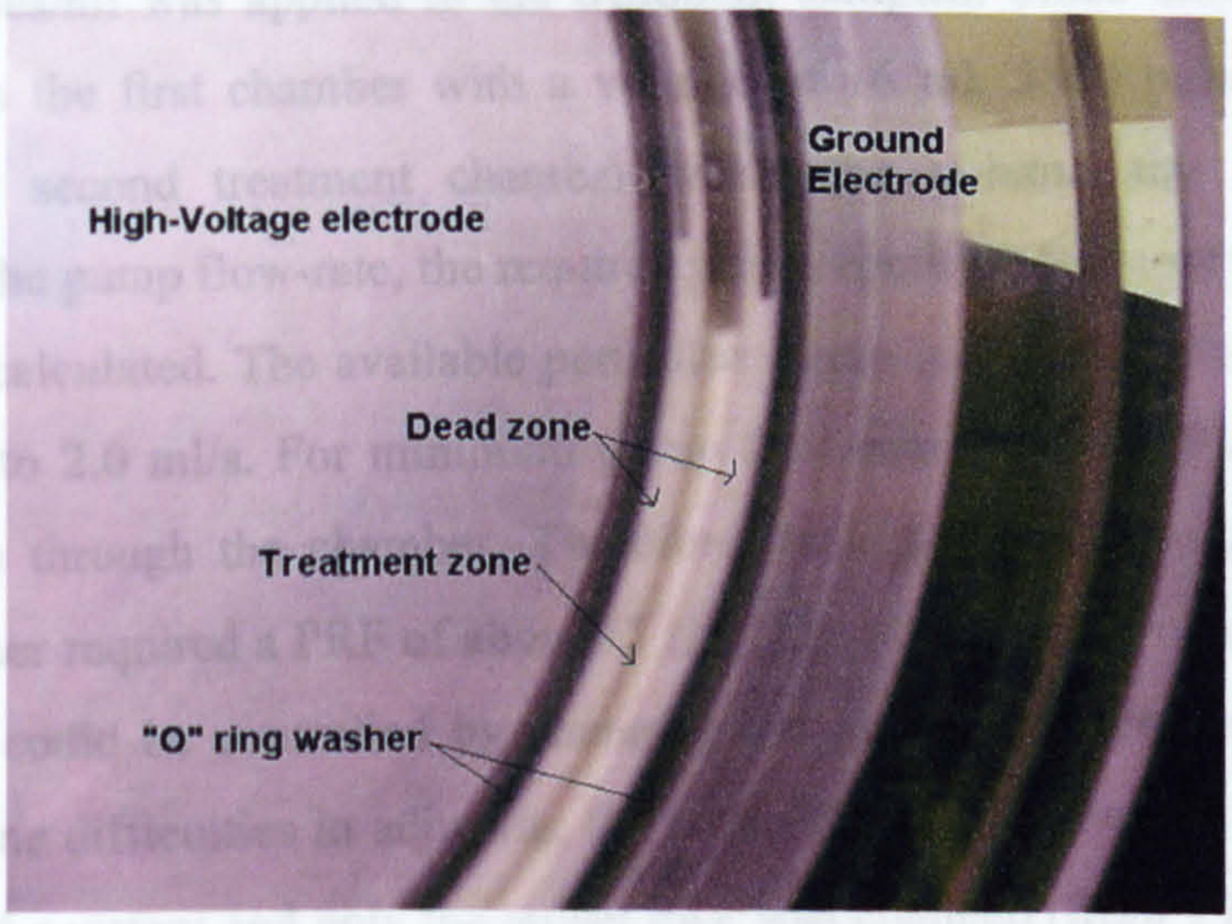

Figure 6.12 Dead zone in the optimised co-axial treatment chamber.

6.7 PEF treatment of microorganisms in flow mode

After modifying the co-axial treatment chamber and providing two small ports for filling/withdrawal of the sample, it was used in a basic re-circulatory system as shown in Figure 6.13.

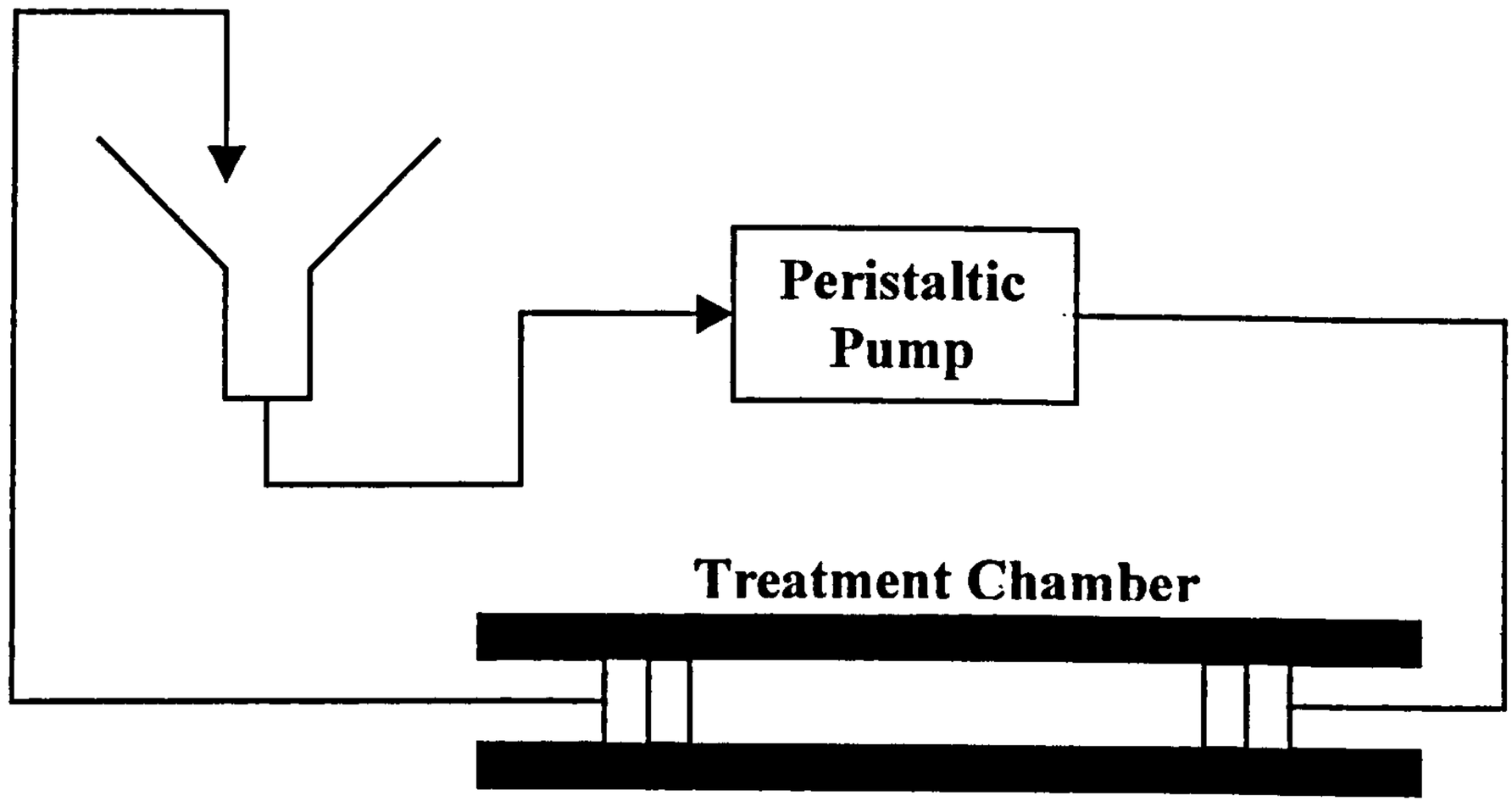

Figure 6.13 Layout of the circulatory treatment system.

To compare the inactivation results of both co-axial treatment chambers, the same number of pulses/ml was applied to the treatment samples. Since 2000 pulses had been applied to the first chamber with a volume of 16 ml, 3500 pulses had to be applied to the second treatment chamber where the volume size was 28 ml. Depending on the pump flow-rate, the required pulse repetition frequency of the pulse generator was calculated. The available peristaltic pump had a controllable flow rate from 0.4 ml/s to 2.0 ml/s. For minimum pump flow-rate, it took 64 seconds for a sample to pass through the chamber. Therefore, to apply a total number of 3500 pulses, the pulser required a PRF of about 55 Hz. The total number of pulses applied to the sample could be controlled by changing the pump flow-rate or pulser PRF. Because of some difficulties in adjusting the pump flow-rate, however, the flow rate was maintained constant and only the pulser PRF was changed (from 1 Hz to 100 Hz) for different numbers of shots. The continuous-flowing system was used for a series of PEF experiments with different types of microorganism. The inactivation of *E.coli* cells (Table 6.4) is presented as an example.

Table 6.4 PEF inactivation of *E.coli* cells treated in continuous-flowing system

Number of pulses	0	962	1923	3500
Normalised (pulse No.)	0	34	68	125
PRF (Hz)	0	15	30	54.8
Energy Input (J/ml)	0	68	136	250
Cell Population (Mean)	4.97×10^{7}	3.23×10^{5}	2.20×10^{4}	4.53×10^{3}

These results show that a log reduction greater than 4 in *E.coli* activity was achieved on applying 3500 pulses. This corresponds to a 62.5 J/ml per log reduction and shows an improvement in the efficiency of the PEF inactivation compared to that achieved with the prototype co-axial treatment chamber, however the initial cell populations were different.

6.8 Summary and Conclusion

The 10 kV optically-triggered IGBT stack was successfully operated using a large number of pulses with different PRF for the PEF treatment of microorganisms. For some inactivation studies, due to a high initial cell population or a rise in sample temperature, the voltage across the stack had to be increased to 12 kV, in order to maintain a constant electric field in the chamber. Although the stack was designed for operating voltages up to 10 kV, it was observed that it could safely handle voltages up to 12 kV for short periods of time (a few tens of seconds), provided that the reference voltage of the protection unit is re-adjusted accordingly. This was one of the main advantages of this system in compare with systems using spark gap switches. The IGBT stack provided stable performance during all the experiments and no over-voltage or misfiring occurred over a period of more than 10^6 pulses. The application of the solid-state pulser was tested in both static and flow PEF treatment systems. A mean microbial inactivation of ~ 3 cfu log units (83.3 J/ml per log reduction) was accomplished using the co-axial treatment chamber. The number of active cells was reduced by about four log (62.5 J/ml per log reduction) in the flow system following optimisation of the treatment chamber dimensions.

Chapter 7

APPLICATION OF THE SOLID-STATE PULSER TO THE LIGHT INACTIVATION OF FOOD-RELATED PATHOGENIC BACTERIA

7.1 Introduction

In chapter 6, a description was given of a pulsed electric field (PEF) system used to inactivate a population of E.coli cells. The PEF system was rapidly pulsed using an optically-coupled stack of IGBTs. In this chapter, another approach to cell inactivation is described, again using an optically-coupled stack of IGBTs. Here the IGBTs are used to switch a Marx generator that drives a UV flashlamp, and the resultant UV light pulses are used to inactivate the bacterial cells. The design and performance of the fully integrated solid-state Marx generator is described. The generator has an output voltage rating of 3 kV and a peak current rating of 2 kA, although the modular approach taken allows for higher voltage and current ratings to be achieved. The generator is constructed using a number of series and parallel-connected 1.2 kV Insulated-Gate-Bipolar-Transistor (IGBT) switched capacitors. Switching of the IGBT modules is controlled by an optical signal. Details are given of how the optimum IGBT gate-drive circuit is achieved using optical components and a pass-through wire to provide the required energies for individual IGBT modules. The generator is demonstrated as the driver of a UV flashlamp used for inactivation of food-related pathogenic bacteria such as *E.coli* and *Salmonella*. The performance of the Marx generator over a period of 10^6 pulses is examined, along with the changes that occur in the spectrum of the UV flashlamp during the same period.

Illness caused by the consumption of contaminated food and food-borne diseases still remains a major cause of death throughout the world. Clearly, the application of methods for either reducing or eliminating the microbiological risks associated with contaminated foods will have a significant effect on the incidence of food-borne disease. Traditionally, pasteurisation or heat processing is used to reduce the level of bacteria, spores, and other agents that cause spoilage of liquid foods or other

perishable media. This can have several disadvantages, including changes in flavour, smell and appearance, and destruction of heat-sensitive compounds such as vitamins and proteins [95,96]. Furthermore, for some high-risk foods such as meats, fruit and vegetables, thermal treatment is not applicable. A possible approach to decreasing the level of microbial contamination on food surfaces and in food preparation environments is through the use of ultraviolet (UV) illumination. Exposure of pathogenic bacteria to UV light within the germicidal wavelength region from 200 nm to 300 nm results in the inactivation of microorganisms [97]. Therefore, UV illumination may have practical application for the disinfection of food and contact surfaces if effective methods of UV generation and delivery can be developed. It has been reported that pulsed UV light, with the capability of delivering peak powers of many megawatts to the flashlamps, can yield higher microbial inactivation rates than conventional UV light systems, which operate continuously and have power levels in the range of 100-1000 W [97,98]. In fact, a pulse-power energisation technique can deliver many megawatts of electrical power to the light source using a modest energy input of a few Joules. This produces a greater intensity of the shorter, bactericidal wavelengths of light, which leads to further effectiveness, and decreases the treatment time from 30 to 60 minutes in continuously UV-operated systems to a few seconds.

In general, flashlamps, used as sources of UV light, can be driven by applying a voltage pulse much lower than the lamp self-breakdown voltage (10-20 kV) by using a trigger pulse of the order of 20-30 kV with a pulse width of a few microseconds to cause the initial ionisation of the gas. In the following sections, the design considerations for a solid-state Marx generator as a driver for UV flashlamps are discussed.

7.2 Solid-state Marx generator

A Marx generator provides one of the most widely used methods of generating high voltage impulses because it features a low voltage power supply for charging and does not require a pulse transformer for generation of the high voltage [99,100]. The Marx generator as shown in Figure 7.1 is comprised of a number of stages, with each stage made of a discrete capacitor and a switch. Voltage multiplication is achieved by

charging the capacitors in parallel, through charging resistors, and then discharging them in series by simultaneously closing the switch [101].

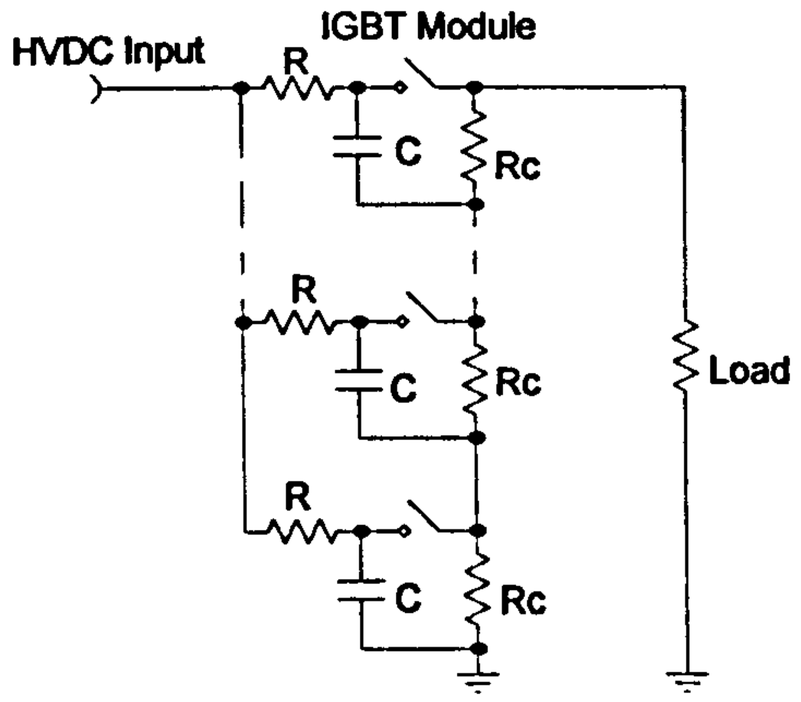

Figure 7.1 Marx generator.

Because of the short lifetimes of the spark gaps normally used for switching, Marx generators tend to have limited lifetime. This limits their use in highly repetitive applications. However, this problem can be solved by using stacked fast medium-voltage IGBTs. Using stacked IGBTs in Marx generators offers a number of advantages, such as high pulse repetition potential, low maintenance, low cost and better flexibility in terms of voltage and current ratings.

7.2.1 Peak current rating of IGBT modules

In chapter 4, stacking of 1.2 kV IGBT modules using GT15Q301 devices was described, and it was shown that this IGBT can operate reliably with a peak current of about 200 A and pulse duration of a few microseconds. This was confirmed using an IGBT module consisting of 5 GT15Q301 devices connected in parallel, and the arrangement shown in Figure 7.2.

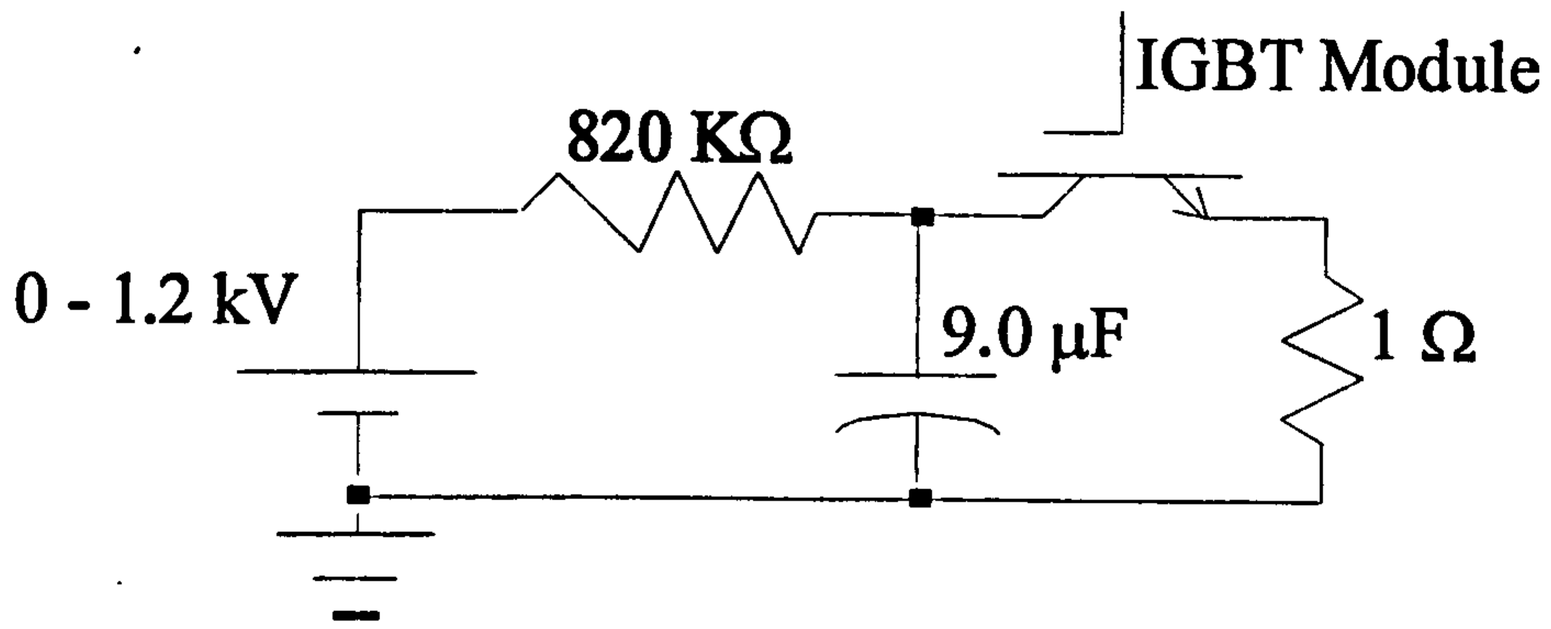

Figure 7.2 Circuit used to check the maximum operating current for IGBT modules.

The charging capacitor in Figure 7.2 was made up of six single 1.5 μF, 1.5 kV capacitors connected in parallel to minimise series inductance. The switching performance of an IGBT module was investigated while the charging voltage was controlled from zero to 1.2 kV. The IGBTs were triggered with an optical signal, and using a drive circuit, fed by an external dc power supply. It was found that IGBT modules could safely handle peak currents of 1 kA at 1 kV.

7.2.2 Marx generator drive circuits

In order to produce 3 kV impulse voltages with a current capability of 1 kA, and by considering the current/voltage ratings of IGBT modules, a prototype Marx generator, consisting of three stages, was designed. The layout of a three-stage Marx generator is illustrated in Figure 7.3. In each stage, two 1.5 μF, 1.5 kV capacitors were connected in parallel to provide an energy per pulse of 1.5 J for a stage voltage of 1.0 kV.

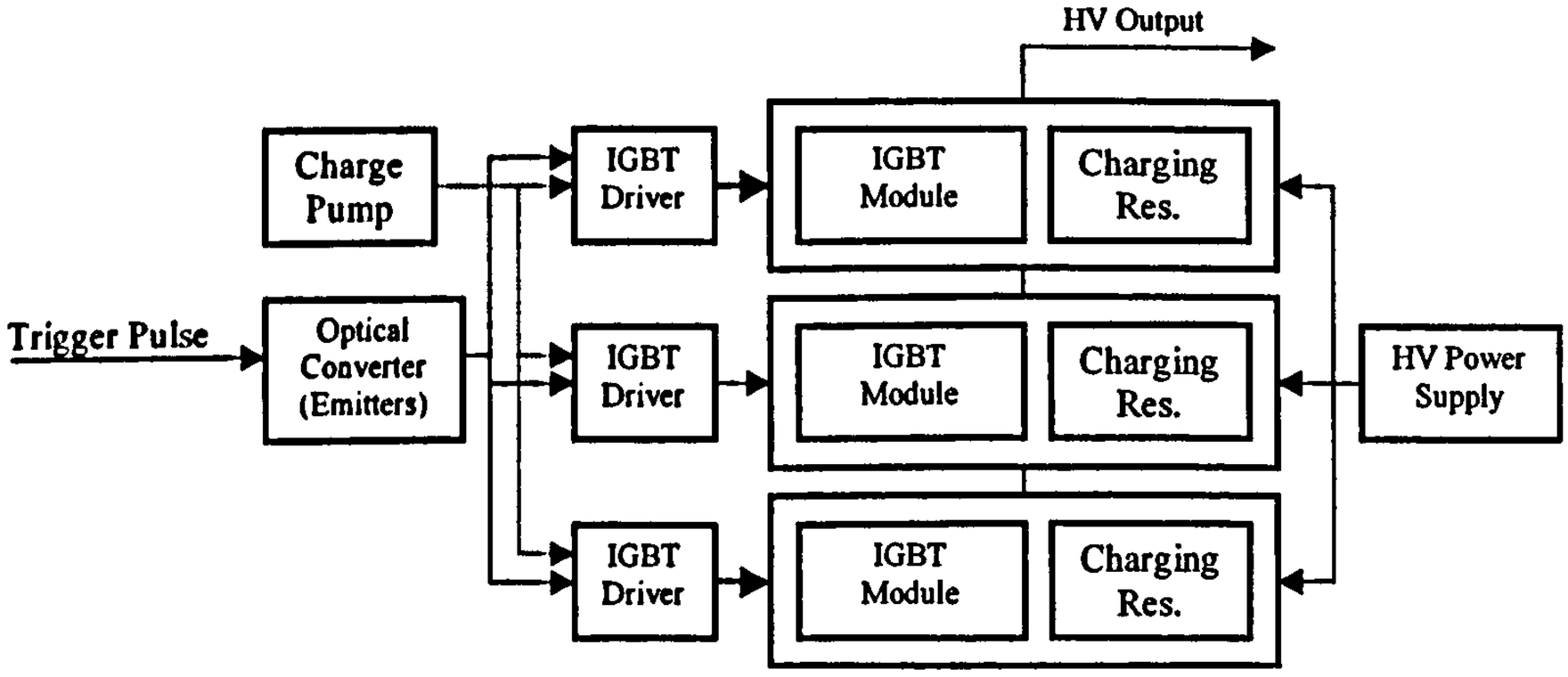

Figure 7.3 Block diagram illustrating the main components of the three-stage Marx generator.

As discussed in chapter 5, driving IGBT modules can be accomplished using magnetic or optical coupling. However, magnetic coupling imposes a limit of pulse duration (about 3 μsec) in triggering signals and requires good insulation between the cores and windings. Optical coupling does not impose these limits in the isolation voltage and pulse duration, although separate isolated dc power supplies are required for each IGBT module. The optical emitters can be driven using the circuit shown in Figure 5.4 of Chapter 5, but some changes in circuit parameters and layout, shown in Figure 7.4, were made to ensure homogeneous switching of the assembly by minimising turn-on delays and voltage variations across the IGBT modules.

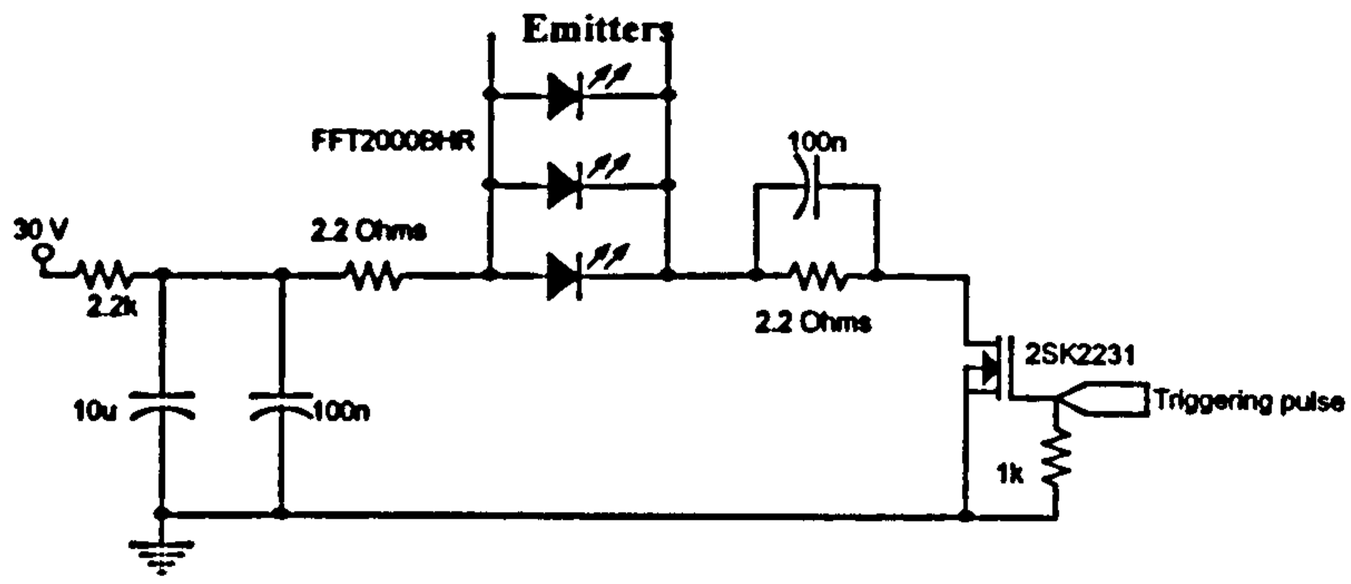

Figure 7.4 Circuit to drive optical emitters.

By employing the same circuit in each module, as shown in Figure 7.5, the optical signals were converted to voltage pulses.

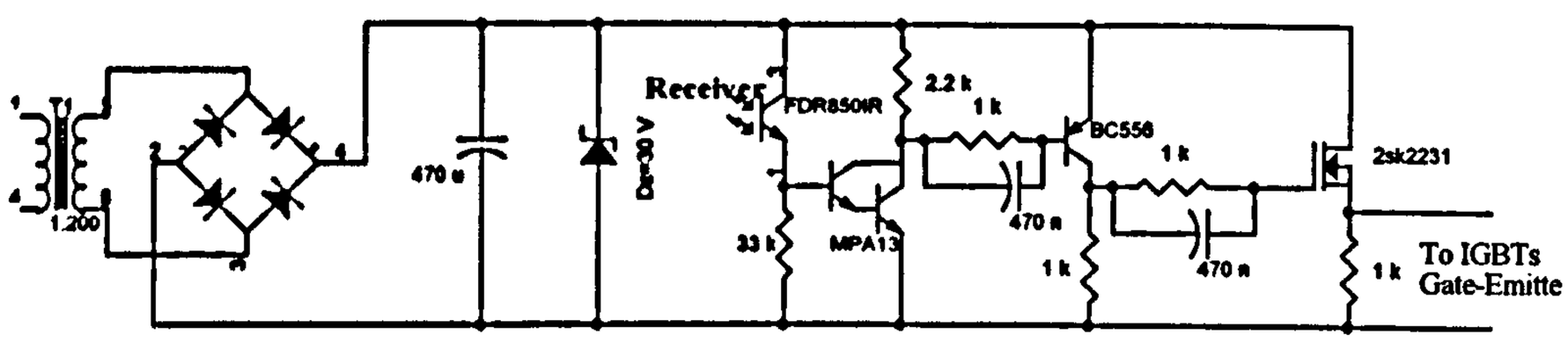

Figure 7.5 Circuit for the conversion of optical signals to voltage trigger pulses.

The dc power for each IGBT module was provided using a transformer with a toroidal core, driven from a charge pump and via a single pass-through winding through the centre of the toroid. Isolation was achieved using well-insulated, high-voltage pass-through wire. The charge-pump circuit is shown in Figure 7.6.

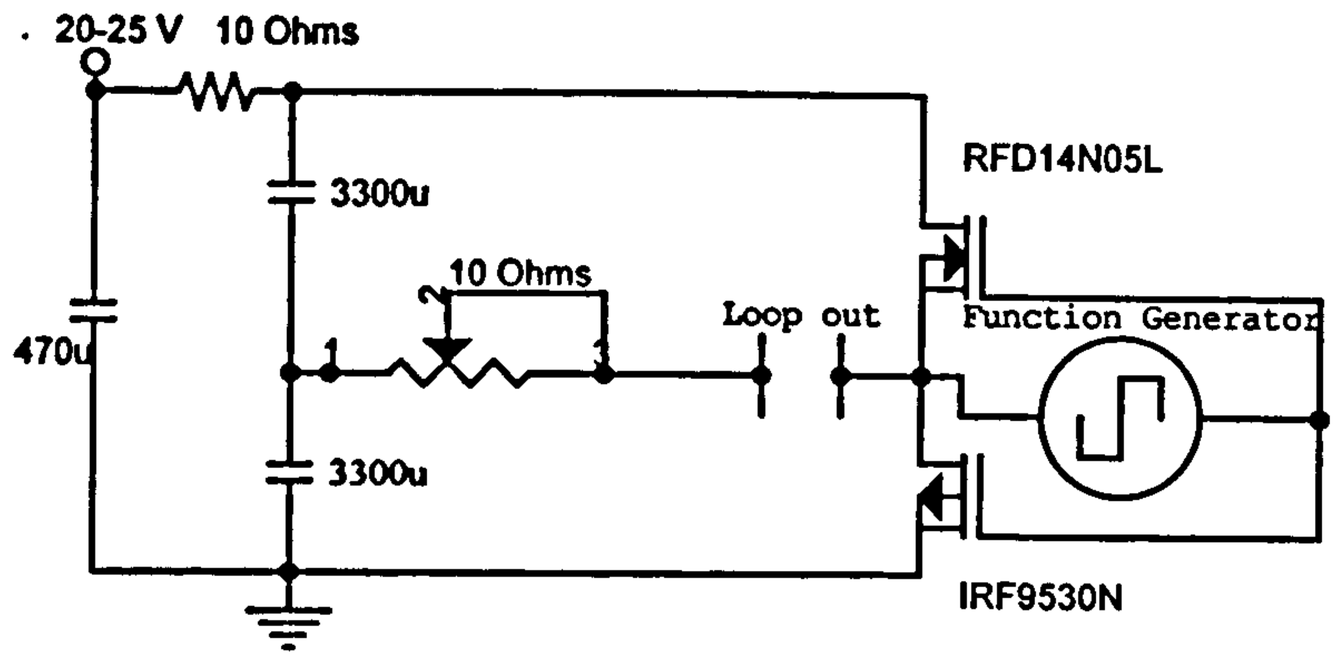

Figure 7.6 The charge-pump circuit.

Two 3300 μF capacitors are charged up to half the voltage of the DC power supply which is between 20 V to 25 V, and then they are discharged separately through the MOSFET switches operating at a frequency of 20 kHz. These pulses drive the primary of the transformer in the circuit shown in Figure 7.6.

7.2.3 A three-stage Marx generator

A photograph of the Marx generator with three IGBT modules is shown in Figure 7.7. The current and voltage ratings are 1 kA and 3 kV respectively. The total energy stored in the capacitors was 4.5 J for a stack voltage of 1 kV and the generator was capable of delivering around 4 J following energy losses in the IGBTs. The energy losses in the IGBTs can be attributed to switching and conduction. During switching, only the self-capacitance of the modules contributes to losses as the switching speed is around 30 ns and the rate of rise of current is more than 1 μs. Therefore, switching losses are negligible. The conduction losses are associated with the average of the current (~707 A) flowing through the equivalent on-state resistor of the IGBT modules (0.036 Ω) for approximately 8 μs. This led to a 0.42 J loss of energy (around 9% of the total stored energy). The generator pulse repetition rate was limited to less than 10 pulses per second (pps) by the power dissipation in the charging resistors.

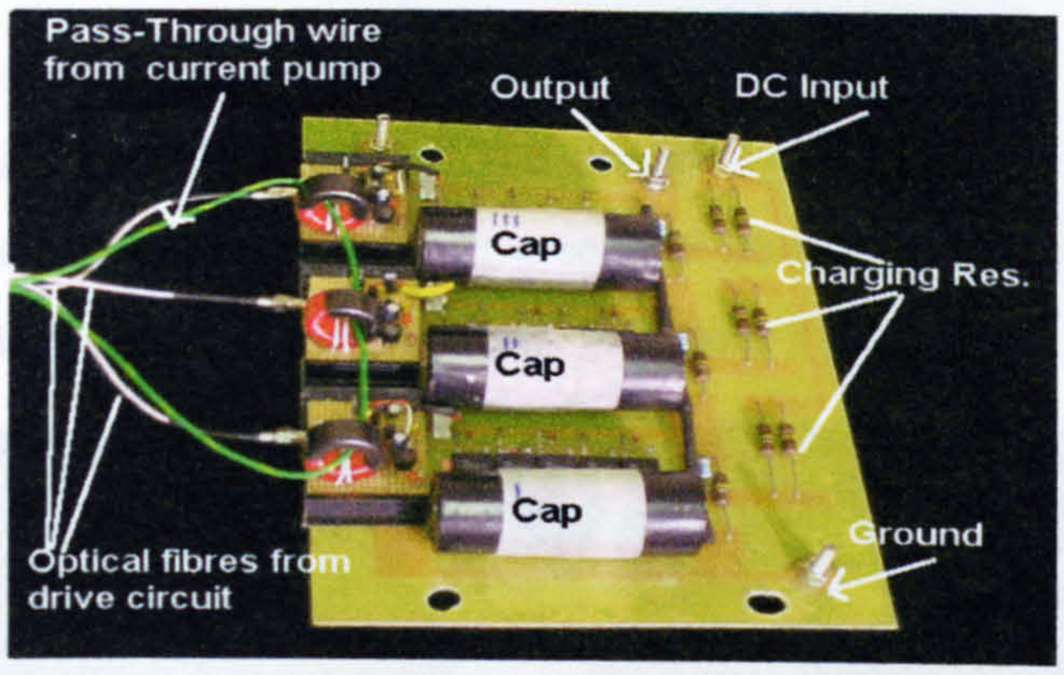

Figure 7.7 Photograph of 3 kV, 1 kA Marx generator made up of three IGBT modules.

Typical current and the voltage waveforms for a 3 Ω resistive load connected at the output of the generator, for a charging voltage of 1 kV, are shown in Figure 7.8.

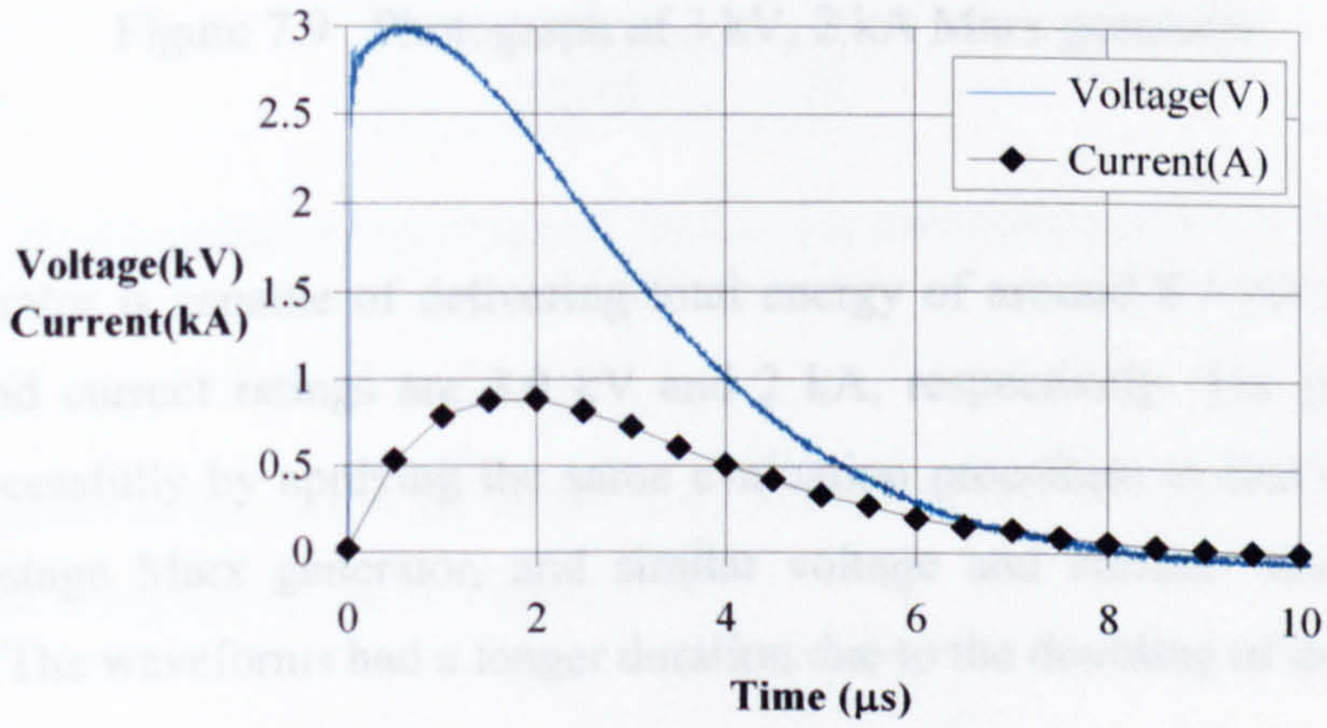

Figure 7.8 Voltage across the capacitors and current waveforms of the 3-Stage Marx Generator with a 3 Ω pure resistive load.

The current waveform was obtained using a *Current Probe DE(CP)-01* manufactured by SAMTECH Ltd with sensing resistance of 30 mΩ and output voltage of 30 V/kA. The voltage waveform was measured using a *Tektronix P6015A 1000X high voltage probe* with maximum voltage of 20 kV DC, 40 kV pulsed, and bandwidth of 75 MHz. A *Tektronix TDS3032* digital oscilloscope with a bandwidth of 300 MHz was used to view and record the voltage signals obtained from the diagnostics.

7.2.4 A double-stack three-stage Marx generator

To demonstrate the flexible nature of the modular approach, and to increase the energy/pulse capability of the generator, a second three-module unit of IGBTs was connected in parallel with the first, as shown in Figure 7.9.

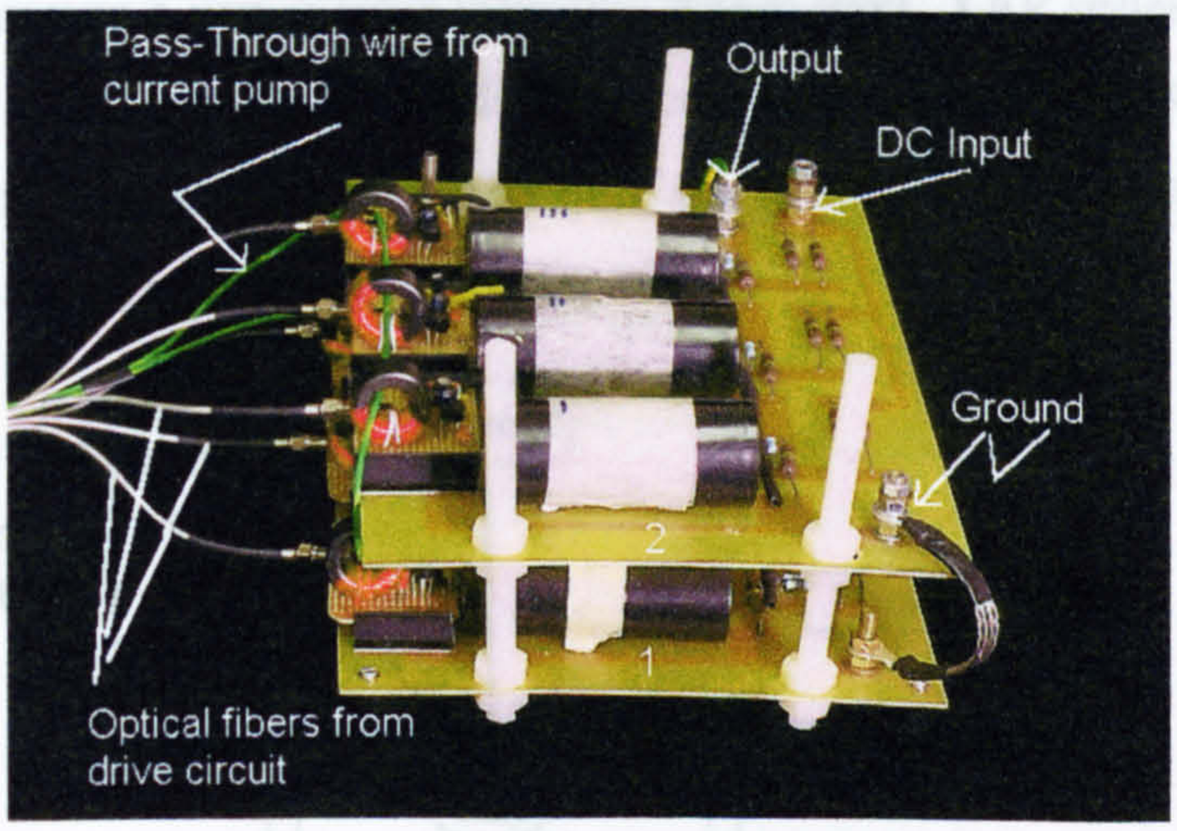

Figure 7.9 Photograph of 3 kV, 2 kA Marx generator

This generator is capable of delivering total energy of around 8 J per pulse and its voltage and current ratings are 3.0 kV and 2 kA, respectively. The generator was tested successfully by applying the same evaluation procedure as that discussed for the three-stage Marx generator, and similar voltage and current waveforms were observed. The waveforms had a longer duration due to the doubling of the circuit time constant.

7.3 Application of the solid-state Marx generator

The effectiveness of UV light in biological inactivation comes about as a consequence of the absorption by DNA molecules of illumination between 200 nm and 300 nm. A test of the capability of the solid-state Marx generator was carried out for pulsing a UV flashlamp to provide efficient emission of UV light in the germicidal wavelength region.

7.3.1 The experimental arrangement

The test was conducted with the assembly of Marx generator, UV flashlamp and sample contained in an optically isolated housing. Measurements were made using a spectrometer and other diagnostics as shown schematically in Figure 7.10. The diagnostic block comprised the voltage and current probes described in section 7.2.3. The UV flashlamp was a xenon lamp (Heraeus Noble-light, XAP series), which was constructed from a fused quartz tube filled with xenon to a pressure of 450 Torr. The tube had a 4 mm diameter bore and 50 mm arc length. It was capable of being operated with an average power of about 100 W.

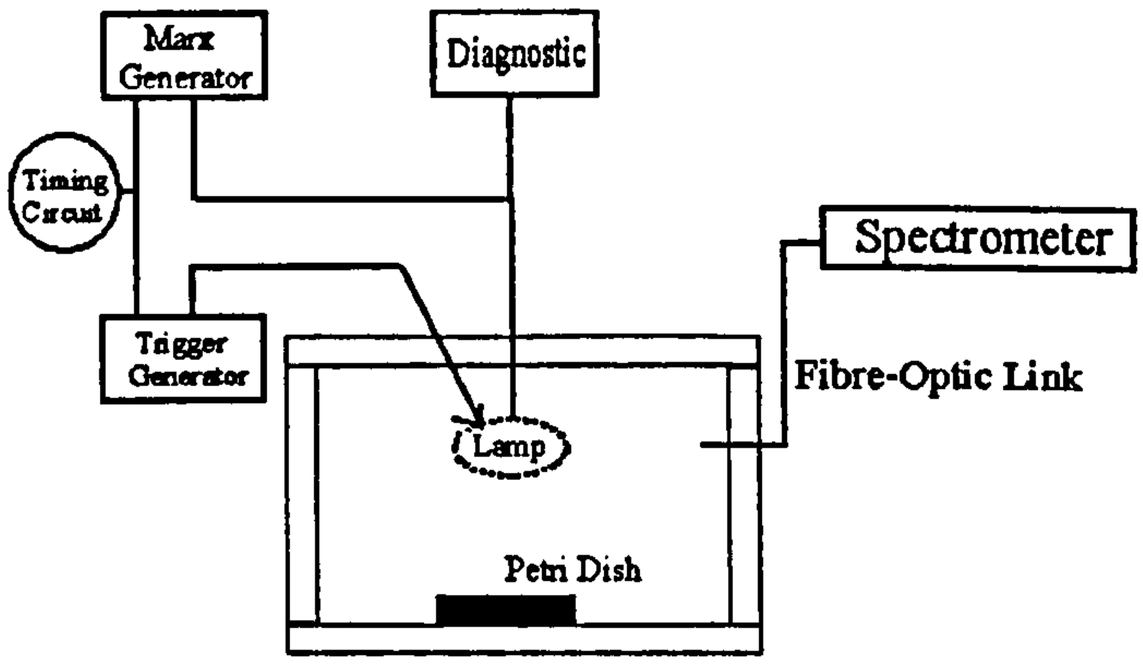

Figure 7.10 Diagram of experimental facility for microbial inactivation using a pulsed UV source.

Initial ionisation of the xenon gas required a triggering pulse of 15 to 20 kV, and this was supplied using the circuit of Figure 7.11.

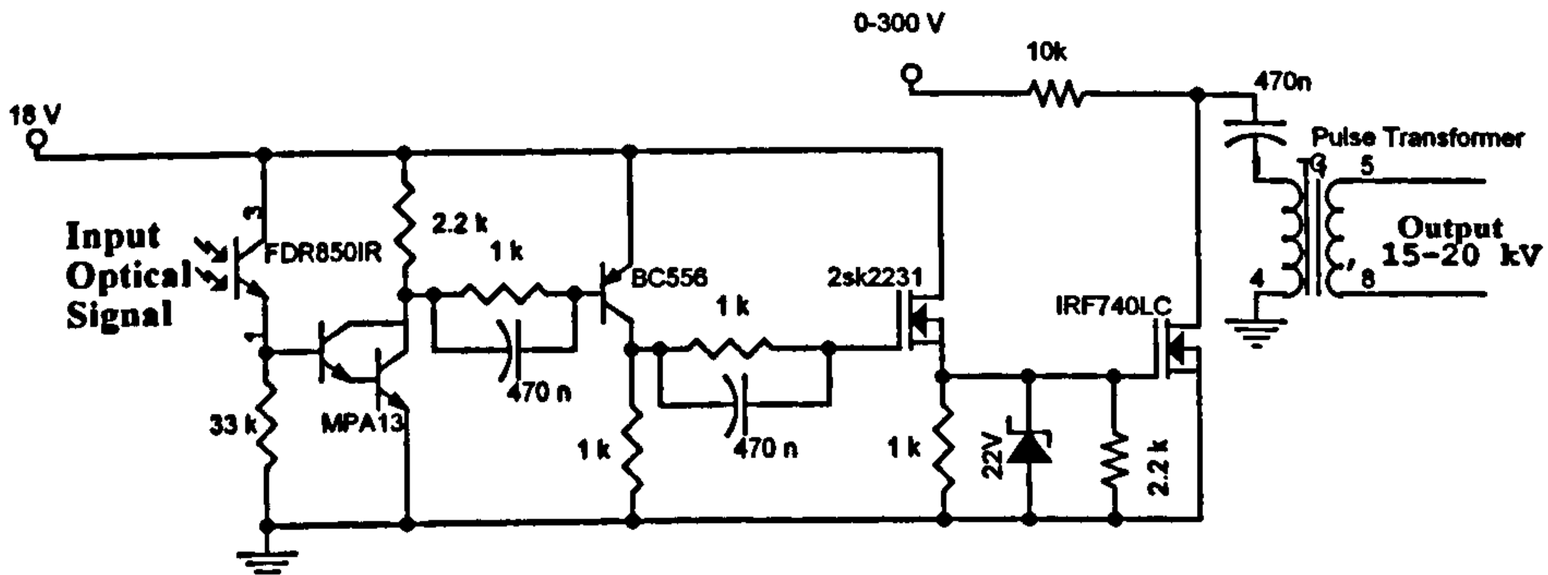

Figure 7.11 External triggering circuit for flashlamp.

A 470 nF capacitor was charged to 300 V and then upon closure of the high-voltage MOSFET, it was discharged through the primary winding of a transformer. This produced a high-voltage impulse across the secondary winding. The high-voltage

triggering pulse was applied to a nickel wire running the length of the lamp with several loops around the lamp envelope. Synchronisation between the external triggering circuit and the pulse generator was provided using the same optical signals generated with the circuit shown in Figure 7.4.

7.3.2 Flashlamp characteristics

The optical emission from the lamp was monitored using a four-channel Ocean Optics SQ2000 fibre optic spectrometer. The spectrometer had a detector (2048-element linear silicon CCD array) with a spectral range of 200-530 nm and a resolution of 1.25 nm. Typical emission spectra and dynamic resistance-voltage characteristics of the flashlamp for pulse energies of 4.5 J and 9.0 J are shown in Figures 7.12 and 7.13, respectively.

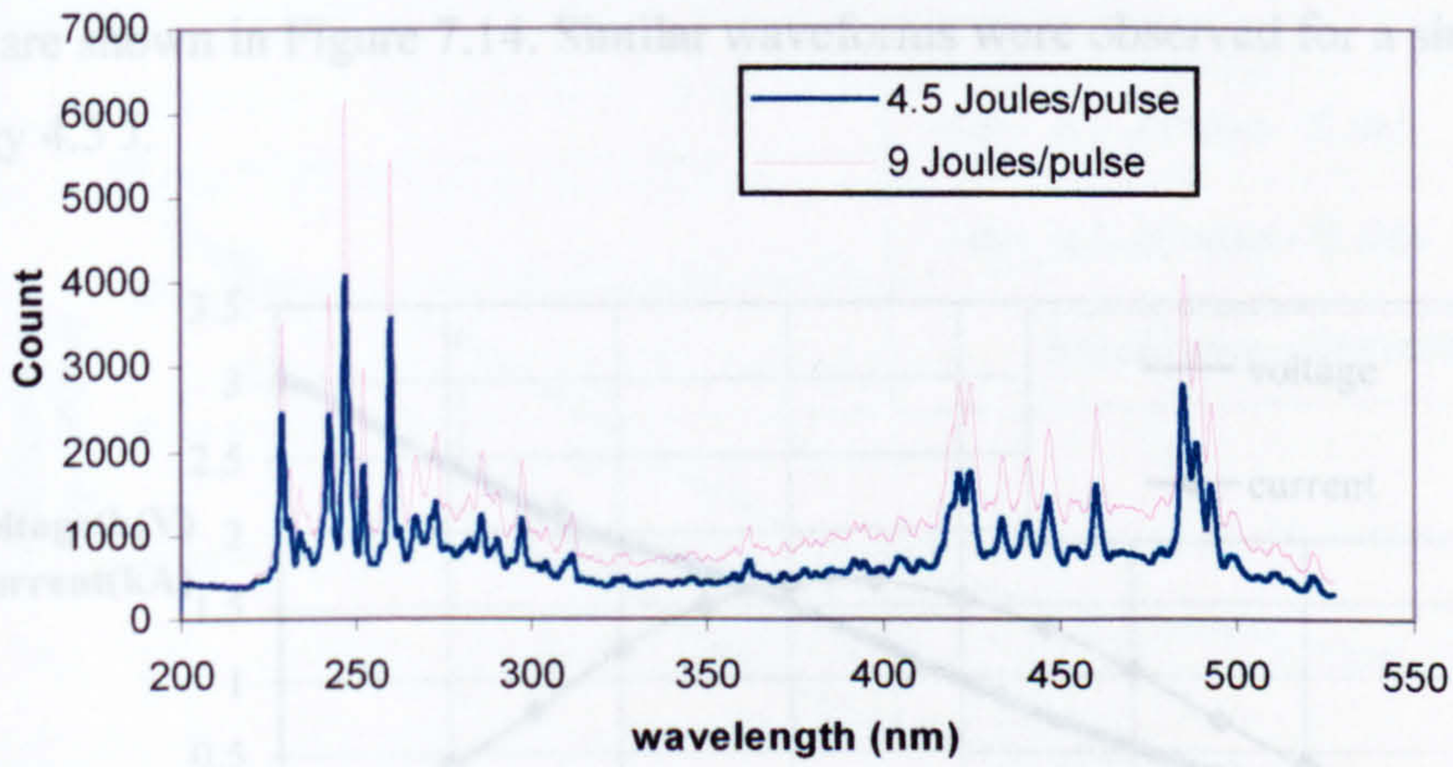

Figure 7.12 Flashlamp spectra for pulses of 4.5 J and 9.0 J.

Following triggering, ionisation of the lamp gas occurs and its resistance begins to fall, dropping to less than 0.5 Ω depending on the total energy delivered to the lamp. Hence the current through the lamp increases rapidly and the voltage across the lamp falls rapidly. As shown in Figure 7.13, the flashlamp has a minimum dynamic resistance of about 0.45 Ω and 0.75 Ω at a voltage of around 500 V when it is driven using 9.0 J and 4.5 J pulses, respectively.

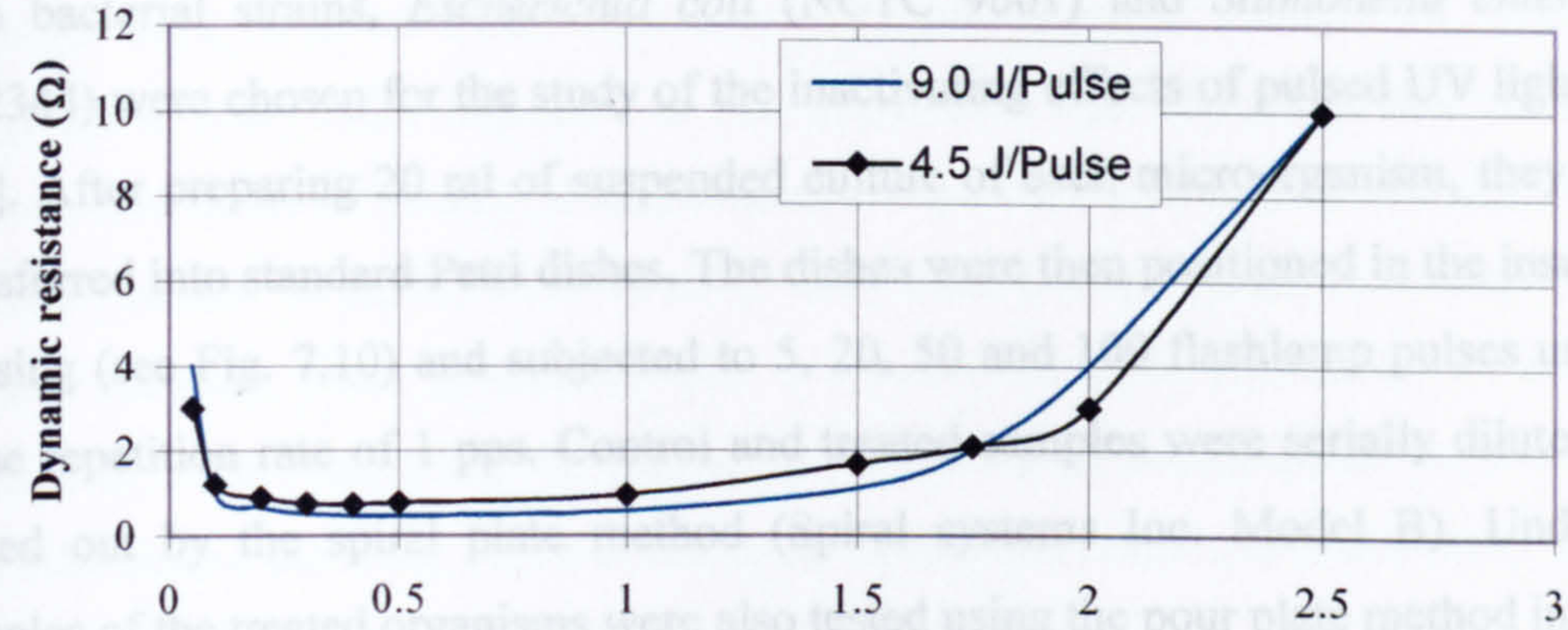

Figure 7.13 Flashlamp dynamic resistance-voltage characteristic for pulses of 4.5 J and 9.0 J.

Typical voltage and current waveforms of the flashlamp for a single pulse of energy 9.0 J are shown in Figure 7.14. Similar waveforms were observed for a single pulse of energy 4.5 J.

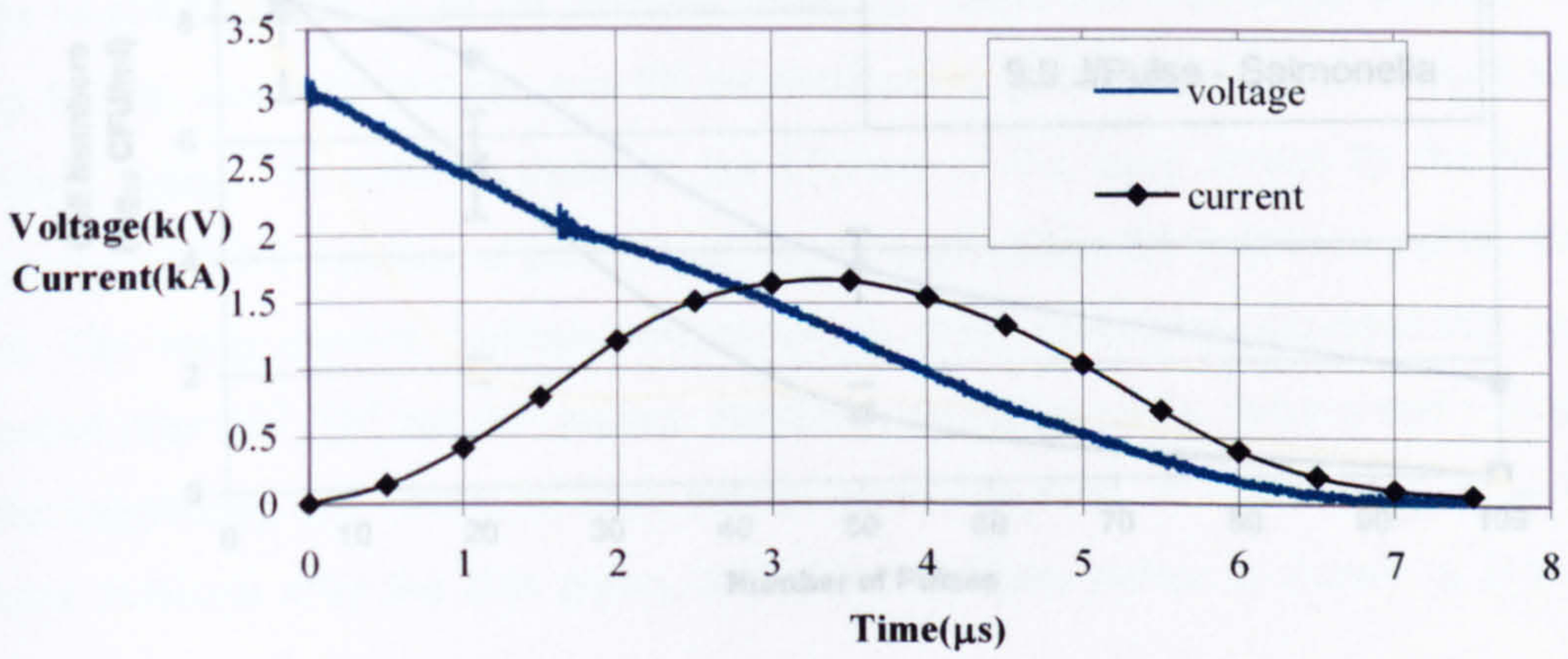

Figure 7.14 Flashlamp voltage and current waveforms for a 9.0 J pulse.

The current passing through the lamp for a pulse of 9.0 J has a larger peak value (~ 1.7 kA) than for a pulse of 4.5 J, where the peak current is 1.0 kA. This is due to the variation of the lamp dynamic resistance characteristic with energy/pulse.

7.3.3 Pulsed UV treatment of microorganisms

Two bacterial strains, *Escherichia coli* (NCTC 9001) and *Salmonella enteritidis* (132344) were chosen for the study of the inactivating effects of pulsed UV light [97, 102]. After preparing 20 ml of suspended culture of each microorganism, they were transferred into standard Petri dishes. The dishes were then positioned in the insulated housing (see Fig. 7.10) and subjected to 5, 20, 50 and 100 flashlamp pulses using a pulse repetition rate of 1 pps. Control and treated samples were serially diluted and plated out by the spiral plate method (Spiral systems Inc. Model B). Undiluted samples of the treated organisms were also tested using the pour plate method in order to detect low numbers of survivors. All plates were incubated at 37 ^{0}C for 24 hours and then counts of Colony Forming Units (CFU) were recorded. The experiment was carried out for energies of 4.5 and 9.0 J/pulse. The results are shown in Figure 7.15.

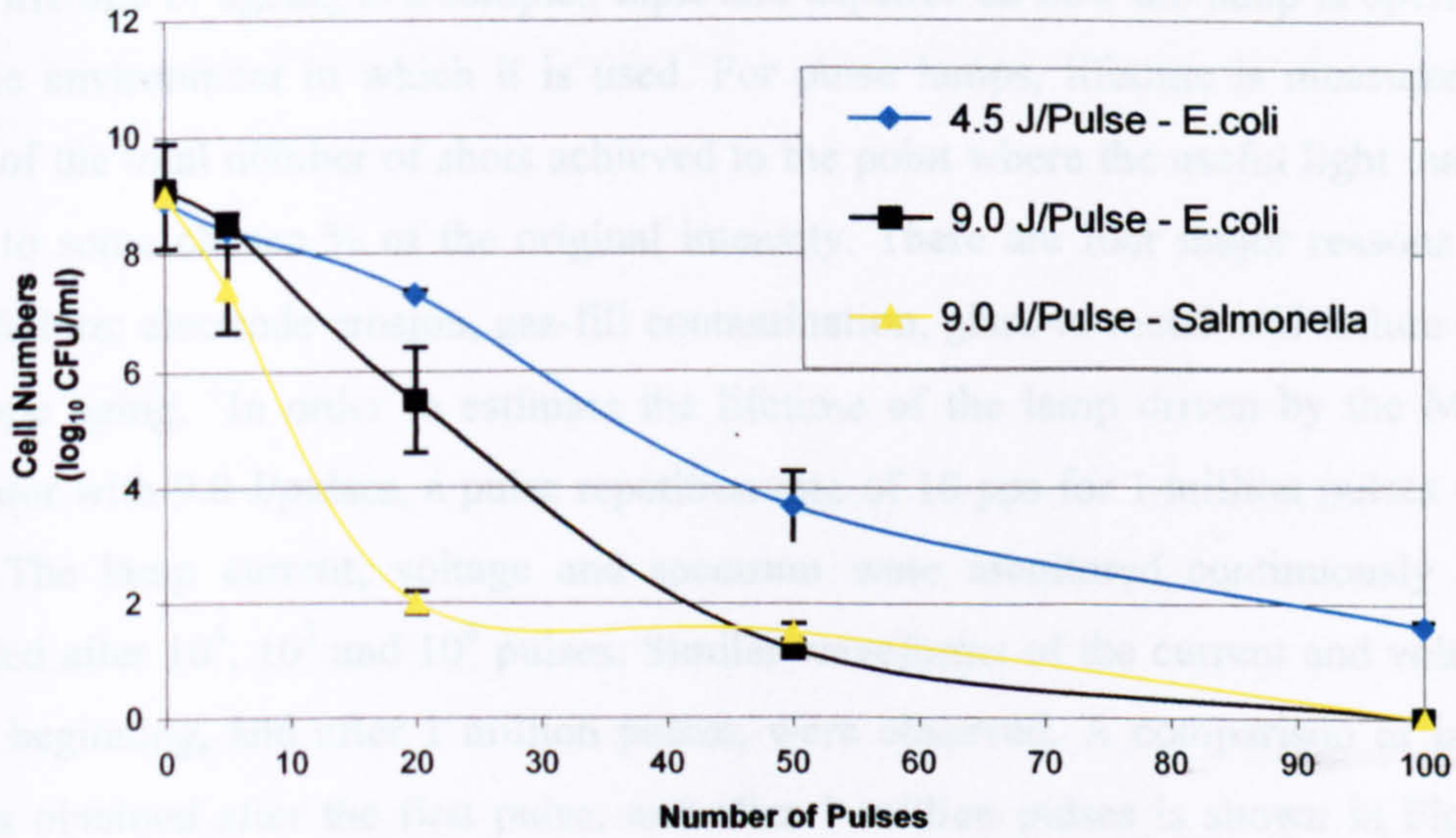

Following analysis of the irradiated samples, both *E.coli* and *Salmonella* showed a 9-log order reduction after treatment with 100 pulses with each pulse providing 9 Joules of radiated energy. 100 pulses of 4.5 Joules/pulse produced a 7-log order reduction for *E.coli*. Only an approximate 0.5-log order reduction was observed to occur after treatment of *E.coli* samples with 5 pulses of 4.5 J and 9.0 J. This relatively low rate of cell reduction over the first few pulses is likely due to the initial very high cell population (1.3×10^{9} CFU/ml) causing a fall-off in UV intensity through the 3.28 mm

depth of the sample. This effect was most likely due to the greater turbidity caused by the larger dimensions of *E.coli* cells compared with those of *Salmonella*. The total energy for a 7-log order reduction in cell population was 900 J and this shows an improvement in the efficiency of inactivation compared, for example, with the xenon-flashlamp results of Anderson *et al* [97]. They used a single-stage, inverting, pulse-forming network, Marx generator, with 3 J/pulse, a nominal peak of 30 kV and duration of 85 ns. Operating the flashlamp with a higher energy/pulse increases the light intensity of the lamp over the whole of its spectral range and particularly within the germicidal band (200 nm- 300 nm), as shown in Figure 7.12.

7.4 Lamp lifetime

Lamp lifetime or ageing is a complex topic and depends on how the lamp is operated and the environment in which it is used. For pulse lamps, lifetime is measured in terms of the total number of shots achieved to the point where the useful light output drops to some chosen % of the original intensity. There are four major reasons for lamp failure; electrode erosion, gas-fill contamination, glass-to-metal seal failure and envelope aging. In order to estimate the lifetime of the lamp driven by the Marx generator with 9.0 J/pulses, a pulse repetition rate of 10 pps for 1 million pulses was used. The lamp current, voltage and spectrum were monitored continuously and recorded after 10^4, 10^5 and 10^6 pulses. Similar waveforms of the current and voltage at the beginning, and after 1 million pulses, were observed. A comparison of lamp spectra obtained after the first pulse, and after 1 million pulses is shown in Figure 7.16.

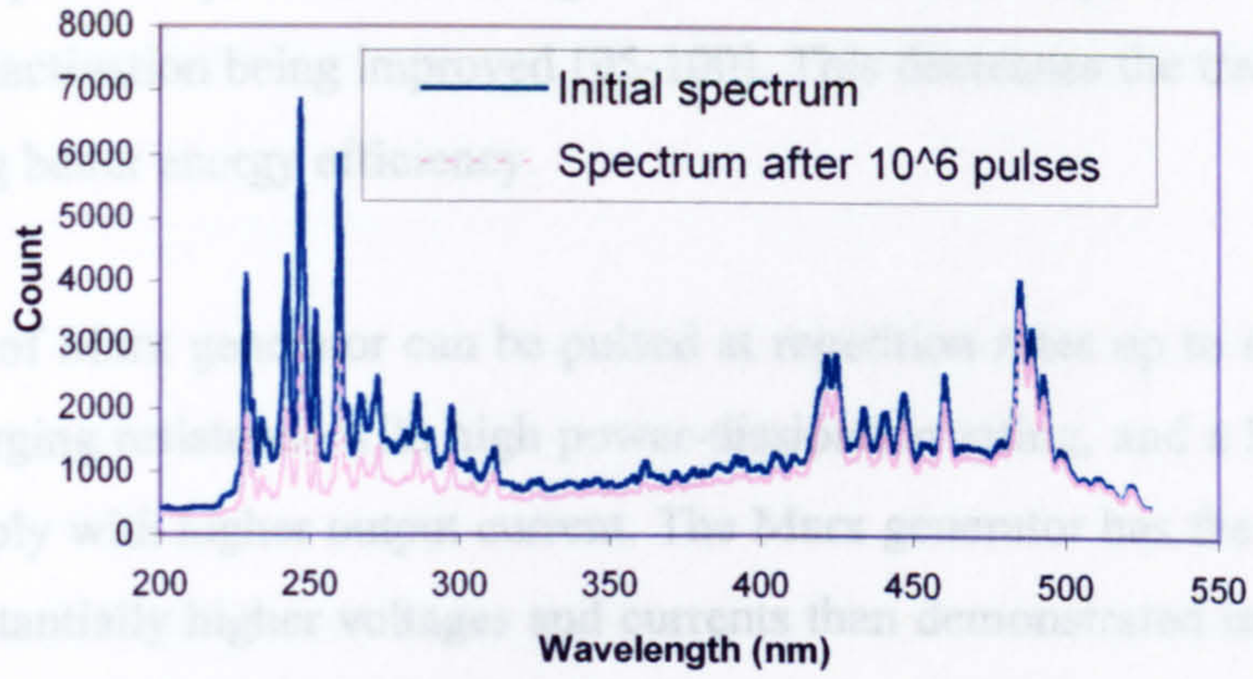

Figure 7.16 Comparison of initial lamp spectrum with the spectrum after 10^6 pulses.

Over time, the output intensity of the flashlamp falls over the whole of its spectral range. The fall in intensity appears greater (more than 50%) in the UV region. This is likely due to build-up on the inner tube wall of a coating that absorbs preferentially in the UV spectral region.

7.5 Conclusion

A modular Marx generator has been designed and evaluated. The capacitors of the Marx generator are switched using series and parallel connected 1.2 kV Insulated-Gate-Bipolar-Transistors (IGBT) that are optically controlled. IGBTs provide fast and repetitive switching, and have the advantage of being cheap and readily available devices. The generator system has modular flexibility to allow a selection of voltage and current ratings to be utilised, with the generator used here having an output voltage rating of 3 kV and a peak current rating of 2 kA. By means of synchronised and optically coupled signals, the new design provides very low pulse-to-pulse jitter (a few nanoseconds).

The performance of the solid-state switched Marx generator was successfully tested over a period of more than 10^6 pulses when it was applied to pulse a xenon flashlamp, with UV illumination from the flashlamp being used for inactivation of microrganisms. The average power of the xenon flashlamp is 100 W but pulsing with the Marx generator provided peak powers of up to 2 MW. High power pulses of UV

illumination appear to provide advantages for inactivation experiments with the efficiency of inactivation being improved [95-100]. This decreases the treatment time while providing better energy efficiency.

The new form of Marx generator can be pulsed at repetition rates up to several kHz, by using a charging resistance with high power-dissipation rating, and a high voltage DC power supply with higher output current. The Marx generator has the potential to operate at substantially higher voltages and currents than demonstrated in the present work. Consequently, it is likely to find application in other pulsed power systems such as those used for dielectric test systems, beam steering, gating and driving grids, and high-power laser-diode drivers.

Chapter 8

GENERAL CONCLUSIONS AND RECOMMENDATIONS FOR FUTURE WORK

8.1 Conclusions

In the first part of the present study, different solid-state switching devices with a stacking capability were investigated and this led to the choice of IGBT.

The dynamic behaviour of IGBTs was studied and it was concluded that it would be possible to accelerate the collector-emitter voltage, and thus the switching speed, by shaping the gate current. This was achieved by charging the input capacitance quickly. It was also confirmed that negative gate bias is not necessary to turn off or hold off an IGBT. However, by using negative gate bias voltage and low gate impedance, spurious triggering due to fast dv/dt, can be avoided totally. It was found that the collector-emitter voltage decreases in two stages (dual degradation) in most of the 1.2 kV IGBTs. Analysis of the simulation results, together with the experimental data, confirmed that the circuit and device parameters, particularly the gate-collector capacitance, determine the IGBT switching performance under fast pulse condition and a reason for dual degradation could be the rapid variations in device parasitic parameters such as gate –collector capacitance and therefore, care must be taken when choosing the 1.2 kV IGBTs for stacking in pulsed applications. It was also confirmed that the dual-degradation phenomenon cannot be due to over-rating the peak instantaneous power, nor is it associated with exceeding the current capability of the device.

The techniques (passive and active snubbers) available to ensure that the voltage is shared equally across the devices in series connection were investigated. It was shown that the active-gate-control methods are slow and unsuitable for fast-pulsed power applications where the pulse lengths are a few hundred nanoseconds, due to relying on sampling the voltage or voltage rise across the IGBTs.

Different techniques of shifting the switching pulses to the high voltage side were studied and tested. It was shown that commercial IGBT driver modules (silicon devices) cannot be used in applications requiring voltages above 1 kV and cascading

IGBTs, because of the variation of delay between input and output signals. Therefore, magnetic and optical isolation were preferred. Several pulse transformers including air-core and ferrite transformers were built and tested. In air-core transformers, the output pulses were fast, but their performance was very sensitive to noise, particularly when the trigger circuit was not far from the high voltage source. For ferrite-core transformers, optimum performance was achieved when the secondary winding had a symmetrical position relative to the primary winding. Single turn, ferrite-core pulse transformers with only one secondary winding were finally chosen for stacking 600 V IGBTs. Results from stacking 600 V IGBTs have shown that these pulse transformers have good operating performance in terms of speed and output-pulse magnitude. However, when driving five 1.2 kV IGBTs in parallel, their primary and secondary winding turns must be increased to three. For optimal synchronisation between switching pulses, the primary windings of the pulse transformers had to be connected in series. However, experimental results showed that by connecting the primary winding in parallel, the output pulses are faster due to lower inductance in the drive circuit, and if identical pulse transformers are used, synchronisation can also be achieved.

It has been shown that most of the 600 V fast IGBTs can be stacked for voltage and current ratings of up to a few kV and a few 100 A respectively. Higher ratings were also possible, but this led to slower switching speed. A prototype 2.5 kV, 250 A stack consisting of 25 × 600 V IGBTs was constructed and tested with a 10 Ω input impedance, Blumlein pulse generator successfully.

Over-voltage protection of IGBTs in stack using available fast non-linear voltage arresters such as *Transil* and *Transient Voltage suppressor* was investigated. Experimental results revealed that these devices can only be used for low voltage IGBTs (<600 V) and by connecting them in series, the difference between their rated voltage and the clamp voltage is increased, and so the voltage rating cannot be improved by placing them in series. This limited their application for stacking 1.2 kV IGBTs. An active method was finally used in stacking 1.2 kV IGBTs. In this method, the immunity of the total stack to short and long-term over-voltages was improved by monitoring the voltage across the bottom stage and finally sending a disable signal to the high voltage power supply to stop charging the pulse forming network (PFN).

A prototype stack of commercially available 1.2 kV IGBTs was designed and built for use as a closing switch in a 25 Ω input impedance, Blumlein pulse generator using a magnetic isolating technique. The switch was operated at voltage and current rating of 10 kV and 400 A, respectively, with a voltage fall-time of about 45 ns. The output pulse had a flattop pulse-width of about 200 ns in 250 ns Blumlein pulse generator.

It was shown that in stacking IGBTs with isolation of more than 10 kV, pulse transformers with bigger cores must be used and this requires additional circuitry. This problem could be addressed in a more efficient way through optical coupling. Initial experiments showed that Opto-coupler devices tend to be slow and have significant device-to-device delay. Therefore, optical emitters and detectors were tested and finally prototype PCB circuits for driving emitters and detectors were developed. The DC voltage required by the drive circuit of the detectors were also provided from the voltage across the IGBT modules by adding some components to the drive circuit. The switching performance of an IGBT module driven by the prototype drive circuit was tested and the comparison showed no significant differences between the switching speeds of modules. It was found, however, that by increasing the number of IGBT modules in series, optical coupling provides better performance than magnetic coupling. Finally, an optically coupled stack of commercially available 1.2 kV IGBTs was designed and built for use as a closing switch in a 25 Ω input impedance, Blumlein pulse generator. The pulser successfully operated at a voltage of 10 kV with its output terminated in a matched load.

In the second part of the present study, the 10 kV optically triggered IGBT stack was successfully operated using a large number of pulses with different PRF for the PEF treatment of microorganisms. Although the stack was designed for operating voltages up to 10 kV, it was observed that it can safely handle voltages up to 12 kV for short periods of times. The application of the pulser was tested in both static and flow PEF treatment systems and the IGBT stack provided stable performance during all the experiments.

In the third part, a modular Marx generator was designed and evaluated using series and parallel connected 1.2 kV IGBTs that were optically controlled. The generator system had modular flexibility to allow a selection of voltage and current ratings to be utilised, with the generator used having an output voltage rating of 3 kV and a peak current rating of 2 kA. The performance of the Marx generator was successfully

tested over a period of more than 10^6 pulses when it was applied to pulse a Xenon flashlamp, with UV illumination from the flashlamp being used for inactivation of microorganisms. The Marx generator could also be pulsed at repetition rates up to several kHz, by using a charging resistance with high power-dissipation rating, and a high voltage DC power supply with higher output current. It had also the potential to operate at substantially higher voltages and currents than demonstrated in the present work.

8.2 Recommendations for further work

The work undertaken during the course of this investigation has only be concerned with 600 V and 1.2 kV IGBTs. It is, therefore, of great interest to examine the switching performance of IGBTs with higher voltage ratings. It has also been shown that the dual degradation phenomenon exists for most IGBTs and the reason(s) for this behaviour could be predicted using the simulation developed. The accuracy and capability of this simulation could be improved by considering all parameters of the Blumlein pulse generator and not using the equivalent circuit. In magnetic isolation, the trigger pulse was directly applied to the IGBT modules. The speed and therefore the synchronisation between triggering pulses can be improved by using a secondary electronic circuit. Over-voltage protection of IGBTs can also be improved with monitoring the voltage across the IGBTs and inactivating the control circuit.

The IGBT stacks and Marx generator can be pulsed at repetition rates up to several kHz, by using a high voltage DC power supply with higher output current. Therefore, it is likely to find applications in other pulsed power systems.

Chapter 9

ACKNOWLEDGEMENTS

I would like to thank Prof MacGregor for his supervision and guidance throughout the course of this research at the university of Strathclyde.

I would like to gratefully acknowledge all the helpful advice and suggestions from Prof Jerry Woolsey.

Thanks also go to Prof J. Anderson, Dr. N. Rowan and Dr. K. Wall for their assistance in bioscience matters.

The help from other members of the pulsed power group and the assistance of the technicians during my study at Strathclyde is much appreciated.

I also wish to thank my wife for all her care, support and understanding, and to my wonderful son Arian for all the love, blessing and warmth he's brought into my life.

10. REFERENCES

1. Brown M P and Smith P W, "High power, pulsed soliton generation at radio and microwave frequencies", *Proc. 11th IEEE Pulsed Power Conf.*, Baltimore, pp 346-54, 1997.
2. Phelps A D R and Cross A W, "High power pulsed microwave and millimetre-wave generation", *IEE Symposium – Pulsed Power 99*, Oxford, Paper No. 10, 1999.
3. Spielman R B, Seamen W A, Long J F, Garcia H, Wagoner R, "Pulsed power performance of PBFA Z", *Proc. 11th IEEE Pulsed Power Conf.*, Baltimore, pp 709-14, 1997.
4. Miller R B, Ballard E O, Barr G W, Bowman and Cochrane J C, " The atlas pulsed power facility for high energy density physics experiments", *Proc. 12th IEEE Pulsed Power Conf.*, Monterey, pp 484-8, 1999.
5. Ramirez J, Prestwich K R, Johnson D L, Corley J P, Denisn G J and Alexander J A, "Performance of the Hermes-III gamma ray simulator", *Proc. 7th IEEE Pulsed Power Conf.*, Monterey, pp 26-31, 1989.
6. Touryan K L, William M, Catherine T, Aimone T and Benze W, "Electrohydraulic rock fracturing by pulsed power", *Proc. 7th IEEE Pulsed Power Conf.*, Monterey, pp 69-72, 1989.
7. Lisitsyn I V, Inoue H and Katsuki S, "Drilling and demolition of rocks by pulsed power", *Proc. 12th IEEE Pulsed Power Conf.*, Monterey, pp 169-72, 1999.
8. Anderson J G, MacGregor S J, Rowan N J, Fouracre R A and Farish O, " Assessment of inhibitory and inactivating effects of pulsed electrotechnologies on foodborne pathogenic microorganisms", *Proc. 13th Inter. Conf. On Gas Discharges and their Applications*, Glasgow, pp 5-14, 2000.
9. MacGregor S J, Farish O, Fouracre R and Rowan N J, " Inactivation of pathogenic and spoilage microorganisms in a test liquid using pulsed electric field", *IEEE Trans. on Plasma Science*, **28**, pp 144-9, 2000.

10. Schoenbach K H, "The effect of pulsed electric fields on biological cells: experiments and applications", *IEEE Trans. on Plasma Science*, **25**, pp 284-93, 1997.

11. Bysritskii V, Yankelevich V, Wood Y, Chauhan T and Isakov S, "Pulsed discharge in the fluidised packed-bed reactor for toxic water remediation", *Proc. 12th IEEE Pulsed Power Conf.*, Monterey, pp 464-7, 1999.

12. Swart P H and Bergmann H M, "Thyratrons versus Thyristors for high power pulse laser excitation", *Proc. 19th Inter. Power Modulator Symposium*, pp 414-20, 1990.

13. Wakeman F J and Green B K, "Improved semiconductor switches for pulse power applications", *Proc. 23rd Inter. Power Modulator Symposium*, pp 135-8, 1998.

14. Vitins J, J.L. Steiner and J.A. Welleman, "High power semiconductor for pulsed switching", *Proc. 7th IEEE Pulsed Power Conf.*, pp 352-7, 1989.

15. Hudgins J L and Portnoy W M, "High di/dt pulse switching of thyristors", *IEEE Trans. on Power Electronics*, Vol. PE-2, No. 2, April 1987.

16. Vorster A, "Replacement of thyratrons by a Mosmatrix", *Proc. 8th IEEE Pulsed Power Conf.* pp 1005-8, 1991.

17. Bonthond J, Ducimetiere and L, Schroder G.H, "High current, high di/dt switching with optimised GTO thyristors", *Proc. 21st Inter. Power Modulator Symposium*, pp 85-7, 1994.

18. Hadizad P and Gundersen M A, "High-voltage recessed –gate GaAs field effect transistors", *Proc. 21st Inter. Power Modulator Symposium*, pp 78-80, 1994.

19. Brylevsky V I, Efanov V.M, Kardo-Sysoev A.F and Sminova I.A, "Power fast modulator thyristors", *Proc. 22nd Inter. Power Modulator Symposium*, pp 39-43, 1996.

20. Paschen F, *Wied Ann*, **37**, p69, 1889.

21. Guenther A and Kristiansen M, *Gas Discharge Closing Switches*, (New York: Plenum Press), 1990.

22. Burkes T R, Craig T R, Hagler J P, Kristiansen M O and Portnoy M, "A review of high power switch technology", *IEEE Trans. on Electron Devices*, **26**, pp 1401-11, 1979.

23. MacGregor S J, Tuema F A, Turnbull S M and Farish O, "The operation of repetitive high-pressure spark gap switches", *J Phys. D: Appl. Phys.*, **26**, pp 954-8, 1993.

24. Turnbull S M, "An investigation into the repetitive operation of high pressure spark gap switches", *Ph.D. thesis*, University of Strathclyde, 1994.

25. Brown A J W and Smith, "A multi-paralleled thyratron, repetitively pulsed power supply for high-power gas lasers", *Proc. 17th Power Modulator Symp.*, Seattle, pp 191-5, 1986.

26. Cavazos T C, McGowan T C and Behr J, "Thyratron evaluation at high power, high repetition rates", *Proc. 19th Power Modulator Symp.*, San Diego, pp 211-4, 1990.

27. McDuff G, "Parallel operation of thyratrons in low inductance discharge circuits", *Proc. 3rd IEEE Pulsed Power Conf.*, Albuquerque, pp 308-10, 1981.

28. Kihara R, Cummings D B and Leighton K S, "Commercial high current ignitron development", *Proc. 7th IEEE Pulsed Power Conf.*, Monterey, pp 18-21, 1989.

29. Kihara R, "Evaluation of commercially available ignitrons as high-current, high-coulomb transfer switches", *Proc. 6th IEEE Pulsed Power Conf.*, Arlington, pp 581-4, 1987.

30. Mazda F F, *Power electronics Handbook*, Oxford (England), Boston: Newnes, 1997.

31. Mohan Ned, *Power Electronics: Converters, Applications, and Design*, (New York: Wiley), 1989.

32. Sankaran A, Hudgins J.L and Portnoy M, "High-energy pulse-switching characteristics of thyristors", *IEEE Trans. on Power Electronics*, Vol. 8, No. 4, October 1993.

33. Jian M and Xi-Jie C, "High repetition rate of solid-state switches technique in solid laser", *Proc. 8th IEEE Pulsed Power Conf.*, pp 204-5, 1991.

34. Dreifuerst G R and Merritt B T, "Development and operation of a Solid-state switch for thyratron replacement", *Proc. 8th IEEE Pulsed Power Conf.*, pp 191-5, 1991.

35. Richardson B, Rush R and Iskander M, "Versatile high voltage solid state MOSFET modulators for driving RF sources", *Proc. 23rd Inter. Power modulator Symposium*, pp 164-7, 1998.

36. Shepherd W, *Power Electronics and Motor Control*, (New York: Cambridge University Press), 1995.

37. Bovino L, Schneider S and Wright J, "The MOS-controlled thyristor (MCT) as an on-off capacitor bank switch", *Proc. 7th IEEE Pulsed Power Conf.*, pp 849-52, 1989.

38. Braun C and Pastore R, "Operation of a high-frequency resonant inverter using MOS-controlled thyristors", *Proc. 20th Inter. Power Modulator Symposium*, pp 278-80, 1992.

39. Pastore R, Braun C and Weiner M, "Developmental MOS-controlled thyristors (MCT) behaviour", *Proc. 19th Inter. Power Modulator Symposium*, pp 391-99, 1990.

40. Pastore R Braun C and Weiner M, "Characterization of 3000 Volt MOS-controlled thyristors", *Proc. 8th IEEE Pulsed Power Conf.*, pp 196-99, 1991.

41. Bayne S B, Portnoy W M, Rohwein G J and Hudgins J L, "MOS-gated thyristors (MCTs) for high power switching", *Proc. 21st Inter. Power Modulator Symposium*, pp 75-77, 1994.

42. Venkataraghavan P and Baliga B J, "The dv/dt capability of MOS-gated thyristors", *IEEE Trans. on Power Electronics*, Vol. 13, No. 4, July 1998.

43. Endo F, Okamura K, Kakizaki K, Takagi S and Kaneko E, "All solid-state exciter for high-power, high-repetition rate excimer laser", *Proc. 22nd Inter. Power Modulator Symposium*, pp 63-6, 1996.

44. Endo F, Okamura K, Yamazaki C, Watanabe Y, Kaneko E and Ohshima I, "Development of semiconductor switch for pulsed power utilizing MAGTs", *Proc. 9th IEEE Pulsed Power Conf.*, pp 650-3, 1993.

45. Hadizad P, Hur J H, Gunderson M A and Fetterman H R, "Design of an opening and closing GaAs static induction transistor for pulsed power applications", *Proc. 7th IEEE Pulsed Power Conf.*, pp 846-8, 1989.

46. Ibuka S, Osada T, Jinqushi K, Suda M and Nakamura T, "Pulsed power generator utilizing fast SI-thyristors for environmental applications", *Proc. 12th IEEE Pulsed Power Conf.*, pp 1441-4, 1999.

47. Ibuka S, Saito K, Yamamoto A, Hanibuchi A and Yasuoka K, "SI-thyristor as á high-power switching device for fast high voltage pulse generators", *Proc. 11th IEEE Pulsed Power Conf.*, pp 954-8, 1997.

48. Kuroda S and Maeyama M, "A study of switching properties of SI-thyristor using high current gate circuit", *Proc. 12th IEEE Pulsed Power Conf.*, pp 1195-8, 1999.

49. Hotta E and Hironaka R, "Performance of pulsed power generator using high voltage static induction thyristor", *Proc. 12th IEEE Pulsed Power Conf.*, pp 788-90, 1999.

50. Hadizad P, Hur J H, Hummel S and Gunderson M A, "High speed static induction transistor for pulsed power applications", *Proc. 19th Inter. Power Modulator Symposium*, pp 343-6, 1990.

51. Bredenkamp L et al, "A bipolar command charge pulser for laser with IGBTs", *Proc. 20th Inter. Power Modulator Symposium*, pp 258-61, 1992.

52. Mazzola M, "A solid-state modulator for environmental applications of pulsed acoustics", *Proc. 12th IEEE Pulsed Power Conf.*, pp 458-60, 1999.

53. Zolfaghari A et al, "Solid-state switch modulator deck for the MIT-bates S band transmitter", *Proc. 23rd Inter. Power Modulator Symposium*, pp 173-6, 1998.

54. Tomek M et al, "Parts obsolescence mitigation in the Harpoon modulator", *Proc. 23rd Inter. Power Modulator Symposium*, pp 150-5, 1998.

55. Okamura K et al, "High-power switching of semiconductor devices", *Proc. 7th IEEE Pulsed Power Conf.*, pp 836-9, 1989.

56. Okamura K et al, "Development of a semiconductor switch for high power copper vapor lasers", *Proc. 11th IEEE Pulsed Power Conf.*, pp 975-80, 1997.

57. Gaudreau M P J et al, "Solid-state pulsed power systems", *Proc. 23rd Inter. Power Modulator Symposium*, pp 160-3, 1998.

58. Gekat F, Ruhl D and G Joachim, "An IGBT-based switch as replacement for thyratrons in Dopper radar transmitters", *Proc. 23rd Inter. Power Modulator Symposium*, pp 110-3, 1998.

59. Rashid M H, *Power Electronics: Circuits, Devices, and applications*, (New Jersey: Prentice Hall), 1993.

60. Baliga B J, *Modern Power Devices*, (New York: Wiley), 1987.

61. Hefner A R, "An investigation of drive circuit requirements for the power insulated gate bipolar transistor (IGBT)", *IEEE Trans. on Power Electronics*, Vol. 6, No. 2, April 1991.

62. Gerster C and Hofer P, "Gate-controlled dv/dt and di/dt limitation in high power IGBT converters", *EPE Journal*, Vol. 5, No. 3, pp 11-16, 1996.

63. Schneider T and Bayerer R, "Advanced module construction for high speed, high current IGBT modules", *Proc. Power Conversion*, pp 143-53, 1990.

64. Musumeci S et al, "Switching behaviour improvement of insulated gate-controlled devices", *IEEE Trans. on Power Electronics*, Vol. 12, No. 4, July 1997.

65. Carmelo L et al, "Assessment of off-state negative gate voltage requirements for IGBTs", *IEEE Trans. on Power Electronic*, Vol. 10, No. 3, May 1995.

66. Musumeci S et al, "A new adaptive driving technique for high current gate controlled devices", *IEEE Trans. on Power Electronics*, pp 480-6, 1994.

67. Licitra C et al, "Optimum driving circuit for IGBT devices suitable for integration", *Proc. Inter. Symposium Power Semiconductor Devices and Ics*, pp 221-5, Tokyo, 1992.

68. Galluzzo A et al, "Switching characteristic improvement of modern gate controlled devices", *The European Power Electronics Association*, pp 374-9, 1993.

69. Abraham L et al, "Investigation on IGBT switching process with variable gate charge current", *The European Power electronics Association*, pp 323-7, 1993.

70. Carmelo L et al, "A new driving circuit for IGBT devices", *IEEE Trans. on Power Electronics*, Vol. 10, No. 3, May 1995.

71. Chokhawala R et al, "Gate drive consideration for IGBT modules", *IEEE Trans. on Industry Applications*, Vol. 31, No. 3, pp 603-11, May/June 1995.

72. McNeil N et al, "Assessment of off-state negative gate voltage requirements for IGBTs", *IEEE Trans. on Power Electronics*, Vol. 13, No. 3, May 1998.

73. Letor R and Melito M, "Safe behaviour of IGBTs submitted to a dv/dt", *Proc. Power Conversion*, pp 25-32, 1990.

74. Chaofeng Huang, et al, " Low jitter and drift high voltage IGBT gate driver", *Proc. 14th IEEE Pulsed Power Conf.*, pp 127-30, 2003.

75. Palmer P R and Githiari A N, "The series connection of IGBTs with active voltage sharing", *IEEE Trans. on Power Electronics*, Vol. 12, No. 4, July 1997.

76. Gediga S et al, "High power IGBT converters with new gate drive and protection circuit", *6th European Conf. on Power Electronics and Applications*, Seville, Spain, Vol. 1, pp 66-70, September 1995.

77. Tromp H T W et al, "A new approach to series semiconductor switch applications", *Proc. 21st Inter. Power Modulator Symposium*, pp 81-4, 1994.

78. Williams B W, *Power Electronics, Devices, Drive, Applications and Passive Components*, (Hong Kong: Macmillan Press), 1992.

79. Githiari A N, "The design of semiconductor switches for high voltage applications", *Ph.D. thesis*, University of Cambridge, 1996.

80. Letor R, "Static and dynamic behaviour of paralleled IGBTs", *IEEE Trans. on Industry Applications*, Vol. 28, No. 2, March/April 1992.

81. Endo F, Okamura K, Kakizaki K, Takagi S and Kaneko E, "All solid-state pulsed power modulator for high power, high repetition rate applications", *Proc. 12th IEEE Inter. Pulsed Power conf.*, pp 1417-20, 1999.

82. Rahimo M T et al, "Analysis of the IGBT/freewheeling diode switching behaviour during turn-on in hard switching applications", Proc. *IEE Power Electronics and Variable speed Drives*, pp 381-6, September 1998.

83. Ruedi H and Kohli P, "IGBT drivers correctly calculated", *CT-Concept Technology Ltd*, Application Note AN-9701, 1997.

84. "A more realistic characterization of power MOSFET output capacitance Coss", *International Rectifier Company*, Application Note AN-1001.

85. Glasoe G N and Lebacqz J V, *Pulse Generators*, (New York: McGraw-Hill), 1948.

86. Sibley M J N (Martin J N), *Optical Communications: Components and Systems*, (Basingstoke: Macmillan), 1995.

87. Senior J M, *Optical Fiber Communications: Principles and Practice*, (Englewood Cliffs, NJ: Prentice Hall), 1992.

88. Bai-Lin Qin, Gustavo V, Canovas B, Swanson B G, Pedrow D and Olsen R G, "Inactivating microorganisms using a pulsed electric field continuous treatment system", *IEEE Trans. on Industry Applications*, Vol. 34, No. 1, pp 43-50, January/February 1998.

89. Jayaram S H, "Sterilization of liquid foods by pulsed electric fields", *IEEE Electrical insulation Magazine*, Vol. 16, No. 6, pp 17-25, November/December 2000.

90. Schoenbach K H et al, "The effect of pulsed electric field on biological cells: experiments and applications", *IEEE Trans. on Plasma Science*, Vol. 25, April 1977, pp 284-292.

91. Gustavo V B et al, *Nonthermal preservation of foods*, (New York: Marcel Dekker), 1997.

92. Duffin W J, *Electricity and Magnetism*, (London: McGraw-Hill Companies), 1997.

93. Wilschut J and Hoekstra D, *Membrane Fusion*, (New York: Marcel Dekker Inc.), 1991.

94. Githiari A N, "Studies on the use of high intensity pulsed electric fields for the inactivation of problematic food-borne microorganisms", *Ph.D. thesis*, University of Strathclyde, 2003.

95. McDonald K and Curry R, "Comparison of pulsed and CW ultraviolet light sources to inactivate spores on surfaces", *13th IEEE Inter. Pulsed Power Conf.*, pp 604-7, Vol. 1, 2001.

96. McIlvaney L et al, "Electrotechnologies for food pasteurisation and sterilisation", Chapter 47, pp 1-8, *Published by IEE*, London, 1998.

97. Anderson J G et al, "Inactivation of food-borne enteropathogenic bacteria and spoilage fungi using pulsed-light", *IEEE Trans. on Plasma Science*, Vol. 28, No. 1, February 2000.

98. MacGregor S J et al, "Light inactivation of food-related pathogenic bacteria using a pulsed power source", *Letters App. Microbiol.*, No. 27, pp 67-70, 1998.

99. Okamura K et al, "Development of the high repetitive impulse voltage generator using semiconductor switches", *12th IEEE Inter. Pulsed Power Conf.*, pp 807-10, California, 1999.

100. Loughlin J O et al, "High repetition rate Marx type generator", *13th IEEE Inter. Pulsed Power Conf.*, pp 242-6, 2001.

101. Kuffel E et al, *High Voltage engineering: Fundamental*, (Oxford: Pergamon Press), 2000.

102. Hobbs B C and Roberts D, *Food Poisoning and Food Hygiene*, (London: E.Arnold), 1987.

Chapter 11

LIST OF PUBLICATIONS

During the course of this study, the following papers were published;

1. Z Ghasemi, S MacGregor, J Anderson and Y Lamont, "Development of an integrated solid-state generator for light inactivation of food-related pathogenic bacteria," *J. Meas. Sci. Technol.*, **14**, No. 6, 2003.

2. K Wall, Z Ghasemi, D Cameron, N. J. Rowan, S MacGregor and J Anderson, "Inactivation of Beer and Lager Spoilage Microorganisms Using Pulsed Electric Fields", 10th International Congress of Bacteriology and Applied Microbiology, Paris, 2002.

3. Z Ghasemi and S MacGregor, "A solid-state pulse generator for use in the PEF inactivation of microorganisms", 9th. Iranian PhD students seminar in Europe, Birmingham, UK, 29-30 June 2002.

4. Z Ghasemi and S MacGregor, "A Solid-State Pulse Generator for Use in The PEF Inactivation of Microorganisms," 10th ICEE, Tabriz, 2002.

5. Z Ghasemi and S MacGregor, "A Comparison into The Performance of 1.2 kV IGBT Devices Under Pulsed Conditions," 8th. Iranian PhD students' seminar in Europe, Manchester, UK, 2001.

6. Z Ghasemi, S MacGregor, A R Dick and F A Tuema, "Fast High-Voltage, High-Current Switching using Stacked IGBTs," IEE Symposium Pulsed Power, London, 2001.

7. Z Ghasemi and S MacGregor, "Power Semiconductor Devices in Pulsed Power Applications," 7th Iranian Ph.D. students seminar in Europe, Manchester, UK, 20-21 May 2000.

Fast High-Voltage, High-Current Switching Using Stacked IGBTs

Z Ghasemi*, S J MacGregor, A R Dick and F A Tuema
Department of Electronic and Electrical Engineering,
University of Strathclyde,
Royal College Building,
204 George Street,
Glasgow, G1 1XW.

Abstract

The development of solid-state switches for pulsed power applications has been of considerable interest since high-power semiconductor devices became available. However, the use of solid-state devices in the pulsed power environment has usually been restricted by device limitations in either their voltage/current ratings or their switching speed. The stacking of fast medium-voltage devices, such as IGBTs, to improve the voltage rating, makes solid-state switches a potential substitute for conventional switches such as hard glass tubes, thyratrons and spark gaps.

This paper reports on a comparative study into the performance of commercially available 1.2 kV IGBT devices. It has been found that dual degradation of the drain-source voltage can be observed in most of the devices and the reasons for this have been investigated.

Further studies have looked at the performance and operation of a high current switch employing fifty 1.2 kV IGBTs in a stacked configuration. Switching times of a few tens of nanoseconds have been measured for a 10 kV charging voltage switched into a 25 Ω input impedance Blumlein pulse generator.

Introduction

A primary switching component is an essential device in any pulsed power system. In recent years, much emphasis has been placed in developing semiconductor switches because of their reported longer lifetime, low degradation and low jitter. The most commonly used high-power semiconductor devices in pulsed power applications are Metal Oxide Semiconductor Field Effect Transistors (MOSFETs) and Insulated Gate Bipolar Transistors (IGBTs), which are commercially available with voltage ratings up to 1.2 kV. MOSFETs have substantially faster switching speeds while IGBTs are generally more efficient, can handle more power and are capable of being manufactured at higher voltage ratings [1]. For high-voltage IGBT devices, in order to keep the electric field at a reasonable level in the drift region, a wide drift region must be used and this leads to a high on-state resistance. A high level of charge has to be injected at the device anode to keep the on-state resistance to a reasonable value. This increases the turn-off time of the device, as well as the switching losses. Therefore, the series connection of lower on-state resistance, medium-voltage devices is more practical for obtaining higher switching speeds. Choosing the proper device, as well as dealing with problems such as unbalanced voltage and current sharing, are important aspects of stacking IGBTs and these are reported in this paper.

Device Selection

* E-mail: z.ghasemi@eee.strath.ac.uk

A comparative study into the performance of 1.2 kV IGBT devices has shown that the drain-source voltage decreases in two stages (dual degradation) in most of the commercially available 1.2 kV IGBTs. The slope of the drain-source voltage is altered when these devices are stressed to enable rapid turn-on [2]. To assess single 1.2 kV IGBT devices in terms of their switching speed, different types of 1.2 kV IGBT devices were examined by connecting them to a Blumlein pulse generator. Results showing the comparisons for two 1.2 kV IGBTs, GT15Q301 and IRG4PH40U are shown in Figure 1.

In Figure 1, the drain-source voltage collapse waveforms for IRG4PH40U and GT15Q301 are shown, as well as the respective Blumlein output pulses. The voltage across IRG4PH40U decreases in two stages. The voltage collapses quickly during the first stage and decreases approximately linearly during the second stage. As shown in Figure 1, this significantly affects the shape of generated output pulse by slowing down the pulse rise and fall times. This dual degradation effect is not observed in the GT15Q301 waveforms.

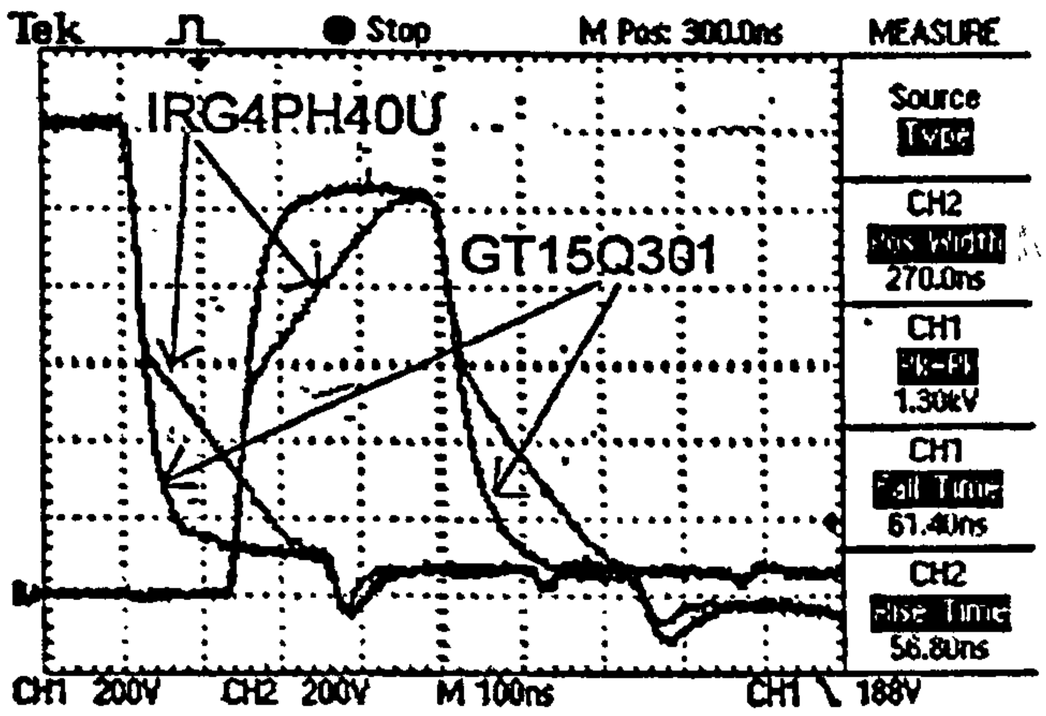

Figure 1: Comparison of the switching behaviour of GT15Q301 and IRG4PH40U under pulsed condition, voltage across the device and output pulse.

Over-rating the peak instantaneous power and variation the parasitic capacitances, particularly the gate-drain capacitor, could be possible reasons for changing the rate of voltage-fall in 1.2 kV IGBT devices. Consequently, the C_{gd}- V_{ds} characteristic of different devices was studied. It was found that the reason for dual degradation of the voltage across the device is a strong variation in the device parasitic parameters, which vary as functions of the drain-source voltage [3]. Operating IGBTs in faster circuits leads to a higher voltage gain, as well as increasing the Miller effect and finally more disruption to the drain-source voltage waveform [4].

The IGBT Gate-drive circuit

Electrically, the gate to source connection in MOS-gate devices such as IGBTs looks like a capacitor and only the gate-source voltage controls the flow of drain-source current. Once the gate-source capacitor is fully charged, no additional energy is required to keep the device on. In pulsed power applications, to increase the switching rate, both during turn-on and turn-off, fast and large current pulses are required. Therefore, in a module consisting of several IGBTs in parallel, the drive circuit should be able to deliver fast current pulses of the order of 100A. Furthermore, for driving a stack of a several IGBT modules connected in series, proper coupling must be applied among the driving pulses. Commercial isolated IGBT gate-driving IC modules with output currents of 10s of amperes such as TC-4426 and HCPL-3120 are available, but their application has been limited due to significant variations in the delay time from one module output to another. A common approach to trigger multiple devices in series is to use a single primary pulse transformer with multiple secondary windings. In this case, the parasitic elements of each secondary winding and its associated element must be minimised in order to avoid increasing the switching time and to

eliminate interference associated with its charging and discharging. The pulse transformer response near the front edge of the pulse was studied. It was found that in order for the output to rise rapidly, the leakage inductance and the shunt capacitance must be kept small. Large step-up ratios, "n", can be obtained only at the price of increasing the rise-time by a factor of "n". Results have shown that pulse transformers with cylindrical ferrite cores have good operating performance in terms of speed and output pulse magnitude. Both the primary and secondary windings consisted of three turns to minimise the leakage inductance. A schematic of the drive circuit is shown in Figure 2 [5].

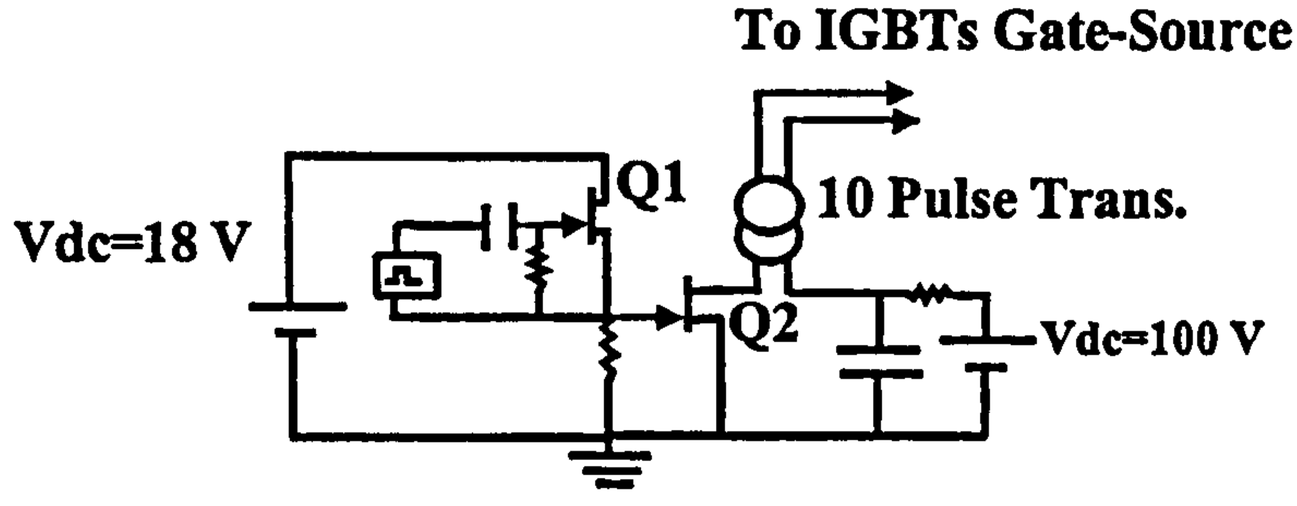

Figure 2: Schematic of electric circuit for driving IGBT modules.

As shown in Figure 2, the drive capacitor is charged to 100 V and is then discharged through the primary windings of isolating pulse transformers. The main switch in the drive circuit, Q_2, consists of three 200 V MOSFETs connected in parallel. The external triggering signal is applied via Q_1 to Q_2. For optimal synchronisation between stages, the primary windings of the pulse transformers should be connected in series. However, experimental results have shown that by connecting the primary windings in parallel, output pulses are faster due to lower inductance in drive circuit and if identical pulse transformers are used, synchronisation can also be achieved.

Switch Description

A photograph of a stack, consisting of fifty 1.2 kV IGBTs in a series/parallel configuration is shown in Figure 3.

In this figure, the stack consists of ten modules in series, with each module consisting of five IGBTs in parallel. The stack was designed so that the circuit layout for all of the devices in the stack is identical. This prevents any timing error in switching.

To ensure that the total voltage across the switch is evenly distributed across each stage during steady state operation, a resistive biasing network has been used. There is an absence of leakage current information in IGBT data sheets. However, this is known to be a function of case temperature. A single module was thermally cycled and its leakage current was measured. The value of steady-state voltage sharing resistor was calculated using the maximum leakage current. Voltage sharing during transient operation was also achieved by using synchronised triggering pulses for each stage.

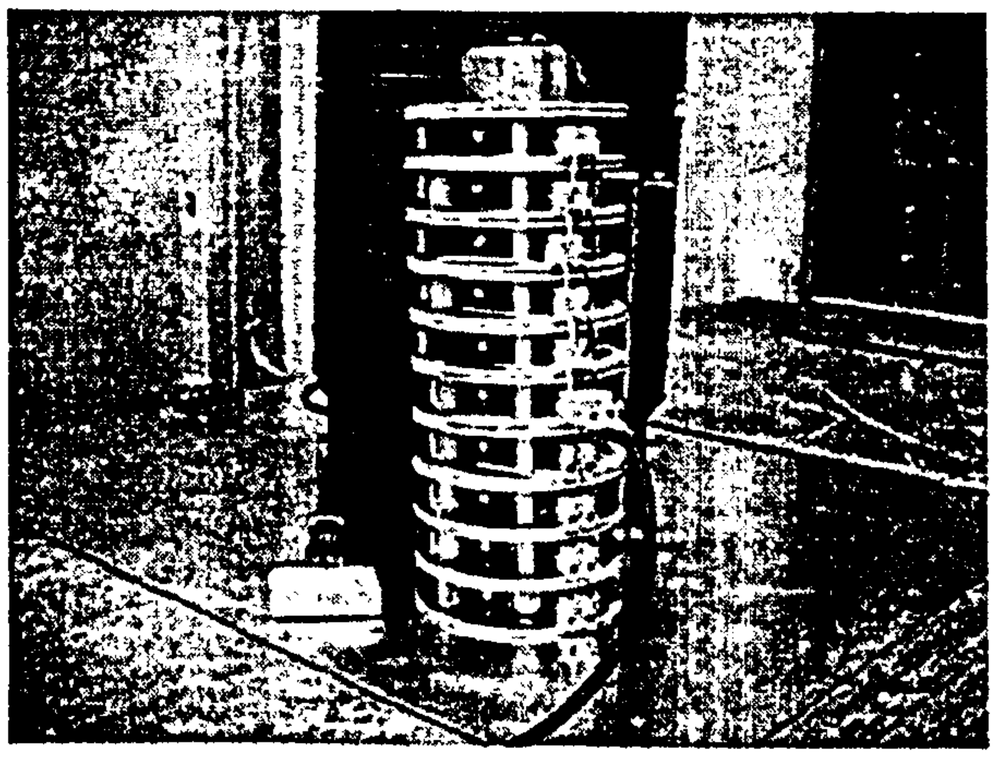

Figure 3: Photograph of 10 kV, 400 A stack of IGBT modules involving 50 1.2 kV IGBTs.

Experimental Results

Experimental results for the turn-on waveform of the switch described previously were obtained by connecting it to a 25Ω input impedance stacked Blumlein pulser having pulse duration of 250 ns. The pulser was terminated in a matched (50Ω) load. The switch was successfully operated at its voltage and current rating (400 A and 10 kV). Voltage sharing was checked by observing the triggering pulses across the gate-source of each module. In addition, voltage waveforms across different stages were monitored simultaneously and no significant over voltages were observed. The voltage waveforms recorded across the switch and generator output are shown in Figure 4.

As shown in Figure 4, the voltage across the stack collapses in less than 50 ns (10-90%), leading to a fast rising pulse at the output of the pulser. The negative voltage appearing across the switch during the conducting stage is a result of a diagnostic instrument and voltage drop across the switch is only a few 10s of volts.

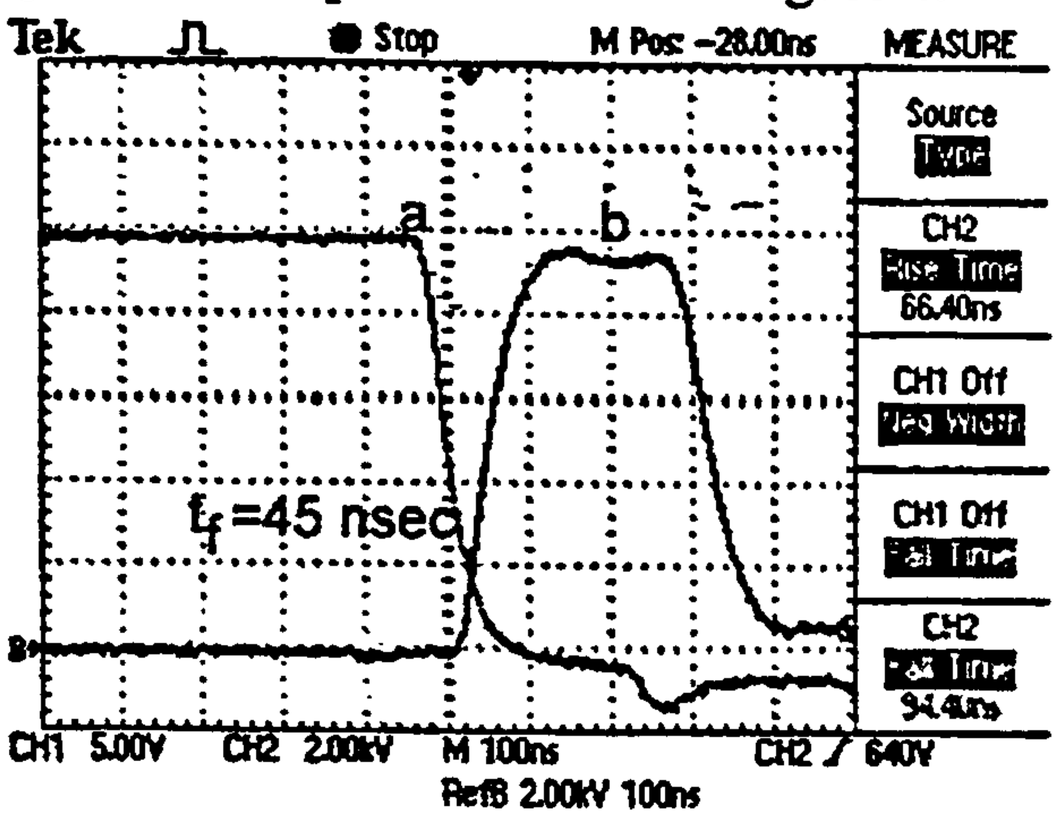

Figure 4: Voltage waveform across the switch (trace "a") and output voltage pulse (trace "b") in 250 ns Blumlein pulser (both traces amplitude 2kV/div and time base 100 ns/div).

Conclusion

Dual degradation of the drain-source voltage can be seen in some 1.2 kV IGBTs. A reason for this behaviour could be fast variations in device parasitic parameters such as gate-drain capacitance. Operating IGBTs in fast pulse circuits leads to a higher voltage gain resulting in an increased Miller effect.

A stack of 1.2 kV commercially available IGBTs has been designed and built for use as a closing switch in a 25 Ω input impedance, Blumlein pulse generator. The switch can operate at voltage and current ratings of 10 kV and 500 A respectively, with a voltage fall-time of about 45 ns.

Future efforts will be directed towards the application of optical coupling of the trigger pulse, which will facilitate an increased number of devices and hence an increased of voltage rating for the switch. This will also serve to improve the switch operating performance in terms of jitter and switching speed.

Acknowledgement

One of us, ZG, would like to thank the ministry of science, research and technology in Iran for financial support.

References

[1] E. G. Cook, "Review of Solid-State Modulators," Lawrence Livermore National Laboratory, USA.

[2] F. Endo et. al, "All-Solid-State Pulsed Power Modulator For High Power, High Repetition Rate Applications," *Proc. 12th. IEEE Int. Pulsed Power Conf., pp 1417-1420, 1999.*

[3] M. T. Rahimo et. al, "Analysis of the IGBT/Freewheeling Diode switching Behaviour During Turn-on in Hard Switching Applications," *IEE Power Electronics and Variable Speed Drives, pp 381-386, 1998.*

[4] B. J. Baliga, "Modern Power Devices," New York, Willey, 1987.

[5] E.G. Cook et al, "Inductive-Adder Kicker Modulator for DARHT-2," Lawrence Livermore National Laboratory, C. A. Brooksby-Bechtel Nevada.

INSTITUTE OF PHYSICS PUBLISHING MEASUREMENT SCIENCE AND TECHNOLOGY

Meas. Sci. Technol. 14 (2003) N26–N32 PII: S0957-0233(03)57226-5

DESIGN NOTE

Development of an integrated solid-state generator for light inactivation of food-related pathogenic bacteria

Z Ghasemi, S Macgregor, J Anderson and Y Lamont

Department of Electronic and Electrical Engineering, University of Strathclyde, Royal College Building, 204 George Street, Glasgow G1 1XW, UK

E-mail: z.ghasemi@eee.strath.ac.uk

Received 6 December 2002, in final form 7 March 2003, accepted for publication 14 March 2003
Published 24 April 2003
Online at stacks.iop.org/MST/14/N26

Abstract

This paper is concerned with the design and performance of a fully integrated solid-state Marx generator, which has been developed to drive a UV flashlamp for use in microbiological inactivation. The generator has an output voltage rating of 3 kV and a peak current rating of 2 kA, although the modular approach taken allows for a number of voltage and current ratings to be achieved. The generator is constructed using a number of series- and parallel-connected 1.2 kV insulated-gate-bipolar-transistor (IGBT) switched capacitors. Switching of the IGBT modules is controlled by an optical signal. Details are given of how the optimum IGBT gate-drive circuit is achieved using optical components and a pass-through wire to provide the required energies for individual IGBT modules. The generator is demonstrated as the driver of a UV flashlamp used for inactivation of food-related pathogenic bacteria such as *E. coli* and *Salmonella*. The performance of the Marx generator over a period of 10^6 pulses is examined, along with the changes that occur in the spectrum of the UV flashlamp during the same period.

Keywords: pulsed generator, solid-state switching, flashlamp driver, pulsed light inactivation

(Some figures in this article are in colour only in the electronic version)

1. Introduction

Illness caused by the consumption of contaminated food and food-borne diseases still remains a major cause of death throughout the world. Recent estimates of the incidence of food-borne infection for the UK and US are around 9 million and 75 million cases per year, respectively [1]. Clearly, the application of methods for either reducing or eliminating the microbiological risks associated with contaminated foods will have a significant effect on the incidence of food-borne disease. A possible approach to decreasing the level of microbial contamination on food surfaces and in food preparation environments is through the use of ultraviolet (UV) illumination. Exposure of pathogenic bacteria to UV light within the germicidal wavelength range 200 to 300 nm results in the inactivation of micro-organisms [2]. Therefore, UV illumination may have practical application for the disinfection of food and contact surfaces if effective methods of UV generation and delivery can be developed. It has been reported that pulsed UV light, with the capability of delivering peak powers of many megawatts to the flashlamps, can yield higher microbial inactivation rates than conventional UV light systems, which operate continuously and have power levels in the range 100–1000 W [2, 3]. In fact, a pulse

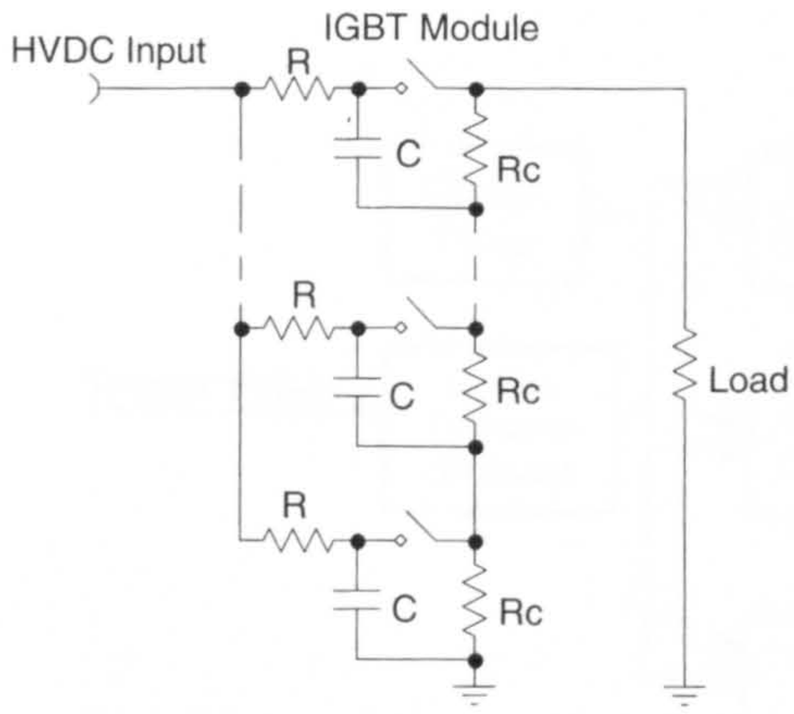

Figure 1. The basic Marx generator.

power energization technique can deliver many megawatts of electrical power to the light source using a modest energy input of a few joules. This produces a greater intensity of the shorter, bactericidal wavelengths of light, which leads to further effectiveness, and decreases the treatment time from 30 to 60 min in continuously UV operated systems to a few seconds.

In general, flashlamps, used as sources of UV light, can be driven by applying a voltage pulse much lower than the lamp self-breakdown voltage (10–20 kV) by using a trigger pulse of the order of 20–30 kV with a pulse width of a few microseconds to cause the initial ionization of the gas. In the following section, the design considerations for a solid-state Marx generator as a driver for UV flashlamps are discussed.

2. Solid-state Marx generator

A Marx generator provides one of the most widely used methods of generating high-voltage impulses because it features a low-voltage power supply for charging and does not require a pulse transformer for the generation of the high voltage [4, 5]. The basic Marx generator as shown in figure 1 comprises a number of stages, with each stage made of a discrete capacitor and a switch. Voltage multiplication is achieved by charging the capacitors in parallel, through charging resistors, and then discharging them in series by simultaneously closing the switch [6].

Because of the short lifetimes of the spark gaps normally used for switching, Marx generators tend to have a limited lifetime. This limits their use in highly repetitive applications. However, this problem can be solved by using solid-state switching devices. The use of solid-state switches has been restricted by limitations in their voltage/current rating or switching speed; however, stacking fast medium-voltage devices, such as insulated-gate-bipolar-transistors (IGBTs), to improve the voltage rating can provide a useful alternative to conventional switches such as spark gaps [7, 8]. This offers a number of advantages, such as high pulse repetition potential, low maintenance, low cost and better flexibility in terms of voltage and current ratings.

2.1. Peak current rating of IGBT modules

A photograph of an IGBT module that consists of five GT15Q301 IGBTs (manufactured by Toshiba) connected in parallel is shown in figure 2. Previous studies into the stacking of 1.2 kV IGBT modules have shown that this module can operate reliably with a peak current of about 1 kA and a pulse duration of a few microseconds. This has been confirmed in the present study using the arrangement shown in figure 3.

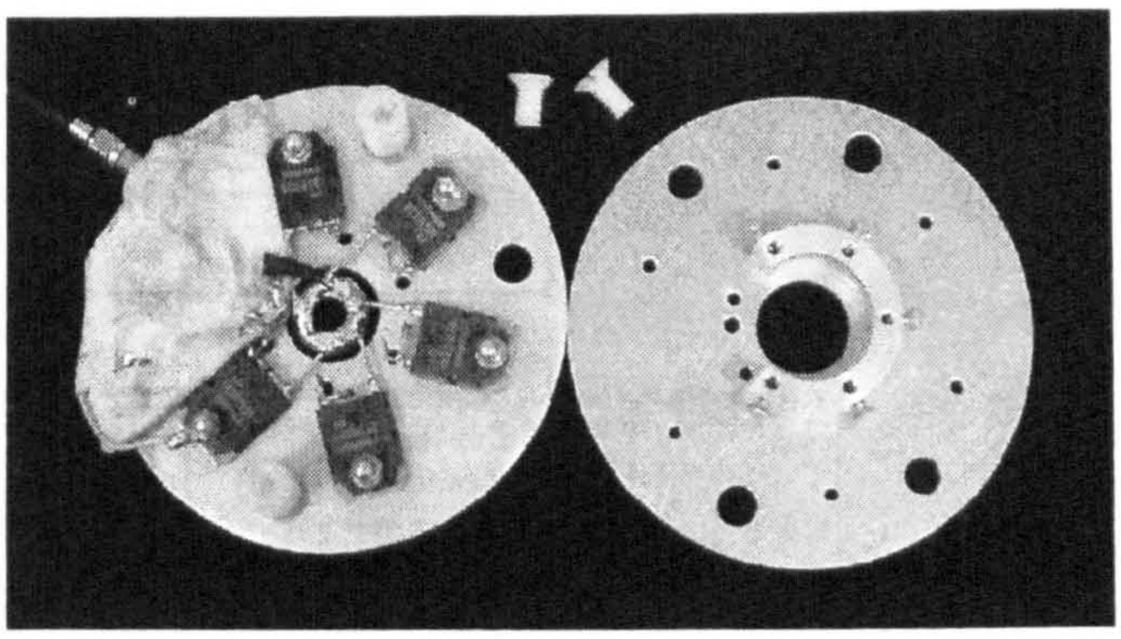

Figure 2. Photograph of a module of five IGBTs in parallel.

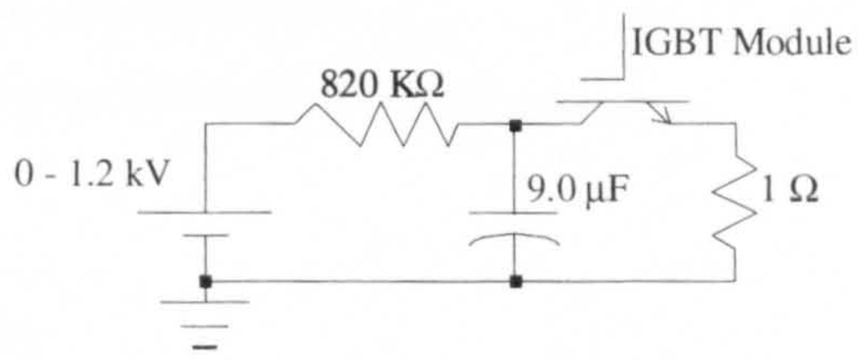

Figure 3. The circuit used to check the maximum operating current for IGBT modules.

The charging capacitor in figure 3 was made up of six single 1.5 μF, 1.5 kV capacitors connected in parallel to minimize series inductance. The switching performance of an IGBT module was investigated while the charging voltage was controlled from 0 to 1.2 kV. The IGBTs were triggered with an optical signal, and using a drive circuit, fed by an external dc power supply. It was found that IGBT modules could safely handle peak currents of 1 kA at 1 kV.

2.2. Marx generator drive circuits

In order to produce 3 kV impulse voltages with a current capability of 1 kA, and by considering the current/voltage ratings of IGBT modules, a prototype Marx generator, consisting of three stages, was designed. A diagram illustrating the layout of a three-stage Marx generator is given in figure 4. In each stage, two 1.5 μF, 1.5 kV capacitors were connected in parallel to provide an energy/pulse of 1.5 J for a stage voltage of 1.0 kV.

Driving single IGBT modules was accomplished using magnetic or optical coupling. However, initial experiments showed that magnetic coupling imposes a limit of pulse duration (about 3 μs) in triggering signals and requires good insulation between the cores and windings. Optical decoupling does not impose these limits in terms of the isolation voltage and pulse duration. However, separate isolated dc power supplies were required in each IGBT module. The optical emitters were driven using the circuit shown in figure 5. A peak current of a few tens of amperes with a small rise-time (50 ns) was passed through all of the emitters. Tailoring of the rate of rise of current to the optical emitters ensured homogeneous switching of the assembly by

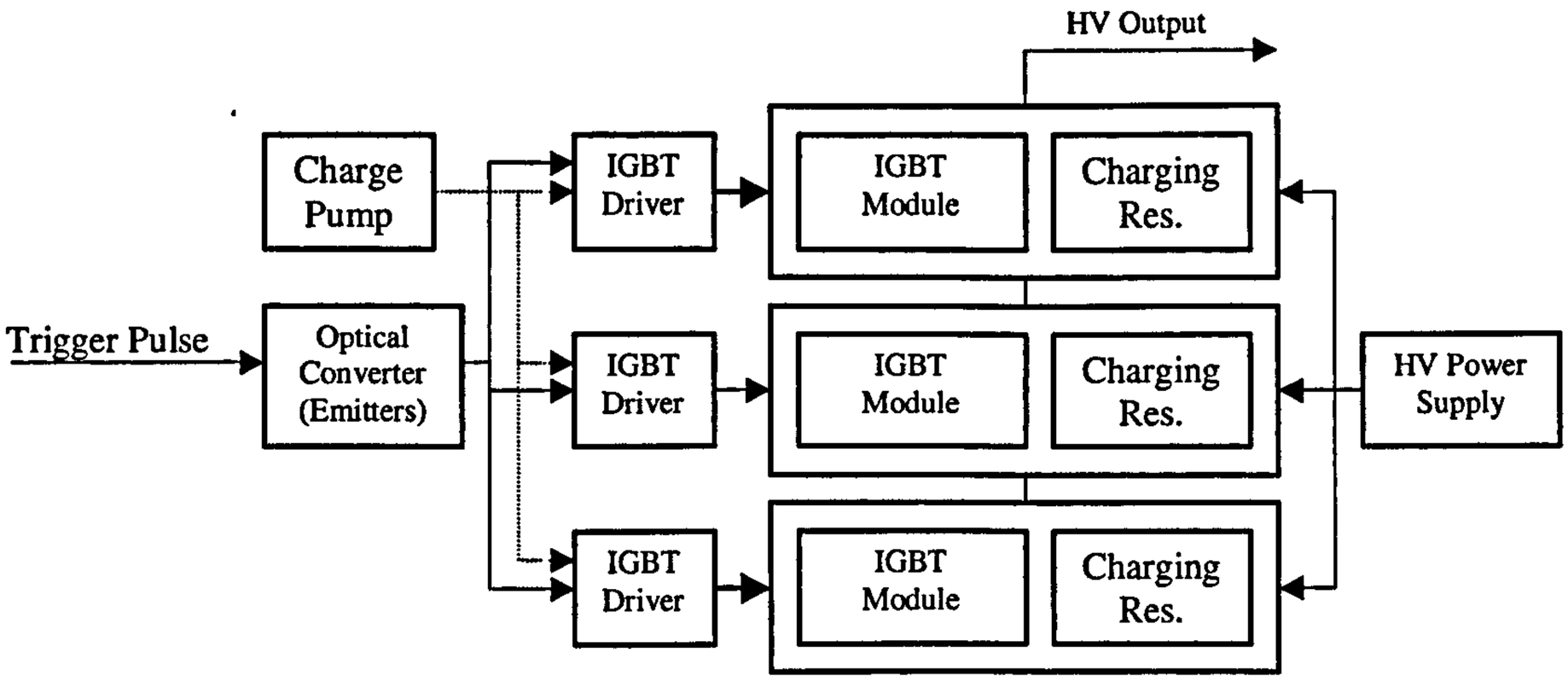

Figure 4. Block diagram illustrating the main components in a three-stage Marx generator.

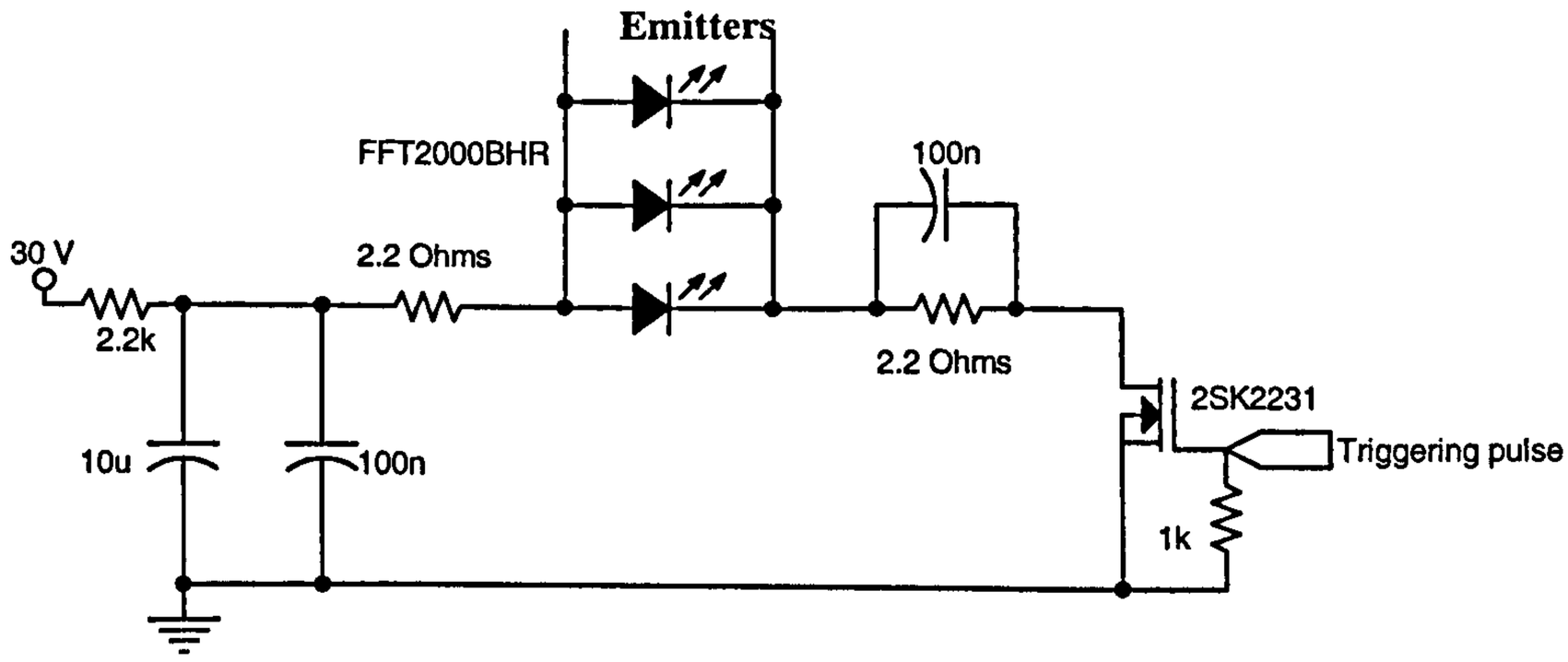

Figure 5. The circuit used to drive the optical emitters.

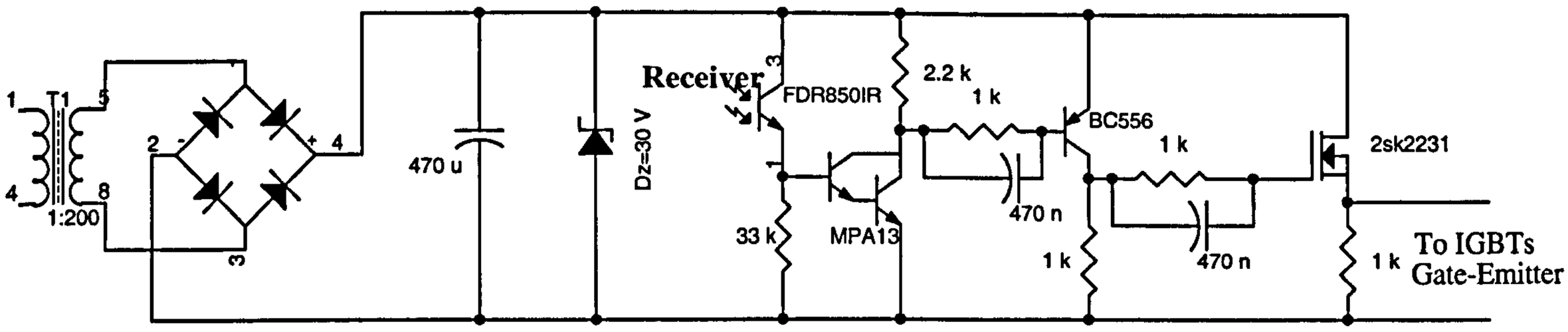

Figure 6. The circuit used for the conversion of the optical signals to the voltage trigger pulses.

minimizing turn-on delays and variation across the IGBT modules.

By employing the same circuit in each module, as shown in figure 6, the optical signals were converted to voltage pulses.

The optical signal is converted to a triggering pulse in three stages. Initially, the optical pulse is converted to a voltage pulse using a Darlington transistor. This provides the required gain for amplifying the current produced by the optical receiver. In the second stage, the pulse magnitude and rate of rise are amplified and finally, in the last stage, the trigger pulse for charging the gate-emitter of the IGBT modules is generated by reducing the output impedance of the circuit using a MOSFET driver. The dc power for each IGBT module was provided using a transformer with a toroidal core, driven from a charge pump and via a single pass-through winding through the centre of the toroid. Isolation was achieved using well-insulated,

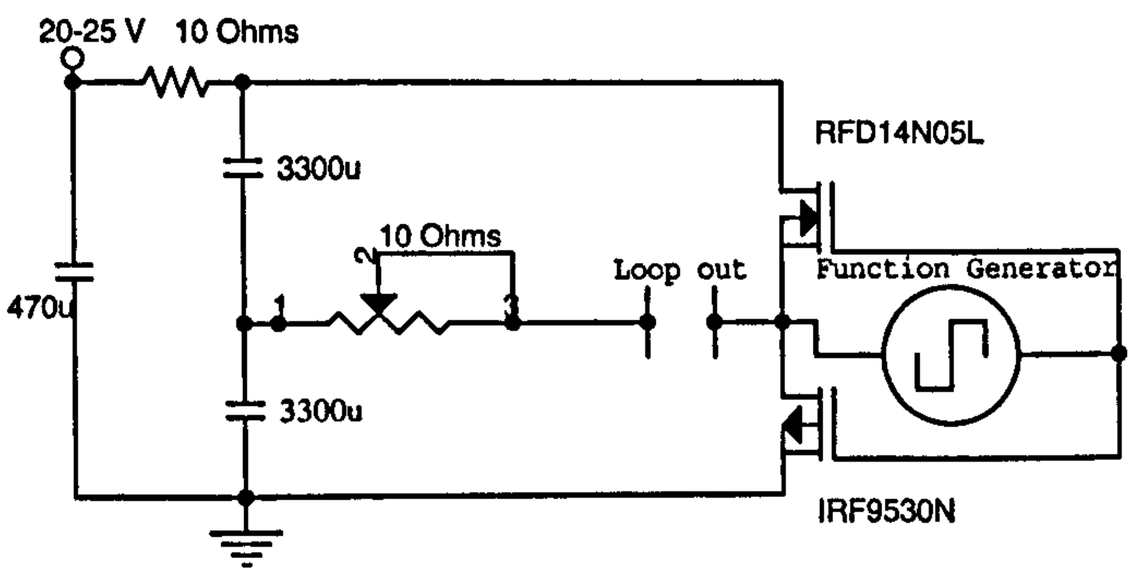

Figure 7. The charge-pump circuit.

high-voltage pass-through wire. The charge-pump circuit is shown in figure 7.

Two 3300 μF capacitors are charged up to half of the

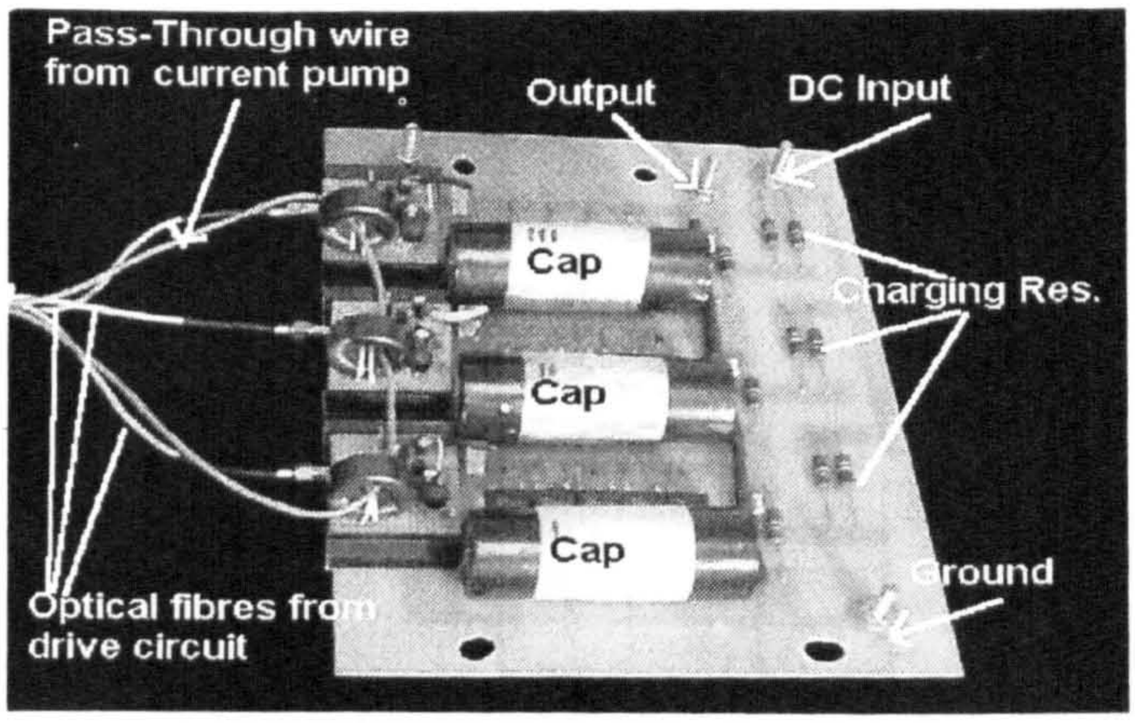

Figure 8. A photograph of the 3 kV, 1 kA Marx generator made up of three IGBT modules.

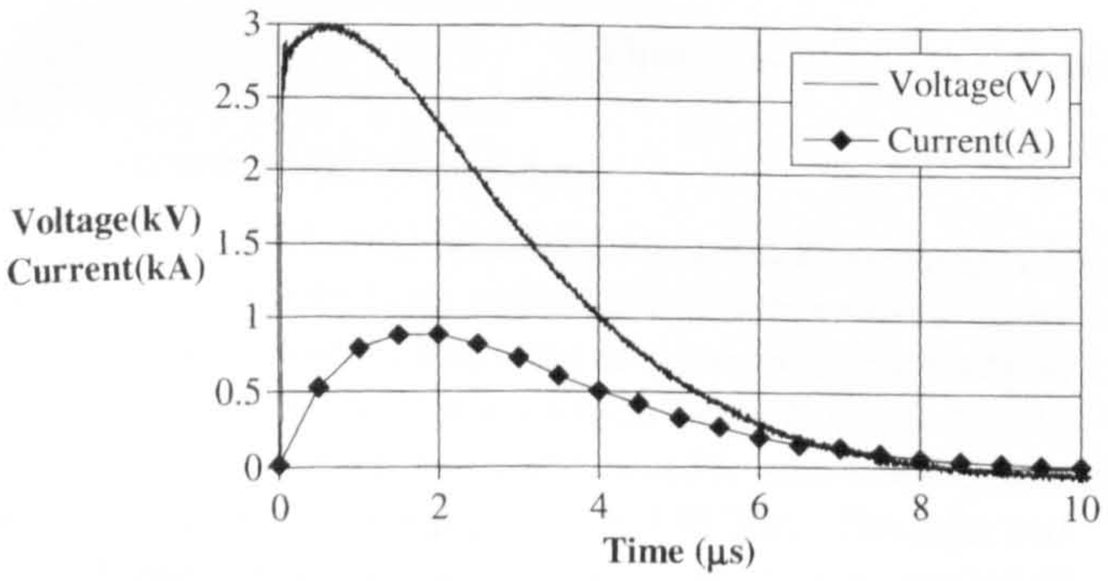

Figure 9. Voltage and current waveforms of the three-stage Marx generator with a 3 Ω pure resistive load.

voltage of the dc power supply which is between 20 and 25 V and then they are discharged separately through the MOSFET switches operating at a frequency of 20 kHz. These pulses drive the primary of the transformer in the circuit shown in figure 6.

2.3. A three-stage Marx generator

A photograph of the Marx generator with three IGBT modules is shown in figure 8. The current and voltage ratings are 1 kA and 3 kV respectively. The total energy stored in the capacitors was 4.5 J for a stack voltage of 1 kV and the generator was capable of delivering ~4 J due to the energy losses in the IGBTs. The energy losses in the IGBTs can be attributed to switching losses and conduction losses. During switching, only the self-capacitance of the modules will contribute to losses as the switching speed is ~30 ns and the rate of current rise is greater than 1 μs. Therefore, the switching losses were negligible. The conduction losses are associated with the average of the current (~707 A) flowing through the equivalent on-state resistor of the IGBT modules (0.036 Ω) for ~8 μs. This led to a ~0.42 J loss of energy (~9% of the total stored energy). The generator pulse repetition rate was limited to less than 10 pulses per second (pps) by the power dissipation in the charging resistors.

The typical current and voltage waveforms for a 3 Ω resistive load connected at the output of the generator, for a charging voltage of 1 kV, are shown in figure 9.

The current waveform was obtained using a Current Probe DE(CP)-01 manufactured by SAMTECH Ltd with a sensing resistance of 30 mΩ and output voltage of 30 V kA^{-1}. The

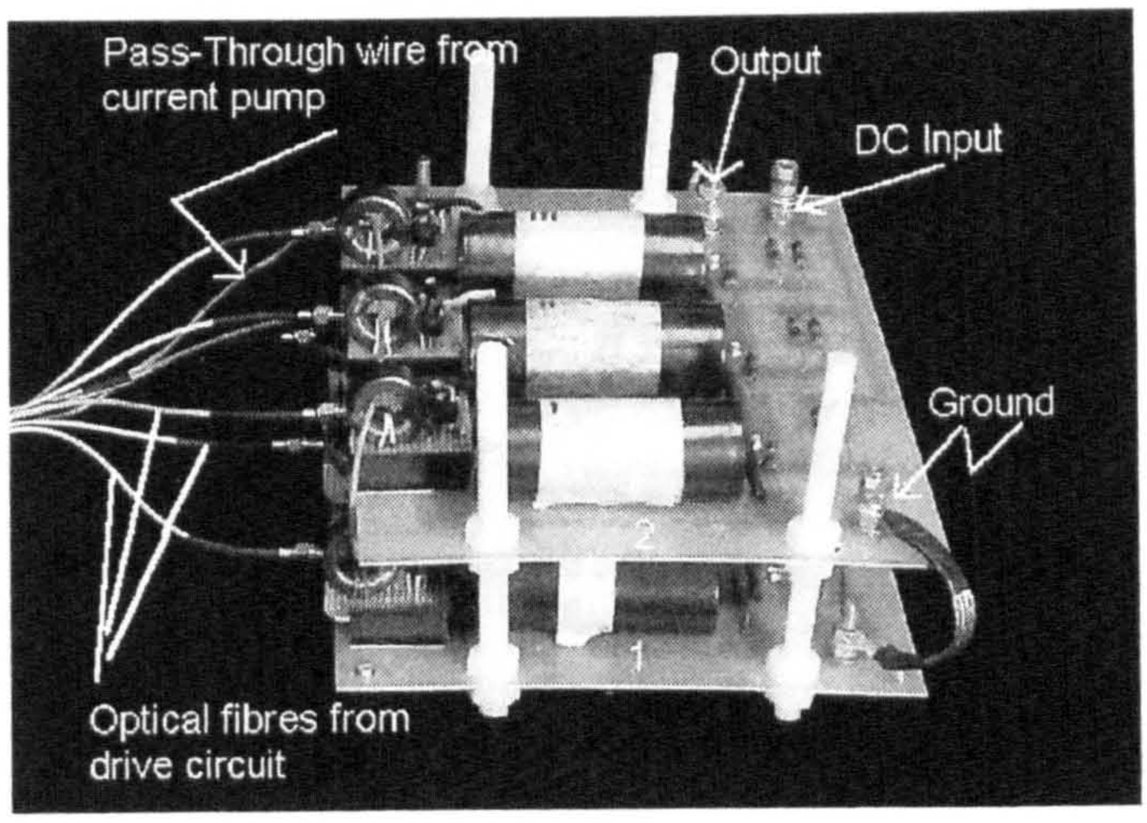

Figure 10. A photograph of the 3 kV, 2 kA Marx generator.

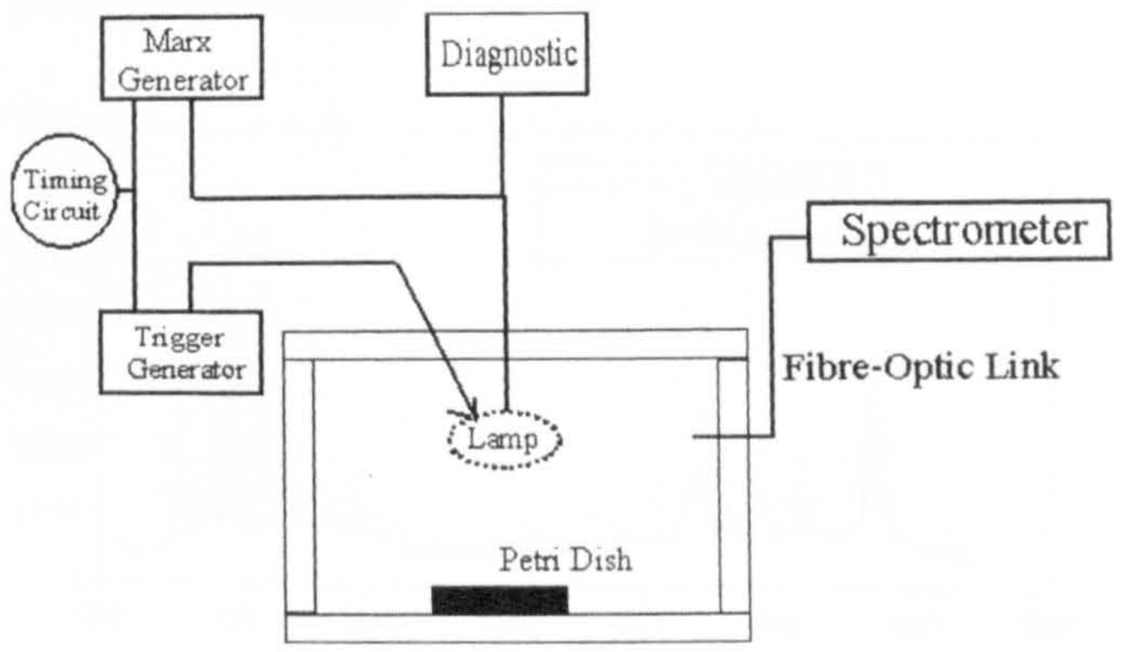

Figure 11. A diagram of the experimental facility for microbial inactivation using a pulsed UV source.

voltage waveform was measured using a Tektronix P6015A 1000X high voltage probe with a maximum voltage of 20 kV dc, 40 kV pulsed and a quoted bandwidth of 75 MHz. A Tektronix TDS3032 digital phosphor oscilloscope with a bandwidth of 300 MHz was used to view and record the voltage signals obtained from the diagnostics.

2.4. A double-stack three-stage Marx generator

To demonstrate the flexible nature of the modular approach, and to increase the energy/pulse capability of the generator, a second three-module unit of IGBTs was connected in parallel with the first, as shown in figure 10.

This generator is capable of delivering a total energy of ~8 J/pulse and its voltage and current ratings are 3.0 kV and 2 kA respectively. The generator was tested successfully by applying the same evaluation procedure as that discussed for the three-stage Marx generator and similar voltage and current waveforms were observed. However, they had a longer duration due to a doubling of the circuit time constant.

3. Application of the solid-state Marx generator

The effectiveness of UV light in biological inactivation comes about as a consequence of the absorption by DNA molecules of illumination between 200 and 300 nm. A test of the capability of the solid-state Marx generator was carried out in the pulsing of a UV flashlamp to increase the UV emission light in the range 200–300 nm.

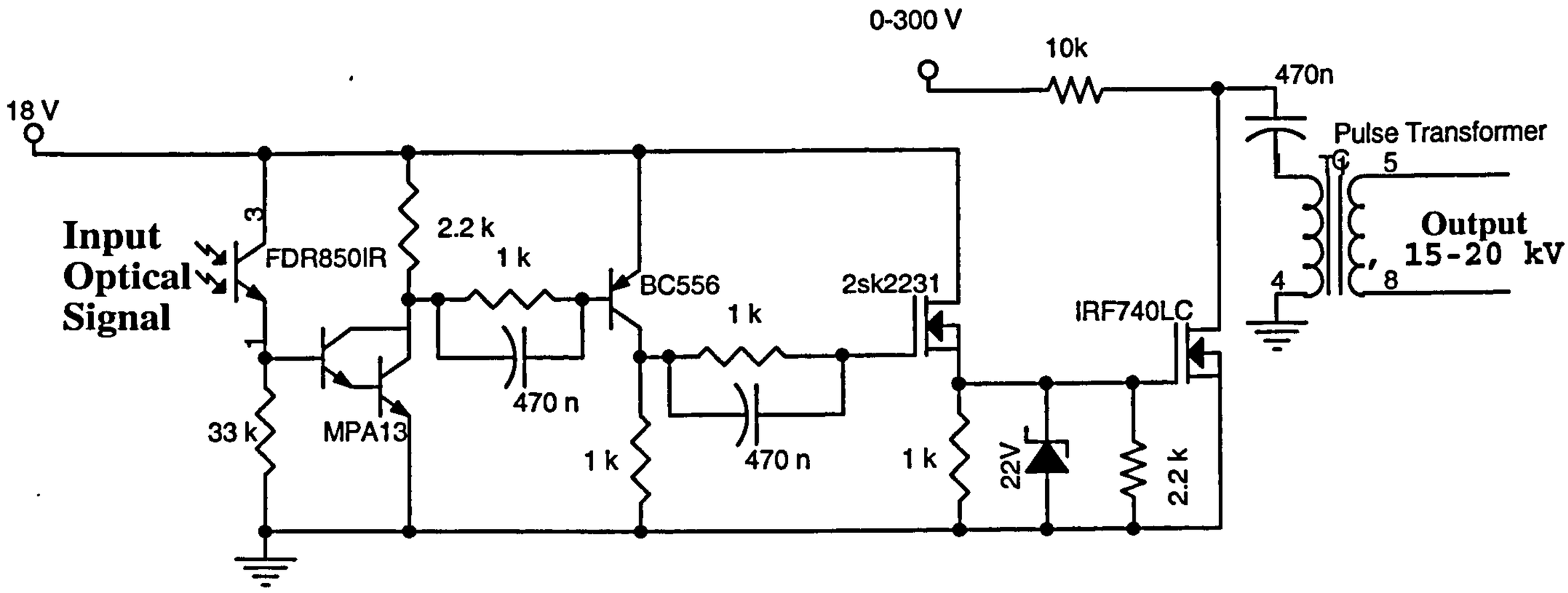

Figure 12. The external triggering circuit for the flashlamp.

3.1. The experimental arrangement

The test was conducted using the Marx generator assembly, UV flashlamp and sample in an optically isolated housing, spectrometer and diagnostic equipment as shown schematically in figure 11. The light source was a xenon lamp (Heraeus Noblelight, XAP series) which was constructed from a fused quartz tube filled with xenon at a pressure of 450 Torr. The tube had a 4 mm diameter bore and 50 mm arc length. It was capable of operating with an average power of about 100 W. The diagnostic block comprises the voltage and current probes described in section 2.3.

Initial ionization of the xenon gas requires a triggering pulse of 15–20 kV, and this was supplied using the circuit presented in figure 12.

A 470 nF capacitor was charged to 300 V and then upon closure of the high-voltage MOSFET, it was discharged through the primary winding of a transformer. This produced a high-voltage impulse across the secondary winding. The high-voltage triggering pulse was applied to a nickel wire running the length of the lamp with several loops around the lamp envelope. The synchronization between the external triggering circuit and the pulse generator was provided using optical signals generated from the same source.

3.2. Flashlamp characteristics

The optical emission from the lamp was monitored using a four-channel Ocean Optics SQ2000 fibre optic spectrometer. The spectrometer had a detector (2048-element linear silicon CCD array) with a spectral range of 200–530 nm and a resolution of 1.25 nm. Typical emission spectra and dynamic resistance–voltage characteristic of the flashlamp for pulse energies of 4.5 and 9.0 J are shown in figures 13 and 14 respectively.

Following triggering, ionization of the lamp gas occurs and its resistance begins to fall, dropping down to less than 0.5 Ω depending on the total energy delivered to the lamp. Hence the current through the lamp increases rapidly and the voltage across the lamp falls rapidly. As shown in figure 14, the flashlamp has a minimum dynamic resistance of about 0.45 and 0.75 Ω at a voltage of around 500 V when it is driven using 9.0 and 4.5 J pulses, respectively.

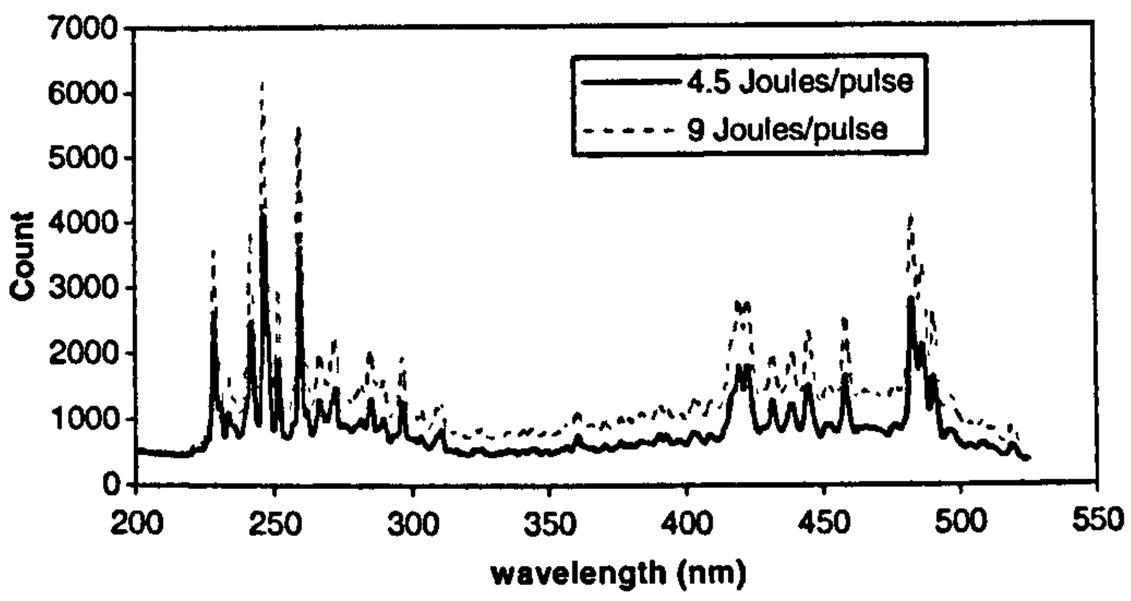

Figure 13. Flashlamp spectra for pulses of 4.5 and 9.0 J.

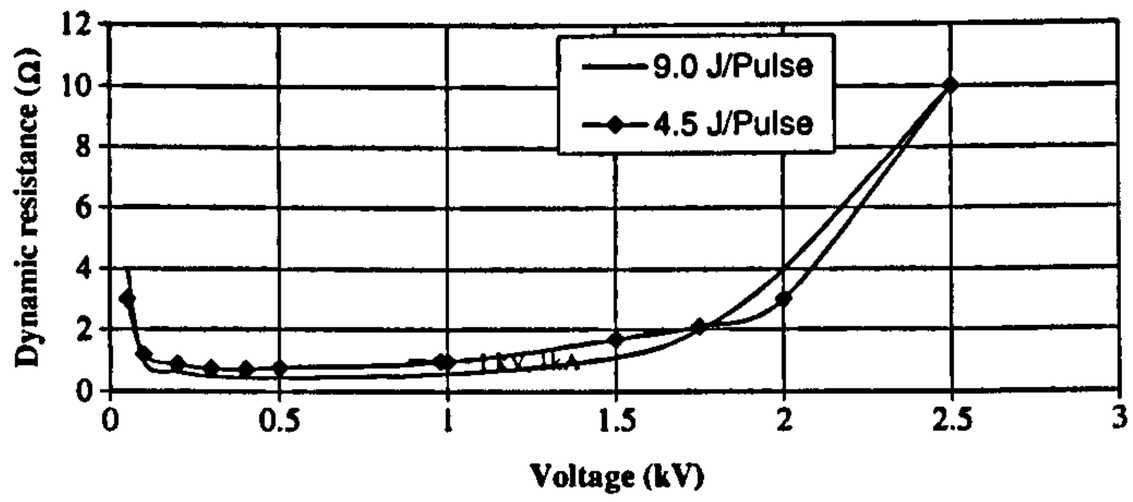

Figure 14. Flashlamp dynamic resistance–voltage characteristic for pulses of 4.5 and 9.0 J.

Typical voltage and current waveforms of the flashlamp during a single pulse with an energy of 9.0 J are also shown in figure 15. Similar waveforms were observed for a single pulse with an energy of 4.5 J.

The current passing through the lamp for a pulse of 9.0 J has a larger peak value (~1.7 kA) than for a pulse of 4.5 J, where the peak current is ~1.0 kA. This is due to the variation of the lamp dynamic resistance characteristic with energy/pulse.

3.3. Pulsed UV treatment of micro-organisms

Two bacterial strains, *Escherichia coli* (NCTC 9001) and *Salmonella enteritidis* (132344), which are small (~2 μm in length), motile, rod-shaped cells that have a gram-negative type cell wall, were chosen for the study of the inactivating effects

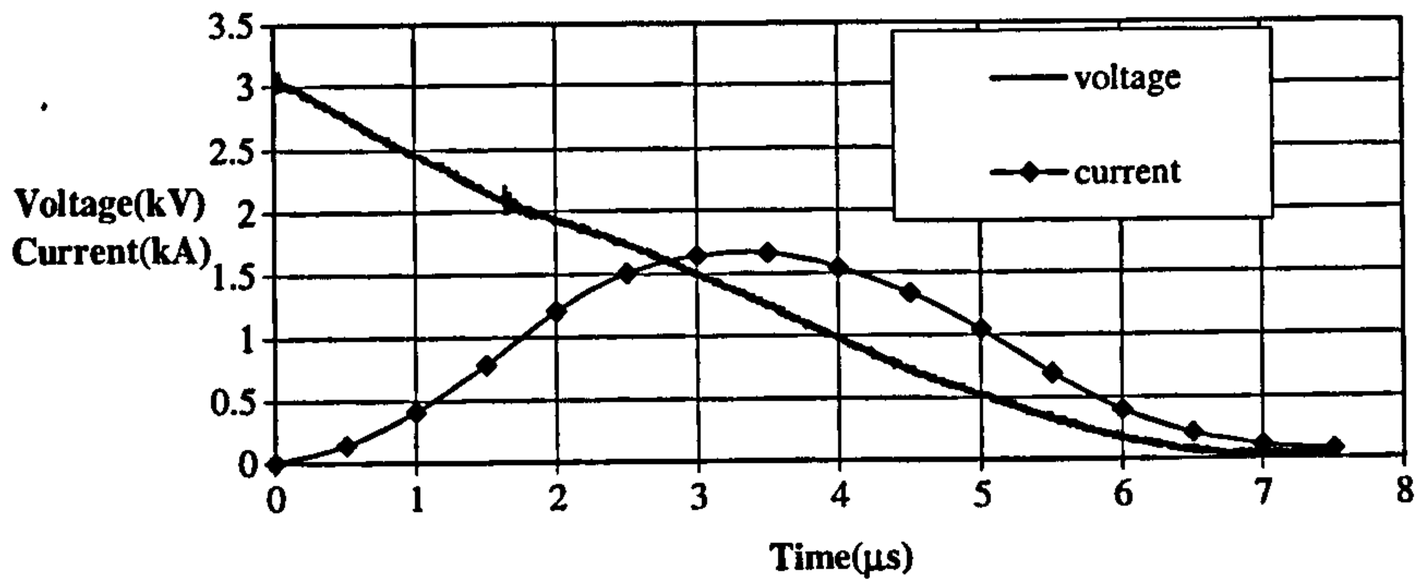

Figure 15. Flashlamp voltage and current waveforms in the 9.0 J pulse generator.

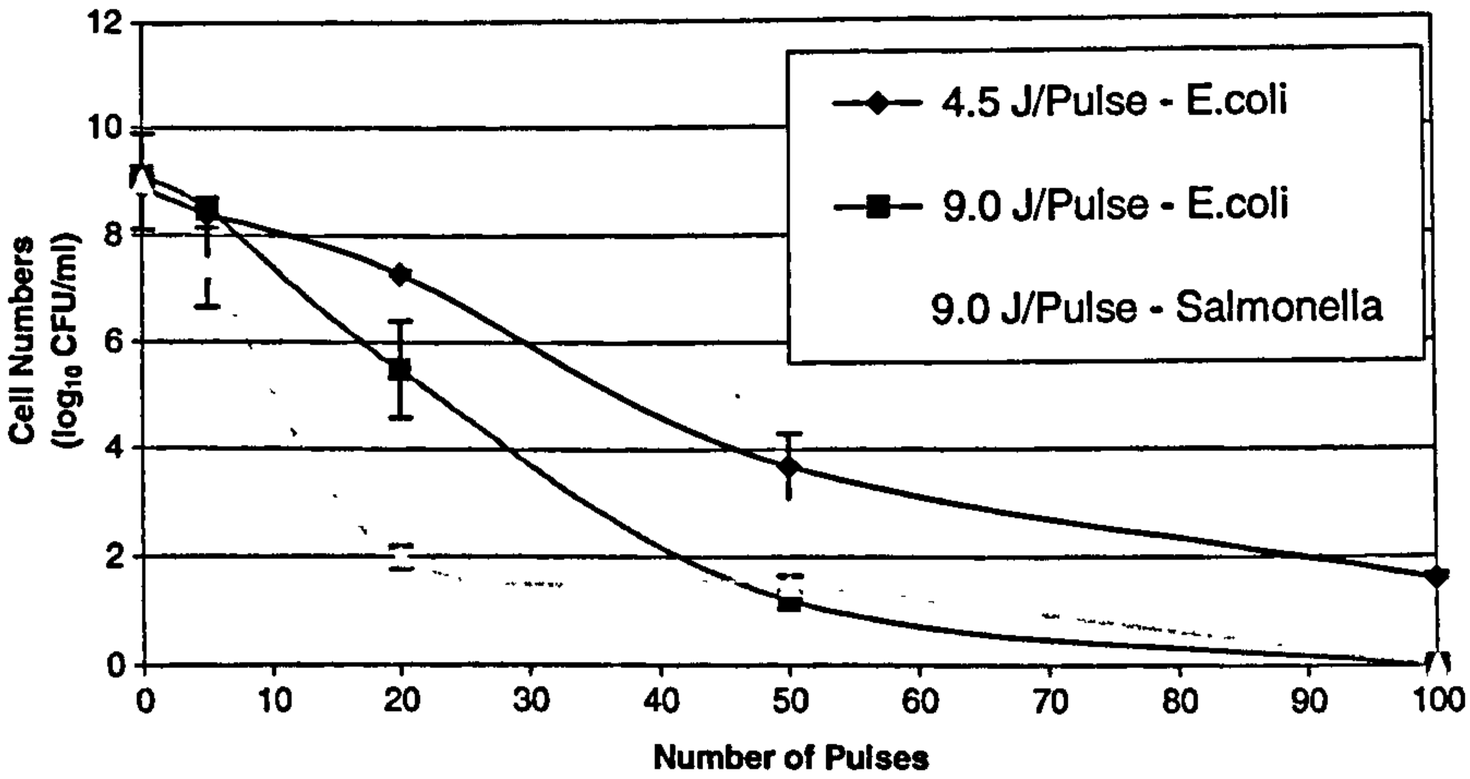

Figure 16. Pulsed UV light inactivation of *E. coli* and *Salmonella*.

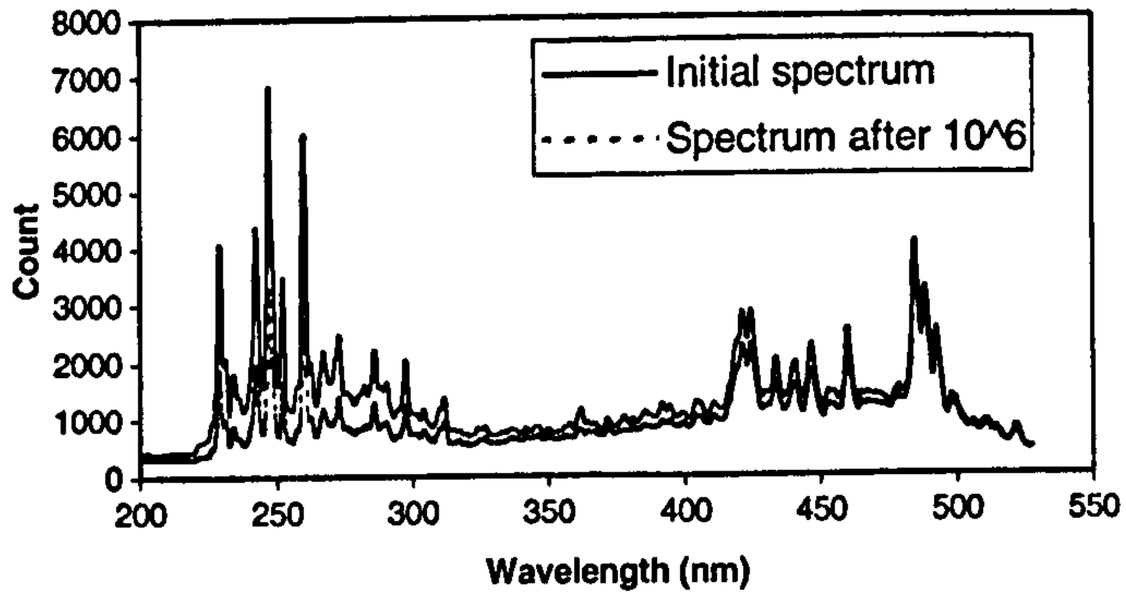

Figure 17. Comparison of the initial lamp spectrum with the spectrum after 10^6 pulses.

of pulsed UV light [2, 9]. After preparing 20 ml of suspended culture of each micro-organism, they were transferred into standard Petri dishes. The dishes were then positioned in the insulated housing (see figure 11) and subjected to 5, 20, 50 and 100 flashlamp pulses using a pulse repetition rate of 1 pps. Control and treated samples were serially diluted and plated out using the spiral plate method (Spiral systems Inc. Model B). Undiluted samples of the treated organisms were also tested using the pour plate method in order to detect low numbers of survivors. All plates were incubated at 37 °C for 24 h and then counts of colony forming units (CFU) were recorded. The experiment was carried out for energies of 4.5 and 9.0 J/pulse. The results are shown in figure 16.

Following analysis of the irradiated samples, both *E. coli* and *Salmonella* showed a 9-log order reduction after treatment with 100 pulses with each pulse providing 9 J of radiated energy. 100 pulses of 4.5 J/pulse produced a 7-log order reduction for *E. coli*. Only an approximate 0.5-log order reduction was observed to occur after treatment of *E. coli* samples with five pulses of 4.5 and 9.0 J. The relatively low rate of cell reduction over the first few pulses is most likely due to the initial very high cell population (1.3×10^9 colony forming units ml^{-1}) causing a fall-off in UV intensity through the 3.28 mm depth of the sample. This effect, which was noticeable with *E. coli*, was most likely due to the greater turbidity caused by the larger dimensions of *E. coli* cells compared with those of *Salmonella*. The total energy for a 7-log order reduction in the cell population was 900 J and this shows an improvement in the efficiency of inactivation compared, for example, with the work of Anderson *et al* [2] where a single-stage, inverting, pulse-forming network, Marx generator with an energy/pulse of 3 J with a nominal peak of 30 kV and duration of 85 ns was used. It is believed that operating the flashlamp with a higher energy/pulse increases the light intensity of the lamp over the whole of its spectral range and in particular within the germicidal band.

3.4. Lamp lifetime

Lamp lifetime or aging is a complex topic and depends on how the lamp is operated and the environment in which it is used. For pulse lamps, the lifetime is measured in terms of the total number of shots achieved to the point where the useful light output drops to some chosen percentage of the original intensity. There are four major reasons for lamp

failure; electrode erosion, gas fill contamination, glass-to-metal seal failure and envelope aging. In order to estimate the lifetime of the lamp driven by the Marx generator with 9.0 J/pulses, a pulse repetition rate of 10 pps for 1 million shots was used. The lamp current, voltage and spectrum were monitored continuously and recorded after 1×10^4, 1×10^5 and 1×10^6 pulses. Similar waveforms of the current and voltage at the beginning and after 1 million shots were observed. A comparison of lamp spectra obtained after the first shot, and after 1 million shots is shown in figure 17.

Over time, the output intensity of the flashlamp falls over the whole of its spectral range. The fall in intensity appears greater (more than 50%) in the UV region. This may be due to a build-up on the inner tube wall of a coating that absorbs preferentially in the UV spectral region.

4. Conclusion

A modular Marx generator has been designed and evaluated. The capacitors of the Marx generator are switched using series and parallel connected 1.2 kV IGBTs that are optically controlled. IGBTs provide fast and repetitive switching, and have the advantage of being cheap and readily available devices. The generator system has modular flexibility to allow a selection of voltage and current ratings to be utilized, with the generator used here having an output voltage rating of 3 kV and a peak current rating of 2 kA. By means of synchronized and optically decoupled signals, the new design provides very low pulse-to-pulse jitter (a few nanoseconds).

The performance of the solid-state switched Marx generator was successfully tested over a period of more than 10^6 pulses when it was applied to pulse a xenon flashlamp, with UV illumination from the flashlamp being used for inactivation of micro-organisms. The average power of the xenon flashlamp is 100 W but pulsing with the Marx generator provided peak powers of up to 2 MW. High power pulses of UV illumination appear to provide advantages for inactivation experiments with the efficiency of inactivation being improved. This decreases the treatment time while providing better energy efficiency.

The new form of Marx generator can be pulsed at repetition rates up to several kilohertz, by using a charging resistance with a higher power dissipation rating, and a high voltage dc power supply with higher output current. The Marx generator has the potential to operate at substantially higher voltages and currents than demonstrated in this work. Consequently, it is likely to find application in other pulsed power systems such as those used for dielectric test systems, beam steering, gating and driving grids and high-power laser diode drivers.

Acknowledgments

The authors gratefully acknowledge the assistance of Professor J Woolsey and one of us (ZG) would like to thank the Ministry of Science, Research and Technology in Iran for financial support.

References

[1] McDonald K and Curry R 2001 Comparison of pulsed and CW ultraviolet light sources to inactivate spores on surfaces *13th IEEE Int. Pulsed Power Conf.* vol 1 pp 604–7

[2] Anderson J G *et al* 2000 Inactivation of food-borne enteropathogenic bacteria and spoilage fungi using pulsed-light *IEEE Trans. Plasma Sci.* **28** 83–8

[3] Macgregor S J *et al* 1998 Light inactivation of food-related pathogenic bacteria using a pulsed power source *Lett. Appl. Microbiol.* **27** 67–70

[4] Okamura K *et al* 1999 Development of the high repetitive impulse voltage generator using semiconductor switches *12th IEEE Int. Pulsed Power Conf. (California, 1999)* pp 807–10

[5] O'Loughlin J *et al* 2001 High repetition rate charging a Marx type generator *13th IEEE Int. Pulsed Power Conf.* pp 242–6

[6] Kuffel E *et al* 2000 *High Voltage Engineering: Fundamentals* (Oxford: Pergamon)

[7] Ghasemi Z *et al* 2001 Fast high voltage, high current switching using stacked IGBTs *IEE Symp. Pulsed Power (London, 2001)* pp 8/1–8/5

[8] Ghasemi Z and Macgregor S 2002 A solid-state pulse generator for use in the PEF inactivation of microorganisms *10th ICEE (Tabriz, Iran, May 2002)* vol 4

[9] Hobbs B C and Roberts D 1987 Food poisoning and food-borne infection *Food Poisoning and Food Hygiene* ed B C Hobbs and D Roberts (London, UK: Arnold) pp 3–120

A Solid-State Pulse Generator for Use in The PEF Inactivation of Microorganisms

Z Ghasemi*, S MacGregor
Department of Electronic and Electrical Engineering,
University of Strathclyde,
Royal College Building,
204 George Street,
Glasgow, G1 1XW,UK

Abstract
The objective of this work was to demonstrate the use of a fast high-voltage, high-power solid-state switch, based on the commercially available IGBTs, as a substitute for conventional switches such as hard glass tubes, thyratrons and spark gaps. The switching performance of a 10 kV stack switch, consisting of fifty 1.2 kV IGBTs in series and parallel is discussed. The switch has been incorporated into a coaxial cable Blumlein pulse generator to investigate the effect of pulsed electric fields (PEFs) on the inactivation of microbial populations suspended in liquids. Electric fields of ~30 kV/cm, and a pulse duration of 1μsec, were generated from the pulser. A reduction of 3.3 log orders in the population of *E.coli* was achieved.

Key Words: IGBT, fast switching, pulse electric field (PEF), pulse generator

I. Introduction

High-voltage pulse generators are used for research and development purposes in a wide range of applications. These include areas such as insulation studies, food preservation, pollution control and medical diagnostics. High-voltage pulses generally fall into three categories, namely Marx and Marx-like impulse generators, pulse transformers and coaxial/stripline generators. Output voltage, energy requirement, pulse voltage profile and cost are factors that normally control the choice of generator [1]. A primary switching component is an essential device in all of these pulse generators. In recent

* E-mail: z.ghasemi@eee.strath.ac.uk

years much emphasis has been placed in developing semiconductor switches because of their reported longer lifetime, low degradation and low jitter. IGBT devices are considered prominent candidates for pulsed power switching. However, problems such as displaying dual degradation in the voltage collapse across the switch have been encountered with the switching performance of IGBTs when rapid switching (<100ns) is required [2,3].

In order to extend the durability of foodstuffs or other perishable media by killing of microorganisms, heat treatment such as pasteurisation or ultra-high temperature processing is the method predominantly used. However, thermal processing causes undesirable side effects, is energy intensive, and can adversely affect the nutritional qualities and flavour of the preserved food. The use of nonthermal sterilisation processes have been studied to overcome these disadvantages.

II. 10 kV pulse generator description

Figure 1 shows the pulse generator layout. A 20-kV Glassman high-voltage dc generator was used to charge a coaxial cable Blumlein pulse generator through a charging resistance of 100 kΩ.

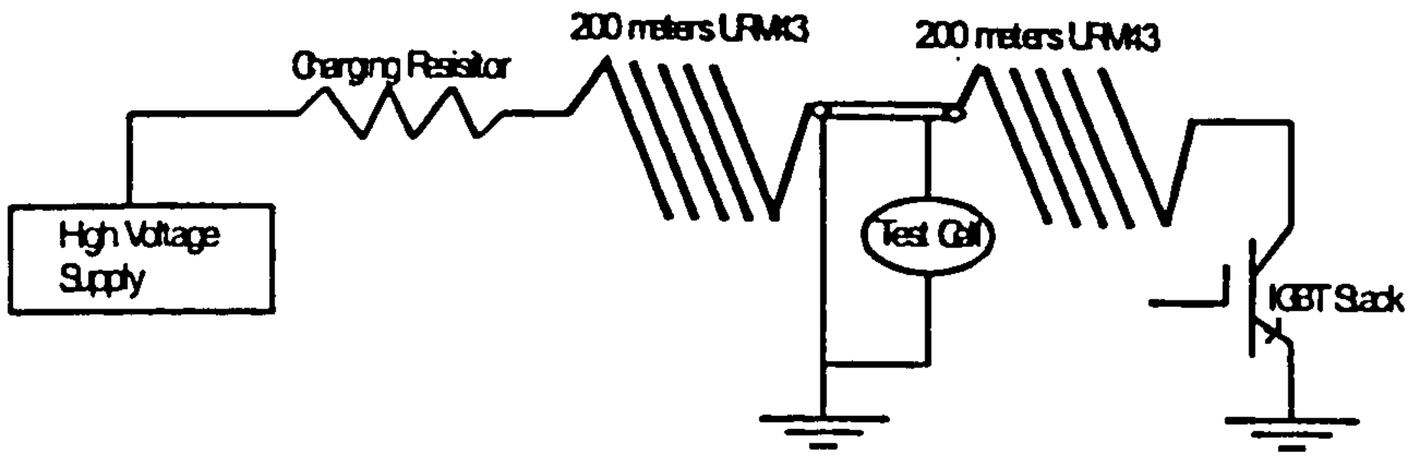

Figure 1. The Pulse generator layout.

The coaxial cable generator was constructed from 400 m of URM43 cable. The high-voltage output pulse from the generator was 1μs in duration, and the generator had an output impedance of 50 Ω, a switching impedance of 25 Ω, and an open circuit gain of two. The pulse generator was charged from one end of the cable and the pulse was generated by switching the inner conductor to ground at the opposite end using a 10 kV stack of 1.2 kV IGBTs. The system was capable of operating at a pulse repetition frequency (PRF) at several kilohertz. However, in this study, the PRF was limited to a

maximum value of 100 Hz due to a limit on the maximum output power of the high-voltage dc power supply.

III. 10 kV stack description

The most commonly used high-power semiconductor devices in pulsed power applications are Metal Oxide Semiconductor Field effect Transistors (MOSFETs) and Insulated Gate Bipolar Transistors (IGBTs), which are commercially available with voltage ratings up to 1.2 kV. MOSFETs have substantially faster switching speeds while IGBTs are generally more efficient, can handle more power and are capable of being manufactured at higher voltage ratings [4,5]. For high-voltage IGBT devices, in order to keep the electric field at a reasonable level in the drift region, a wide drift region must be used and this leads to a high on-state resistance. A high level of charge has to be injected at the device anode to keep the on-state resistance to a reasonable value. This increases the turn-off time of the device, as well as the switching losses. Therefore the series connection of medium-voltage devices is more practical for obtaining higher switching speeds. The slope of the drain-source voltage collapse can be distorted when IGBT devices are stressed to facilitate rapid turn-on, displaying dual degradation. The problem caused by this behaviour on the circuit performance could be reduced by using a saturable inductance or a magnetic assist in series with the switch to create a delay between the voltage fall and current rise [2,3]. However, applying this remedial method to most types of high-speed pulse generators, such as Blumlein cable generators, causes perturbations and deviations in the shape of the output pulse. A comprehensive assessment was carried out on the switching performance of different types of single 1.2 kV IGBT devices. As an example, the switching behaviour of two similar IGBTs in terms of switching parameters has been shown in Figure 2.

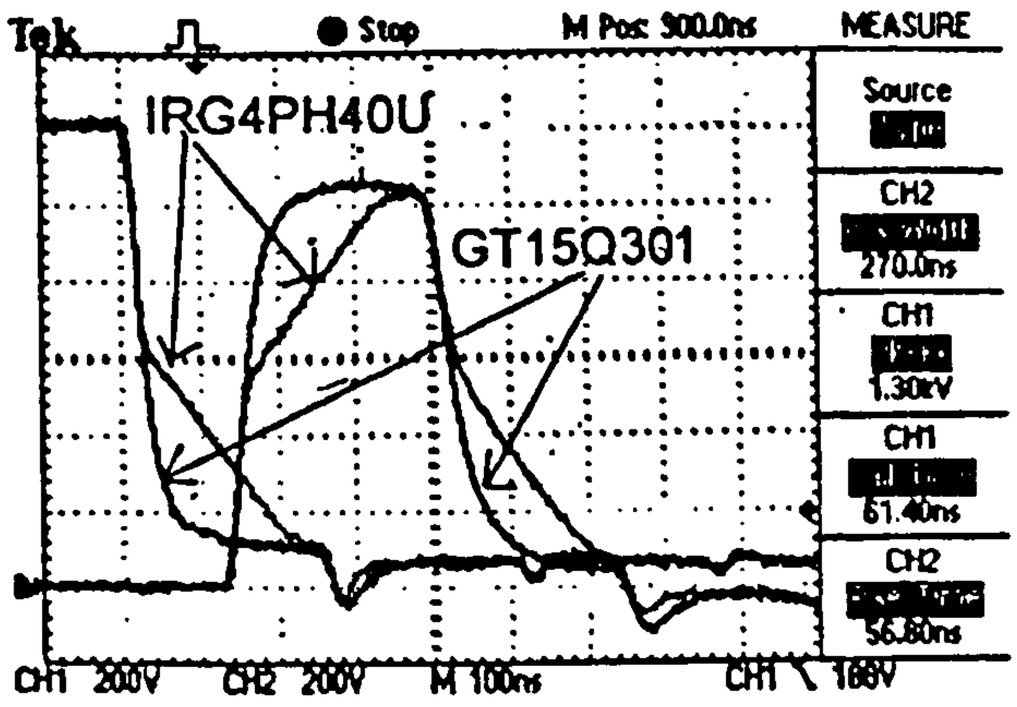

Figure 2. Comparison of the switching behaviour of GT15Q301 and IRG4PH40U under fast pulsed condition, voltage across the device and output pulse.

As can be seen in Figure 2, dual degradation phenomenon in IRG4PH40U significantly affects the shape of generated output pulse by slowing down the pulse rise and fall times. This dual degradation effect is not observed in the GT15Q301 waveforms. It has been shown that a reason for the dual degradation observed with drain source voltage could be the rapid variations in device parasitic parameters such as gate-drain capacitance [4].

Another aspect of stacking IGBTs is the drive circuit. In a module consisting of several IGBTs in parallel, the drive circuit should be able to deliver fast current pulses of the order of 100A. Furthermore, for driving a stack of several IGBT modules connected in series, proper coupling must be applied among the driving pulses. The application of commercial isolated IGBT gate-driving IC modules such as TC-4426 and HCPL-3120 has been limited due to significant variations in the delay time from one module to another. In this project, pulse transformers with cylindrical ferrite cores having three turn primary and secondary windings have been used. A schematic of the drive circuit has been shown in Figure 3.

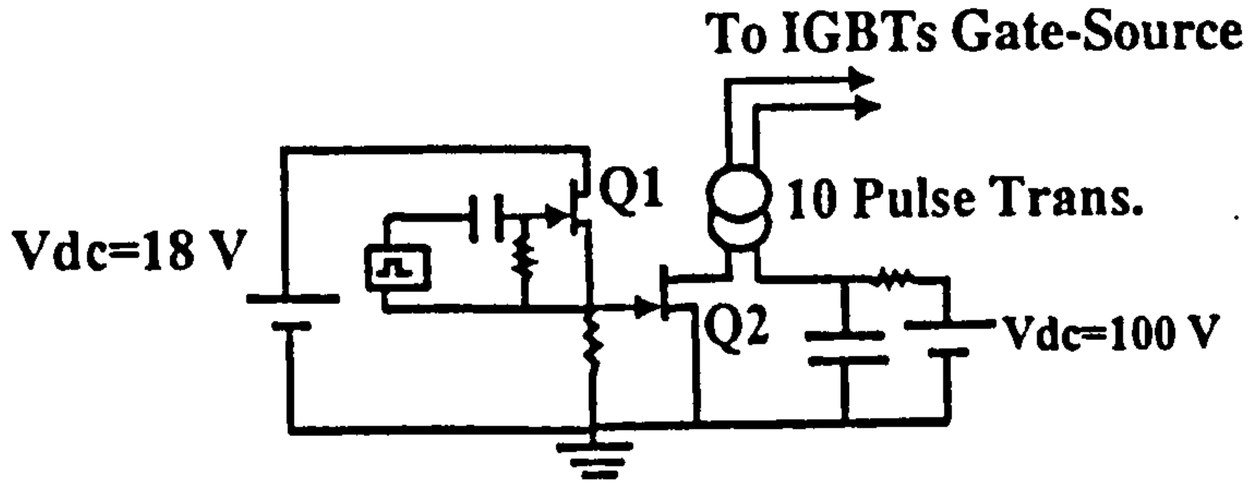

Figure 3. Schematic of electric circuit for driving IGBT modules,

A photograph of the stack, consisting of fifty 1.2 kV IGBTs in a series/parallel configuration, is shown in Figure 4. The stack consists of ten modules in series, with each module consisting of five IGBTs in parallel.

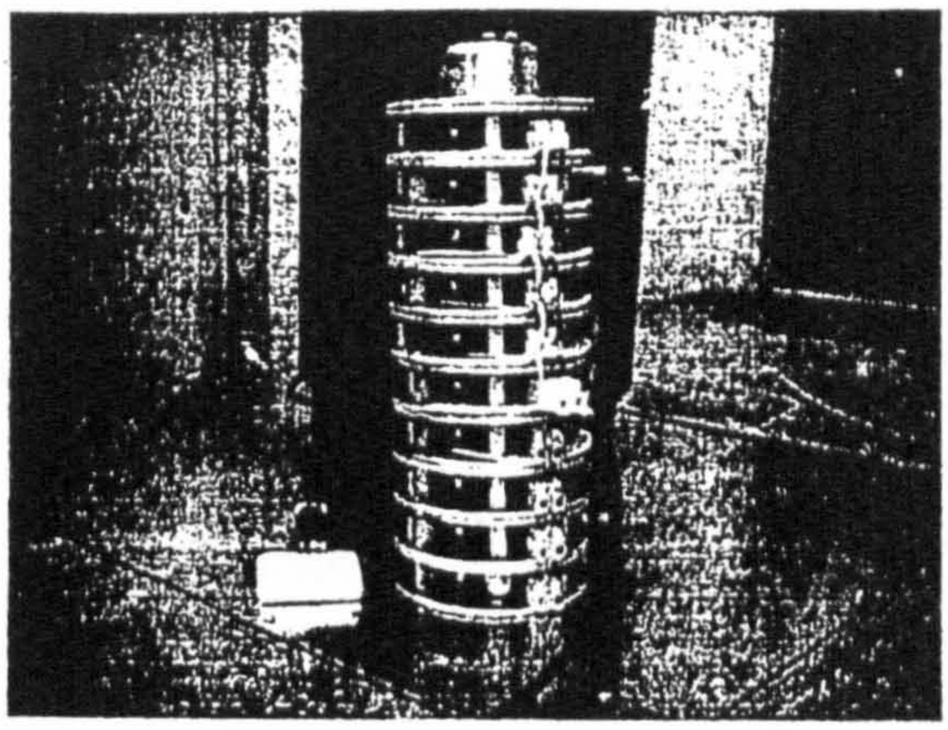

Figure 4. Photograph of 10 kV, 400 A stack of IGBT modules involving 50 1.2 kV IGBTs.

The voltage waveforms recorded across the switch and the generator output are shown in Figure 5.

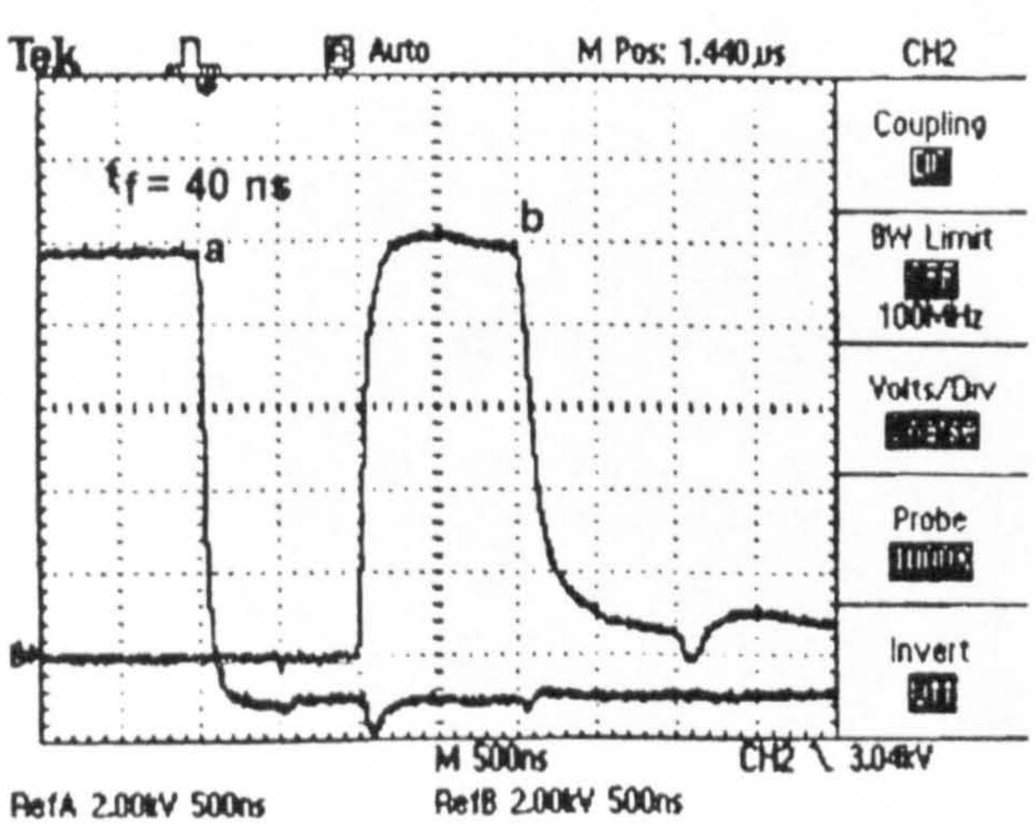

Figure 5. Voltage waveform across the switch (trace "a") and output voltage pulse (trace "b") in 1µs Blumlein pulser (both traces amplitude 2 kV/div and time base 500 ns/div).

As shown in Figure 5, the voltage across the stack collapses in less than 50 ns (10-90%), leading to a fast rising pulse at the output of the pulser.

IV. Application of the switch in microorganisms inactivation

The application of high intensity pulsed electric fields (PEF) is one of the nonthermal methods of food preservation. In this method, an electric field is applied to the fluid food in the form of short pulses with pulse durations ranging from a few microseconds to milliseconds [6]. One important component of the processing system is the treatment chamber and several designs of static and continuous chambers have been suggested [7]. The electric field between two electrodes has to be uniform in order to achieve the maximum treatment efficiency. It also has to be limited to 30 kV/cm because of the electrical breakdown of air above the food. In this study, numerical electric field optimisation was used to design the treatment chamber. The optimisation criterion was to find electrodes dimensions that provided a relatively uniform high-intensity electric field in the treatment region. It was also desirable to match the impedance of the test chamber to the source impedance of the pulse generator in order to eliminate reflected pulses so that the total treatment time would be well defined. A photograph of the optimised PEF test chamber has been shown in Figure 6.

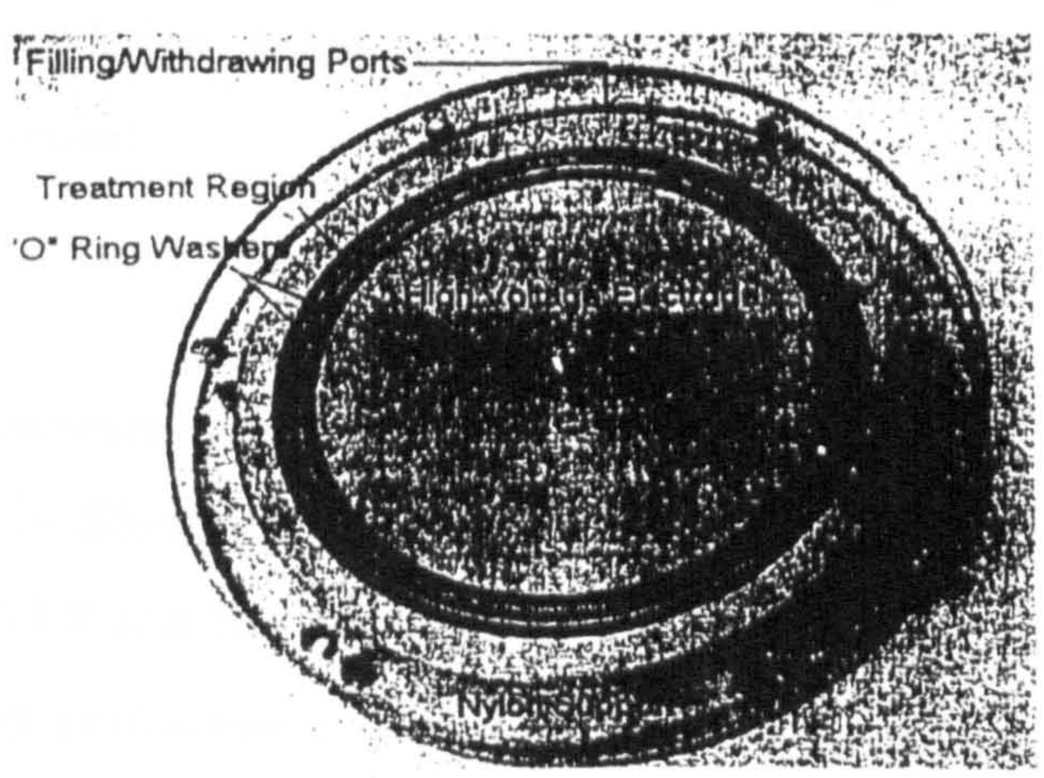

Figure 6. Photograph of 10 kV, 50Ω PEF test cell.

V. Inactivation of Escherichia coli

Escherichia coli is a bacterium and is one of the most characteristic members of the normal intestinal flora of mammals. *E.coli* and other coilform bacteria are pathogens, responsible for such intestinal flora infections as bacterial dysentery, typhoid fever, and bacterial food poisoning [8]. Inactivation of *E.coli* was performed after the treatment cell

was sterilized by autoclaving at 121 C° for 15 minutes. The samples to be treated were circulated in a closed-loop, PEF treatment system. This comprised a holding reservoir, treatment chamber, inner connections and pump. The flow rate of the system was 0.44 ml/sec and the total volume of the chamber was 28 ml. The level of microbial inactivation was assessed by taking samples from the reservoir during experiments. The results were expressed in the form of colony forming units per ml (CFU/ml) as shown in Table 1.

Table 1. PEF Inactivation of *E.coli* cells treated in a continuous-flowing system

Number of pulses	0	57	570	1140
Normalised (pulses/ml)	0	2	20	40
PRF (Hz)	0	1	10	20
Energy Input (J/ml)	0	4	40	80
Cell Population (CFU/ml)	8.55E+07	1.97E+07	9.67E+04	4.83E+04
Cell Population (Log)	7.93	7.29	4.99	4.68

The results show that the greater the number of PEF pulses applied, the larger the reduction in cell population. A log reduction of 3.3 in the number of cells was achieved by applying 40 pulses/ml.

VI. Conclusion

A stack of 1.2 kV commercially available IGBTs has been designed and built for use as a fast closing switch in Blumlein pulse generators. The switch can operate at voltage and current ratings of 10 kV and 500 A respectively, with a voltage fall-time of about 45 ns. The stack switching performance was investigated in a 50Ω output impedance pulse generator, while a coaxial treatment chamber with a gap spacing of 3 mm and impedance of 50Ω had been connected at the output of pulser. The results have shown that the application of pulsed electric fields is an effective method for the inactivation of liquids contaminated with high concentrations of microorganisms. PEF treatment of *E.coli* cells in a continuously flowing test system reduced the number of suspended cells to a level of 4.83E+04 CFU/ml (a ~ 3.3 log order reduction) after 1140 pulses from an initial concentration 8.55E+07 CFU/ml.

Future efforts will be directed towards the application of optical coupling of the trigger pulse, which will facilitate an increased number of devices and hence an increased of voltage rating for the switch and pulse generator.

References

[1] I. C. Somerville, et. al, "An efficient Stacked –Blumlein HV Pulse Generator," Meas. Sci. Technol., pp 865-868, 1990.

[2] F. Endo, et. al, "All-Solid-State Pulsed Power Modulator For High Power, High Repetition Rate Applications," *Proc. 12th. IEEE Int. Pulsed Power Conf.*, pp 1417-1420, 1999.

[3] H. T. W. Tromp, et. al, " A New Approach to Series Semiconductor Switch Applications," *Proc. 21st. International Power Modulator Symposium*, pp 81-84, 1994.

[4] Z. Ghasemi, et. al, "Fast High Voltage, High Current Switching Using Stacked IGBTs," *IEE Symposium Pulsed Power*, pp 8/1-8/5, London, 2001.

[5] E. G. Cook, "Review of Solid-State Modulators," Lawrence Livermore National Laboratory, USA.

[6] Shesha h. Jayaram, "Sterilization of Liquid Foods by Pulsed Electric Fields," IEEE Electrical Insulation Magazine, Vol. 16, No. 6, pp 17-24, November/December 2000.

[7] Gustavo V. Barbosa, et. al, " Nonthermal preservation of foods," New York, Marcel Dekker, 1997.

[8] Bai-Lin Qin, et. al, "Inactivating Microorganisms Using a Pulsed Electric Field Continuous Treatment System," IEEE Transactions on Industry Applications, Vol. 34, No. 1, Jan. 1998.

Inactivation of Beer and Lager Spoilage Microorganisms Using Pulsed Electric Fields

K.Wall, Z. Ghasemi, D. Cameron, N.J. Rowan., S.J. MacGregor and J.G. Anderson.
Electronic Pasteurisation and Sterilisation Technologies (EPAST) Group, University of Strathclyde, Glasgow, UK.

Background

This study focuses on the effectiveness of high intensity Pulsed Electric Fields (PEF) on the inactivation of a range of beer/lager spoilage microbes. Whilst few microbes can tolerate the acidic alcoholic environmental conditions of lager and beer, microbial spoilage can still occur. As PEF is a non-thermal electrotechnology it is likely that less nutritive loss or adverse changes in sensory characteristics will occur. This study reports on the susceptibility of a range of lager and beer spoilage yeast (*Saccharomyces carlsbergensis* and *Zygosaccharomyces bailii*) and bacteria (*Obesumbacterium proteus*) to the lethal action of PEF-treatment.

Methods

Microbial Strains and Growth Media:

- *S. carlsbergensis* (IHEM 2683) was grown to a cell population of 10^7 in Malt Extract Broth (OXOID) for 24hrs at 30°C.
- *O. proteus* (LMG 3045) was grown to a cell population of 10^8 in Nutrient Broth (OXOID) for 24hrs at 30°C.
- 2 strains of *Z. bailii* (MUCL 27812 + MUCL 28823) were grown to a cell population of 10^7 in Malt Extract Broth (OXOID) for 48hrs at 30°C.

Pulsed Electric Field (PEF) treatment

Test cultures were suspended in 0.04% bacteriological peptone (Wt/vol) and were subjected to high intensity PEF (30KV/cm) in a uniform flowing test chamber using a range of pulses as described in MacGregor *et al* (1). The testing arrangement is shown schematically in **Figure 1**.

Test samples were serially diluted and enumerated by spiral plating. Agar used was Malt Extract Agar (OXOID) with *S. carlsbergensis* and *Z. bailii* and Nutrient Agar (OXOID) with *O. proteus*. Cellular damage induced by PEF was examined using Scanning Electron Microscopy (SEM), as described by Rowan *et al* (2). Untreated and PEF treated SEM images of *S. carlsbergensis* are shown in **Figure 2 (a)** and **(b)** respectively.

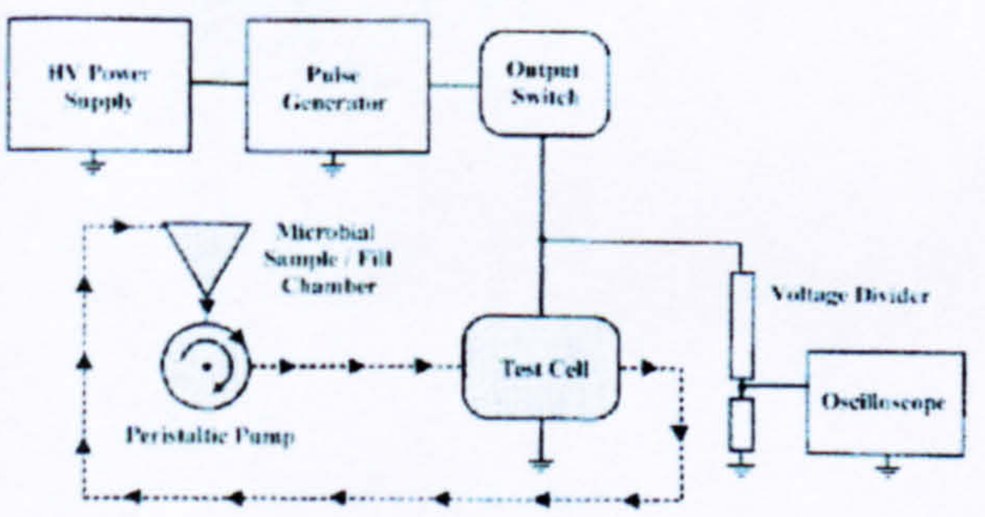

Figure 1. Experimental arrangement for PEF treatment of flowing liquids

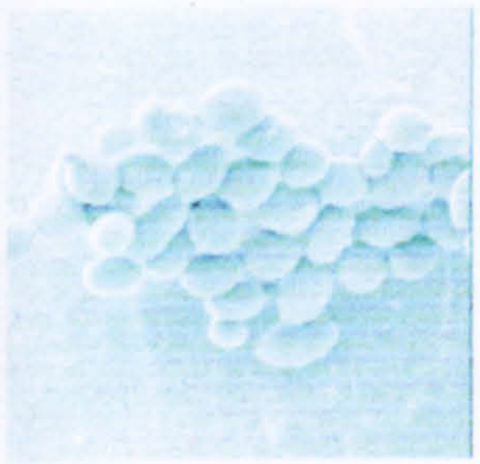

Figure 2(a) SEM of untreated *S. carlsbergensis* cells

Figure 2(b) SEM of PEF treated *S. carlsbergensis* cells

Results and Discussion

- Inactivation data for lager and beer spoilage microbes that were subjected to PEF treatment are presented in **Figure 3**.
- From the results shown in **Figure 3** it can be seen that the PEF had a strong biocidal effect on the test organisms. For all of the test organisms the inactivation rate was greatest during the first 2000 pulses. The long inactivation tails that occurred with further processing were at least partly associated with the type of culture recirculation system used.
  - For the strain of *Z. bailii*, 27812 there was a 3.2 log reduction and for 28823 there was a 3.5 log reduction and these microorganisms were the least susceptible to PEF
  - For *S. carlsbergensis*, there was a ~4 log reduction
  - For *O. proteus*, a ~6 log reduction was achieved
- The SEM images in **Figure 2(a)** and **(b)** show evidence of cell shrinkage, indicating that subjecting *S. carlsbergensis* to PEF caused significant damage at the cellular level. The cell shrinkage is most likely due to the loss of cytoplasmic contents through irreversible pores in the cell membrane caused by PEF. This is known as Electroporation and leads to cell death.
- The results obtained using the current system indicate that the test bacterium seems to be more susceptible to PEF damage than the yeasts.
- In the experiments reported here, the test microorganisms were suspended in bacteriological peptone during PEF treatment. Further work is underway to develop a test cell that can be used for the direct PEF treatment of contaminated beer and lager. It may well be that the presence of alcohol in these products will further enhance the microbiocidal effects of PEF treatment.

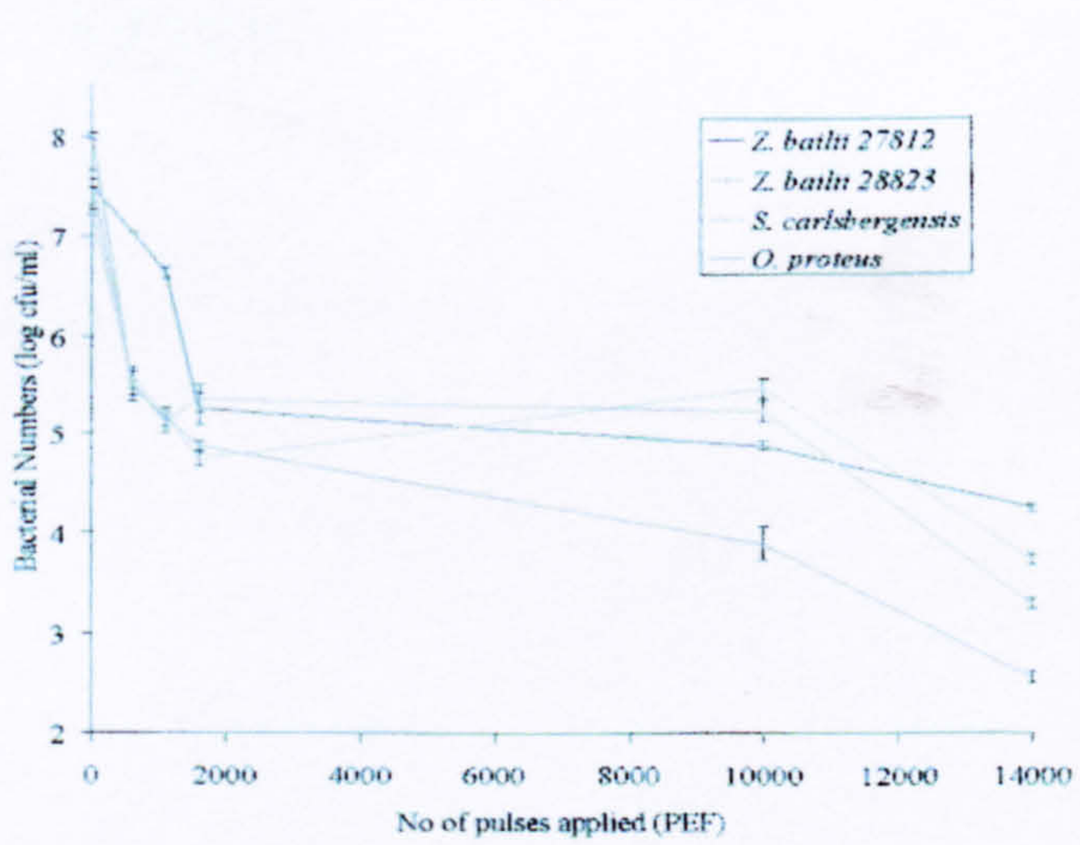

Figure 3: Comparison of PEF inactivation of various beer/lager spoilage microbes

References

1. **MacGregor, S.J., Farish, O., Fouracre, R., Rowan, N.J. and Anderson, J.G.** 1996. Inactivation of Pathogenic and Spoilage Microorganisms in a Test Liquid Using Pulsed Electric Fields. *IEEE Transactions on Plasma Science*, 28(1) 144-149.
2. **Rowan, N.J., MacGregor, S.J., Anderson, J.G., Cameron, D. and Farish, O.** 2001. Inactivation of *Mycobacterium paratuberculosis* by Pulsed Electric Fields. *Applied and Environmental Microbiology*. 67: 2833-2836

EPAST GROUP

Enquires contact Karen Wall: **karen.wall@eee.strath.ac.uk**

پنجشنبه ۸۱/۰۲/۲۶ سالن ۱ گرایش: قدرت

SP13 ماشین و الکترونیک صنعتی ساعت ۱۰:۳۰-۱۲:۱۰

روسای جلسه: دکتر سقائیان نژاد از دانشگاه: صنعتی اصفهان

دکتر شرکت معصوم محمد علی از دانشگاه: علم و صنعت ایران

افزایش پایداری خودرو برقی چهار - چرخ - محرک بوسیله منطق فازی

POW-305 کاظمی رضا فرهنگی شاهرخ تهامی فرزاد

تحلیل پایداری و کنترل پیشگیرانه توسانات موتورهای پله‌ای

POW-181 فیض جواد عباسی خلیل بانان علی

طراحی بهینه موتور القایی سه فاز قفس سنجابی برای خودروی برقی

POW-104 بناء شریفیان محمد باقر فیض جواد

A Solid - state pulse generator for use in the PDF inactiration of microorganisms

s. Macgregor z ghasemi **POW-331**

Switch Mode Power Supplies (SMPS) & EMI Emissions: causes and perdictions

M.H.Nagrial A.Hellany **POW-326**